Abstract

Visual working memory (VWM) is defined as the process of temporarily storing relevant information online for processing and manipulation while no visual information is at present. Like high-level regions in the brain, evidence from recent studies suggested that visual areas (V1-V3) might be also actively involved in remembering features such as orientation and spatial frequency. The work presented in this thesis extended to other visual attributes, including motion coherence and contrast, with more detailed psychophysical and neuroimaging evidences to support the role of early visual areas in human visual working memory. The mnemonic characteristics of those visual traits were explored from *temporal* and *spatial* aspects using conventional psychophysical and functional brain imaging.

Along the temporal domain, a variety of durations were applied to examine observers' ability to maintain visual information in memory. Differential performance was found for motion coherence and visual contrast. Subjects' performance for remembering contrast degraded as time increased; yet information for motion coherence was retained almost perfectly. These results support the multi-channel theory that models the process occurred in early visual cortex when different visual features were perceived.

In addition, the procedure of "memory masking" was used in studies of both visual attributes with different properties. Compared to the baseline performance when no additional stimulus was present during the delay period, the mask stimulus declined the precision of WM, indicating that the ongoing memorization was interrupted by the perception of a task-irrelevant stimulus, which is mainly processed in early visual areas. Moreover, for motion coherence, it was found that a mask with similar characteristics along the interested dimension showed the most disruptive effect. This result supports the representation specificity of stimuli held in WM. We also displayed the mask stimulus at different time points during memory period, either at the beginning, in the middle or at the end of the delay interval. Our findings show that these time points of mask presence had similar influence.

Besides answering the question of whether early visual cortex was engaged in VWM, we also addressed the issue of *how* visual information is processed and held in these areas. Taking advantage of the patterns of random pixel noise with a range of contrasts, we revealed that the visual system might exploit the "image-like" representation to discriminate stimuli with different contrasts, rather than only extracting and retaining the luminance differences.

With the advent of up-to-date imaging technology, we also used Magnetic Resonance Imaging (MRI) in this thesis to investigate the neural correlates of visual WM of contrast in human brain. In addition to the conventional fMRI analysis, we executed multivariate pattern analysis (MVPA) in this thesis. This analyzing method takes all the information within the interested regions into account instead of the average activity, allowing more precise understandings of the structure and neural mechanism of WM. By using MVPA, we confirmed our results from the psychophysical parts in the thesis, showing that distinctive spatial patterns were evoked in early visual areas when different contrasts were perceived as well as remembered.

Along the spatial domain, the work presented in this thesis provides further evidence of behaviour and brain activity when stimuli were displayed in different hemifields. Our findings showed the extra time and information cost when information relating the contrast of a stimulus was transmitted across hemispheres. Moreover, we unravelled the effect of spatial attention on primary visual cortex while visual features at different spatial locations were processed and memorized.

Acknowledgement

I am extremely grateful to my supervisors, Dr. Denis Schluppeck, Professor Tim Ledgeway, and Professor Paul McGraw for their excellent academic advice and intellectual inspiration, their encouragement and support throughout the whole course of my Ph.D study. They did not only proofread my work, but also helped me build up my confidence through powerful encouragement when I needed. I feel privileged to carry my research under their supervision. I particularly thank Denis for his enormous kindness, sincere care, and patience as my first supervisor who helps me come through the most challenging time during the past four years, including those times when I was in hospital.

Many thanks to Julien Besle, Alex Beckett and Yin Wang for their academic support and kindly sharing their knowledge with me. I am grateful to all office mates who have cared for me and encouraged me. I also benefit greatly from useful discussions and support from the Notts Vision group.

I wish to give my heartfelt thanks to people who supported me mentally and medically. My dearest friends in the fellowship have been a constant source of care. Thanks to Dr. Lim Weishen who offered me treatment and made my return to Ph.D study possible.

My major debts are to my dearest parents who brought me into this world. They have given me tremendous and valuable love, encouragement and unconditional support. Their endeavour (i.e. companying me in a completely unfamiliar country, and learning English!) was of inestimable value in enabling me to bring this research study to a successful conclusion. This work is dedicated to them. 亲爱的爸爸妈妈， 感谢你们对我无私的爱！我爱你们！将这本博士论文献与你们！

Last but not least, I thank School of Psychology and the International Office of the University of Nottingham, and all other organisations that supported me financially, which helps me concentrate on my research and makes my dream of becoming a Ph.D. come true.

Table of contents

Chapter 1: Introduction

1.1 The visual cortex

1.1.1 From eye to brain

The first stage of processing visual stimuli happens just after light enters the eye through the cornea, the pupil, passes through the lens and vitreous humor and arrives at the retina. The photosensitive receptors on the retina then translate this visual information carried by light into electrical energy, triggering a rapid cascade of neural responses throughout the brain. The earliest report showed that neurons in visual areas in cat, including in the retina, thalamus and cortex, all share a common property that they only respond to a small area of the visual field, which is known as the receptive field (RF) of the neuron. The size of receptive fields varies depending on location along the visual processing hierarchy as well as which part of the visual field is represented. For example, the foveal representation has the smallest RF and the densest population of cone photoreceptors in the retina. The resulting visual field sampling density of ganglion cells from the cones, which are more sensitive to the details of visual image (Rodieck, 1973; Wassle et al., 1990), is the highest in the fovea. As one moves up the visual stream, the size of RF becomes progressively larger for cells – a trend that has been confirmed across species, including humans and macaques (Desimone & Gross, 1979; Gattass et a., 1981; Harvey & Dumoulin, 2011; Amano et al., 2009).

From each retina, most of the visual signals are projected-forward to the optic nerves, which include groups of fibers originating from the nasal and the temporal parts. The nasal fibres cross at the *chiasma opticum,* while the fibers from the temporal halves ultimately project to the ipsilateral cortex. Then information arrives at the lateral geniculate nucleus (LGN), which is a thalamic relay along the visual pathway from retina to the visual cortical areas (Figure 1.1). Like neurons in the retina, LGN cells are monocular and have relatively small circularly shaped, concentric On- or Off- center receptive fields (Figure 1.2). The LGN on each side contains six major laminae, four dorsal, parvocellular layers and two ventral, magnocellular

laminae. It has been shown that these two types of layers receive input from two distinct retinal channels (Figure 1.3) (see reviews Benedek et al., 2006, Callaway, 2005).

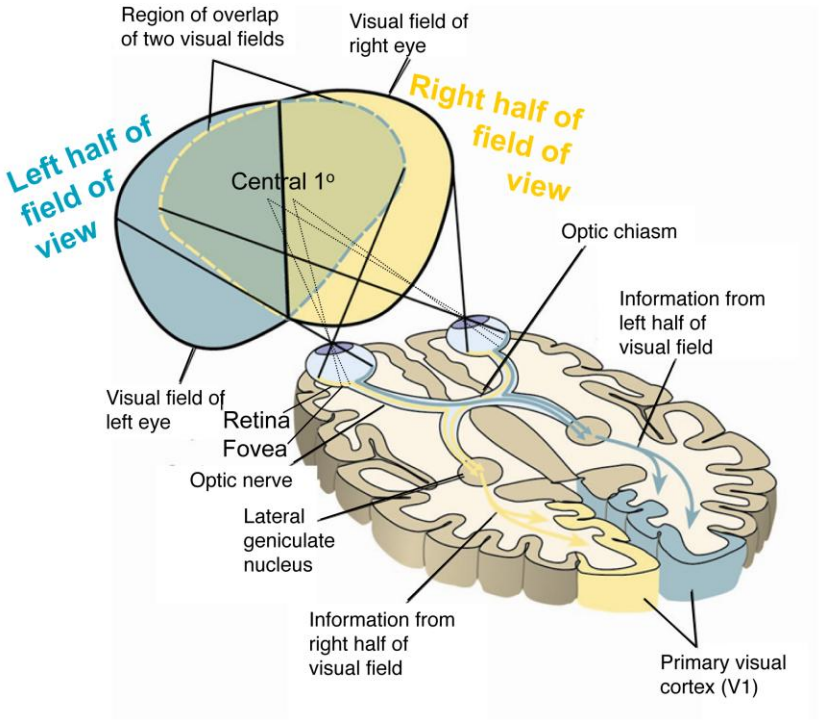

Figure 1.1: Pathway of visual system. Light enters the eye through the cornea, the pupil, passes through the lens and vitreous humor and arrives at the retina. From each retina, most of the visual signals are projected-forward to the optic nerves, which include groups of fibers originating from the nasal and the temporal parts. The nasal fibres cross at the chiasma opticum, while the fibers from the temporal halves ultimately project to the ipsilateral cortex. Then information arrives at the lateral geniculate nucleus (LGN), which is a thalamic relay along the visual pathway from retina to primary visual cortex, the first station in cortical area (Figure modified based on www.empiricalzeal.com/wp-content/uploads/2012/06/visual-pathway-small.gif).

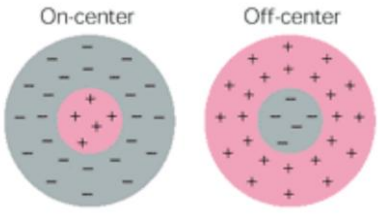

Figure 1.2: The receptive fields of cells in the retina and LGN. Cells in these two regions fall into two classes: on-center and off-center. The receptive fields of these neurons have a center-surround organization due to antagonistic excitatory (+) and inhibitory (-) regions (Figure and legend adapted from Kandel et al., 2000).

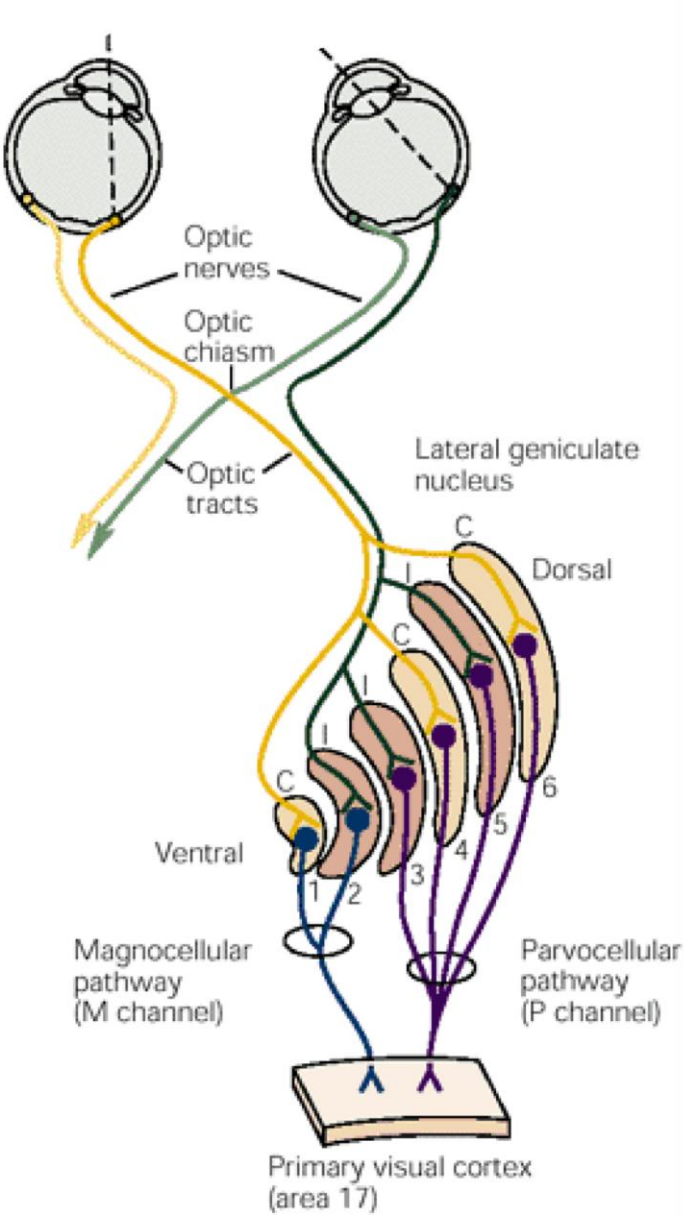

Figure 1.3: Organisation of the lateral geniculate nucleus. Inputs from the right hemiretina of each eye project to different layers of the right LGN. Layers 1 and 2 comprise the magnocellular layers; layers 3 through 6 comprise the parvocellular layers. All of these project to area 17, the primary visual cortex. (C, Contralateral input; I, ipsilateral input). (Figure and legend adapted from Kandel et al., 2000)

After relaying in the LGN, information from one half of the visual field almost exclusively projects to V1, or striate cortex, (the first cortical station) in the contra-lateral hemisphere (Henschen, 1893). Human V1 is located in and around the calcarine sulcus on the medial surface of the occipital lobe, spanning the area of occipital pole, covering approximately 4700

mm^2 cortical surface on average (Andrews et al., 1997). The average number of neurons in V1 in each hemisphere of an adult human is estimated to be ~140 million (Leuba & Kraftsik, 1994). These cells are distributed in six basic layers defined by Nissl-stained method in mammals. It has been demonstrated that the information relayed in the magno- and parvo-pathways of LGN projects primarily to layer 4 of V1. Some early studies have proposed that these two systems remain completely segregated within this layer (Wong-Riley, 1979). However, succeeding findings have shown the organization of cortical circuits in V1, indicating that the output from different groups of LGN cells are intermingled extensively beyond the input layers in V1 (Callaway & Katz, 1993; Yabuta & Callaway, 1998; Yoshioka et al., 1994). Several lines of evidence have illustrated that the two different streams, established in the retina and LGN, remain partially segregated but continue on with significant crosstalk (Fitzpatrick et al., 1994; Lund & Boothe, 1975; Wiser & Callaway, 1996).

Neuroanatomists have found that the cells in human occipital cortex (which has a thickness of around 2~3 mm) (Fischl & Dale, 2000; Lüsebrink et al., 2013) are organized into a columnar arrangement orthogonal to the cortical surface. Moreover, these columns span ~$1\times1mm^2$ in monkey and ~$2\times2mm^2$ in human (Hubel & Wiesel, 1963; Blasdel & Salama, 1986a; Das & Gilbert, 1997; Maldonado et al., 1997; Ohki et al., 2006; Adams et al., 2007). The neurons from a particular cortical column have similar receptive field properties. This anatomical structure was found to be an important property of V1, which will be further described in the following paragraphs.

After this first station in cortex, the information is fed on into other areas (termed V2, V3, V4, MT/V5 and so on) (see Figure 1.4). In this sense, V1 is indispensable as it plays a role of central distributor along the visual processing pathway, which runs from retina to extrastriate cortices. Therefore, some of the properties of this region are shared with other visual areas, one of which is their retinotopic organization. I will outline the visual retinotopic architecture in the next section.

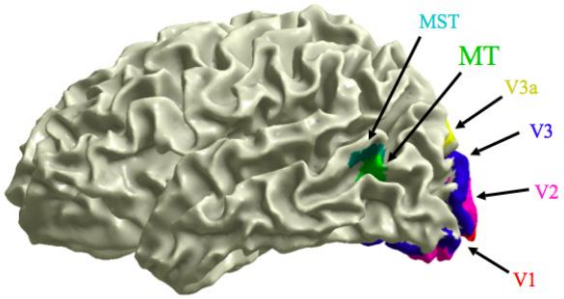

Figure 1.4: Lateral view of the human cortical hemisphere showing the representation of visual areas. Colours indicate different visual areas. (Figure adapted from www.cns.nyu.edu /~david/courses/perception/lecturenotes/motion/motion.html).

1.1.1.2 Visual Retinotopy

Details of human visual retinotopy were discovered first in clinical patients and found to be consistent with the marked visual cortical areas from earlier animal experiments (Felleman & Van Essen, 1991; Tootell et al., 2003). It was found that cortical lesions in V1 caused scotomas or phenomenal blindness confined to a corresponding region of the visual field. The property of the human visual system preserving the spatial structure and layout of the visual field is termed retinotopy: at the earliest stage, the receptive field centres of the retinal ganglion cells sample the visual field via an orderly mosaic organization which is represented in the lateral geniculate nucleus in a visual map. What is more important, the early visual cortex maintains the spatial arrangement of this image. In other words, information is a specific reflection of retinal geometry: adjacent points in the retina are projected to adjacent locations in the contra-lateral hemisphere. Since this property imitates the fixed correlation between the visual field and the retina, the visual field maps are also called *retino*topic maps. However, some regions on the retina are expanded as a function of visual field eccentricity. For instance, the central fovea is represented over a larger area of the cortical surface. This amount of enlargement is usually quantified as the cortical magnification factor (CMF) (see Figure 1.5) (Daniel & Whitteridge, 1961).

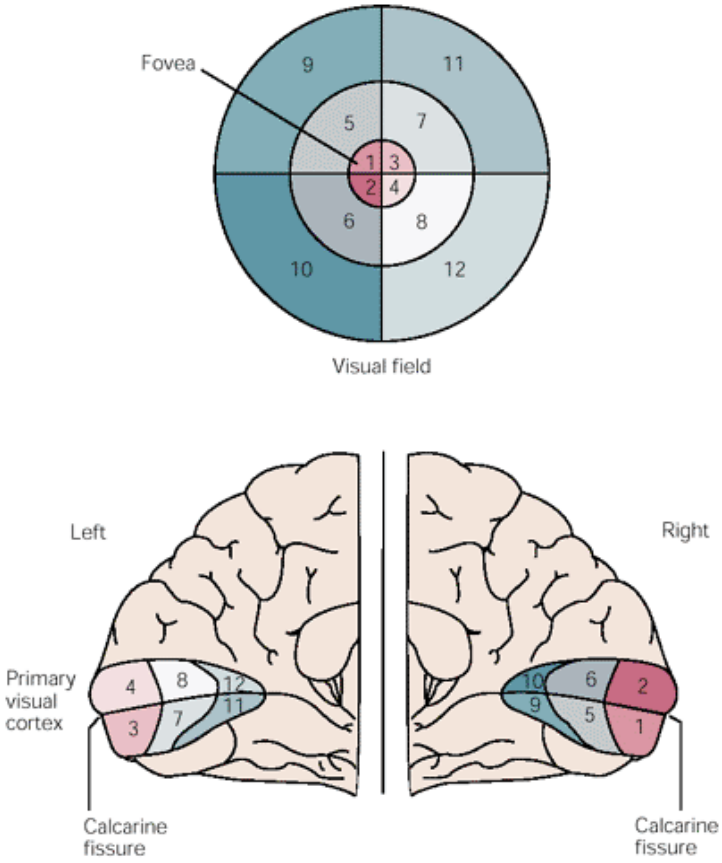

Figure 1.5: Retinotopic organization of the primary visual cortex. Areas in the primary visual cortex are devoted to specific parts of the visual field, as indicated by the corresponding numbers. The upper fields are mapped below the calcarine fissure, and the lower fields above it. The striking aspect of this map is that about half of the neural mass is devoted to representation of the fovea and the region just around it. (Figure and legend adapted from Kandel et al., 2000)

Before the advent of fMRI in the field of neuroscience, PET has been used to image the activity in V1 of normal human subjects non-invasively. These data confirmed the visual maps derived from previous neurology and electrocorticography in patients undergoing surgery (Brindley & Lewin, 1969; Dobelle & Mladejovsky, 1974; Dobelle et al., 1979). However, spatial detail and maps in individuals were beyond the ability of PET, which called for the application of more advanced methods and technology. Back in 1991, Horton and Hoyt initially conducted anatomical MRI on patients with focal lesions in occipital cortex. Subsequent functional MRI experiments, especially using BOLD fMRI further increased the reliability of identifying the visual field maps. Early travelling-wave fMRI measurements

revealed three clearly delineated regions near the calcarine sulcus in the occipital lobe (DeYoe et al, 1996; Engel et al, 1997; Sereno et al., 1995).

1.1.1.2 Organization and layout of visual field maps

First, the visual field is split into two hemifields along the vertical meridian. V1 in one hemisphere represents the whole contralateral visual hemifield roughly and is centred on the calcarine sulcus. A visual stimulus that travels from superior vertical meridian of the visual field to the inferior vertical meridian is represented in V1 as a displacement of neural activity from the inferior limb of the calcarine to the superior limb. In the orthogonal direction, the representation in V1 goes from central to the peripheral visual field as one moves from the occipital pole to anterior calcarine (Figure 1.6).

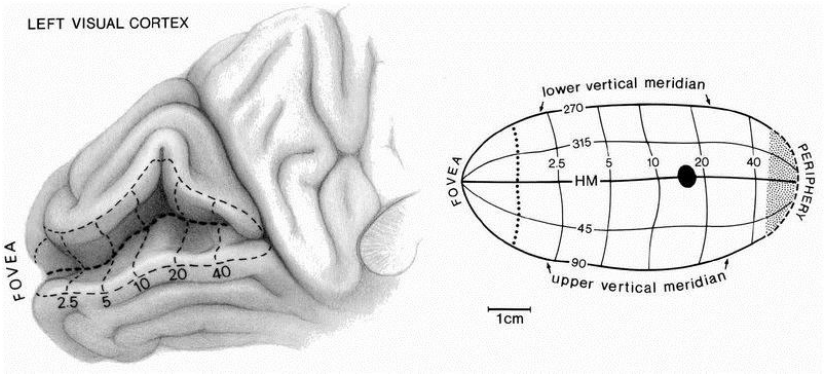

Figure 1.6: Left: the representation of the visual field on the surface of human occipital cortex. The figure shows the medial aspect of the occipital lobe with tissue on either side of the calcarine sulcus pushed apart. Right: representation of visual field coordinates as they would appear on the cortex if completely unfolded and flattened. Numbers show either meridional angle or eccentricity in degrees. The dark circle is the blind spot; HM: horizontal meridian. Note the orthogonal intersections of lines of constant eccentricity and meridional angle. Modified from Horton (2006).

Similar to the organization in many species (Allman & Kaas, 1971; Hubel & Wiesel, 1965; Talbot & Marshall, 1940; Talbot, 1942; Thompson, Woolsey & Talbot, 1950; Zeki 1969), fMRI experiments demonstrated that there are two additional extrastriate maps in *human* visual cortex (V2 and V3) that span the area of 10-30 cm^2 (Dougherty et al., 2003). V2 and V3

contain discontinuous hemifield maps, which are segregated along the localized meridian (Figure 1.7) (De Yoe et al., 1994; Engel et al., 1997; Sereno et al., 1995). Each of them has two edges representing the horizontal meridian and the vertical meridian. It was suggested that its special division might contribute to the achievement of binocular integration. The approach of displaying such retinotopic organization onto a map, which was used in this thesis, will be outlined in the Retinotopic mapping section in Chapter 2 (see more details in General method).

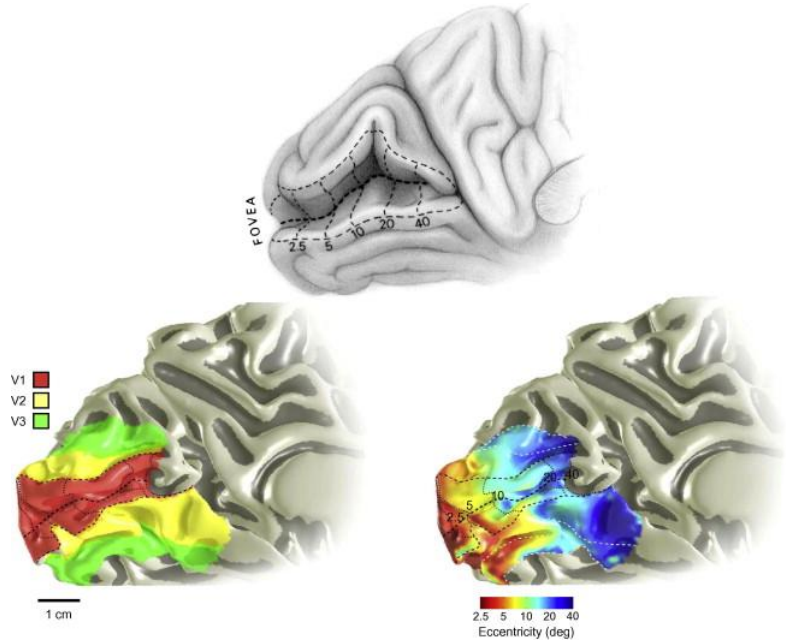

Figure 1.7: The visual field eccentricity map in human primary visual cortex (V1). The image at the top is the same as the top graph shown in Figure 1.6, a sketch of the estimated eccentricity map in calcarine cortex as deduced from lesion data (Horton & Hoyt, 1991). The image on the lower left shows the arrangement of V1, V2 and V3 in a single human subject. The image at the lower right shows the eccentricity map in the same subject. The color bar for this image represents log-scaled eccentricity. The field map locations and eccentricity map were measured with fMRI (Dumoulin & Wandell, 2008).

While fMRI offers clear boundaries of visual fields, it faces the similar difficulty of distinguishing the visual fovea as single-unit electrophysiology and cytoarchitectonic approaches (Dougherty et al., 2003; Schira et al., 2009; Zeki, 1969). In the majority of papers, the foveal regions of V1 to V3 are delineated as the 'confluent foveal representation'. Several reasons may contribute to this difficulty, including fixation instability and the artefact of large

veins. In addition, the width of the fovea on the maps is smaller than the voxel size in most routine experiments (3mm). Despite these problems, a recent study using high-resolution fMRI showed that the fovea of V1, V2 and V3 could be separately represented (Schira et al., 2009). One study also measured the localization precision of such fMRI experiments and found that the traveling wave is able to localize activity to within 1.1mm of visual cortex (Engel et al., 1997).

The work presented in this thesis mainly focuses on V1-V3 and MT/V5+, whose maps can be defined reliably and uncontroversially in every subject, despite the individual variability in respect of sizes and locations on gyri/sulci of those visual areas.

1.1.2 Establishing the neural representations of different visual features

In parallel with the work defining retinotopic maps in the human visual system, a considerable body of research has emerged, aiming to understand the maps with regard to functional specialization. Such work complements electrophysiological and psychophysical studies that have provided a wealth of information on the neuronal characteristics of different early visual areas, such as the ocular dominance, selectivity for stimulus orientation and spatial frequency, neuronal response to contrast, and selectivity for motion in early visual cortex as well as MT/V5. Neuroimaging, especially fMRI, is becoming increasingly informative for exploring the neuronal correlates for different visual areas in the human brain. In the first instance, work has replicated findings revealed by electrophysiology from animals, including the function of primary visual cortex (V1) in responding to orientation, contrast and motion, and the characteristics of MT/V5 in analysing moving stimuli. In this thesis, I will review some relevant evidence of neuronal properties derived through these three complementary methodologies: single unit electrophysiology, psychophysics, and neuroimaging.

1.1.2.1 The orientation selectivity of the primary visual cortex

Cellular basis of orientation selectivity

The encoding of orientation of visual stimuli is one of the most well-known characteristics of neurons in primary visual cortex (V1). Because the LGN does not show much orientation selectivity, this has made V1 a site of intense interest for visual neuroscience. It is worth pointing out that, some recent research has showed that even LGN cells may have a degree of orientation and direction selectivity, albeit on a much lesser scale (Xu, et al., 2002). A bulk of experiments has studied orientation selectivity in V1 on the level of microstructure and physiology. Hubel and Wiesel (1963) also discovered the differentiated properties of neurons in V1 with linear stimuli (bars and edges), based on which they introduced three categories of V1 neurons: simple, complex and hypercomplex cells. Different from the concentric RF of LGN and retina cells (Figure 1.2), the RF of simple cells in the primary visual cortex is organized into elongated ON and OFF subfields (Figure 1.8). The long axis of these fields is parallel to the preferred orientation of the cell. Though complex cells are also tuned for orientation, there are no distinct ON and OFF zones which makes their response insensitive to the position of the stimuli or phase of sinusoidal stimuli on the RF. Based on those findings, Hubel & Wiesel proposed a hierarchical feed-forward model, where they hypothesized that the RF of the complex cells was a convergence of simple cell inputs from deeper layers. This model has been supported by many experiments (see e.g, Alonso & Martinez, 1998; Chung & Ferster, 1998), yet it does not fully capture the complexity of RF in the cortex. Some discrepant findings suggested that the selectivity of some neurons is strongly dependent on the intracortical modification (i.e. excitation and inhibition) that shapes the response of cortical cells within a network, generating heterogeneity of orientation tuning response across the visual cortex (Sclar & Freeman, 1982; Skottun et al., 1987; Gardner et al., 1999; Muller et al., 1999; Dragoi, Sharma & Sur, 2000; Dragoi & Sur, 2001). A parsimonious model of simple cells of V1 receptive fields is based on a simple Gabor filter and it has been proposed that simple cells compute a linearly weighted sum of the input along both temporal and spatial dimensions. Then, its response is normalized by the responses of surrounding neurons and

passed through response nonlinearity (squaring or rectification). Complex cells, on the other hand, sum over the outputs of a local pool of simple cells with comparable tuning characteristics but different spatial locations or phases (Heeger, 1991; Geisler & Albrecht, 1997; Schwartz & Simoncelli, 2001; Cavanaugh, Bair & Movshon, 2002). Some studies, however, have suggested that there might be a continuous spectrum with 'simple' and 'complex' cells at the extremes (Chance et al., 1999; Abbott & Chance, 2002; Mechler & Ringach, 2002). Finally, the hypercomplex cells exhibit end-stopping properties in that their response declines when an elongated stimulus in the RF exceeds a particular length.

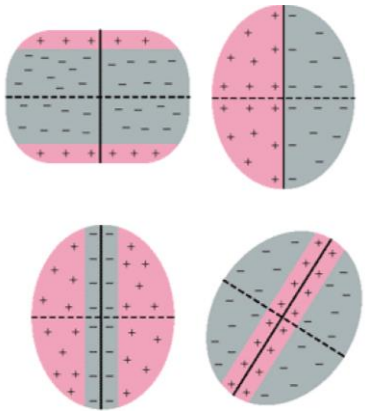

Figure 1.8: The receptive fields of simple cells in V1. They have narrow elongated zones with either excitatory (+) or inhibitory (-) flanking areas. Despite the variety, the receptive fields of simple cells share three features: (1) specific retinal position, (2) discrete excitatory and inhibitory zones, and (3) a specific axis of orientation (Figure and legend adapted from Kandel et al., 2000).

Anatomical architecture of orientation selectivity

A prominent architectural feature of V1 anatomy is that neurons with similar properties are clustered in a structure of columns, including columns with orientation specificity. These functional units run perpendicular to the surface of the cortex across the entire cortical grey matter. Within each of these vertical columns, the neuronal response to orientations approximately stays invariant, but it displays a slight difference across adjacent successive columns. This means that for a specific orientation stimulus, some of the neurons in V1

respond maximally to it as their preferred orientation, some cells are less responsive and others almost silent (Figure 1.9).

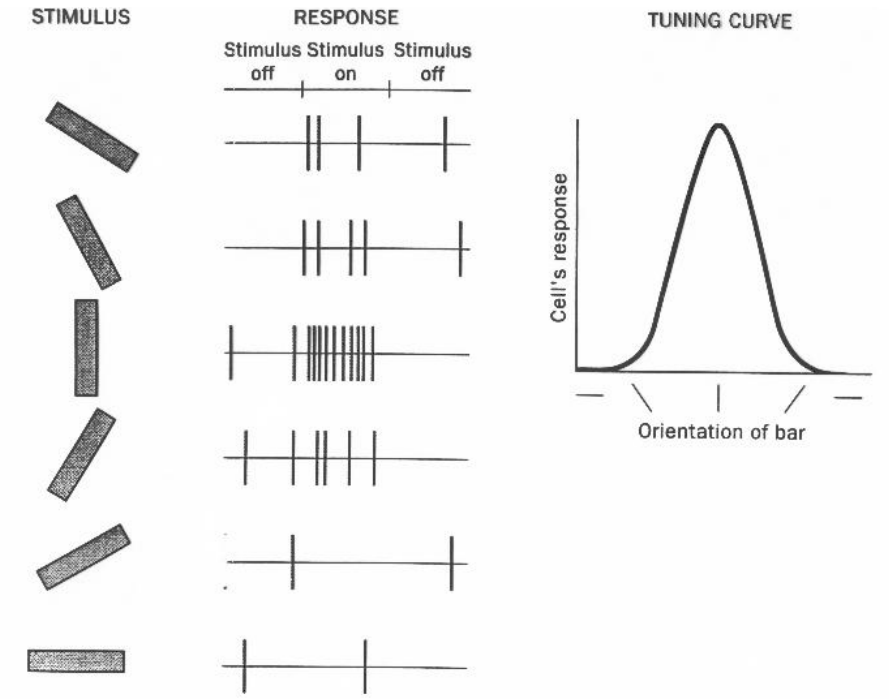

Figure 1.9: Orientation tuning of a simple cortical cell. This cell responds best to a vertical bar, and responds less as the bar is tilted in either direction, which is illustrated as a tuning curve on the right of the figure (Figure adapted from cogsci.bme.hu/~ikovacs/SandP/-prepI_3_1.html).

The detailed spatial structure of the orientation preference was unveiled with optical imaging by Blasdel & Salama (1986b) and Grinvald, et al., (1986) in monkeys (Figure 1.10). In one of their analyses, they calculated the dominant angle from summed responses to all stimulus orientations for all the pixels acquired from the cortical surface, and colour coded to indicate the preferred angle for each individual pixel. They found that the map of orientation preference is inhomogeneous. Later applying the same methods to area 17 of cat, Bonhoeffer & Grinvald (1991) also found that the orientation selectivity shows a pinwheel-like organization. For nearly half of the pinwheels, the representation of orientation changed in a

clockwise direction (as seen from above), leaving the other half in a counter-clockwise sequence with each pinwheel containing a full set of unique orientations domains.

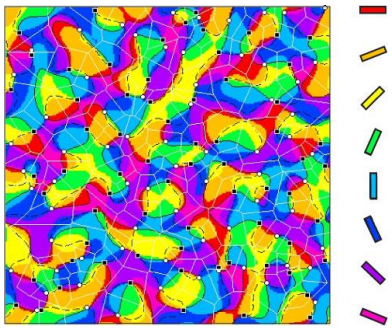

Figure 1.10: Layout of orientation preference observed in area V1 of macaque monkey. The colour plots show that iso-orientation domains – regions of constant colour – are periodically spaced thin strips with a variable width and pointed terminations. The cortex preferences usually rotate, either clockwise or counter-clockwise at a roughly constant rate. The direction of rotation will typically continue unchanged for 1 – 2 mm and then reverse unpredictably. Scale bar = 1mm. Modified from Blasdel & Salama (1986b).

Functional architecture of orientation selectivity

Some researchers have posited that spatially organized feed-forward inputs (an elongated array) from LGN contribute to this orientation preference (Hubel & Wiesel, 1963), whereas others have argued that orientation selectivity is a property that arises from intracortical circuitry. By examining the relative contribution of linear and nonlinear mechanisms, single unit recordings from simple cells indicated that a cortical mechanism plays a more prominent role than feed-forward input from LGN in the process of orientation tuning (Gardner et al., 1999). In addition, these investigators suggested that this cortical interaction also ensures an equivalent orientation representation independent from the RF's size and shape for the striate cells in cat.

Over the last decades, several electrophysiological and optical imaging experiments in both animal and humans have reproducibly confirmed that the primary visual cortex (V1) processes the orientation information and that single neurons selectively encode particular orientations. But few earlier experiments have been able to study human cortex directly.

However, with the recent advancement of fMRI, the property of orientation selectivity and the basis of orientation perception have also been studied in the human brain. It provides consistent evidence about the representation of orientation but at a coarser spatial scale than electrophysiology or optical imaging. Because fMRI pools the response of neuronal ensembles over several millimetres, it tends to cancel out orientation selective responses at the level of individual voxels. As a result, it is possible that the measured average fMRI signal does not exhibit any orientation specificity. Multivariate statistical analyses have been used to successfully demonstrate orientation selectivity in human V1 using fMRI (Haynes & Rees, 2005; Kamitani & Tong, 2005b; Kay et al., 2008), but some results have raised doubts whether multivariate analysis can reveal biases produced by uneven sampling of columnar level maps. For example, a recent fMRI study has colocalized the orientation map with retinotopic organization (Freeman et al., 2011) and convincingly shown a large-scale radial bias of orientation preference in V1 (Sasaki et al., 2006), though it is in conflict with other conjecture based on fine-scale columnar architecture (Swisher et al., 2010).

Other spatial selectivity

The stimulus dimensions of orientation and spatial frequency are fundamental to the early analysis of visual input. Concordantly, the response of simple cells can be modelled by linear filters that are selective for certain spatial frequency and orientations (Jones & Palmer, 1987). In psychophysical experiments inspired by the electrophysiology findings (Campbell et al., 1969), the relation between orientation and spatial frequency has been investigated by measuring the orientation sensitivity (thresholds) to sinusoidal stimuli with various spatial frequencies (Schade, 1956; Westheimer, 2001). Discrimination thresholds for orientation and spatial frequency tasks are also dependent on stimulus contrast. Both of them rise sharply at low contrast and progress to asymptote at moderate contrasts.

1.1.2.2 Early visual areas respond to stimulus contrast

Contrary to the other neuronal characteristics of striate cells, early electrophysiology research put much less emphasis on the response as a function of luminance contrast. However, since the detailed description of the contrast response function in animal striate cortex (Albrecht & Hamilton, 1982), more studies have been conducted to explore the properties of neuronal response to contrast.

Single cell contrast response function

While retinal cells process primarily the absolute light levels, it was found early on that cortical neurons mainly respond to relative changes in illumination, i.e. contrast. Electrophysiological recordings showed that the relationship between neuronal response and the stimulus contrast exhibits a monotonic increase (Albrecht & Hamilton, 1982, Anzai et al., 1995; Dean, 1981; Tolhurst et al., 1982). Specifically, the function is well described by a monotonic S-shape, with strongly nonlinear responses at both low and high contrasts, and the linear part explains the enhancement of neuronal response as a function of contrast. These three sections of the contrast response curve are sometimes referred to as compression, saturation and overall gain, respectively. For quantitative analysis, this contrast response relation can be fitted with the Naka-Rushton function:

$$R = R_{max}\frac{C^n}{C^n + C_{50}^n} + b, \qquad \text{(Eq. 1)}$$

where R_{max} is the maximum amplitude of response, C_{50} is the semi-saturation contrast at which the curve reaches half height, *n* is the power-function exponent denoting the steepness of the fitting curve, and *b* is the background discharge (see 1.12, a). This function has been found to be a good description of the relationship between stimulus contrast and single neuron responses in macaque V1 (Hubel & Livingstone, 1990; Edwards et al., 1995) and in owl monkeys, a nocturnal primate (O' Keefe et al., 1998).

Population contrast response functions

-Electrophysiological evidence

The contrast response function (CRF) across a number of neurons has been found to be in good agreement with the response property of single cells in V1 detected by single-unit recordings. Electrophysiological data from non-human primates indicates that the regional CRF can be fitted by a power law with exponent ~0.6 (Heeger et al., 2000).

-Psychophysical evidence

Contrast discriminability is well described by measuring the psychophysical thresholds as a function of contrast increment. The resulting contrast discrimination function in such experiments is dipper-shaped. As background (fixed) contrasts are added, instead of rising with the contrast, the increment threshold drops below the detection threshold (Campbell & Kulikowski, 1966; Nachmias & Sansbury, 1974; Stromeyer & Klein, 1974). This initial dip is usually described as a facilitation effect: the increment threshold is even lower than the detection threshold. Then as the background contrast is increased, the increment of thresholds elevate steadily, which is called a masking effect (Legge & Foley, 1980; Foley & Yang, 1991; Teo & Heeger, 1994, 1995). This masking effect can be related to the normalization model in which each cell in striate cortex has a nonlinear acceleration but it is also suppressed by a divisive inhibitory pool of responses of other neurons (Heeger, 1992; Foley & Boynton, 1993). This measurement of contrast discrimination has been validated as an indirect mean for estimating population CRF (Boynton et al., 1999; Zenger-Landolt & Heeger, 2003). For instance, the expansive portion of the CRF predicts the facilitation effect, while the compressive section corresponds to the masking effect at high contrast.

-Functional MRI evidence

Over the last decades, fMRI has been exploited for the measurement of CRF. Besides V1 (Schumacher, et al., 2011), it was found that the response in other early visual areas also increases monotonically as a function of stimulus contrast, including V2 and V3 (Boynton et al., 1999; Gardner et al., 2005). Moreover, an even better match was observed between the psychophysical measurement of human behavior and the population response of the primary

visual cortex via BOLD fMRI (see Figure 1.11) as well as other serial recordings of multiple units (Geisler & Albrecht, 1997).

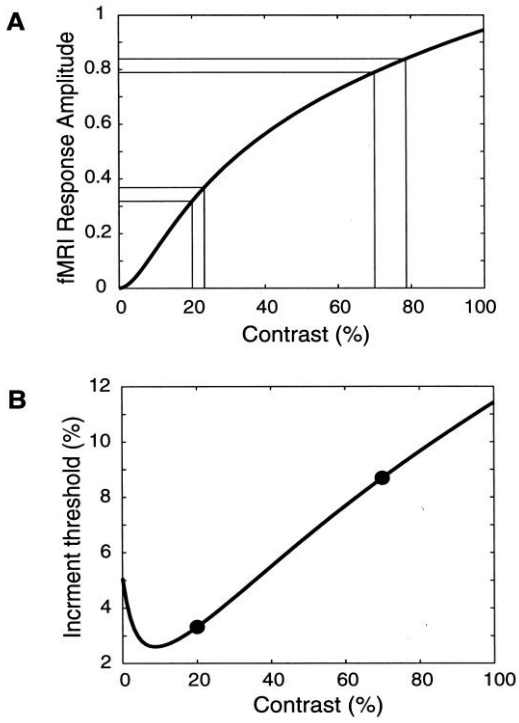

Figure 1.11: Illustration of the link between neuronal contrast–response functions and psychophysical TvC curves. **A**, A typical contrast–response function. **B**, TvC curve predicted from the contrast–response function in **A**. The thin lines in **A** and the filled circles in **B** illustrate an example of the relationship between the two curves. Figure and legend adapted from Boynton et al. (1999).

Change of contrast response function

The CRF can differ (between individuals or under varying experimental conditions) in several ways, yielding three types of changes (shown in Figure 1.12 b-d): the CRFs can shift horizontally along the contrast axis, indicating a change in *contrast gain* (c in Figure 1.12); or the response gain, which affects the response to lower contrasts less than those to higher contrasts (Figure 1.12 d). Finally, the activity gain, meaning the CRF could also show a vertical shift as a result of an overall increment of the function baseline (Figure 1.12 b). The following subsection briefly outlines the mechanism thought to underlie the first effect of CRF changes: contrast gain control.

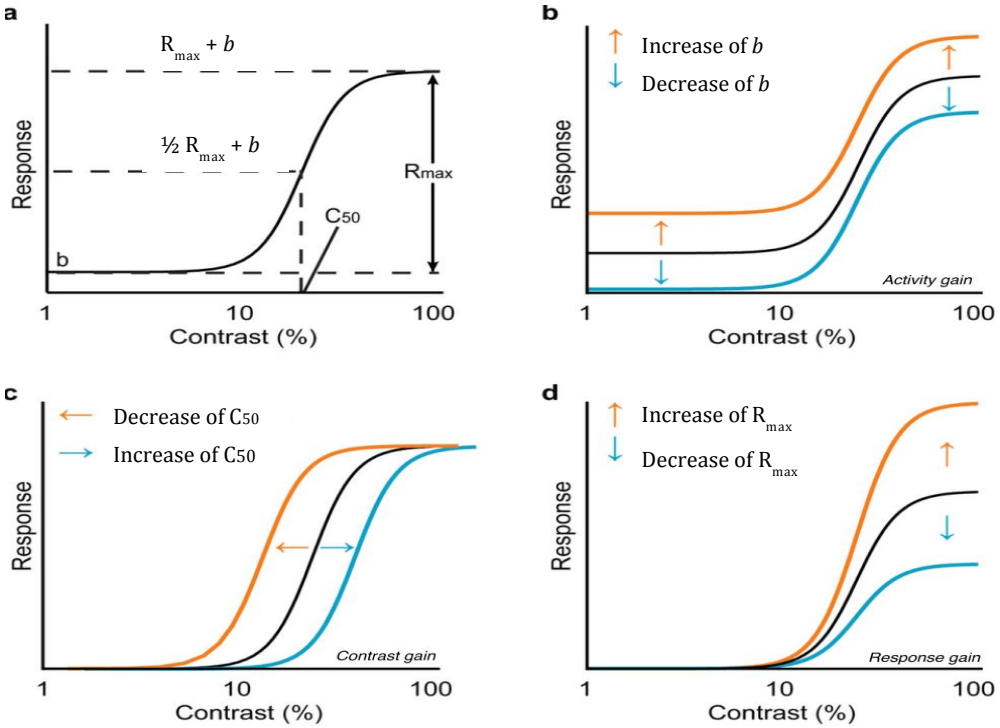

Figure 1.12: **a**, the contrast-response tuning curve was fitted using the Naka-Rushton function, where R_{max} is the peak (maximal) response, *b* the background discharge, and C50 the contrast value at 1/2 R_{max} (contrast sensitivity). **b-d**: Three kinds of gain control are considered: **b**, baseline control, **c**, contrast gain control and **d**, response gain control, which are characterized by changes in *b*, C50, and R_{max}, respectively. For example, response facilitation (orange) and suppression (blue) modulates the contrast-response function differently according to the type of gain control (see arrows). (Figure adapted from Soma et al., 2013)

Contrast gain control

Early investigations found contrast adaptation as a cortical function only. However, over the last decades, it has been corroborated that both parvocellular cells and magnocellular cells in LGN manifest a contrast gain effect. Similar to the LGN neurons (Sclar 1987) and retinal ganglion cells (Shapley & Victor 1978), responses from V1 also exhibit horizontal shift in the CRF after adapting to a prolonged contrast (perceptual adaptation): after prolonged adaptation, larger contrasts are needed to elicit the same level of response.

-Electrophysiological evidence

Numerous studies using single-unit methods in V1 of anesthetized cats (Bonds, 1991; Ohzawa et al.; 1982, 1985; Sclar et al., 1985), monkey and prosimian (Allison et al., 1993; Carandini et al., 1997; Sclar et al., 1989) have confirmed this effect as a result of adaptation. Moreover, striate cells in cat visual cortex showed different sensitivity to contrast adaptation. It was

found that for the majority of cortical neurons, their contrast-response functions shift laterally along a log-contrast axis, making the response functions center around the mean contrast level of a range of the stimuli (Ohzawa, Sclar & Freeman, 1985).

-Functional MRI evidence

FMRI has been used to measure the average BOLD response within demarcated regions of interest as a function of stimulus contrast. Using this method, investigators have characterized the mechanism of attentional modulation and adaptation of the CRF in early visual areas of the human brain. One study identified that covert attention boosted both the baseline activities and contrast gain (Kastner & Ungerleider, 2000). It was posited that the latter effect might increase the neuronal sensitivity to lower stimulus contrast. By imaging early visual cortex with an event-related functional MRI, Gardner et al. (2005) also found the contrast gain changes caused by adaptation in human V1, V2 and V3.

Spatial variation of contrast response

Despite the aforementioned universal neuronal properties, it was found that neurons in both the LGN and primary visual cortex show substantial variability in their responses. As outlined earlier, the LGN consists of six distinct layers. The four dorsal layers contain parvocellualr neurons, which are characterized by lower contrast gain and a more linear contrast response function. The other two ventral layers contain larger magnocellular neurons. This type of cell has high-contrast gain and saturates at relatively low levels of contrast. This segregation of contrast characteristics is extended to distinct layers in the primary visual cortex. For example, it was pointed out that the contrast threshold was lower inside cytochrome oxidase blobs than outside (Tootell, Hamilton & Swtkes, 1988), an effect that was missed by previous single-unit recordings. In addition, different cells exhibit different contrast gain control, which is reflected by the variation of the location of dynamic response range among the neuronal population. These findings raise one interesting question: whether there is any systematic clustering of neurons with higher and lower responsiveness to contrast in this area? One study optically imaged the response to a variety of stimuli in cat V1 (Lu & Roe, 2007). The optical

response was described as a function of contrast in that report. However, they failed to find a spatial specificity across the cortical surface. That study also investigated whether stimulus contrast might affect other orderly distributed visual representations. By measuring stimulus orientation maps at various contrasts, their data excluded an interaction between contrast and orientation preference. Given that the orientation map shows a pinwheel organization, they reasoned that only if neurons contributing to a particular pixel response shared similar contrast property, would the orientation tuning of pixel response keep invariant at different contrast levels. Based on pixel-by-pixel analysis, their results indicated that this contrast response is uniform across V1 (Lu & Roe, 2007).

The relationship between CRF and other stimulus dimensions

Previous studies have shown that for most simple cells the properties of neuronal preference are not largely influenced by increases in contrast (Albrecht, 1978; Albretcht & Hamilton, 1982; Sclar & Freeman, 1982; Li & Creutzfeldt, 1984), including spatial-frequency tuning, orientation tuning, and direction selectivity. Evidence from electrophysical recordings in V1 complex cells in monkeys illustrated that the contrast of a stimulus mainly modulates the response latency when manipulation occurs only along the contrast dimension (Gawne et al., 1996; Albrecht 1995).

1.1.2.3 Motion processing in MT/V5

The neuronal correlates of motion perception have drawn a considerable interest over the last decades. In particular, the perception of visual motion and the processing of motion information in area MT/V5 has been used as a powerful model system for understanding the computations achieved by neurons within particular areas and across neurons in connected areas. I will consider "motion perception" as the process of inferring the properties of moving elements in a scene based on visual input. The following sections will outline the relevant background literature on the properties of MT/V5 related to the work in this thesis.

Identifying MT/V5

The cortical area MT/V5 was first described in experiments with monkeys. It was identified as an extrastriate visual area that is firmly linked with the analysis of movement (Britten et al., 1992; Movshon et al., 1986; Newsome & Pare, 1988). Subsequent animal reports consistently showed that an area between lateral occipital and temporal cortex is distinctively motion sensitive (Gattass et al., 1981; Van Essen et al., 1981; Desimone & Ungerleider, 1986; Maunsell & Van Essen, 1987). Homologously to the macaque monkey, investigators also localized MT and adjacent main cortical fields involved in motion processing in humans (Maunsell & Van Essen, 1983) (see Figure 1.2). Findings from PET, which measures the changes in regional cerebral blood flow (Lueck et al., 1989; Zeki et al., 1991; Watson et al., 1993) confirmed these regions in humans to exhibit significantly stronger response to moving stimuli compared to stationary stimuli. The human homologue of MT is often also referred to as V5 or the 'human MT complex' / hMT+. It is typically found on the lateral surface on the occipital lobe within a dorsal or posterior limb of the inferior temporal sulcus (Huk, Dougherty, & Heeger, 2002). Patients with lesions in this region as well as healthy volunteers who encountered temporary interference from transcranial magnetic stimulation (TMS) in hMT+ uniformly demonstrated deterioration of motion perception (Beckers & Zeki, 1995).

Over the last decade, many functional MRI experiments have looked at processing of motion in MT/V5 (Zeki et al., 1991; Tootell & Talor, 1995), and have characterized the receptive fields of neurons in this area, which are dominated by the contralateral visual hemifield. Furthermore, using a motion-defined rotating wedge stimulus (coherently moving dots versus stationary background), fMRI has been used to detail the retinotopic organization in distinct subregions, allowing the delineation of human MT and MST (Huk, Dougherty & Heeger, 2002).

Direction selectivity of MT/V5

Neurons in many visual cortical areas are selective for certain fundamental properties of visual stimuli (Albright, 1984; Maunsell & Newsome, 1987; Born & Bradley, 2005;

Andersen, 1997). *Direction selectivity* is one of defining properties of neurons in MT/V5. It refers to the phenomenon that cells respond best when a stimulus moves in a particular direction within the RF of the cell.

Lesion experiments support the idea that MT/V5 is a crucial component in the neural machinery for analyzing and *perceiving* motion. It has been demonstrated that in experiments, where animals were trained to identify the moving directions of a group of correlated dots, psychophysical thresholds were elevated significantly after chemical lesions to MT/V5 in monkeys. Hence, loss of MT/V5 caused a selective impairment of motion perception (Newsome & Pare, 1988), indicating MT/V5 plays a crucial role in identifying direction of motion.

The effect of motion coherence on MT/V5 response

The firing rate of MT/V5 neurons is modulated by the strength of a motion stimulus. In this thesis, the strength of motion signal is defined specifically as the coherence of random dot kinematograms (RDK) or 'motion energy'. It can be varied from 0% to 100%. The motion energy is highest when all dots move in the same direction (100% coherence). One of the motion coherences we used in Chapter 4 was 40%, meaning that 40% of the dots move in the same direction while the other 60% moves in random directions. The following sections provide some relevant evidence of the response of MT/V5 neurons to the strength of a motion stimulus from electrophysiological and neuroimaging experiments.

-Electrophysiological evidence

Early visual areas including V1, V2 and some extrastriate areas, including MT/V5 are all activated at the onset of dynamic noise regardless of the presence of coherent motion (Movshon et al., 1986; Rodman & Albright, 1989; Movshon & Newsome, 1996). However, single-unit physiological experiments have demonstrated that neurons in V5 are strongly and selectively driven by a coherent stimulus moving in one particular direction (Snowden et al., 1991), a property not shown as conspicuously in V1 and V2. Furthermore, the firing rate of

single neurons in MT/V5 increases as the proportion of coherent dots in a RDK to the preferred direction increases (Britten et al, 1992).

-Neuroimaging evidence

Following on from PET experiments in which human MT/V5 was initially localized, some studies used fMRI with its improved temporal resolution to explore the dependence of signal amplitude and temporal latency on the level of motion coherence. Their results support the suggestion that motion coherence is a crucial modulator of the responses in hMT. Moreover, this increase of activation of neurons has a positive linear relation to the coherence levels (from 0% to 100% coherence) (Heeger et al., 2000; Rees et al., 2000). However, there are also conflicting data. For instance, one positron emission tomography (PET) study found the contrary result that incoherent motion is more effective than coherent motion in activating MT/V5 (McKeefry et al., 1997). They attributed their result to surround suppressive interaction, which is proposed based on the evidence from electrophysiological experiments. Born & Tootell (1992) illustrated that there are at least two anatomically separated subgroups of cells in MT/V5. Neurons in one group have receptive fields that are surrounded by an antagonistic RF and another group do not exhibit this antagonism. Functionally, it has been suggested that they process local (Allman et al., 1985; Tanaka et al., 1986) and global motion respectively. For neurons with an antagonistic surround, response reduction occurs if the stimulus (preferred motion) extends into the suppressive surround, whereas the response steadily increases for the other subpopulation of neurons (Born & Tootell, 1992; Reppas et al., 1997). These findings suggest that MT/V5 neurons are highly heterogeneous in their response properties. Therefore, when measuring the global response of neuronal response in this area, many factors should be considered before making a conclusion.

Other properties of MT/V5 neurons

Some of the experiments in this thesis used a moving grating stimulus with different contrasts. Though we did not investigate the average response across neurons in MT/V5 in those

contrast experiments, we considered some of the following issues when we designed the experiments. Therefore, I will briefly review these relevant neuronal characteristics.

-Dependence on stimulus contrast

The response of MT/V5 neurons does not only depend on the strength of visual motion as described, but also luminance contrast. An early human fMRI study analysed the relationship between these two stimulus properties (Tootell et al., 1995), and also stated that the BOLD fMRI responses in hMT+ decrease at and near equiluminance (as determined for each participant individually). Their data indicated that neurons in MT/V5 have high sensitivity to contrast as well. And they ascribed these properties to the magnocellular stream, which exhibit a higher sensitivity to the contrast of visual image than parvocellular (dorsal) stream.

-Component and pattern selectivity

MT/V5 is characterized by neurons directionally selective to motion, but previous electrophysiological studies further identified that these neurons illustrated differential selectivity to moving stimuli. By using 'plaid' stimuli composed of two superimposed moving gratings with different orientations, it was found that a portion of cells in MT/V5 (approximately 20%) selectively responds to the unitary pattern motion of the stimulus (Rodman & Albright, 1989; Stoner & Albright, 1992), whereas others are responsive to the direction of the components of the plaid when their directions were different (Movshon et al., 1986; Stoner & Albright, 1992). Data collected from rhesus monkeys showed that the sensitivity to motions of the component gratings is strengthened when non-coherent motion is perceived. On the other hand, evidence from human MRI experiment also supports that the activity of pattern-motion cells in human MT/V5 is a reflection of motion coherence perception (Huk & Heeger, 2001).

-External effects on MT/V5 response

In addition to the diversities due to the selective properties of neurons in MT/V5 themselves (internal/local), there are some external factors that affect the MT/V5 response, including bottom-up and/or top-down neuronal input inherited from other areas and attentional

modulation. For instance, both macaque and human MT have been shown to receive prominent input from cells in the magnocellular stream. And for attentional modulation, substantial changes in activity have also been observed in MT/V5+ when subjects were instructed to attend to a specific moving direction (Corbetta et al., 1990; Treue & Maunsell, 1996; Beauchamp et al., 1997; O'Craven et al., 1997; Gandhi et al., 1999). In a series of seminal experiments it was also illustrated that the firing rate of individual MT/V5 neurons has a high correlation with the psychophysical performance of the monkey performing a task (Salzman et al., 1992; Britten et al., 1992).

1.1.2.4 The differential and associated properties of MT/V5 and V1

Besides MT/V5, other areas including V1 and V3 also show differential responses between stationary and moving dots stimuli. However, the properties of neurons in MT/V5 and other earlier visual cortex differ substantially and are thought to play very different roles in the analysis of motion signals. It has been posited that while V1 is an area for initial motion processing, responses of MT/V5 neurons are crucial for (and causally linked) to motion *perception*. I briefly summarize their differences in four particular aspects, which are relevant to this thesis:

Motion sensitivity

Both single-unit electrophysiological experiments and MRI experiments have looked at responses to moving and stationary stimuli in both areas MT/V5 and V1 in the macaque and rhesus monkeys (Albright, 1984; Snowden et al., 1992; Cao, 2001; Tolias et al., 2001). The results indicated that the spikes measured from neurons in MT/V5 has higher magnitude in responsive to moving stimuli than those in V1. But on the other hand, responses to stationary stimuli were of a similar level in the two areas (Albright, 1984). These results again suggested that MT/V5 plays a special role in motion perception and that neurons in this area are significantly more sensitive to motion.

Direction selectivity

Many neurons in area V1 also demonstrated direction selectivity. However, this property is linked to the orientation tuning of neurons. Specifically, cells in V1 respond to the moving edges of a particular orientation while travelling through the receptive field. Because of the relatively small size of V1 receptive fields, this leads to ambiguity of the motion direction, which is well known as the "aperture problem". On the other hand, neurons in MT/V5 are able to code the genuine global direction by integrating the orthogonal components of motion within an object (Movshon & Newsome, 1996; Andersen, 1997; Qian & Andersen, 1994).

Motion coherence

Neurons in early visual areas V1 to V3 did not respond differentially to coherent and incoherent motion stimuli whereas human MT/V5 did (McKeefry et al., 1997). Moreover, other evidence has shown that the average response evoked by motion dynamic noise is more enhanced in V1 than in MT/V5 (Braddick et al., 2001).

Motion opponency

As introduced, neurons in MT/V5 respond preferentially to a particular direction. However, perceptual studies discovered the existence of motion opponency in this region when two moving gratings were superimposed (Levinson & Sekuler, 1975; Mather & Moulden, 1983; Van Santen & Sperling, 1984; Stromeyer et al., 1984; Lubin, 1992; Qian et al, 1994; Zemany et al, 1998). Some electrophysiological studies also found that MT/V5 responses could be inhibited by populations of neurons sensitive to an opposite direction (Snowden et al., 1991; Bradley et al., 1995). By analogy, fMRI study revealed that the activity of a single moving grating was selectively suppressed in the presence of another grating that moved in the opposite direction; whereas the response of primary visual cortex is independent of the existence of other directions of movement (Snowden et al., 1991). Therefore, considering motion opponency in MT/V5 is important for understanding this area's role in motion perception in humans.

Connections between V1 and MT

Preliminary studies have confirmed that direction tuning is evident in layer 4B of V1 as well as other layers (Hawken et al., 1988; Ringach et al, 2002; Gur et al., 2005). This pronounced direction bias was assumed to be the source of the high degree of direction tuning of MT/V5 cells (Movshon & Newson, 1996), which receives direct input from those cells. Additionally, both V1 and MT/V5 showed velocity selectivity yet the range of velocities driving cells in MT/V5 was higher than for V1. It has therefore been proposed that the response of a particular cell in MT/V5 receives the summed afferent inputs from V1, reflecting the increased range of selectivity.

1.2 Visual working memory

Visual working memory (VWM, visual WM) is a fundamental cognitive process that maintains perceptual information in an active state for the purpose of decision-making and action. The concept was developed from short-term memory (STM), which is considered to be a system able to maintain information for ~15 to 30 seconds before its decay and disappearance (Brelsfor et al., 1968). Though similar to STM, the idea of *visual* WM emphasizes a processing-orientated activity at the interface of perception and behavioural manipulation for the completion of a complex task. The initial reports of WM were dominated by memory experiments with visual objects, which could differ in elementary visual features including shape, colour, size and length. Based on the results from these experiments, a multi-component model of WM was postulated and later revised by Baddeley and Hitch (1974). This model consists of a central executive system with limited capacity, two subsidiary systems including a phonological loop and visuospatial sketchpad, and a fourth subsystem, termed the episodic buffer (see Figure 1.13). Since the introduction of this model, a great number of studies, including the study of visual components, have been conducted to further explore the mechanism of WM. One of the most common paradigms used in those

experiments is the delayed discrimination task with a variety of retention intervals between the two target stimuli. This paradigm is still extensively employed.

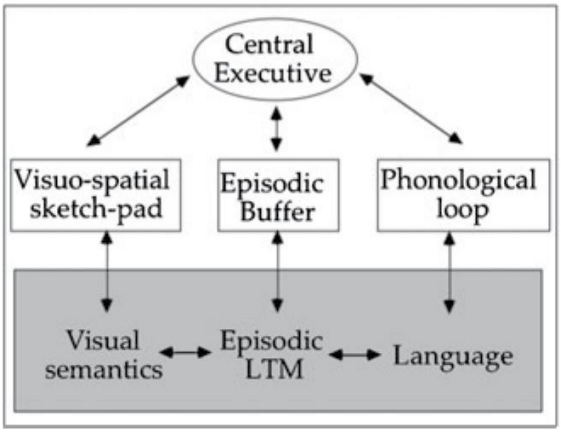

Figure 1.13: A model of working memory. Working memory consists of a central executive, which controls and co-ordinates the operation of two subsystems: the phonological loop and the visuo-spatial sketchpad. The phonological loop is mainly responsible for memory of spoken and written material, whereas visuo-spatial sketch pad stores and processes information in a visual or spatial form. The episodic buffer acts as a 'backup' store which communicates with both long term memory and the components of working memory (Adapted from Baddeley, 2000).

Visual WM can be distinguished from so-called *iconic* memory (Sperling, 1960). It was found that the iconic memory decays substantially after 1 second, whereas information kept in WM can last for at least 15 seconds or until interference from the same spatial location is introduced (Phillips, 1974). Other differences from iconic memory are that WM is known to have a limited capacity and is dependent on stimulus complexity. It is thought that WM is able to hold only three or four objects in memory efficiently (Baddeley, 2003). Additional evidence of the storage capacity of WM comes from the phenomenon of change blindness. Observers often fail to detect the change of one element in images that are shown in sequence and in alteration with brief blank displays, indicating that only incomplete information is kept between repeated presentations of images. On the other hand, visual WM is also distinct from visual long-term memory (LTM) in that it does not have comparable capacity and retention stability as information stored in long-term memory (Phillips and Christie, 1977a). In the work presented in this thesis we used mostly experimental stimuli and designs, which were

within the temporal range of WM to minimize confounding interactions of LTM and iconic memory.

Another array of experiments concerning the mechanism of WM aims at accessing the fidelity of maintaining detailed low-level visual features (Magnussen, 2009; Magnussen, 2000). Rather than memorizing the integrated representation of several basic visual attributes in objects, subjects were asked to concentrate on one basic dimension of the stimulus, hold information about it in memory for a period of time, and then discriminate the mnemonic representation of the first stimulus with an incoming stimulus. Observers typically need to discriminate which stimulus has a higher or lower value along the specific stimulus dimension. This paradigm is also referred to as the 'match-to-sample task'. The difference between the sample and match is manipulated for the attribute in question, such as spatial frequency, orientation, contrast and so forth. From the perspective of psychophysics, researchers can evaluate the fidelity of the feature representation by measuring the discrimination threshold as a function of the manipulated difference. Then, the constancy of this representation can be examined by lengthening the durations between the sample and test stimuli. The discrimination thresholds should increase if the memory decays in the temporal domain.

Evidence from neurophysiology and neuroimaging (both in animals and humans) indicates that stimulus-specific sustained activity during the delay intervals is a potential neural correlate of the on-going WM. Previous studies have shown that some low-level attributes can be maintained without much loss of information over time (i.e. Magnussen, Greenlee & Thomas, 1996; Vogels & Orban, 1986; Harvey et al., 1986; Fahle & Harris, 1992; Bisley & Pasternak, 2000). But where in the brain is the content of visual information stored? Researchers have provided potential answers to this question with different neuroimaging methods. The results from these studies can be divided into two groups. One camp proposed the view that visual content is retained in high-order cortex during short-term memory but not early visual areas, whereas another has provided evidence that visual WM and visual

perception for low-level features recruit the same neural circuits. According to the latter hypothesis, early visual areas, which are traditionally thought to just encode the stimulus, are also responsible for retaining the information in memory. Despite the large number of investigations in this field, the underlying neural mechanism of VWM is still under debate.

1.2.1 Neuronal correlates of high-level working memory

So far, a relatively clearer picture has been established for the part played by the higher-order cortical areas in the process of VWM. For example, studies using various methods have supported the idea that the prefrontal cortex (PFC) is an indispensable region for WM despite some disagreement about the specific roles of its subdivisions. Early lesion studies revealed intense deficits of short-term memory after selective ablation of this region (Jacobsen 1936; Milner 1963; Goldman-Rakic 1987). Since then, subsequent experiments have paid special attention to this area. A substantial number of neurophysiological experiments in animals showed that neurons in PFC continued to discharge when monkeys were maintaining the information about a stimulus in a delayed match-to-sample task without stimulation from sensory input (Fuster & Alexander 1971; Kubota & Niki 1971; Funahashi et al., 1989). It was also found that some cells in PFC exhibited persistent activity even when distractors were presented (Fuster, 2008). PFC lesions in monkeys, however, led to a loss of tolerance to external interference, as indicated by the impairment of WM performance (Malmo, 1942). Moreover, the strength of activity in the persistently activated areas showed a positive correlation with the behavioural performance in animal studies, indicating, for example, that the fidelity of remembered spatial locations is reflected in the delay-interval activity (Curtis & D'Esposito, 2004).

These animal results have been supported by functional MRI and PET studies in humans. They uniformly found maintained elevation of signals in PFC during the delay period (for review, see Curtis & D'Esposito, 2003). Similar to the lesion results from animals, human patients with lesions, including PFC, were also reported to have disruption of WM (Chao & Knight, 1995). One study even showed that the magnitude of the BOLD signal reliably

predicted the task performance on a trial-by-trial basis in humans (Constantinidis et al., 2001). Furthermore, using PET, investigators tracked the change of rCBF in PFC and found that WM for objects ('what') mainly activates the inferior prefrontal cortex, whereas the superior prefrontal cortices are highly active when spatial locations ('where') are required to be remembered. Based on these similarities to evidence from monkeys, it is assumed that human WM is also associated with the activations of two anatomically distinct and functionally specialized pathways, including the occipitotemporal pathway or 'ventral stream', and the occipitoparietal pathway or 'dorsal stream' (Figure 1.14). This assumption has been further corroborated by the findings of sustained response outside PFC (Haxby et al., 2000; Curtis & D'Esposito, 2003). Taking advantage of the wide spatial coverage of fMRI, Pessoa et al., (2002) searched the entire brain for areas contributing to WM and established a network of regions involved. Besides dorsolateral prefrontal cortex (DLPFC), they localized frontal eye field (FEF), superior parietal cortex (SPL), intraparietal sulcus (IPS) and anterior part of supplementary motor area (Pre-SMA). Other reports agreed that temporal cortex, parietal cortex, and premotor cortex are also actively engaged in maintaining information in WM depending on the type of stimulus (D'Esposito et al., 1998; Jonides et al., 1998; Rowe et al., 2000).

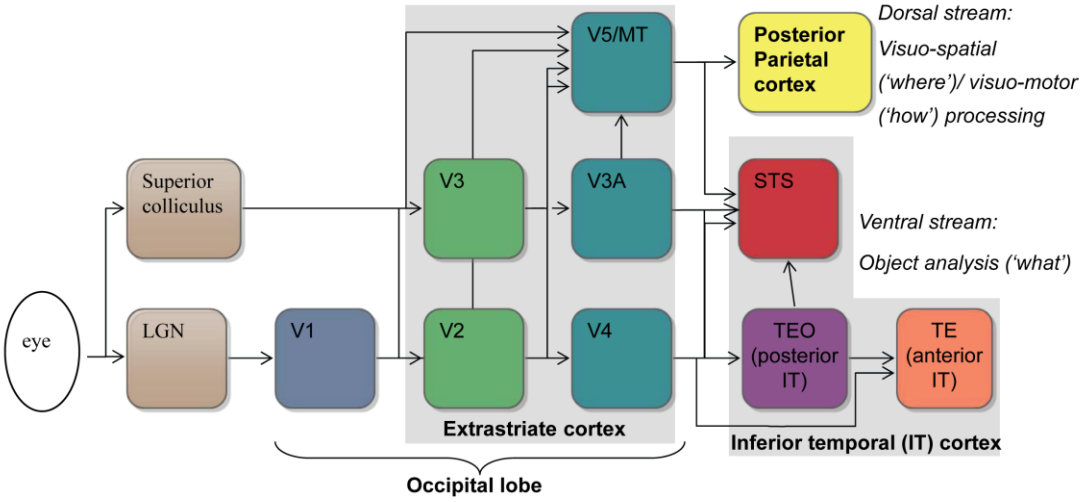

Figure 1.14: Diagram summarizing the current view of the pathways of dorsal and ventral streams. It describes two information processing streams originating in the occipital

cortex, *dorsal* (which goes to parietal cortex) and *ventral* (which goes to temporal cortex), which exhibit relative specialization in object recognition (*what*) and spatial vision (*where*), respectively. Physiological studies of cell properties also support the functional distinction between ventral and dorsal pathways. Neurons within the ventral stream (in distinct modules within V1 and V2, area V4, and inferior temporal areas TEO and TE) respond selectively to visual features relevant for object identification, such as colour, shape and texture. Neurons within the dorsal stream (in other modules within with V1 and V2, areas V3, V3A, middle temporal area MT, medial superior temporal area MST, and additional areas in inferior parietal cortex) instead respond selectively to spatial aspects of stimuli, such as the direction and speed of stimulus motion (Goodale & Milner, 1992).

As briefly stated before, one emerging view proposes that VWM recruits the visual perceptual areas to maintain the representation of memorized items (Awh et al., 1999; Super et al., 2001). For instance, a subregion of the inferior temporal (IT) cortex known as the fusiform face area (FFA) not only demonstrated transient activity during perceptual processing (Kanwisher et al., 1997; Andrews et al., 2002), but also showed sustained face-selective response to stimuli during a memory task (Druzgal & D'Esposito, 2003). Paralleling this result, another study reported that the parahippocampal place area (PPA), which is defined by its specific response to images of places, is also highly involved in the retention process when buildings and houses were needed for memory (Ranganath et al., 2004). Among the multiple areas in the cortex that contribute to the process of WM, IT is regarded as the final stage of the pathways. The prevailing explanation for the observed activity in this area during the delay interval was that the top-down signal from PFC controls the gain of its activity (Knight et al., 1999; Ranganath & D'Esposito, 2005), as well as supresses the sensory processing of the distractors in lower-order regions (Jensen et al., 2002; Klimesch et al., 1999; Worden et al., 2000). However, recently evidence to the contrary has been growing, calling for re-evaluation of this PFC-dependence of activity in IT (Warden & Miller, 2007; Kusunoki et al., 2009). Several studies alternatively interpret the role of PFC as attentional control or selection instead of supporting the core of WM. Along the same lines, the selective neuronal activity in sensory visual areas during the delay interval also point to the idea that these regions may take a more important and active part than previously realized. The work in this thesis placed emphasis on

studying the role of sensory visual areas in the process of WM, and the following section will outline a general literature review. Additional details will be introduced in each chapter.

1.2.2 Neuronal correlates of low-level working memory

In contrast to the function of higher cortical areas in the brain, the role of early visual cortex in WM is much more elusive. As introduced, by using the typical delayed-discrimination task in which subjects had to retain a representation of a past stimulus, many studies failed to observe the neuronal contribution from the early visual areas. This suggested that these areas are only involved in visual perception and related processing. About a decade ago, a single-unit recording experiment on spatial WM with monkeys found that a perceptual signal was maintained strongly in the absence of a stimulus when memory was required to perform the task (Super et al., 2001). The authors excluded the possibility of sustained activity induced by visual persistence. Moreover, they showed that task irrelevant interference could disrupt WM performance. Combined together, the study provided initial evidence that primary visual cortex is not only a crucial component for perception but also a potential correlate of temporary storage of visual information.

Results from such experiments have led to the 'sensory recruitment model', which hypothesizes that visual areas are dual-functional and relevant to both perceptual coding and mnemonic representation. For instance, some experiments have shown that the basic dimensions of visual stimuli for memory are represented separately as they are coded in sensory areas. For instance, memory for spatial frequency is not influenced by changes along the memory-irrelevant dimension (e.g. orientation) (Bradley & Skottun, 1984; Magnussen et al., 1998). In addition, in a dual task when observers were asked to simultaneously judge two *independent* features, their performance remained relatively unaffected (Greenlee & Thomas, 1993). However, impairment occurred when they were asked to remember two elements along one single dimension (Magnussen & Greenlee, 1997).

Another approach of exploring the neuronal mechanisms of WM is to use a memory-masking paradigm. If delay activity is selectively retained in sensory visual cortex, then a masker stimulus within the same visual dimension should interfere with the mnemonic representation of the remembered stimulus. For example, by manipulating the spatial frequency of mask gratings, Magnussen et al. (1991) found that the mask only interferes when its feature is different from the target stimuli, and its effect reached maximum when the disparity was ±1 octave. Moreover, studies using this masking paradigm also supported the hypothesis of 'sensory recruitment model'. They showed that varying the mask along the task-irrelevant dimensions did not affect the discrimination performance, indicating that separate and specialized channels are utilized for memorizing low-level visual features. Based on this, we can further infer that memory and perception share similar neuronal correlates in the sensory visual cortex. Similar phenomena were found in delayed discrimination tasks of other basic visual features.

Recently, more fMRI experiments have been used to investigate the mechanism of WM, given the advantages of this neuroimaging method for image acquisition with good spatial resolution and relatively good temporal resolution. Several lines of evidence found maintained activation during short delay durations between two stimulus presentations, even though no stimulus was present (Cornette et al., 2002; Greenlee et al., 2000). For instance, one study suggested that neurons in the middle temporal visual area (MT) might also be involved in the short-term storage of visual motion information (Born & Bradley 2005). Additionally, using event-related fMRI, investigators assessed the pattern of neuronal activation evoked by gratings of the same or the orthogonal orientation when subjects performed a discrimination task for spatial frequency (Baumann et al., 2008). Their result revealed activation in both primary visual cortex and extrastriate visual cortex. They also found significant differences in BOLD signal in these sensory areas when the stimulus changed along a task-irrelevant dimension (same versus orthogonal orientation) but not in prefrontal and intraparietal cortex.

Based on this contrasting result, they suggested that retention of basic stimulus elements is maintained by the system of low-level WM in the early visual cortex.

However, some other fMRI studies on WM failed to detect the overall enhancement of delayed activity in early visual regions (e.g. Harrison & Tong, 2009). Among these reports, Offen et al (2009) tracked the BOLD signal change in primary visual cortex during a WM and attention-demanding task, respectively. Unlike the delay-period activity recorded in temporal or prefrontal cortex, they found a strong, global suppression of activity in primary visual cortex during the WM task instead. They argued that the early visual cortex did not engage in the process of WM but rather received a top-down attentional modulation. However, they objectively pointed out the limitation of using sustained activity as the indication of functional involvement. Analogously, a recent study also challenged this traditional assumption, holding that an overall increase of delayed activity does not necessarily reflect stimulus-specific memory (Sligte, et al., 2013). The persistence might merely subserve the processing of other stimulus dimensions rather than that of the relevant feature. Alternatively, they emphasized the necessity of showing content-specific activity in relation to visual WM.

In the light of the open questions reviewed above, we developed both psychological and fMRI experiments using a new combination of elements outlined above in order to understand more about the mechanism of visual working memory. Further details about this thesis are outlined in chapter 3.

1.3 Principles underlying Magnetic Resonance Imaging (MRI)

Since Purcell (Purcell & Pound, 1946) and Bloch (Bloch & Packard, 1946) first discovered the magnetic properties of atomic nuclei, it has been well known that when the nuclei of certain elements in a static magnetic field receive an oscillating (RF) pulse, they are knocked out of equilibrium and relax back into alignment *precessing* at a frequency that depends on the type of nucleus, the strength of external magnetic field and the chemical environment.

Following the development of spectroscopy techniques in the domain of *chemistry* and the discovery of how to turn information from magnetic resonance measurements into *images*, MRI has evolved into a widespread imaging tool for collection of both anatomical and functional information (Wehrli & Atlas, 1991; D'Esposito et al., 1999a).

The improvements in magnetic field gradients, the invention of echo-planar imaging (Mansfield, 1977) and related technology has allowed further improvements in fast acquisition techniques and the use of different contrast mechanisms (Lakrimi et al., 2011; Burton & Small, 1999; Lebihan, 1992).

In particular, the introduction of blood oxygenation level-dependant (BOLD) imaging has opened a novel and non-invasive approach for modern neuroscience (Thulborn et al., 1982; Casey & Davidson, 2002). In this chapter, the basic theoretical foundations of nuclear magnetic resonance (NMR) that are relevant to the work presented in this thesis will first be reviewed. Then the principle of BOLD imaging will be addressed considering its special role in functional imaging.

1.3.1 Nuclear Magnetic Resonance

1.3.1.1 Spin, Precession

Hydrogen atoms consist of a proton and an electron that occupies an orbital. Each atom has associated with it a property called 'spin', which depends on the spins of its constituent particles and is equal to the sum of the spins of its unpaired electrons. For ^{1}H nuclei the spin is ½ (Shannon & Roemer, 1990). The 'classical' picture of this is that these particles rotate about their central axis and produce a net nuclear angular momentum because their nuclei have an uneven number of protons with a magnetic moment. When spinning particles are charged and are placed in an external static magnetic field they create a diminutive magnetic field. Similar to small bar magnets, they align to either the same or opposite directions of the external magnetic field. But unlike magnets, because of the existence of spinning and angular

momentum, charged nuclei, when knocked out alignment, return back to equilibrium/ alignment in a gyroscopic motion, which is referred to as precession (Figure 1.15).

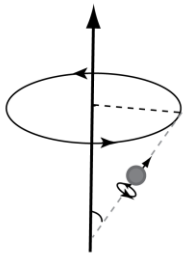

Figure 1.15: Single spin. Once a magnetic field is applied, the magnetic moment of a spin precesses around the magnetic field axis similar to gyroscope at the Larmor frequency, keeping a constant angle between the spin magnetic moment and the field.

The speed of precession depends on the magnetic field strength as well as the *gyromagnetic ratio*, representing an intrinsic characteristic of magnetically active nuclei (which is the ratio of magnetic moment and angular momentum). This is a constant for given nuclei, for ^{1}H $\gamma \sim$ 42.6 MHz/Tesla (Hashemi et al., 2003). Their frequency of precession in the field can be calculated using the Larmor Equation:

$$\omega_0 = B_0 \times \gamma, \qquad \text{(Eq. 2)}$$

where B_0 is the strength of the external magnetic field, γ is the gyromagnetic ratio, and ω_0, as the result of this equation, describes the speed of precession (Van Geuns et al., 1999).

The direction of precession can be either parallel or anti-parallel with the direction of the external magnetic field. Protons in the anti-parallel direction are in low-energy state and are often labelled as 'spin up', while 'spin down' protons are in the opposite direction with high energy. 'Spin up' (low energy) only slightly outnumber 'spin down' (high energy), inducing a net magnetisation **M**, which has the same direction as the external magnetic field (Figure 1.16). **M** has no transverse component because even though protons precess about the vertical direction like a gyroscope, they are out of phase and thus the contributions to transverse magnetization from different protons cancel each other out. When the strength of B_0 becomes

stronger, the net magnetisation turns larger because the number of 'spin up' protons in the low energy state increases. An illustration of this is shown in Figure 1.17. Any transition between these two states requires an energy change, which can be induced by absorption or emission of electromagnetic radiation of frequency (RF) (Caldemeyer & Buckwalter, 1999).

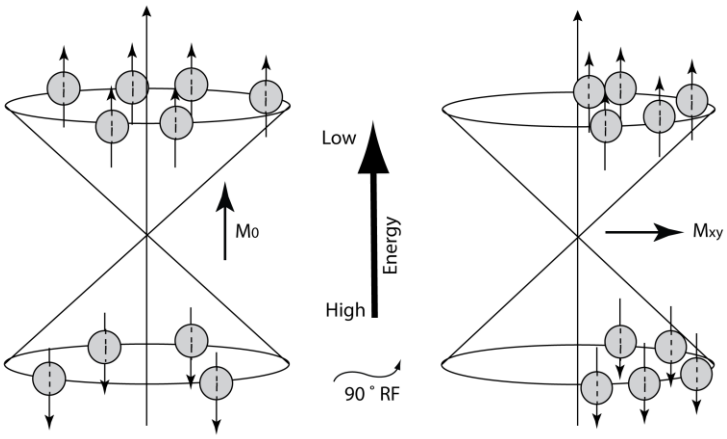

Figure 1.16: When placed in a magnetic field B_0, protons fall into either the lower energy state where they are parallel to B_0, or the higher energy state that corresponds to a counter-aligned to the magnetic field. The protons in the lower energy state in an entire sample are slightly outnumbered by the high-energy state proton spins (Left). The application of RF pulse can equalize the number of protons in both energy states (Right).

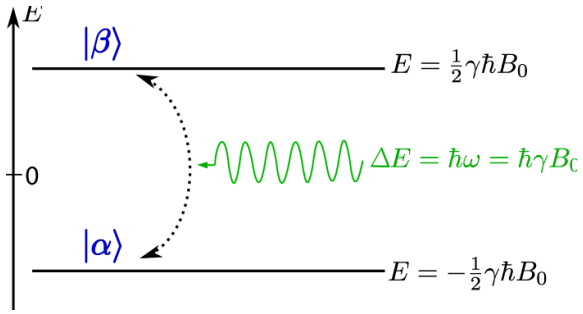

Figure 1.17: Energy level diagram of the hydrogen nucleus (spin 1/2) in a magnetic Field B_0. Transitions can be induced between spin states by irradiating with photons of energy E equal to the energy level splitting (Replicated from Sanchez-Panchuelo, 2009).

1.3.1.2 Radio frequency

When an appropriate radiofrequency wave or pulse is applied, it generates an oscillating electromagnetic field (RF field, B_1), perpendicular to the main external magnetic field (B_0). If the RF pulse is at the same Larmor frequency as the tissue it is applied to, protons inside are

then flipped to this new magnetic field (B_1), and the spins begin to precess in phase. As the RF pulse continues, some protons absorb energy from the low energy state and are promoted into the higher energy state, causing the net magnetisation vector to 'tip' from the vertical Z-axis to the transverse X-Y plane (Figure 1.18 **B**), when considered in a frame of reference rotating at the Larmor frequency. In the laboratory frame of reference, this appears as a complex spiral motion (Figure 1.18 **A**). By dividing the vector **M** into two components (**Mxy** as a transverse magnetization vector and **Mz** a longitudinal magnetization vector), we can analyse the change of **M** as two simultaneous yet independent processes. After a pulse is applied, protons absorb energy and commence nutational motion in phase, and as a result, net magnetisation on the Z-axis reduces, while **Mxy** increases. This process continues till **M** completes flipping to a certain angle. If **M** flips 90°, the applied RF is referred to as a 90° pulse (Figure 1.19), which forces protons into the transverse plane with a null **Mz**. The flip angle depends on the amplitude (strength of B_1) and duration of the RF pulse. A 180° pulse can be produced by using twice the strength or twice the duration compared to a 90° pulse. It makes **Mz** inverted to the opposite direction along the Z-axis without inducing phase coherence in the X-Y plane, constructing a net magnetization of –**M** (Foltz & Jaffray, 2012).

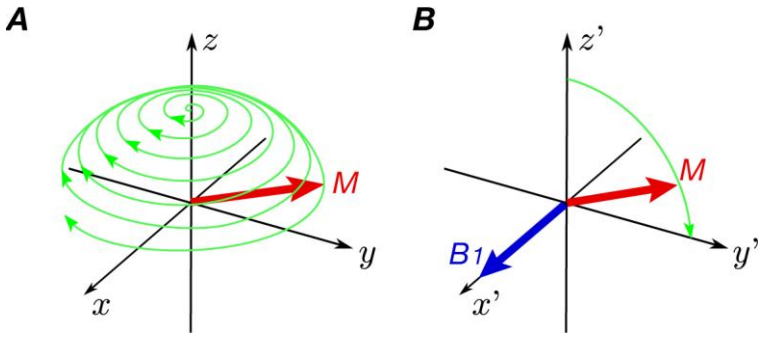

Figure 1.18: The evolution of the bulk magnetisation vector M under the application of an RF pulse at the resonant frequency in (A) the laboratory and (B) the rotating frame.

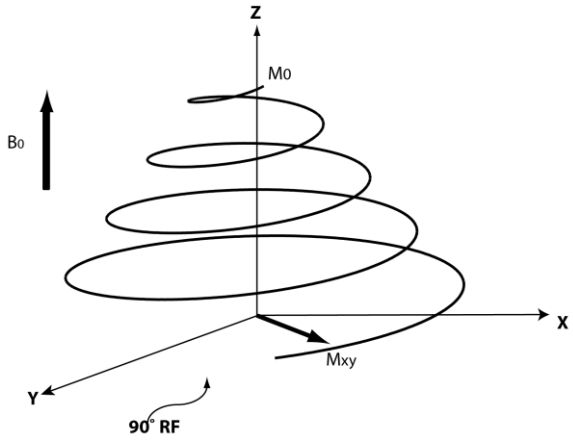

Figure 1.19: A RF pulse that makes the spiral motion of the magnetization vector flip into the X-Y plane is called a 90° RF pulse.

1.3.1.3 Relaxation and MR signal detection

The application of RF disturbs the original energy equilibrium by changing the number of spins in two energy states. When RF discontinues, the spin system subsequently initiates a process of returning to the original state with a net magnetisation at equilibrium, and this process is termed *relaxation*. By decomposing **M** into **Mz** and **Mxy**, relaxation can be explained by the following: the **Mz** vector recovers to its original magnitude (M_0) along the longitudinal axis; at the same time, the transverse magnetization **Mxy** decays to zero at a much faster rate (Figure 1.20). The corresponding relaxation time for these two components was measured as longitudinal relaxation time (or T1 relaxation time), and transverse relaxation (or T2 relaxation time). In terms of energy change, these processes can be considered as the following: during the *longitudinal* relaxation, spin-lattice relaxation occurs when some of the spins restore to the low energy state from higher energy state by exchanging energy with the surrounding lattice. *Transverse* relaxation represents an inherent energy exchange among protons themselves, and thus is often also called spin-spin relaxation (Gibby, 2005).

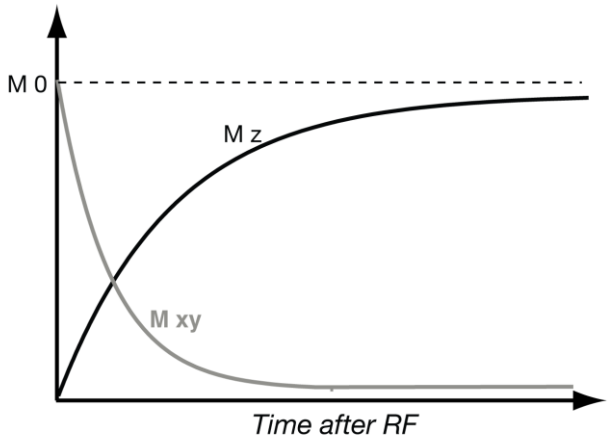

Figure 1.20: The rate of decay of transverse magnetization (T2) in the horizontal X-Y plane is much more rapid than the recovery of longitudinal magnetization to Z-axis (T1).

According to Faraday's Law of Induction, if a magnetic field is moved through a conductor, a current will be produced in the conductor. In the case of MR imaging, after the termination of the RF pulse, all spins are in phase, lined up and precess at the same frequency ω_0 in the same direction, which means that the associated magnetic fields created by each spin are also precessing in phase (Tanaka, 2000). When they are of the same direction as a receiver coil, a very large current that is oriented perpendicular to B_0 in the transverse plane, which we call the signal, can be induced and detected (Figure 1.21 A). The frequency of the signal is equivalent to the frequency ω_0. Figure 1.21 B illustrates the relationship between transverse magnetization and the received signal at different time points. The coil receiver (in the illustration of A) can only detect the magnetization along the Y-axis in the X-Y plane. Therefore, at time points t1 and t3 there is no signal, whereas at t0 and t2 the signal reaches maximum. A sinusoidal curve with the frequency of ω_0 correctly describes such fluctuation of the received signal over time.

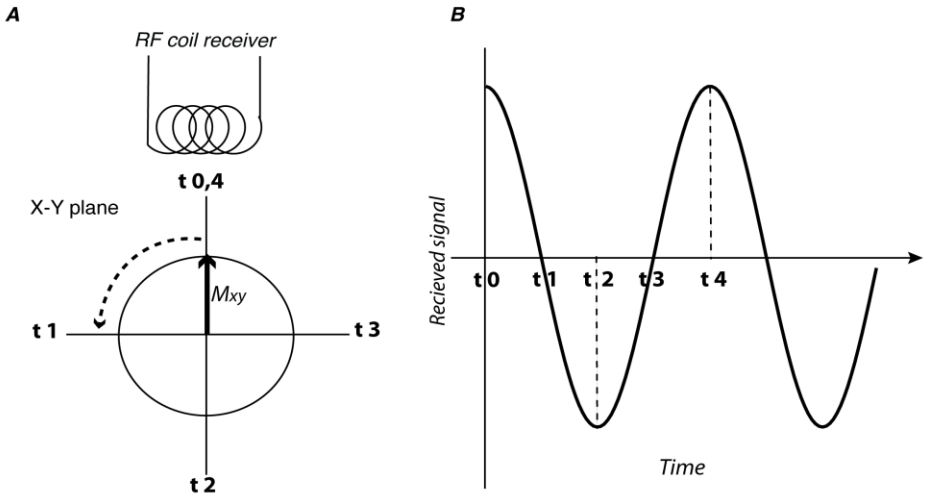

Figure 1.21: **A**, Induction and detection of fMRI signal. **B**, The relationship between transverse magnetization and the received signal at different points in the temporal domain (adapted from Hashemi et al., 2003).

1.3.1.4 Free induction decay

The signal detection delineated above is an ideal situation. In reality, however, the coherence of spinning remains only for a short while, and then precession turns into a de-phasing state (McGowan, 2008; Morin & Gray, 1990). As a result, the amplitude of the signal attenuates rapidly under an exponential envelope. This is referred to as the Free Induction Decay or FID (Figure 1.22).

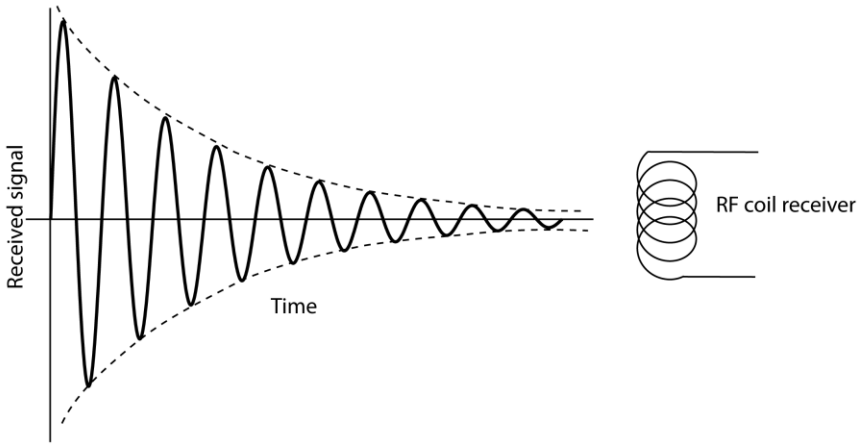

Figure 1.22: FID is referred as the decaying sinusoidal waveform of the received signal.

Loss of signal is not only attributed to the spin-spin interaction among protons as outlined above, but also the inhomogeneity of the external magnetic field. Since B_0 is not homogeneous in real systems, spins in different spatial locations have slightly different precession frequencies, which means that some protons that precess faster tend to offset those that precess slower, and this subsequently accelerates de-phasing. Therefore, the actual decay time, which is known as T_2*, can be represented by two factors in the following equation: T_2 (pure spin-spin interaction) and T2′ (magnetic field inhomogeneity).

$$\frac{1}{T_2^*} = \frac{1}{T_2} + \frac{1}{T_2'} \qquad \text{(Eq. 3)}$$

1.3.2 Magnetic Resonance Images – Contrast and Weighting

1.3.2.1 Tissue contrast (T1 and T2 weighting)

T1 and T2 relaxation times are important parameters for MR imaging (Stanisz et al., 2005). Since different tissues have varying relaxation times, it will take different time for the corresponding **M** vectors to restore to the initial amplitude. Based on these differences, we can distinguish one tissue from others. Figure 1.24 and Figure 1.25 illustrate tissues with different T1 and T2 relaxation time. For instance, according to Table 1.1, three main tissues in the human brain have their distinctive relaxation times (Ethofer et al., 2003; Gelman et al., 1999; Stanisz et al., 2005). White matter's (WM) **Mz** recovers more rapidly than Grey Matter (GM) and CSF, so if we measure the signal earlier than 1300ms after the cessation of the RF pulse (short TR), both of the substantial tissues will be suppressed and become dark in the MR images, in comparison to the relative bright image intensities show by WM (Gelman et al., 1999; Ethofer et al., 2003). Figure 1.26 shows images obtained with short TR based on the differential T1 relaxation time of brain tissues.

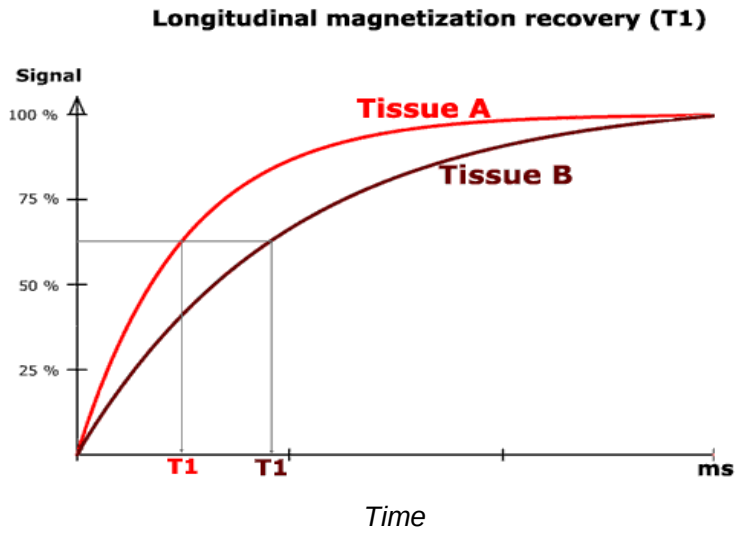

Figure 1.24: The tissues A and B with different T1s.

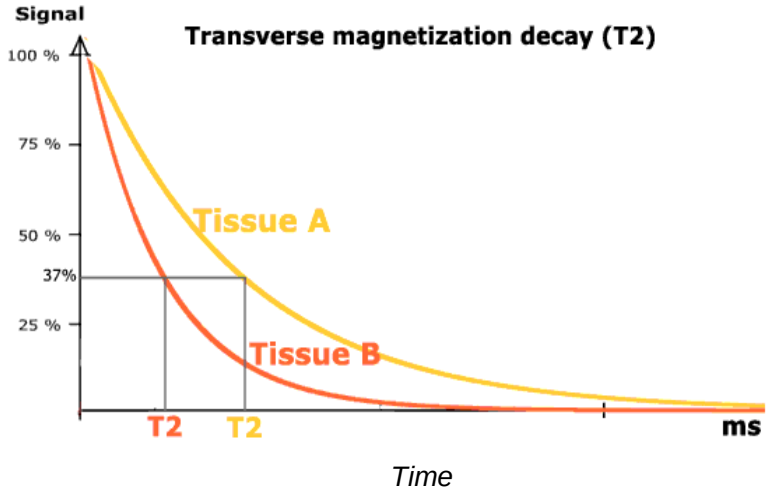

Figure 1.25: The tissues A and B with different T2s.

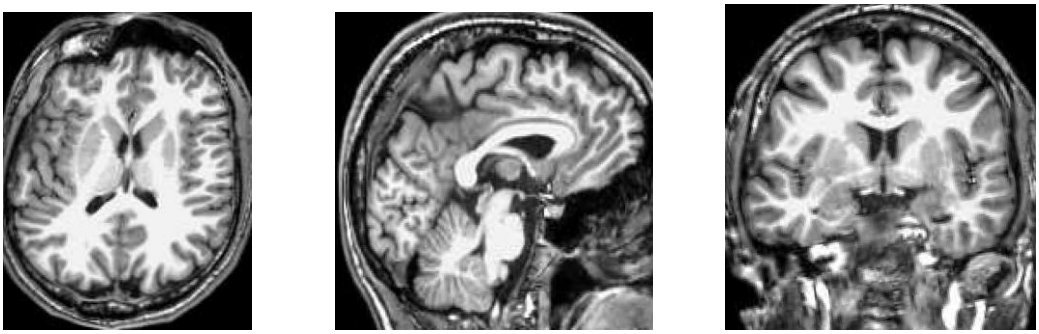

Figure 1.26: T1-weighted imaging obtained from axial, sagittal and coronal direction (from left to right). WM shows higher image intensity than GM and CSF (darkest signal illustrated in ventricles).

Table 1.1: T1 and T2 values at 3T magnetic field MRI

Tissue Type	**T1 value (ms)**	**T2 value (ms)**
White matter (WM)	~1110	~56
Grey matter (GM)	~1470	~71
Cerebrospinal fluid (CSF)	~3120	~160

Images that emphasize the contrast in accordance with T2 values of different tissues and along with **Mxy** are denoted as T2-weighted images. This is in contrast with T1-weighted image, which enhances the discrepancy of **Mz** by taking full advantage of the difference in T1 relaxation time of different tissues.

1.3.2.2 TE and TR

The existence of inhomogeneity of magnetic field seems to preclude the possibility of getting pure T2-weighted images, yet there are methods to compensate such inhomogeneity. A sequence of pulses can be applied to achieve this purpose. Take the very common 'Spin Echo' sequence for example. After a 90° RF pulse is applied, the vertical **M** vector tipped into the transverse plane. As it stops, **Mxy** gradually reduces due to de-phasing. But if a 180° RF pulse is applied to reverse all the directions of de-phasing spins after a period of time (e.g. *t*), the incoherent spins will then re-phase to **Mxy** within another *t* period to produce a repeated strong signal echo (Figure 1.23). The time **Mxy** needs to proceed back is measured as the **Time to echo (TE)**, which is the duration between the application of the 90° and 180° RF pulse. However, the regained **Mxy** does not have the same initial amplitude, hence, it is necessary to start a new sequence beginning from another 90° pulse. And the duration between these two consecutive RF pulses is indicated as the **repetition time (TR)**. Both TE and TR are crucial time variables since they determine which tissues will be highlighted in differentially weighted images.

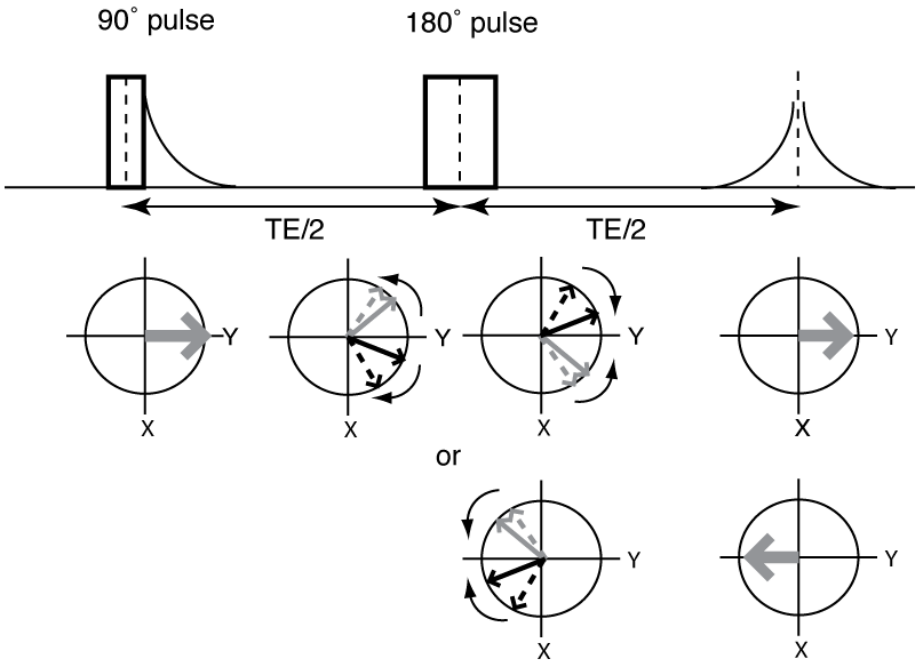

Figure 1.23: Scheme of a spin echo sequence. After a 90° RF pulse, an FID is formed. The application of 180° pulses can refocus the transverse magnetization vector to generate echoes.

1.3.2.3 Paramagnetism and Diamagnetism

Diamagnetic and paramagnetic substances induce a weak magnetic field (either parallel or anti-parallel) when they are placed in an external magnetic field (Rodriguez, 2004). For the tissue with diamagnetic substances, such as air in the sinuses and bone tissue, they possess no unpaired orbital electrons, thus the effective magnetic field is reduced because the field they produce is opposite to the main field. On the contrary, paramagnetic substances have unpaired orbital electrons, and consequently their induced magnetic field boosts the effective magnetic field, leading to the increased signal on T1-weighted images. Oxyhemoglobin and Deoxyhaemoglobin, two variants of hemoglobin, are two representatives of diamagnetic and paramagnetic substances, respectively.

People have been using their properties to introduce contrast between different tissues, or observe changes between different cognitive states in a given region of interest for clinical and research purposes. The mechanisms underlying functional MRI, and specifically the

imaging of blood-oxygen-level-dependent (BOLD) changes in the brain will be illustrated in detail in the section on functional MRI.

1.3.3 Conclusion

To summarize, the concepts of precession, the induction and detection of MR signal, and the process of relaxation have been reviewed in this chapter. In general, an oscillating magnetic field at the Larmor frequency applied orthogonally to a static magnetic field, B_1, will trigger a bulk magnetisation that aligns to B_0 flipped into a certain plane. So when the operating oscillating field ceases, a signal is emitted and can be detected during the process of recovery to the original bulk magnetisation. Hydrogen with one proton is abundant in the human brain, thus possessing a significant net magnetic moment. Strong signals from hydrogen protons can thus be detected using MR imaging to ultimately explore the anatomy and function of the brain, and in the case of this thesis specifically the mechanism related to the processing of visual information.

Chapter 2: General Methods

Introduction

In this thesis, we performed experiments with a variety of psychophysical methods for both piloting and continued data sets of behavioural studies. The aim of piloting experiments was to establish behavioural thresholds to allow us to pick a reasonable range of parameters for follow-on experiments. We used *Yes-No* tasks, (spatial) two-alternative forced choice and (temporal) two-interval forced-choice experiments with different delay intervals (which we refer to as *delayed discrimination tasks*) to characterize the property of memory as a function of manipulations for different visual features, such as motion coherence, orientation and contrast. Here, I will briefly review the background and history of the psychophysical techniques and paradigms used in this thesis. Details on the choices of parameter and any changes from standard paradigms are highlighted in the Methods sections of the different experimental chapters.

2.1 Psychophysics

2.1.1 Signal Detection Theory

To analyze behavioural data from Yes-No experiments, we made use of the framework of *signal detection theory* (SDT), which has played an important role in the analysis of sensory processes (Coren et al., 1994). SDT provides a quantitative link between the strength of a sensory stimulus, a hypothesized internal decision variable, and the subject's choices. One of the fundamental assumptions of SDT is that there are always some uncertainties in the signals that allow us to make decisions (Green & Swets, 1966). The theory allows estimation of decision-related variables from perceptual reports, such as sensitivity, specificity and observer criterion. The basic principles including SDT and methods of psychophysics that are relevant to our work are outlined in the following sections.

The theory of signal detection (SDT) is a model used to estimate how people actually behave in detection tasks (Tanner et al., 1954). In the most common situation, subjects observe a stimulus and then make a decision about whether a particular "signal" is present or absent. There are thus, two categories: the observation is due to the noise alone (N) or a signal added to a noise background (S+N). Internally, the stimulus is assumed to be represented by a (scalar) quantity, or decision variable, that is low for noise and high for signal + noise. The noise is assumed to vary randomly and if it is very high, subjects are more likely to make an error by mistaking it as a signal (a so-called *false alarm*). Conversely, when the noise level is low subjects may consider the stimulus as containing only noise, even though there is a weak signal added to it (a *miss*).

I designed a detection task and collected data to illustrate the relationship between noise (N) and signal + noise (S+N). Observers were asked to perform a Yes-No task by making a judgment of the presence or absence of a coherent motion signal (similar to what is displayed in Figure 2.1) by giving a long series of trials at a fixed signal intensity.

Visual stimulus and task

In this experiment, subjects' task was to detect a signal – a short interval of coherent motion at a coherence level of 20% – in the presence of directional noise (random dot motion with 0% coherence). Figure 2.2 illustrates a scheme of this experiment. The stimuli were displayed on a CRT monitor with a resolution of 800 × 600 pixels and effective frame rate of 60 Hz. It contained moving "white" pixel dots (density, 2 dots/deg^2) within a circular aperture of radius 10° of visual angle. Each dot was 4 × 4 pixels in size and they moved on each frame at a velocity of 3°/s. The direction of moving dots was randomly set from 0-360° if there was a coherent movement. For any given new frame, noise dots changed direction while all signal dots (coherently moving dots) travelled in the same direction and were replotted along a straight trajectory with a spatial displacement of 0.05 deg. The probability for the presence or absence of coherent movement was approximately the same. There was a small fixation cross (size, 1°) at the centre of a "black" background (0.01 cd/m^2). Preceding each trial, the

fixation-cross changed to yellow to indicate the onset of each trial, allowing subjects to attend to an impending stimulus. And at the end of each trial when the colour of the fixation changed to cyan, subjects were asked to give a response as "yes, I saw a target- a coherent movement" (key press 1) or "no, I did not see a target- no coherent movement" (key press 2). Participants were told to make a judgment as quickly as possible, and then received feedback: the fixation-cross changed to green after correct trials, or to red after incorrect trials. During the intertribal interval (ITI), the fixation-cross remained white.

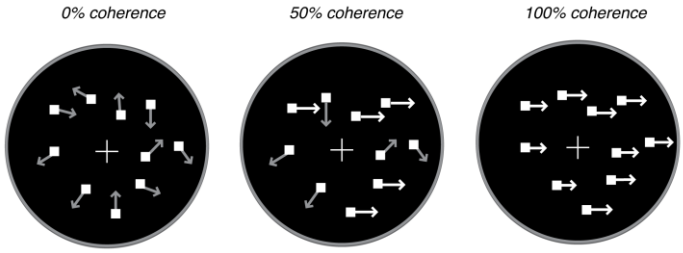

Figure 2.1: Different coherence levels of moving dots. In the actual experiment we used more white dots on black background (arrows indicating direction of motion are only present for illustration).

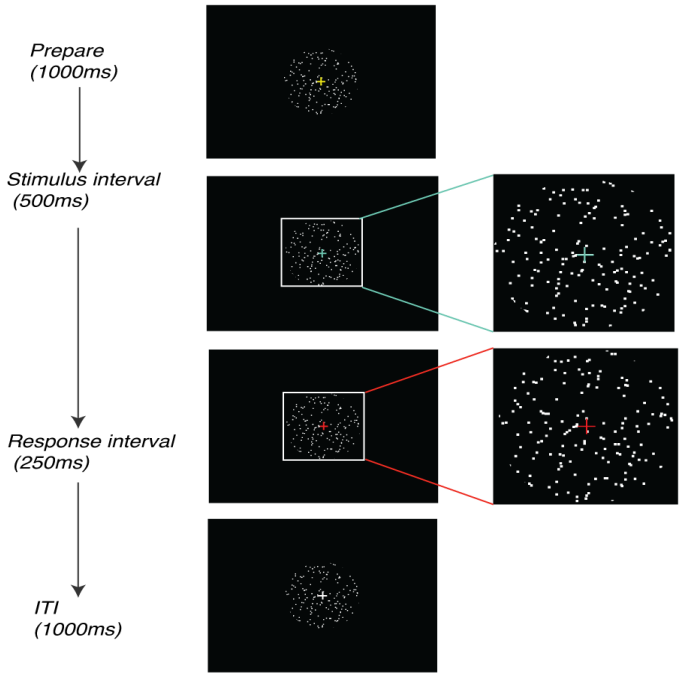

Figure 2.2: The paradigm of the simple Yes-No task for threshold detection with one trial. Subjects were instructed to fixate at a central cross, while dots with either a coherent motion or a random motion were displayed for 500 ms. Subjects need to judge whether there was a coherent movement by pressing a corresponding button.

The distribution of noise (N) and signal + noise (S+N)

Figure 2.3 shows the hypothesized distributions of the internal decision variable for S+N and N plotted with our data. In this figure, the S+N is always greater than noise alone. But when the strength of the signal decreases, there will be more overlap of these two distributions, making it more difficult to make a correct decision.

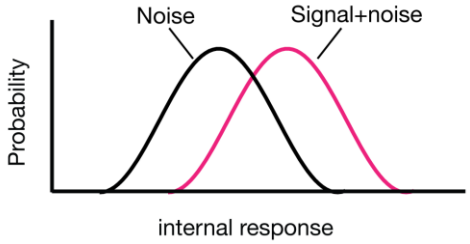

Figure 2.3. A probability of occurrence curves of noise (black curve) and signal + noise (pink curve).

Two types of noise that may corrupt a signal are external noise (which we can apply to a stimulus) and internal noise (that is present inside the observer). They prevent observers making the correct decision or limit the subject's performance. *External noise* refers to the fluctuations introduced by the external environment. One example of this is the changes in the temperature of a visual display, which may change the number of emitted photons from a fluorescent screen over time. If an observer is performing a luminance detection task at threshold, such changes in stimulus intensity may affect the behavioural responses (Schonhoff & Giordano, 2006). For random dot kinematograms (RDKs), the level of external noise can be controlled quite carefully by manipulating the amount of *coherence*. At 0% coherence (Figure 2.1, left), one end of the spectrum, there is no motion signal consistent with one particular direction of motion present. At 100% coherence (Figure 2.1, right), the other end of the spectrum, the external noise in the signal is minimal. *Internal noise* refers to fluctuations in the representation of the signal inside the observer, which can be due to cognitive states (e.g. attention) and other physiological factors (Lucas, 1967). Taking the luminance detection as an example, even if the stimuli were presented by the same experimental apparatus, the internal conditions are not identical on each trial because of slight changes in physiological

state. These fluctuations in the internal representation may lead to different perception and perceptual decisions. The task structure is simple, but in most of the situations there is always some amount of uncertainty due to the existence of noise, leading to four possible outcomes when subjects give their response (illustrated in Figure 2.4).

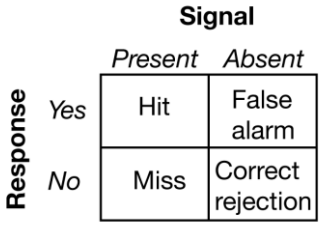

Figure 2.4: Hit (signal present and subject responds 'yes'), false alarm (signal absent but subject says 'yes'), miss (signal present and subject responds 'no'), and correction rejection (signal absent and subject says 'no').

In the basic signal detection model, the distribution of the internal decision variable is assumed to be *Gaussian* and to have the same variance for the S and S+N distribution (variance=1 for mathematical convenience). To calculate the observer's sensitivity and bias, the proportions of hits and false alarms can then be transformed into quantiles of the standard normal distribution (Z scores) (Kay 1998). The calculations for these quantiles are briefly outlined below.

The curve shown in Figure 2.5 represents a situation where the signal strength is sufficient to result in only a slight overlap of the N and S+N probability distributions. The solid vertical line corresponds to the location of the criterion (beta), which is used to make a decision. If the stimulus level is higher or at least equal to the level of the criterion, then the observers' response falls into the distribution of S+N and they respond 'yes / target present'. The proportion of the area under the curve to the right of the criterion gives the proportion of 'yes' decisions. Therefore, the hit rate and the false alarm rate can be determined by calculating the areas under the S+N and N distribution curves, respectively. But if the level of the internal variable is lower than that criterion, they choose N and respond 'no / signal absent'.

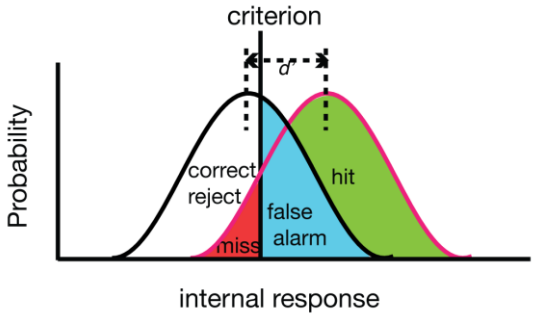

Figure 2.5: The hit rate is equal to the proportion of the area of the S+N distribution (shadow in green) that is above criterion (Vertical solid line). The false alarm rate is equal to the proportion of the area of the noise distribution (N) that is above criterion (cyan shadow), whereas the left of the criterion represents the miss (shadow in red) and correct rejection (white shadow). *d*', the distance between the peaks of two curves.

One commonly used method of considering the *behavioural* data from Yes-No tasks is the so-called Receiver Operating Characteristic (ROC), in which the proportion of *hits* is plotted against the proportion of *false alarms* (Wickens, 2002). Each point on an ROC curve is determined by the location of the observer's criterion on the X dimension. As the criterion is changed from high to low, the false alarm rate and the hit rate both increase, forming a ROC curve (Peterson et al., 1954). Specifically, if the point is near the bottom of the ROC curve where the slope value is large, the criterion is high; if the point is near the top of the curve where the slope is slight, the criterion is low. The exact value of beta is equal to the slope of the ROC curve at a particular point (A plot of a variety of ROC curves obtained by using the simple Yes-No task in the psychophysical experiment above, Figure 2.2).

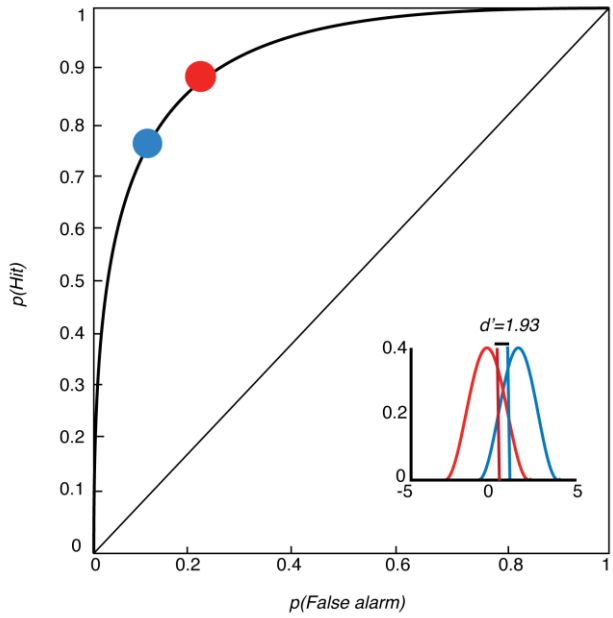

Figure 2.6: Relation between the ROC curve and the theoretical noise and signal + noise distributions. Variation in the criterion results in different points along the ROC curve. As the criterion is lowered, the predicted point on the ROC curve becomes higher. Red point (Hits= 0.89, False Alarm=0.25) corresponds to the red vertical line, which represents the lower criterion, compares to the blue point (Hits=0.75, False Alarm=0.11) and its corresponding higher criterion.

SDT also affords a method to measure the observer's *sensitivity* and *criterion* location. d' is a variable equal to the difference between the means of S+N and N distributions divided by the standard deviation of the N distribution (which is often taken to be 1) (see Figure 2.5). Because the location of the S+N distribution in relation to that of the N distribution is a function of stimulus intensity and properties of the sensory system, d' is a pure index of stimulus detectability that is not contaminated by the location of the observer's criterion. A family of d' is shown in Figure 2.7. This graph also gives information about the distributions of S+N and N. The curve through the red point that is closest to the diagonal red line in Figure 2.7 shows the condition for which there is little separation between the N and S+N distributions. In this case, the external signal may be too weak to have a measurable effect on the nervous system. It can be seen that as the separation between N and S+N distributions

increases, the predicted ROC curve rises more rapidly and departs from the positive diagonal of the graph by a greater amount.

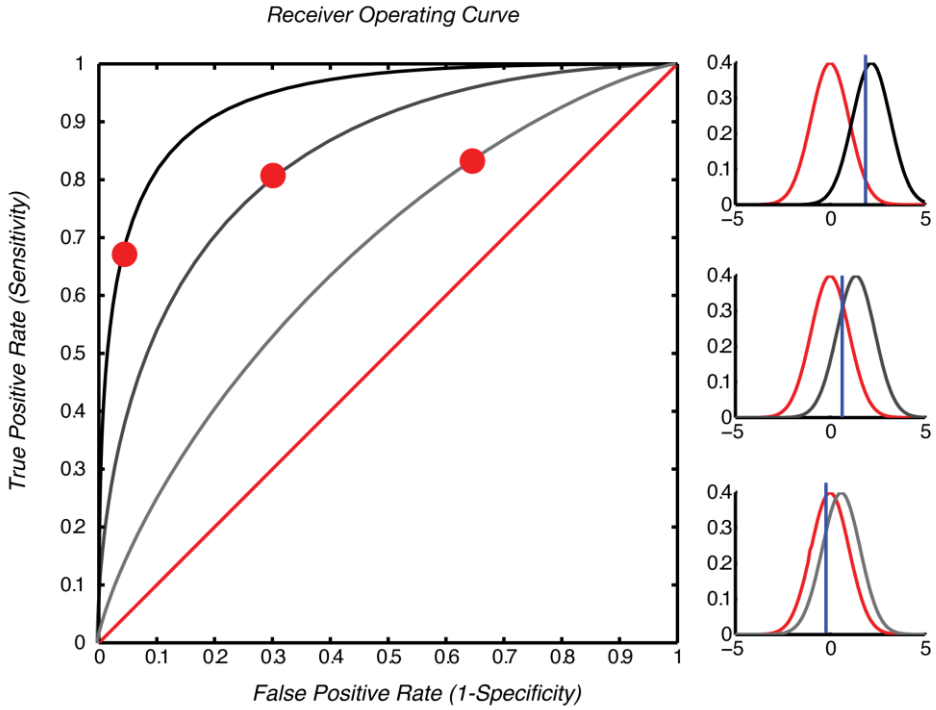

Figure 2.7: A family of ROC curves corresponding to d' values (three graphs on the right show increased d' values from bottom to top) and different criterions (shifting from left to right in the graphs on the right from bottom to top). As the d' values increases, the

In terms of the Yes-No procedure in this detection task, it is a very simple method for obtaining a threshold — find the lowest stimulus intensity that subjects report the existence of coherent movement for a particular proportion of trials (often chosen by the experimenter to be 75% or 90%). However, it has a few drawbacks. One problem is that it does not exclude the contamination of the sensitivity caused by response bias. For example, the subjects may have a tendency of committing false alarms by reporting the presence of infrathreshold or absent stimuli, making the measured value of detection of the signal lower than the actual threshold. Another worse scenario could be that subjects give responses without even observing the stimuli. Thus, the simple version of a Yes-No task may not reflect the accurate threshold if observers fail to report truly what they perceived. On the other hand, there are

some problems due to the cut-off level (criterion) that subjects use to make a decision. Observers could shift their criterion to influence the detection results, which means that the self-made criterion is not objective and stable enough to get a correct threshold. In order to avoid this subjectivity and control over the response bias, we used two-interval forced choice designs to acquire a more accurate estimation of threshold.

2.1.2 Measuring thresholds for the discrimination task

The discrimination threshold is the minimum *difference* between stimuli that an observer can discriminate reliably, also called the differential threshold. This term originated from the method of the just noticeable difference (JND) (Coren et al., 1994). One widely applied procedure for getting the differential threshold in a discrimination task is the two-interval forced choice (2IFC) design. In such a procedure, subjects are asked to compare and discriminate stimuli in two observation intervals and then report the interval containing the stronger/lower sensory information. It can be combined with either the method of *constant stimuli*, in which a fixed range of stimuli is randomly and repetitively presented or an *adaptive psychophysical method*. The following sections include a brief review of *constant stimuli* and *adaptive* methods with empirical examples.

2.1.2.1 Constant Stimuli

To measure the differential threshold of stimulus coherence, we performed a discrimination task with the method of constant stimuli. In the two-interval forced choice experimental design, subjects were asked to make discrimination judgments between two (or more) alternatives.

Visual Stimulus and Tasks

For this coherence of moving dots experiment, properties of the stimulus were kept the same as the Yes-No task. A coherence level of 40% was used as a fixed for the two stimulus intervals in each trial. The coherence level for the *signal* interval was obtained by randomly adding one of the four coherence values (2%, 4%, 8% and 16%) to the fixed. There was a delay interval between the two stimuli. Direction of motion for both stimuli in each trial was

kept constant at 0° (rightwards motion) for different trials. The graphical representation of the paradigm is shown in Figure 2.8. Rather than responding coherent motion present "Yes or No", observers were instructed to judge which interval contained the dots with higher motion strength overall at the offset of the second stimulus by pressing a button, which was instantly followed by feedback.

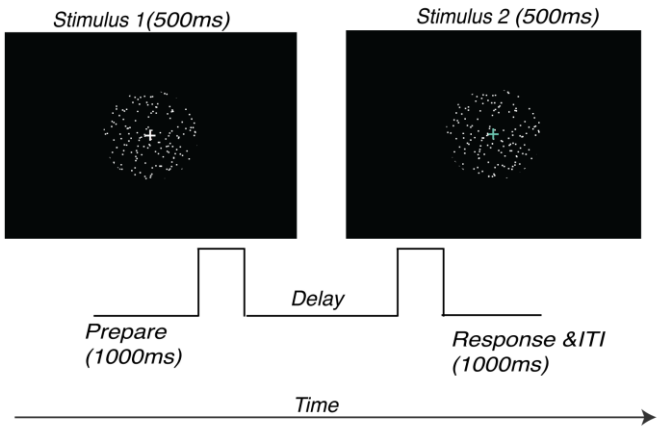

Figure 2.8: Paradigm of stimuli for the simple two-alternative forced choice discrimination task in psychophysical experiment, employing RDKs. Subjects were instructed to fixate centrally, while moving dots with a coherence level chosen randomly from five levels (40%, 42%, 44%, 48% and 56%) were presented during the first stimulus interval (500ms). Subjects need to hold the coherence level of this stimulus during the delay interval (300ms) until the presence of the second stimulus, and judge which stimulus had a higher coherence level.

Psychometric curves

Using this 2IFC design and the above parameters, we obtained the percent correct (P(c)) for different step-sizes of coherence based on the fixed coherence level. Typically, as the size of difference increases, the P(c) also elevated (examples shown in Figure 2.9). If we plot the P(c) against the size of the coherence difference (equal to the step-size levels), we get an approximately ogival curve with P(c) ranging from 0.5 (chance level) to 1 (100% correct). These plots are psychometric curves (Urban, 1910).

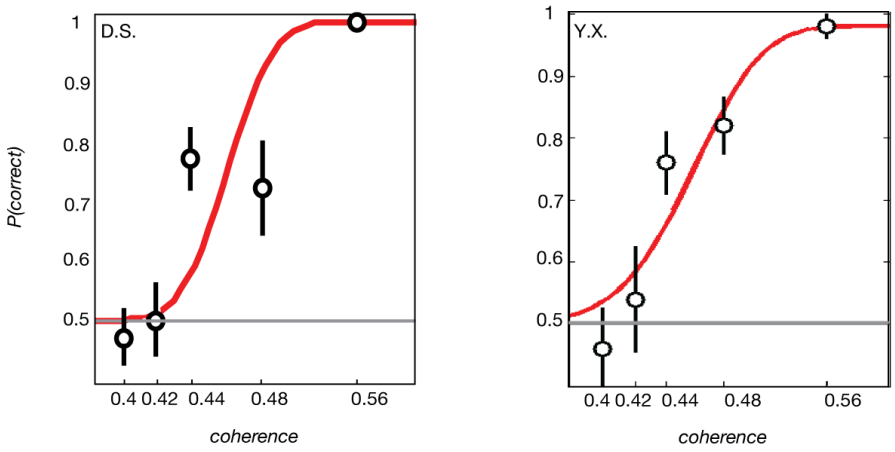

Figure 2.9: Proportion of correct as a function of difference of coherence levels for two subjects. X-axis presents the percent of dots moving coherenctly to the right direction (0º).

Curve fitting

The last step of analysing data from psychophysical experiments is curve fitting. It is crucial for acquiring a correct measure of threshold. We used a method based on Bootstrapping to fit the psychometric functions in this thesis. It is a method for estimating the variability of a statistic from a limited sample. A parametric bootstrap fits the psychometric curve by drawing samples repeatedly from a model instead of the original collected data points. Each time, a sample of random numbers with replacement was selected from a parametric model, in our case, the Weibull function. After 1000 resamples, the best-fitting curve is found with the method of maximum likelihood. Finally the bias and skewness in this new distribution was adjusted. From such a fit, thresholds and their 95% confidence intervals can be estimated. Sigmoid nonlinear regression was used to fit the psychophysical data, (psignifit toolbox, version 2.5.6) for Matlab (http://bootstrap-software.org/psignifit), and the corresponding value of stimulus intensity (coherence, orientation or contrast difference) at 75% correct performance was defined as the threshold.

Experiment Modification

One could get a reliable threshold using the 2IFC procedure and the robust fitting method. However, during pilot studies, I found that after a few trials, if the first coherence level was obviously higher or lower than the second stimulus, the subjects could give a response

without even observing the later stimulus. It then reduced the efficiency of the 2IFC. Therefore, in a modified version of the psychophysical experiments for investigating the working memory of motion coherence, I changed the fixed coherence levels to two values (30% and 40%), one of which was randomly selected as the base coherence, to which one of the increments of coherence levels was added.

As a result of *interleaving* these two fixed levels, there would be a overlap of the coherence levels between the first and second stimuli, making the coherence level during the second interval difficult to predict, ensuring that the subjects had to pay attention to both presentations of the stimulus (see more details in Chapter 4).

2.1.2.2 Adaptive staircase procedure

In contrast to the classical method of *constant stimuli* outlined above, an adaptive staircase procedure is a method where stimulus intensity starts from a pre-defined point around the threshold and then makes changes depending on the performance history. Specifically, staircases often start from an intensity level that is easily detected or discriminated. The stimulus is then reduced by a step-size downwardly towards threshold while the subject responds correctly, until the observer responds with an error. This then triggers a reversal of direction of stimulus change (intensity level begins to increase). After a number of trials and reversals, the data points converge around threshold. Many different types of staircase designs with different decision rules about changes of step-size, and up-or-down rules are available, but a discussion of the details of these is beyond the scope of this thesis.

Visual stimulus and task

With an analogous two-interval forced choice experimental design and an adaptive procedure, subjects were asked to make discriminations between two oriented contrast-reversing sinusoidal gratings (spatial frequency: 0.75 cycle/° of visual angle; maximum contrast), within a circular aperture (radius: 5° of visual angle). In one of the stimulus intervals, a grating tilted at either 45° or 135° was present for 0.5s. The orientation in the other stimulus interval was increased or decreased by an angle starting from 10°. Two stimulus intervals were separated

by an interstimulus duration (0.25s). A 2-down-1-up staircase with fixed step-size (3°) was used. This means that if subjects make two consecutive correct responses, then the intensity level is decreased by one step-size. Once the participant responds incorrectly, the level is increased by the same size. At the end of each trial, observers pressed a button after making a judgment of which interval contained a more clock-wise grating. Feedback was given. The threshold can then be estimated from the average of these reversals (Figure 2.10) or by fitting the whole trial history.

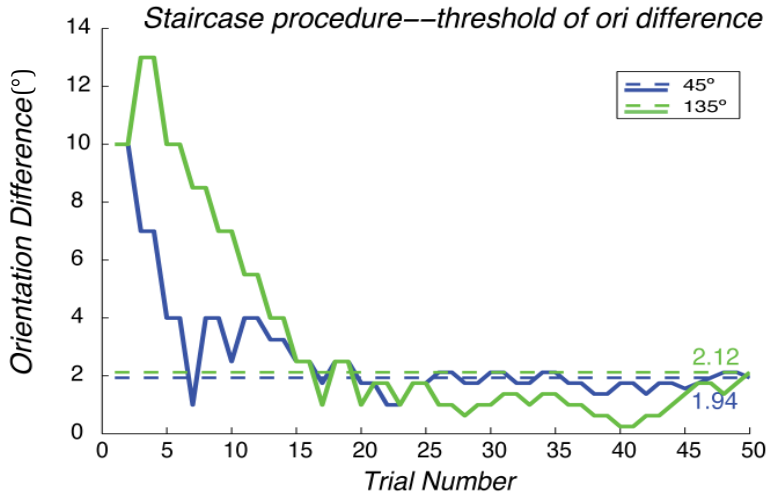

Figure 2.10: 2-down-1-up staircase procedure used in an orientation discrimination task. Solid coloured lines: the orientation difference for gratings based on orientations of 45° (Blue) and 135° (Green). Dashed coloured lines indicate the discrimination thresholds for the two orientations.

Compared to the method of constant stimuli, this method is more efficient and flexible. It does not require a large number of data points to obtain a psychometric function and the sample points are properly maintained around the threshold. Therefore, some of the previous MRI functional experiments used this method to manipulate performance with the precision of threshold and slope estimation in the scanner.

In the work presented in this thesis, we implemented a version of this adaptive method and used it in the retinotopy scans to control the subjects' attention and keep the gaze at fixation in

the scanner. For this, the luminance of the fixation cross was manipulated by an adaptive staircase method (2-down-1-up). Another application of adaptive methods is in our last experiment outside the scanner. In those parts, we used it in an orientation discrimination task (in the psychophysics setup) to measure the discrimination threshold in order to investigate whether the task difficulty modulates the neuronal activity in working memory (Chapter 8).

2.2 Gamma correction

The input-output characteristic of displays is often nonlinear, as the emitted light intensity (output) changes disproportionally to the voltage (input). Their relationship is described in the following equation:

$$y = ax^g, \qquad \text{(Eq. 4)}$$

where y is the output luminance, a is a constant, x is the monitor gun intensity, and g is the gamma value.

For our contrast experiment, we need to ensure the value of stimulus contrast precisely reflects the luminance difference of stimuli displayed on the screen. Thus, it is necessary to correct the gamma (non-linearity) to make the voltage level of pixels in the monitor and light intensity (luminance) linearly related. We used a sensitive psychophysical approach to adjust gamma. It takes advantage of one of the properties of "second-order motion" to conduct gamma correction. Previous studies have found that the human visual system requires some form of nonlinear processing to detect the direction of motion for second order, contrast-modulated (CM) stimuli (Benton & Johnston, 1997; Ledgeway & Hutchinson, 2006). Therefore, if we can find the gamma value that makes the second-order motion undetectable, we effectively adjust the output intensity to be linear to input voltage as previously shown (Ledgeway & Smith, 1994b, Ledgeway, 1994). The stimulus is constructed by alternating frames of sinusoidal gratings (spatial frequency, 1 cycle/degree) either first-order luminance-

modulated noise or contrast modulated two-dimensional random noise (Noise contrast, 50%) across space (github.com/psychopy/psychopy/blob/master/psychopy/demos/coder/experiment %20control/gammaMotionNull.py). In a forced-choice task, the observer was asked to indicate the direction of motion when the sinusoidal waveform was displayed by 25 cycles: whether the stimulus moved upwards or downwards by pressing up and down buttons correspondingly. During the process of 1-up and 1-down adaptive staircase procedure (initial step size, 0.5; total number of reversals of staircase, 12), observers could integrate the successive frames in the sequence and perceive motion reliably when the display system was far from linear. But as the gamma value dynamically adjusted, the direction became ambiguous (Ledgeway & Smith, 1994b). Then we estimated the monitor gamma by averaging the last four reversals of staircase; this averaged value was used in the relevant stimulus codes to linearize the monitor. The final gamma applied for our contrast experiments in this thesis was decided based on the mean result from three observers (4 repetitions for each observer) whose values were stable.

2.3 Functional brain imaging

2.3.1 Blood oxygenated-level dependent imaging

While behavioural measurement yields very important information, they provide no direct knowledge of neuronal substrates or pathways involved in cognitive tasks (Menon & Kim, 1999). By contrast, blood-oxygen level dependent (BOLD) functional magnetic resonance (fMRI) is able to provide both temporal and spatial information about the underlying neuronal activity in relation to a given sensory stimulus or cognitive event. Due to these conspicuous advantages of fMRI, it has been extensively applied in the field of neuroscience. Here, the basic principles underlying this technique will be outlined for reference.

2.3.1.1 The principle of blood-oxygen level dependent (BOLD) fMRI

It is thought that when neurons fire a series of action potentials, say, in response to a sensory stimulus, a complicated sequence of events follows in a variety of structures including glial

and other support cells, the somata, dendritic trees and terminals of the axons. These changes then trigger a complex interplay between vascular response (i.e. cerebral blood flow and cerebral blood volume), blood oxygen extraction, vascular coupling, neuronal modulation (e.g. subthreshold activity, excitation-inhibition networks, feed-forward and feed-back pathways) and local metabolism, the details of which are still being elucidated. As a result, the concentration of deoxyhemoglobin changes, altering the local field inhomogeneity and influencing the transverse relaxation time (T2*) of the activated area, which can be measured as signal increase or decrease on T2*-weighted images (Fox & Raichle, 1986). Figure 2.11 is a simplified diagram showing the change of oxygen consumption and blood flow evoked by neuronal activity.

Despite the fact that BOLD fMRI reflects the concentration ratio change of deoxyhemoglobin to oxyhemoglobin in the brain tissue, the time series obtained with fMRI does not offer a direct representation of the neuronal response to cognitive or perceptual events (Silver et al., 2010). Therefore, it is extremely important to understand the relationship between the measured fMRI signal and neuronal activity. There is a large body of research that has aimed to capture a clearer picture of this relationship, which will be reviewed in the coming sections.

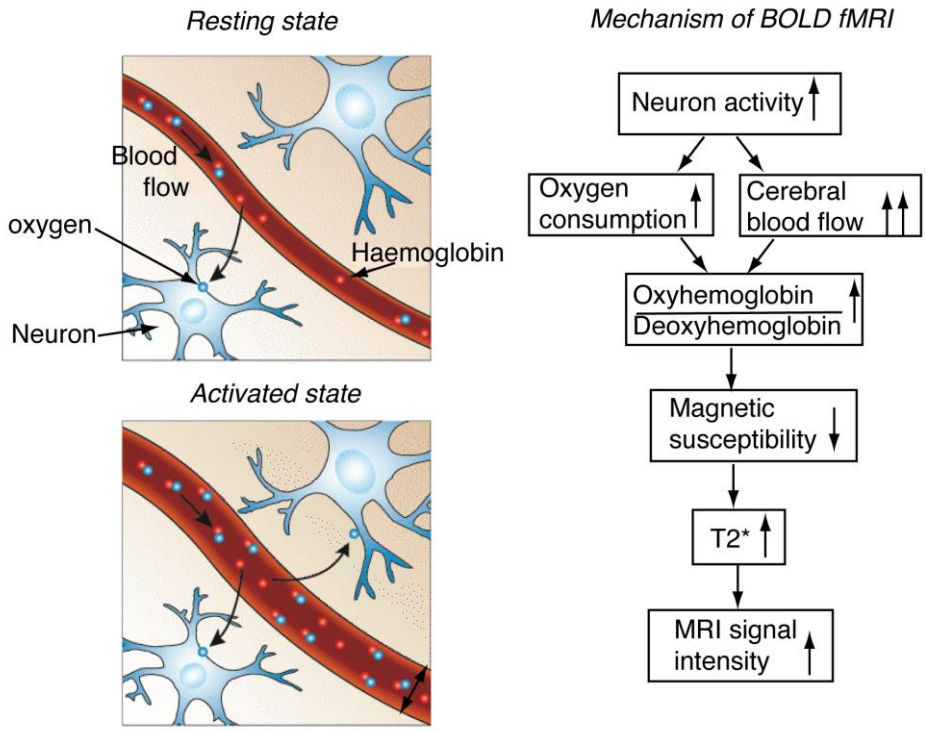

Figure 2.11, Images on the left show a diagrammatic representation of tissue in the resting and active states (modified based on diagram of www.fmrib.ox.ac.uk/research/introduction-to-fmri/what-is-fmri/what-does-fmri-measure-cont). Right panel shows a simplified mechanism of BOLD fMRI as a result of neuronal activity. When the neuronal activity increases, the consumption of blood oxygenation raises as a consequence, causing a momentary decrease of blood oxygenation. However, the increase of blood flow over-compensates this oxygen demand, and consequently increases the ratio of oxyhemoglobin and deoxyhemoglobin. According to the magnetic properties of these two substances (see Chapter 1), their concentration changes increases the signal of T2*, which we would observe as an enhanced signal on T2* images.

2.3.1.2 What does blood oxygenation level dependence fMRI measure?

When the local brain tissue is active, the increased demand for oxygen paradoxically leads ultimately to an even higher oxygenation level. It was hypothesized that this is caused by the increase of regional cerebral blood flow (rCBF). Though previously observed, this change had not been exploited until early 1990s when Ogawa and his colleagues demonstrated that measurement of rCBF might reflect the neuronal activity evoked during the process of perception (Ogawa et al., 1990). Since then, many studies have explored the relationship between neuronal activity evoked oxygenation change and regional blood flow. For example, one study using deoxyglucose autoradiographic methods reported comparable results from

both human and animal brains, suggesting that the density of vasculature is correlated with the number of synapses (Sokoloff et al., 1977). In addition, it was found that the dense vascularization is in close correspondence with an enzyme that is involved in oxidative metabolism (Sokoloff, 1977).

Other studies have been investigating the spatial scale of fMRI measurements. Invasive studies on animals measured neuronal activity at different spatial resolutions to detect on which scale and exactly what activity fMRI signals reflect. Different approaches have been used including single-unit recording, multi-unit activity (MUA) and local field potential (LFP). Among these methods, LFP measures the low frequency component of extracellular field potentials (Kamondi, Acsady & Buzsaki, 1998). Results from visual experiments on anaesthetized and alert monkeys showed that BOLD responses are slightly better predicted by LFPs than multiple-unit or individual spiking activity (Mathiesen et al., 1998). Moreover, increases in the LFP range are better predictors of BOLD activity than other measures (Logothetis & Pfeuffer, 2004). For instance, by simultaneous recordings of hemodynamic responses, LFPs and transient single and multi-unit activity in V1, investigators found that the activity underlying the LFPs remains elevated for the period of the visual stimulus, whereas the spike-density function and the MUA showed strong adaption and returned to baseline a few seconds after the offset of the stimulus (Figure 2.12). This evidence also indicates that BOLD activation may reflect the neural activity pertaining to the input and the local processing, rather than the output of the region (Logothetis 2008). On the other hand, selective blocking of MUA with various substances did not significantly affect the BOLD responses (Mathiesen et al, 1998). These findings are in agreement with the statement that the BOLD response mainly reflects the mostly slow intracortical activity elicited from a neuronal ensemble rather than the weighted sum of signals over a small area of grey matter (covering approximately $2\times2.5\times7$ mm^3) (Arezzo, Legatt & Vaughan, 1979; Huang & Buchwald, 1977).

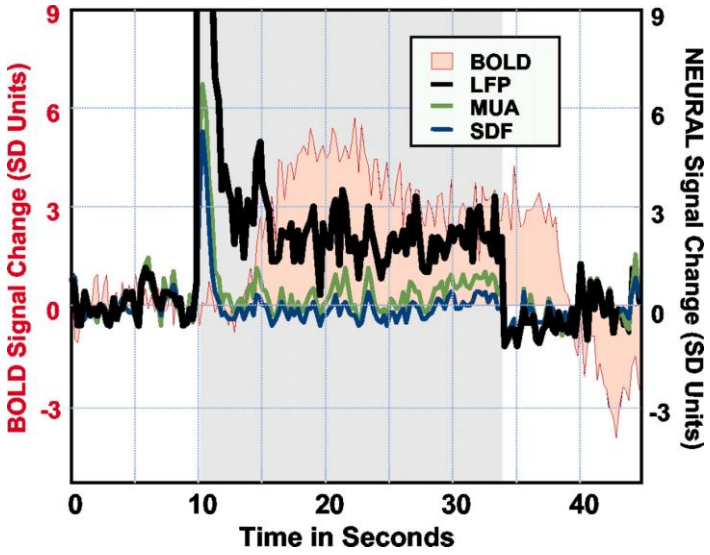

Figure 2.12 Response in striate cortex to a visual stimulus of 24s. Both single- and multi-unit responses adapted a couple of seconds after stimulus onset, with LFP remaining the only signal correlated with the BOLD response. SD, spike-density. Adapted from Logothetis et al. (2001).

2.3.1.3 Linear system analysis

Although complicated biological and physiological processes are occurring while neurons respond during a cognitive task, the measured fMRI responses to some stimuli are well described by a linear transform model (Boynton et al., 1996; Friston, Jezzard and Turner, 1994). This model was established to interpret the relationship between fMRI response and underlying neural activity. It approximates the fMRI signal as a consequence of the averaged neural response over several millimeters in space and a temporal summation over a few seconds. According to this model, the BOLD response should conform to the properties of a linear system including scaling and additivity. Studies supports the idea that signals obey *scaling* by measuring the relation of fMRI response and average neuronal response to the strength of a motion signal (coherence of dots), respectively (Heeger et al., 2000; Britten & Newsome, 1998). It was found that the BOLD signal increased proportionally to the neuronal firing rates in MT (Rees, Friston & Koch, 2000). Figure 2.13 summarizes the linear systems framework of visual stimulus and BOLD response. Heeger and his colleagues also extended their observation to other elementary visual features (e.g. contrast). They made the assumption that fMRI signals correspond to neural firing rates. If this were the case, then the

BOLD response would also change in proportion to stimulus contrast given the monotonic relationships between average firing rates and stimulus contrast. Their results revealed a similar relationship between the spiking rates across a large population of neurons in V1 (measured in monkeys) and the fMRI signal for contrasts of stimuli (in human subjects) (Boynton et al, 1999; Geisler & Albrecht, 1997; Heeger et al., 2000). In the light of this evidence, most of the current analysis methods and tools (i.e. SPM, FSL) assume that the output fMRI response of an arbitrary experimental design can be predicted by convolution of a hemodynamic response function with stimulus design time course that captures expected changes in neural firing rate. The following sections outline the temporal and spatial features of this linear model, respectively.

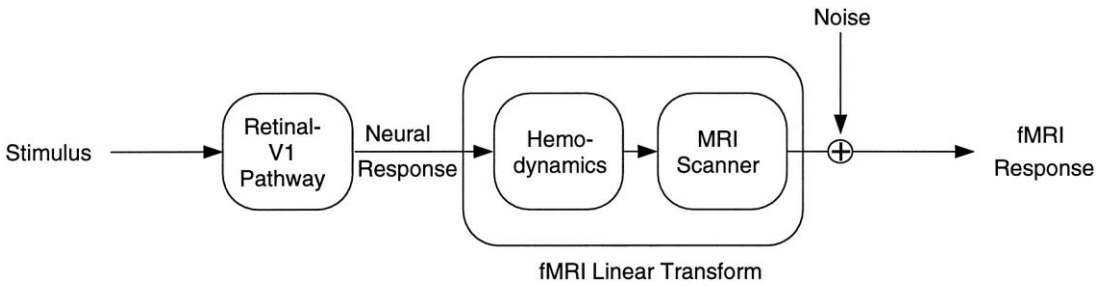

Figure 2.13: The linear systems framework for fMRI. Adapted from Boynton et al. (1996). A linear model seems to describe functional MRI responses to combinations of stimuli in the visual cortex well. Experimental evidence shows that BOLD signal changes are roughly linear with visual stimulus duration and contrast once the non-linearities in the neural response are accounted for, and even rapid visual stimuli show approximate superposition typical of a linear system.

(1). Temporal features of fMRI

Before examining the temporal features of a linear system, it is necessary to measure the BOLD change elicited by a single stimulus. Initially, investigators had observed the time series of fMRI signal change in V1 at 1.5 T, and found that the fMRI signal responds approximately 2 seconds after the presence of a stimulus (Savoy et al., 1995; Kim, Richter & Ugurbil, 1997). Since BOLD fMRI measures the change of rCBF induced by blood volume alteration and oxygenation changes, its signals represent *slow reactions* to brain activity in response to external stimuli or internally generated neural events. Nevertheless, there are

reliable delayed responses to the onset of events. Evidence has shown that the variability of the onset delay in simple visual experiment is small (Savoy et al., 1995; Savoy et al., 1994). After the delayed onset of BOLD response, the time-to-peak of the response can occur up to 13s later (Richter et al., 1997; Menon, Luknowsky & Gati, 1998). Then it takes another few seconds for the response to settle and return to the baseline activity. They also found that further increasing the duration of a stimulus would not further increase the activity amplitude due to neuronal saturation. Yet the width of response peak increased, indicating that the width of fMRI response reflects the processing duration of a stimulus (Savoy et al., 1994). On the basis of these observations, one could correlate the temporal features of fMRI response with neuronal activity.

Moreover, the understanding of the temporal features of the BOLD response to individual stimuli facilitated the establishment of the linear transform model. From the temporal perspective, it posits that the response to a long stimulus is formed from the summation of the responses to shorter stimuli. Different experiments measured the fMRI response to different numbers of stimuli, and compared the result with the sum of individual activity (Dale & Buckner, 1997; Horner & Andrews, 2009). The data supported another property of the linear relational model: *additivity* (Figure 2.14). Along the same line, a time resolved event-related fMRI technique provided a method of discriminating hemodynamic differences in reaction to neuronal activity (Buckner et a., 1996).

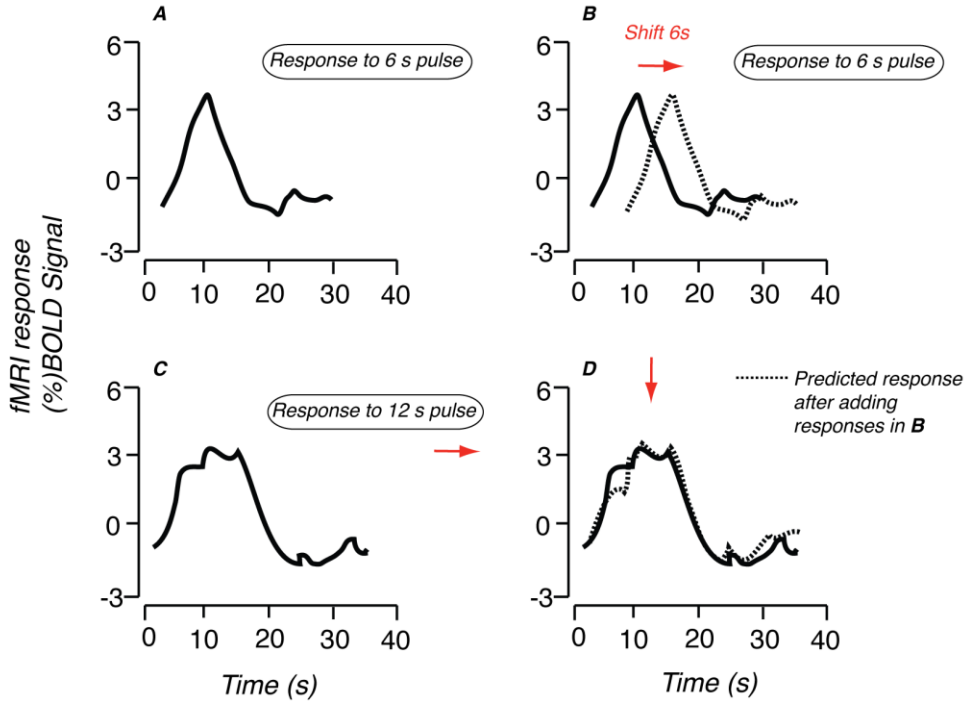

Figure 2.14 Measured functional magnetic resonance imaging (fMRI) responses from the visual cortex for 6- (A) and 12-s (C) stimulus presentations. B shows the two separate fMRI responses with a delay of 6s. D. temporal summation of the two fMRI responses showed in B, and compared with the responses to a 12s pulse in C, which are very similar to each other. Adapted from Boynton et al. (1996).

(2). Spatial relations between fMRI and neuronal responses

In addition to the linearity / temporal summation, co-localization of fMRI and neuronal response is also indispensible for spatial localizing the underlying activity for a cognitive task. Compared to other neuroimaging methods, including electroencephacegraphy (EEG) and magnetoencaphalography (MEG), fMRI achieves a relatively high spatial resolution (Menon & Kim, 1999). However, BOLD signal changes can covary with microvasculature, such as the capillary bed in the cortex (< 10 mm), as well as bigger vascular structures such as the large draining veins at the scale of millimetres (Menon et al., 1993; Lai et al., 1993; Lee, Glover & Meyer, 1995; Logothetis et al., 2001). It has been suggested that the signal change from microvascular contributions has a higher spatial correlation with the site of neuronal activity, whereas the macrovasculature could lead to the response site being mis-localized to centimetres away from the actual location (Kim et al., 1994). Despite this limit, it was found

that single and brief presentations of stimuli could suppress this vascular artefact (Menon & Kim, 1999).

A large array of fMRI experiments has provided supportive evidence for the correspondence between the BOLD signal and neuronal activity in space. For instance, the typical retinotopic maps showed that visual stimuli presented next to each other in the visual field correspond to the nearby regions of visual areas (Engel et al., 1994). This case was presumed to occur only when the large draining vein signal could be successfully deemphasized (Logothetis & Pfeuffer, 2004). Therefore, the retinotopic maps may suggest that the biological and hemodynamic factors in those large veins are constant throughout the scanning time. Similar co-localization has also been presented in somatosensory cortex using tactile stimuli with a block design (Puce et al., 1995; Yousry et al., 1995; Schulder et al., 1998; Ruge et al., 1999; Cannestra et al., 2001; Sanchez-Panchuelo et al., 2012b). Based on these reports, many fMRI experiments have used localizer scans to first delineate the specific areas that are responsive to the stimuli/events. For example, the Fusiform Face Area (FFA), an area in the fusiform gyrus that is heavenly involved in face processing, is defined for each individual by locating the region that responds more strongly to faces compared to other objects in ventral temporal cortex (Haxby et al., 2001; Poldrack, 2006; Poldrack, 2007; Friston, 2006; Saxe et al., 2006).

2.3.1.4 The existence of nonlinearity

One variation of the relationship between fMRI and neuronal activity comes from the hemodynamic response function (HRF) (see more in the section on the general linear model in this chapter). Even though the HRF is often modelled as a linear, time-locked transform of the underlying neuronal activity (Friston et al., 1995), many experiments have shown the nonlinearity of the BOLD signal in time in certain circumstances (Boynton, et al., 1996; Birn, Saad, & Bandettini, 2001; Buxton, Wong, & Frank, 1998; Friston, et al., 2000; Vazquez & Noll, 1998; Huettel et al., 2009). One circumstance in which the HRF is known to violate linearity is for very short stimulus durations and inter-stimulus intervals. Although pronounced hemodynamic responses can be observed, the responses depart from linearity

when the interval between stimuli is too short. In fact, response amplitudes could be reduced, and duration for the recovery to baseline could be prolonged (Richter et al., 1997; Menon, Luknowsky & Gati, 1998). Thus, it is not recommended to use inter-stimulus intervals (ISI) of less than one second if analysis assumes linearity. However, some experimental designs even make use of this refractory effect by presenting very closely spaced stimuli. Subsequent stimuli only elicit smaller hemodynamic responses due to adaptation (Kileny, Ryu, & Abbas, 1980; Logothetis, 2003; Logothetis et al., 2001; Wilson et al., 1984; Kanwisher et al., 1997; Grill-Spector et al., 2001).

Even though a few reports have pointed out the significant nonlinear responses in the higher visual areas (Avidan et al., 2002; Mukamel et al., 2004) and variance of HRF in different regions of interest (Birn et al., 2001; Boynton & Finney, 2003; Soltysik et al., 2004) and stimulus category (Horner & Andrews, 2009), a majority of researchers confirmed that the BOLD response in sensory areas (V1-V3 and MT/V5) generally obeys linearity (Hoge et al., 1999; Miezin et al., 2000; Vazquez & Noll, 1998; Gu et al., 2005; Glover ,1999; Rees et al, 1997). Thus, we used the canonical HRF to estimate the response amplitude in Chapter 8 of this thesis in addition to the deconvolution approach used elsewhere in the thesis.

2.3.1.5 The advantages of BOLD fMRI

Despite many underlying assumptions and the existence of a small nonlinearity between neuronal response and fMRI, the measurement of responses in early visual cortex are well captured by a linear approximation. Besides, magnetic resonance imaging and in particular BOLD fMRI has many incontestable advantages: it is a completely non-invasive method; measurements of the responses across the whole brain are possible (unlike single unit electrophysiology); and it is also relatively easy to measure different aspects of cortical anatomy. Meanwhile, with on-going developments of the technique, BOLD fMRI is able to reach a relatively good combination of both spatial and temporal resolution of the images. The successful application of Echo Planar Imaging (EPI) makes it possible to scan regions of interest in a relatively large area within seconds while keeping a good spatial resolution (e.g.

$3mm^3$ voxels with 1.5s TR and 30ms TE). This technique acquires multiple lines of imaging data after a single RF excitation. Therefore, typical EPI imaging at 3T magnetic field allows 20-30 slices of data collection within a few seconds. Moreover, several experiments at very high magnetic field are currently trying to push the spatial resolution of fMRI to the scale of cortical columns (Cheng, Waggoner, Tanaka, 2001; Goodyear & Menon, 2001; Menon & Goodyear, 1999). It is a technique that some believe facilitates the further exploration of decoding the functional organization of neuronal populations (Bartels, Logothetis, & Moutoussis, 2008).

2.3.2 fMRI Design Methods

Functional MRI data are usually acquired in either a blocked design or an event-related design (although some experiments have attempted to combine these two approaches). A brief review of these two experimental designs is as follows.

2.3.2.1 Block design

The "on" and "off" model of block designs has been extensively applied in MRI for more than a decade (Brockway, 2000; Loubinoux et al., 2001; Machielsen et al., 2000; Rombouts et al., 1998; Rombouts et al., 1997; Friston et al., 1999; Buxton et al., 1998; Glover, 1999). This is the simplest way to evaluate the correlation between one independent variable (e.g. contrast of a visual stimulus) and a dependent variable (usually the modulation in the fMRI signal). Trials under the same condition for an independent variable are grouped together over time (termed as blocks) to see whether the presence of the independent variable makes a significantly different effect versus its absence (see Figure 2.15 **A**). For instance, investigators (Grill-Spector, 2003; Malach et al., 1995) used blocks with objects interleaved with blocks with scrambled images or blanks to localize object-related cortical areas that are preferentially activated by objects, including the lateral occipital complex (LOC). Given the straightforwardness of this design method, it is often applied to detect voxels with significant activity under certain conditions. In the present work, we used a block design with ON blocks

of visual stimuli versus OFF blocks of another condition (fixation on a grey background) to help localize and refine the regions of interest relating to the visual stimuli in this thesis.

However, there are some drawbacks of blocked designs (D'Esposito et al., 1999a). First, the length of each block needs to be sufficiently long to allow the hemodynamic response to have adequate time to return to the baseline, providing a large enough response to compare between two conditions. In addition, blocked designs should have as many transitions between conditions as possible to easily remove the low-frequency noise and to get a good estimate of signal changes. Besides this time-consuming disadvantage for long blocks, the succession of stimuli presented during blocks causes the superposition of individual hemodynamic responses on top of each other. This makes it clear that blocked designs are not ideally suited to reveal the shape of the hemodynamic response function and its change over time.

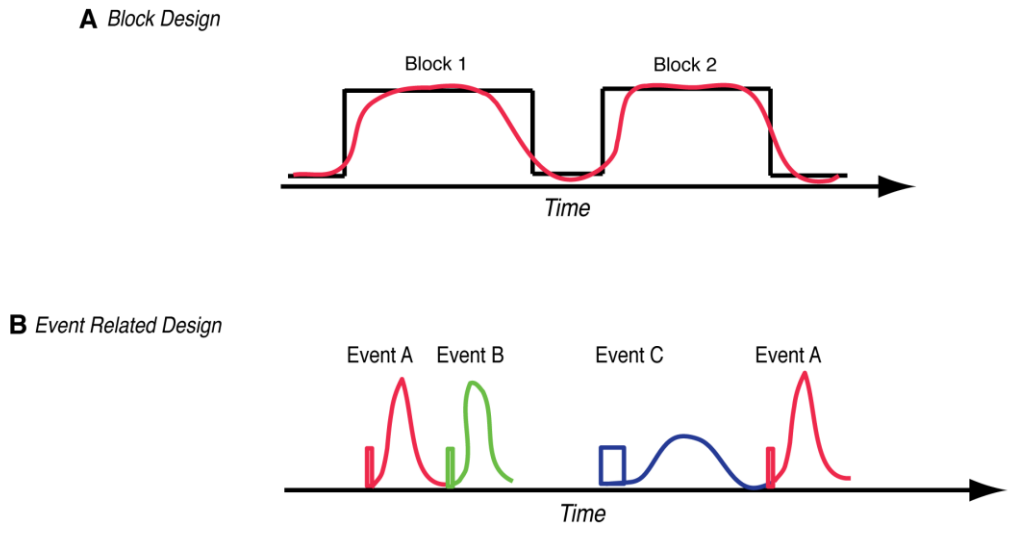

Figure 2.15: Example of block **A** and event-related designs **B** for fMRI experiments. A. Block design paradigm requires the task block which is interleaved with time blocks of rest. B. Event related paradigm. Since response summation is an approximately linear fashion, the responses to rapidly presented stimuli can be extracted from the data if the events are presented randomly. Colours illustrate possible responses evoked by different types of events.

2.3.2.2 Event-related design

The other commonly used design method is called the 'event-related' design. It is a method of presenting separate and short-duration events whose timing and order may be randomized

(Rosen et al., 1998). It measures transient changes in brain activity associated with discrete stimuli (Amaro et al., 1999; D'Esposito, 1999a; Friston et al., 1998; Josephs, Turner, & Friston, 1997; Rosen, Buckner, & Dale, 1998; Wiener et al., 1996; Zarahn, Aguirre, & D'Esposito, 1997). Thus, we expect that the event-related design is optimal to get the maximal and accurate change of BOLD signal for variable blocks (Dale, 1999). One of the earliest uses of event-related fMRI was to explore a working memory paradigm (D'Esposito, et al., 1999b). In that experiment, different trials were intermixed in order to separate the events of encoding and maintenance in working memory. Figure 2.15 **B** shows one example with transient and sustained responses evoked by different types of events. The outcomes can demonstrate the regions in the brain that are involved in the activity of encoding (transient activity) and maintenance (sustained activity), and suggested that their roles in each corresponding process were different. These examples illustrated that the event-related design is good at measuring the pattern of signal change over time within an active voxel in response to the experimental manipulation (Burton & Small, 1999; Josephs & Henson, 1999).

Since one of the main aims of this thesis was to probe the role of early visual areas in working memory by observing the activity during the delay time between two stimulus intervals, an event-related design provides a good and flexible means for achieving this (Celsis et al., 1999; Liu et al., 2001; Loubinoux et al., 2001). First, an event-related design allows different trials or stimuli to be presented in arbitrary sequences, thus eliminating potential confounds, such as habituation, anticipation, set, or other strategy effects on our targeted process (D'Esposito et al., 1999c). Second, it is sensitive to the change of hemodynamic response during variable delay intervals ranging from very short periods to relatively long ones, allowing us to estimate the cortical responses to each component during the intrinsic process of working memory (Courtney et al. 1997; Zarahn et al. 1999; Zarahn et al. 1997). Even though the BOLD signal is sampled at discrete intervals determined by the repetition rate of scanning (TR) and event-related design needs high temporal resolution to obtain signal changes, the currently available

technology on standard 3T scanners is more than sufficient to guarantee the presentation of time-resolved signal changes (Ress, Backus, & Heeger, 2000).

2.3.3 Data pre-processing

The following sections focus on reviewing some of the steps for processing the acquired functional images in spatial and temporal domains (Figure 2.16). These processes aim to (1) reduce the noise-induced variability in the signal, (2) make data ready for statistical analysis and (3) prepare the display of data in the context of the two-dimensional cortical surface. For our particular analyses, some of the steps commonly used in other domains were unnecessary or undesirable. All of the preprocessing that was applied was performed using a combination of free imaging analysis tools (mrTools, Heeger lab, NYU; mrVISTA, Wandell lab, Stanford; FMRIB Software Library; Freesurfer, http://surfer.nmr.mgh.harvard.edu/) and custom-written extensions written at the University of Nottingham. Originally, cortical segmentations and unfolding were performed using SurfRelax (Larsson, 2001), but in later analyses, we moved to an automated process with Freesurfer (MGH).

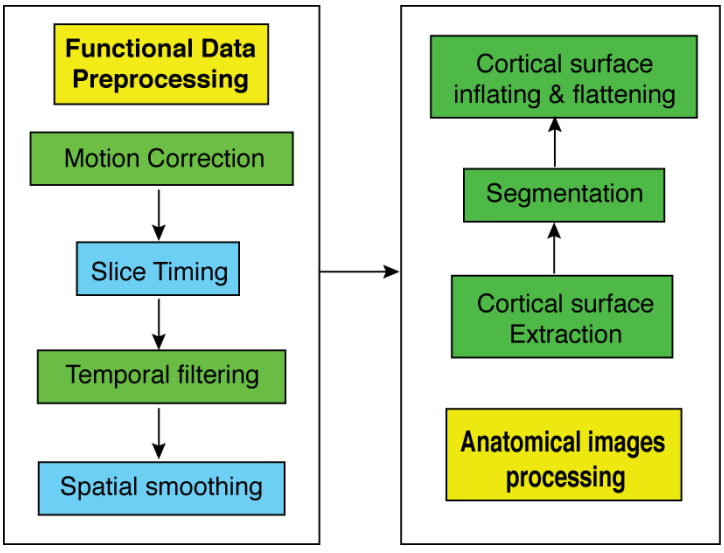

Figure 2.16: Workflow of pre-processing and image visualization for fMRI data. Squares with green colour indicate the steps we performed for obtaining cortical surface maps.

2.3.3.1 Motion correction (fMRI)

Even with padding and the use of vacuum pillows slight head motion may still be inevitable during the scanning and can induce artefacts, consequently causing the invalid identification of "active" voxels (Figure 2.17). It is, therefore, necessary to perform motion correction to compensate for the head motion and minimize its effect on analysis. A reference image is selected and the rest of the images are registered to it by translation and/or rotation (rigid body transform).

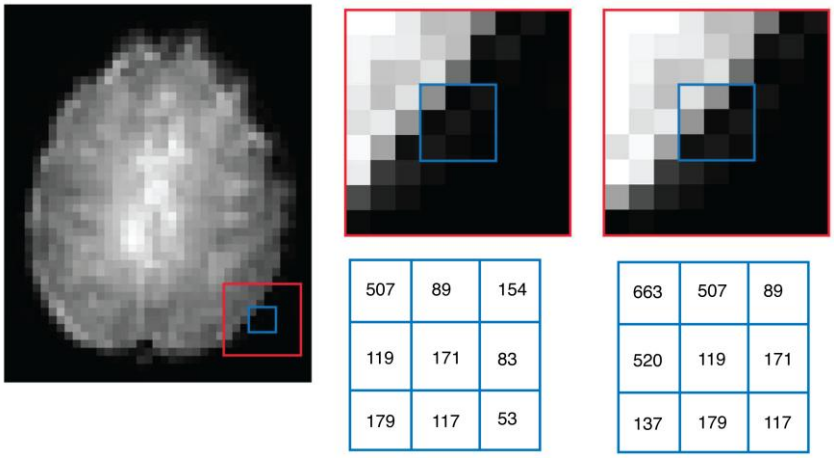

Figure 2.17: Effects of head motion on fMRI data. Large intensity transitions exist at tissue boundaries, including the edges of the brain (Left). The magnified views show the position of the brain before head motion (Middle) and after a movement of one voxel to the right (Right). The numerical intensity values for the voxels within the blue square are shown below. Note that the intensity in a given voxel may change by more than a factor of 5 solely due to head motion. This compares to a change of only 1 to 2% for real brain activity. Figure and legends adapted from Huettel et al. (2009).

Figure 2.18 plots head motion over an experimental session. In this thesis, we used the tools implemented in mrLoad (Heeger lab, NYU) for motion compensation (correction). It mainly contains two types of correction (Nestares & Heeger, 2000). For a session with more than one scan, it corrects the motion between scans first. The compensation function treats each scan as a single unit to conduct alignment by computing the mean T2* map across the functional images within one scan. We specify a reference scan to which the rest of the scans will be aligned. Typically, the reference scan is the one closest to the anatomical collection in time.

Besides this "between scans alignment", the motion compensation function also performs a similar rigid-body alignment "within each scan". The frames are lined up to a chosen base frame. These displacements in 3D also provide the foundation for the coregistration between anatomical and functional images (see more detail in section of coregistration).

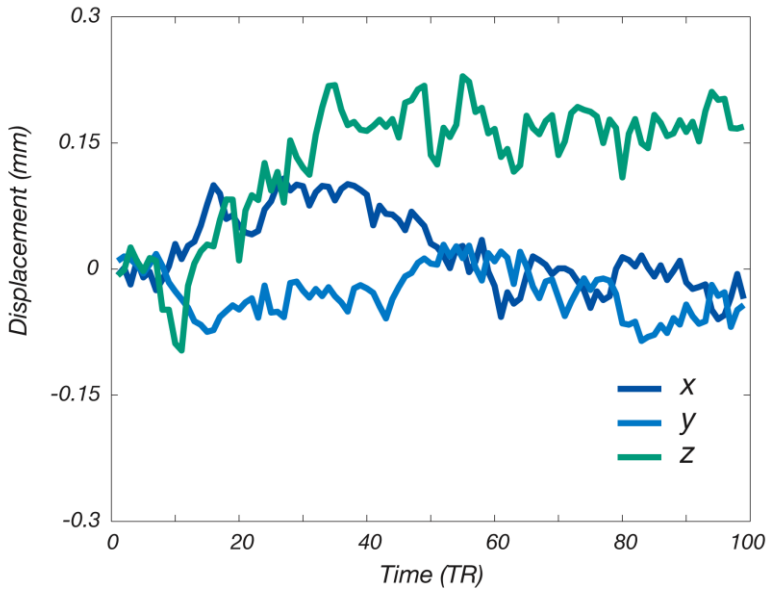

Figure 2.18: Plots of translational head motion from a single fMRI session. Translational effects comprise movements from left-to-right (x-axis), forward-to-backward (y-axis), and top-to-bottom (z-axis). Adapted from Nestares & Heeger, (2000).

2.3.3.2 Slice-timing correction (fMRI)

If slices in an imaging volume are acquired in an interleaved 2D acquisition sequence, the time discrepancy between two spatially adjacent slices could be much greater than two slices that are far apart. This inter-slice gap, which can be up to ½ of a TR, depending on how slices are interleaved, should be corrected if one wants to apply the same statistical analysis to every slice, assuming all slices in a volume are collected at the same point in time. However, such temporal realignment to the beginning of the TR requires interpolation of the time series (e.g. using sinc-interpolation), which brings along its own set of problems. In addition, because the TR in the fMRI experiments was relatively short (only 1500ms), small inaccuracies due to slice timing are unlikely to affect the estimation of hemodynamic responses in individual subjects. For the data in this thesis, we therefore chose not to apply slice-timing correction.

2.3.3.3 Spatial smoothing (fMRI)

The purpose of applying spatial smoothing to fMRI images is to increase the signal to noise ratio by decreasing the uncorrelated noise in space (Oppenheim, 1978; Triantafyllou, 2006). In certain analysis workflows, it is also required to guarantee the validity of the assumed spatial model of noise (e.g. assumption of spatially Gaussian noise with particular characteristics for *Gaussian random field theory*) (Friston et al., 1995). The effect of smoothing also is to, ultimately, help clustering the activity of voxels adjacent to each other, thus reducing the problem for multiple comparisons in statistical analysis (Poline et al., 1995; Siegmund et al., 1995). However, for retinotopic mapping and the region-of-interest based approaches used in this thesis, spatial smoothing is not required and rarely desirable. We therefore did not apply any spatial smoothing (beyond that inherently incurred by the interpolation of the 4D fMRI data during motion correction).

2.3.3.4 Temporal filtering (fMRI)

Small instabilities in the electronics of the scanner and the physiological movement can induce low frequency drift as well as high-frequency components in the measured BOLD signal (Edelstein et al., 1986; Parrish et a., 2000). The low frequency confounds can be removed by use of a high-pass filter. High-frequency noise in time series can be smoothed temporally with a low pass filter (Raj et al., 2001). In many circumstances both types of filters are combined in a *bandpass* filter, which filters out frequencies both below and above a particular pass band. Typically, temporal filters ensure a better estimation of parameters in statistical analysis.

To remove slow temporal drift in fMRI time series, we applied high-pass filtering to the data. For the retinotopic mapping data at each voxel, a low-pass filtered version of the timeseries was subtracted from the original timeseries, in effect high-pass filtering (for example Larsson et al., 2010; Montaser-Kouhsari et al., 2007; Larsson & Heeger, 2006; Offen et al., 2009; Offen et al., 2010; Sanchez-Panchuelo et al., 2012a; Levy et al., 2007). For the GLM analysis and classification analysis, we used standard high-pass filtering (0.01Hz cutoff) as routinely

used in many applications (Offen et al., 2009; Sapountzis et al., 2010; Dinstein et al., 2008; Liu et al., 2011).

2.3.3.5 Segmentation and unfolding of the cortical surface (anatomy)

Since visualizing the 2D topography not only presents the activity over a large-scale field within a single image, but also conveniently reveals the response within the sulci in cortex, we adopted an approach to unfold the convoluted 3D structure of the grey matter into a 2D flattened surface. The steps related to this processing are summarized in the forthcoming sections. This outline makes reference to the steps used by SurfRelax (Larsson, 2001), but largely equivalent, automated processing is available in Freesurfer (MGH).

Extraction of cortical surface

As a result of inhomogeneities of the magnetic field, even the same tissue in the structure of interest may contain different intensities, leading to possible confusion when marking the boundary between WM and GM with simple intensity thresholding. Thus the initial step is to normalize the intensity variations in the T1-weighted MPRAGE anatomical MR images with a non-parametric heuristic approach (Lasson, 2001). After this step, each cerebral hemisphere in the brain and the brain stem were computationally separated according to the image intensity of different structures. This step also fills cavities in white matter as well as separates the WM from subcortical nuclei. This preprocessing aims to prepare for the WM and GM segmentation properly.

Lasson (2001) devised a method for cortical segmentation by using a voxel-based deformable template. First, the WM volume in each target individual brain was used to derive a template volume with spherical topology. This is taken as a starting estimate for obtaining a fitted cortical surface between the grey matter and white matter. Then a parameterized erosion and dilation are used to deform onto the WM, which insures that the final extracted WM volume has a correct anatomical configuration (e.g. no “handles” or holes). Compared to many other tools for the similar purpose, Larsson’s method for WM and GW classification provides a more precise delineation of the interface between GM and WM. Figure 2.19 is a

demonstration of coloured surfaces (curvatures) after segmentation. Finally, in order to optimize the fit between the outer and inner layers of the grey matter ("pial" and "white matter" surfaces, respectively), a similar deformation method was applied repetitively onto the original (but intensity-normalized) anatomical image.

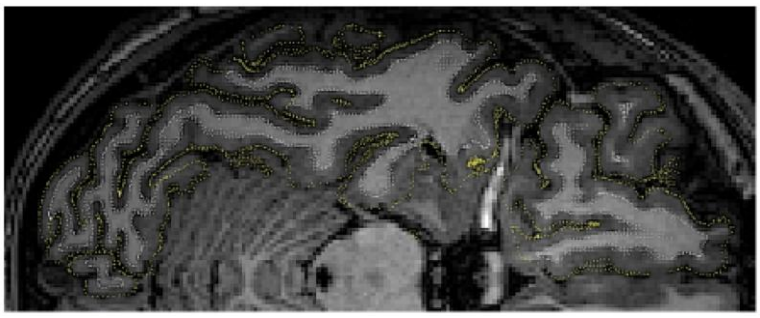

Figure 2.19: The extracted surface between the grey and white matter for the left hemisphere. Yellow curvature, outer-surface of GM; White curvature, interface between GM and WM.

Coregistration

The spatial resolution of the functional EPI images obtained for this thesis was 3mm isotropic. This resolution is still regarded as relatively low compared to the resolution of an anatomical image (usually, 1 mm isotropic). Thus, researchers routinely overlay the functional and derived statistical images on the high-resolution anatomical images to link cortical function with anatomy (for example Larsson et al., 2010; Montaser-Kouhsari et al., 2007; Larsson & Heeger, 2006; Beckett et al., 2012; Sanchez-Panchuelo et al., 2012a; Schluppeck et al., 2005). An unfolded 2D cortical surface for displaying information from BOLD imaging, further, makes the visualization more direct and easier for observers (Figure 2.20). The next section briefly summarizes the method of cortical unfolding.

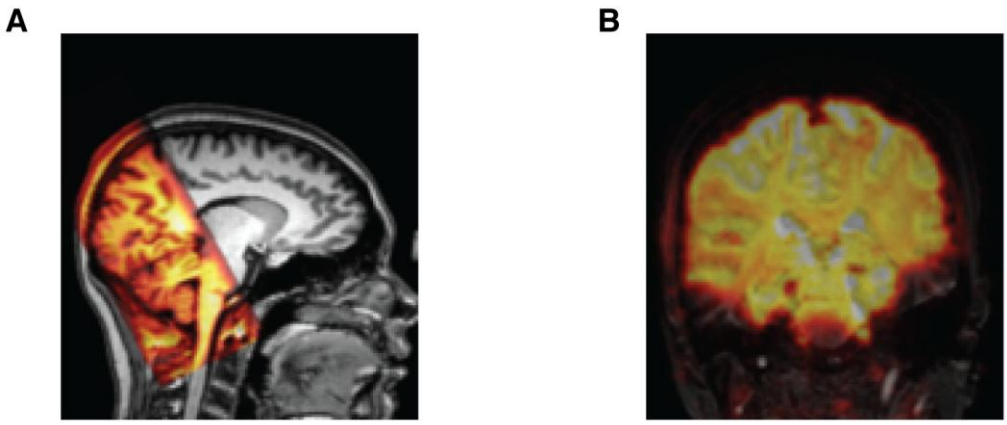

Figure 2.20: **A**. High-resolution anatomical images (in gray) are overlaid by low-resolution anatomical images (in red) obtained in the same session as the functional images. **B**. Functional images (red) overly on the corresponding low-resolution images displayed in A.

Cortical surface inflating and flattening

Although the cortical surface already provides a better display for the spatial relationship between different activated locations on each hemisphere, the cortical surface is still folded with sulci varying from subject to subject anatomically. Moreover, it is often the case that the shape and distribution of some activated regions is "hidden from view" inside the sulci but equally important (Witzel et al., 2001) (see Figure 2.21 A and B). Hence, it is advantageous to "inflate" the brain surfaces and flatten parts of them into a two-dimensional map with unfolded configuration, especially for smaller regions in the brain (Figure 2.21 C).

To make the process of inflation less time-consuming, the algorithm first reduces the number of nodes for initial relaxation/flattening by performing resampling to a lower-resolution surface. Then it tries to move these chosen nodes towards their corresponding vertices on a plane while retaining the approximate distance between neighbouring points. The displacement parameters for each point on the low-resolution mesh are then fed into the matching vertices in the higher-resolution surface. Similar steps of resampling, moving and smoothing are iteratively performed, until finally the parameters are applied to the original surface, the points of which then end up on an inflated or smoothed version of the

corresponding surface (FreeSurfer: Martinos Center for Biomedical Imaging, MGH, Harvard).

Flattening an inflated surface of the occipital lobe does induce some, but limited geometric distortions but vastly improves visualization: the same method as surface inflating, described in the previous paragraph, can be used to project the folded surface onto a plane.

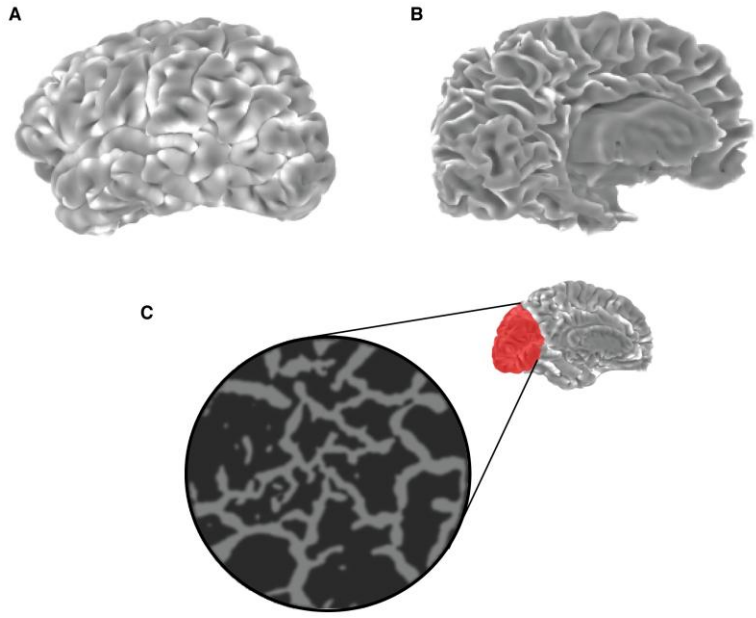

Figure 2.21: **A**. 3D outer surface of grey matter of the left hemisphere. **B**. 3D inner surface of grey matter of the left hemisphere **C.** An inflated and flattened patch from the occipital area (shown in red) in left hemisphere. The original sulci and gyri are represented by different grey scale (darker black – sulci; lighter black – gyri).

2.3.4 Human Retinotopic Mapping

In the past decade, several studies clearly established that visual areas are topographically organized both in animals and humans (DeYoe, et al., 1996; Engel, et al., 1994; Shadlen, 1994). The organization of cortical retinotopy in the early visual areas has been reviewed in Chapter I. Although the local neighbourhood relations for those areas are faithfully maintained in humans, the exact correspondence between anatomical structure and the retinotopic maps is highly variable across individuals (Larsson & Heeger, 2006; Andrews et al., 1997; Henriksson et al., 2012; Yamamoto et al., 2012). Thus, we employed an

individualized delineation for early visual regions (V1, V2 and V3) in our experiments. This is also important for defining the Regions of Interest (ROIs) in the early visual areas for the functional experiments that follow. In this section, I focus on how we delineated the retinotopy on the visual cortical surface using BOLD fMRI.

2.3.4.1 Visual stimuli

We used the standard traveling-wave method with ring and wedge stimuli to measure visual field maps (DeYoe et al., 1996; Engel, Glover, & Wandell, 1997; Engel et al., 1994; Larsson & Heeger, 2006; Sereno et al., 1995). In this method, subjects fixate at the center of the screen while a series of high contrast patterns are presented periodically. Our stimuli consisted of radial and high-contrast checkerboard pattern that were masked to either concentric rings or rotating wedges (Figure 2.22). The visual field alternates between the flickering checkerboard and a grey equi-luminant background in order to evoke a reliable response and to form an apparent contrast between stimulated neurons and those outside a voxel's 'receptive' field.

The ring stimuli are annuli at different diameters, all centered at the fixation cross. In each scan with *expanding* rings, the size of the stimulus varies from minimal eccentricity to maximal and then returns to the minimal to start a new cycle. A full cycle is completed in 24s. The order of eccentricity steps was reversed for *contracting* rings. The wedge stimuli, on the other hand, are made up of a sector with a central angle of 45° that rotates around the fixation point. It moves in discrete 20° steps to finish a full circle in either the *clockwise* or *anti-clockwise* direction in each individual scan. The responses to the rings and wedges are used to estimate the eccentricity and polar angle of the visual field representation, respectively. And with the conjunction of both responses, we can estimate the visual field position in polar coordinates.

Scans of the outlined stimulus families (contracting/expanding rings and positive/negative rotating wedges) were interleaved within a session. Throughout every scan, subjects were asked to perform a fixation-dimming task that was controlled by a staircase procedure for the purpose of attention control (Offen et al., 2009).

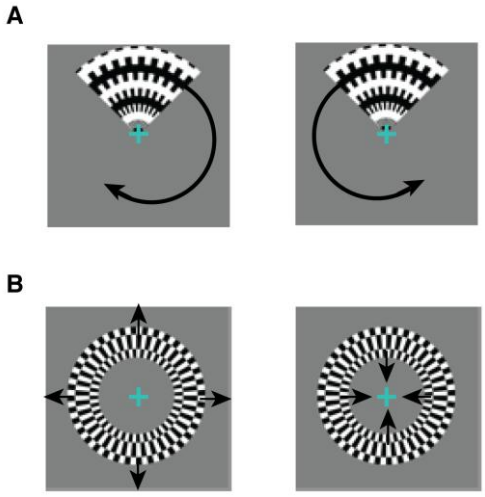

Figure 2.22: A contrast pattern example at eccentricity or angle. Cyan cross, fixation point. Arrows, directions of stimulus pattern: **A,** Wedge clockwise or counter-clockwise rotation; **B,** Concentric rings, expansion or contraction.

2.3.4.2 Functional data collection

MR imaging was performed at 3 T (Philips Achieva, Philips Healthcare, Best, the Netherlands) using an eight-channel SENSE head coil. Foam padding was used to minimize head movements. For blood-oxygen-level dependent (BOLD) fMRI, we used a standard T2* (gradient-echo) echo planar imaging pulse sequence (voxel size $3\times3\times3mm^3$, TE = 35ms, TR = 1500ms, flip angle 75º, FOV = $192 \times 192mm^2$). 32 slices were taken oriented approximately perpendicular to the calcarine sulcus. We used parallel imaging (acceleration SENSE factor 2). In the same session we also acquired high-resolution anatomical T1-weighted MPRAGE images of the whole brain for segmentation and cortical flattening.

2.3.4.3 Functional data analysis

We performed standard analysis with steps for pre-processing and statistical analysis. All these analyses were implemented with custom-written software (mrTools, http://www.cns.nyu.edu/heegerlab/; mrVISTA, Wandell lab, Stanford University) and tools included in the FSL distribution (FMRIB Software Library). Details of the methods are published elsewhere (Offen et al., 2009; Levy et al., 2007; Schluppeck et al., 2006; Offen et al., 2010), but briefly: time series for each voxel were Fourier transformed to calculate

statistical maps for correlation (or coherence), phase and amplitude of the measured response at each voxel (Figure 2.23). The coherence coefficient quantifies the modulation of BOLD signal in response to the visual stimulus (at the frequency corresponding to a wedge/ring cycle) compared with noise (Figure 2.23 lower panel right). The value would approach 1 if the signal is highly correlated with the stimulus, and be close to 0 when the strength of signal modulation was weak compared to the noise. For defining the maps, voxels with greater than 40% correlation (C > 0.4) between the retinotopic stimulus and response were included in our analysis (Figure 2.24). The *phase* at each voxel shows the best-fitting sinusoid at the frequency of stimulus repetition and therefore signals the position of the stimulus in the visual field to which the voxel responded maximally (Figure 2.25). A map containing such information from all the voxels within the scanning coverage can be used to define visual areas.

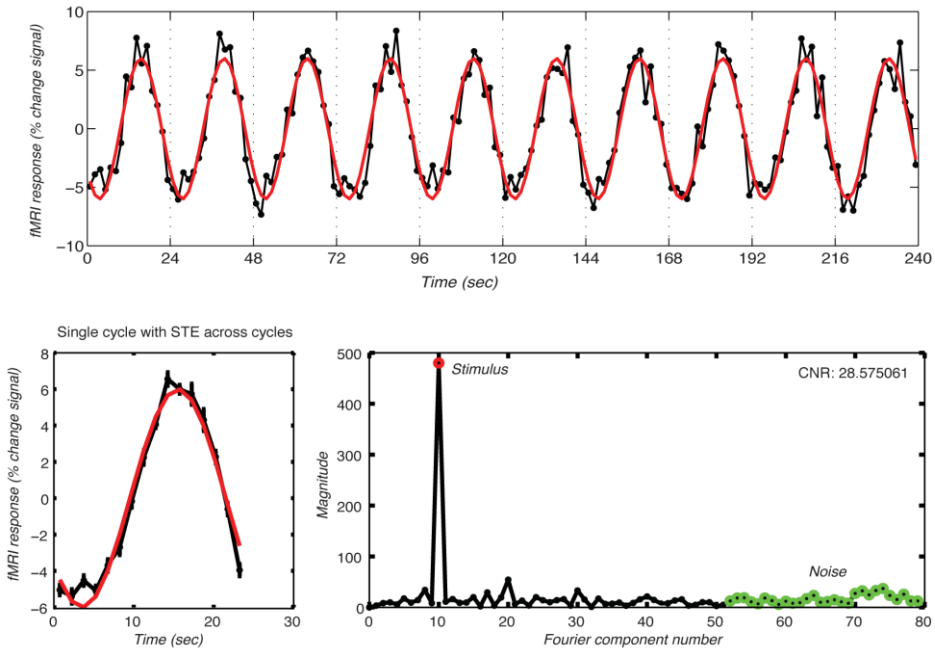

Figure 2.23: Time course of example voxels in a retinotopic mapping data set. The dynamic responses evoked by the wedge stimulus are well modulated. Upper panel, time course of voxel over the averaged, 4-minute scan (black, measured signal; red, sinusoidal fit). Lower panel left, fMRI response average across 10 cycles (colours as in A). Lower panel right, Amplitude spectrum of signal shown in A. The magnitude of the response at the task stimulus frequency (10 cycles per scan) was significantly higher than noise (compare signal marked by red point, with noise, marked by green symbols).

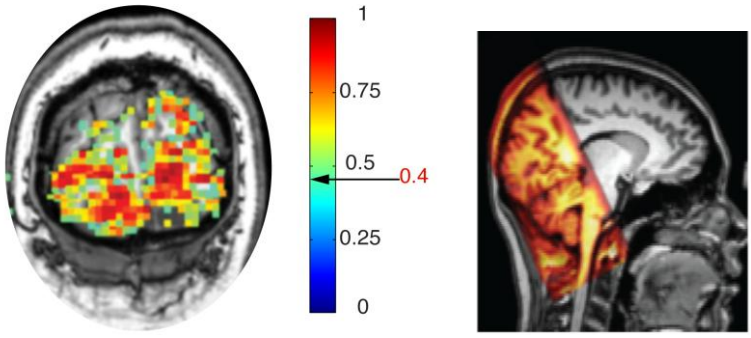

Figure 2.24: Coherence maps when using the expanding/contracting rings as a visual stimulus thresholded at 0.4. The example coronal slice on the left panel is one of the oblique slices through occipital cortex shown on the right.

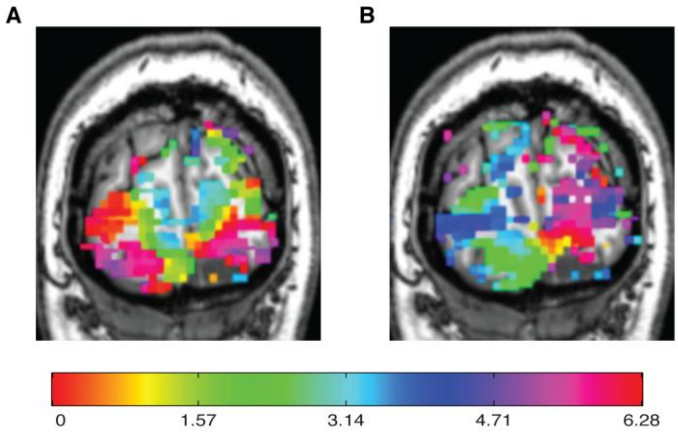

Figure 2.25: Phase maps of eccentricity (stimulus of rings, **A**) and angular (stimulus of wedges, **B**) at the coherence value thresholded at 0.4.

2.3.4.4 Result of retinotopic mapping

For better visualization of the activity induced by the visual stimulus within our regions of interest, we display the functional images on flattened cortical maps. Using the inflation and flattening method summarized in the data pre-processing section of this chapter, we found the well-known strong correlation between responsive visual voxels and stimuli on the flattened occipital patch in our individual subjects. Specifically, we overlaid the responses to wedge and ring stimuli to identify the eccentricity and angular organization of the visual areas.

Eccentricity map

The stimuli of expanding or contracting rings were used to obtain a phase-encoded eccentricity map. As the eccentricity increases, the cortical voxels progressively respond to

the stimuli presented from fovea to periphery in sequence, mapping the anterior to posterior regions of the visual field (along the direction of the calcarine sulcus) (see Eccentricity in Figure 2.26 A).

Angular map

The representation of angular positions for stimuli (wedge) in the visual field is measured with the periodic BOLD signal in the angular dimension. The angular map is color-coded according to the location of the travelling wave phase (see Angular rotation in Figure 2.26 A). As reviewed in Chapter 1, it is known from previous neurophysiological evidence that the visual area borders fall along the upper and lower vertical meridians (VM) and horizontal meridian (HM) in early visual areas (V1, V2 and V3) and are delineated by reversals in the angular representation. Here, I illustrate how each of the cortical regions of the visual system referred to in my work is defined (result shown on flattened maps in Figure 2.27).

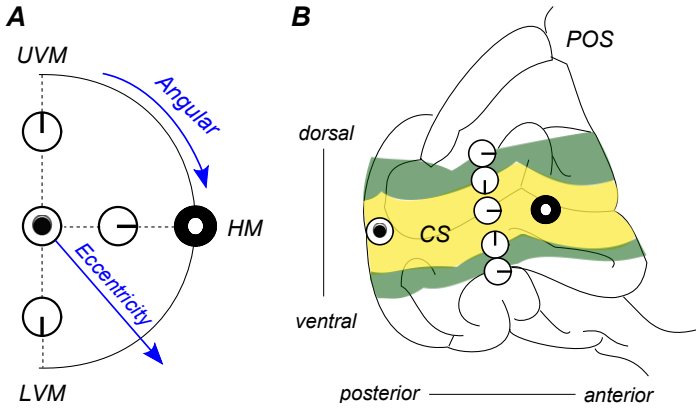

Figure 2.26: Retinotopic organization of visual areas in the left hemisphere. **A** Representation of the visual field. Central fixation is represented by the black dot on the white surround and the periphery by the white dot in the black surround. Eccentricity, upper vertical meridian (UVM), lower vertical meridian (LVM) and horizontal meridian (HM) are also labelled. **B** Sketch of the medial surface of the left occipital lobe showing approximate positions of areas V1 (yellow area) and V2 (green area). The positions of the calcarine sulcus (CS) and parieto occipital sulcus (POS) are also shown. Adapted from Wandell, (1999).

V1: The primary area has a complete representation of the contralateral hemifield. The upper vertical meridian (UVM) and the lower vertical meridian (LVM) define the ventral border and the dorsal border of V1, respectively. The horizontal meridian (HM) lies in the middle,

corresponding to the location of the fundus of calcarine sulcus. As one moves from the center to the border, in a dorsal direction for example, the representation of visual field changes from HM to UVM. A mirrored projection of this is present when moving from the center to the ventral border.

V2*:* UVM and LVM, respectively, also sketch one of the borders of the two distinct parts for V2. Dorsal V2 (V2d) and ventral V2 (V2v), each of which represent a quarter of a reversed contralateral visual field. The V2/V3 border is formed along the HM representation.

V3*:* Analogous to V2, this region is divided into two quadrants. V3d (V3v) follows V2d (V2v) as one shifts dorsally (ventrally), representing the upper (lower) quarter-field. But the representations of V3d and V2d (V3v and V2v) are mirrored.

The outlined estimations of corresponding angular position of voxel response would be straightforward without the hemodynamic delay. By combining the two directions of stimulus presentation (clockwise with counter-clockwise and expanding with contracting), we can compute the delayed hemodynamic response and the phase of the stimulus coded in the visual areas.

I manually delineated the early retinotopic areas for each subject based on the eccentricity map and angular map; the most important information for defining visual field boundaries comes from the angular phase map, however. This allowed me to derive the ROIs used in other functional imaging experiments to investigate the activation relevant to the process of working memory in human early visual areas.

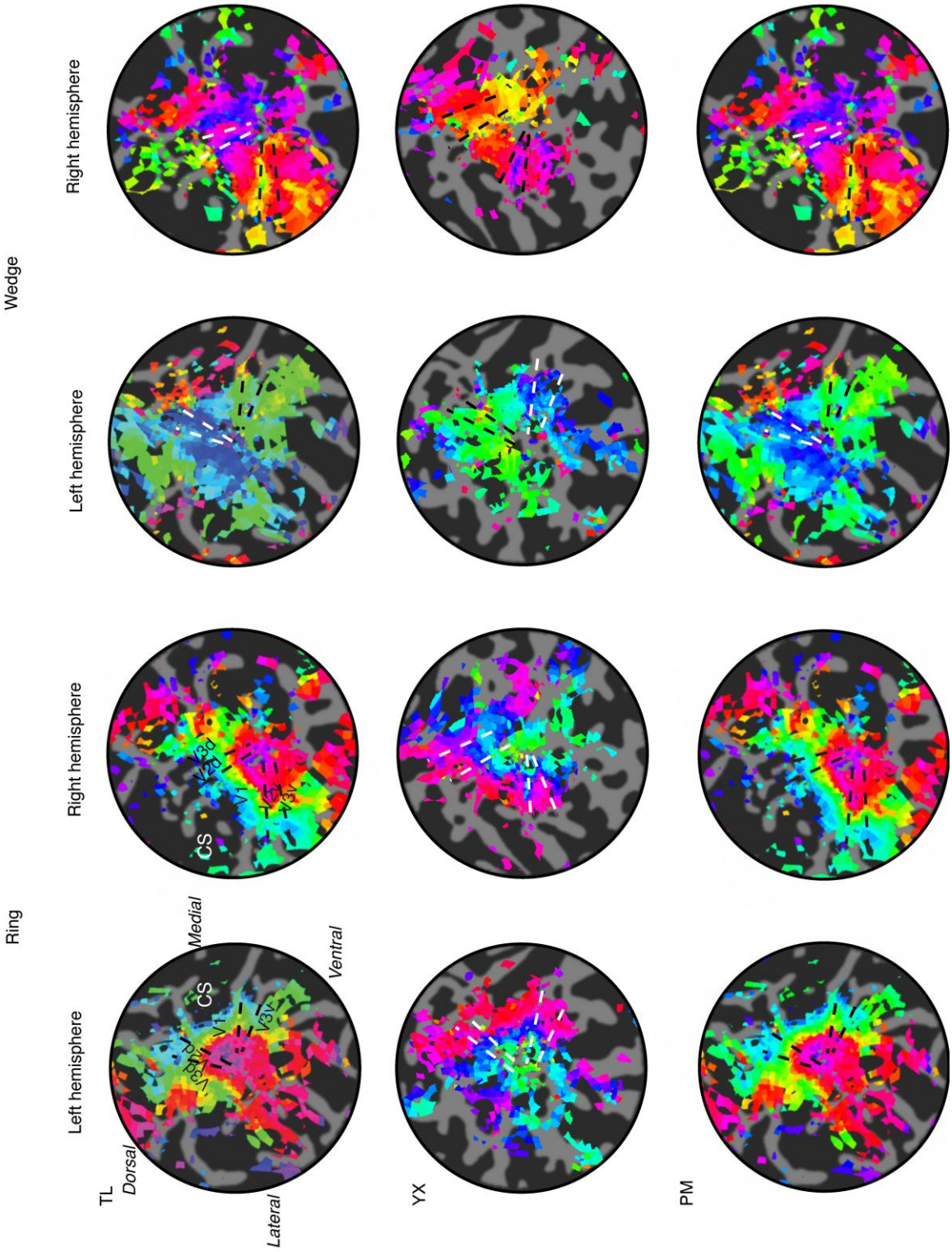
Wedge
Ring
Right hemisphere
Left hemisphere
Right hemisphere
Left hemisphere
CS
V1
V2d
V2v
V3d
V3v
Medial
Ventral
Dorsal
Lateral
TL
YX
PM

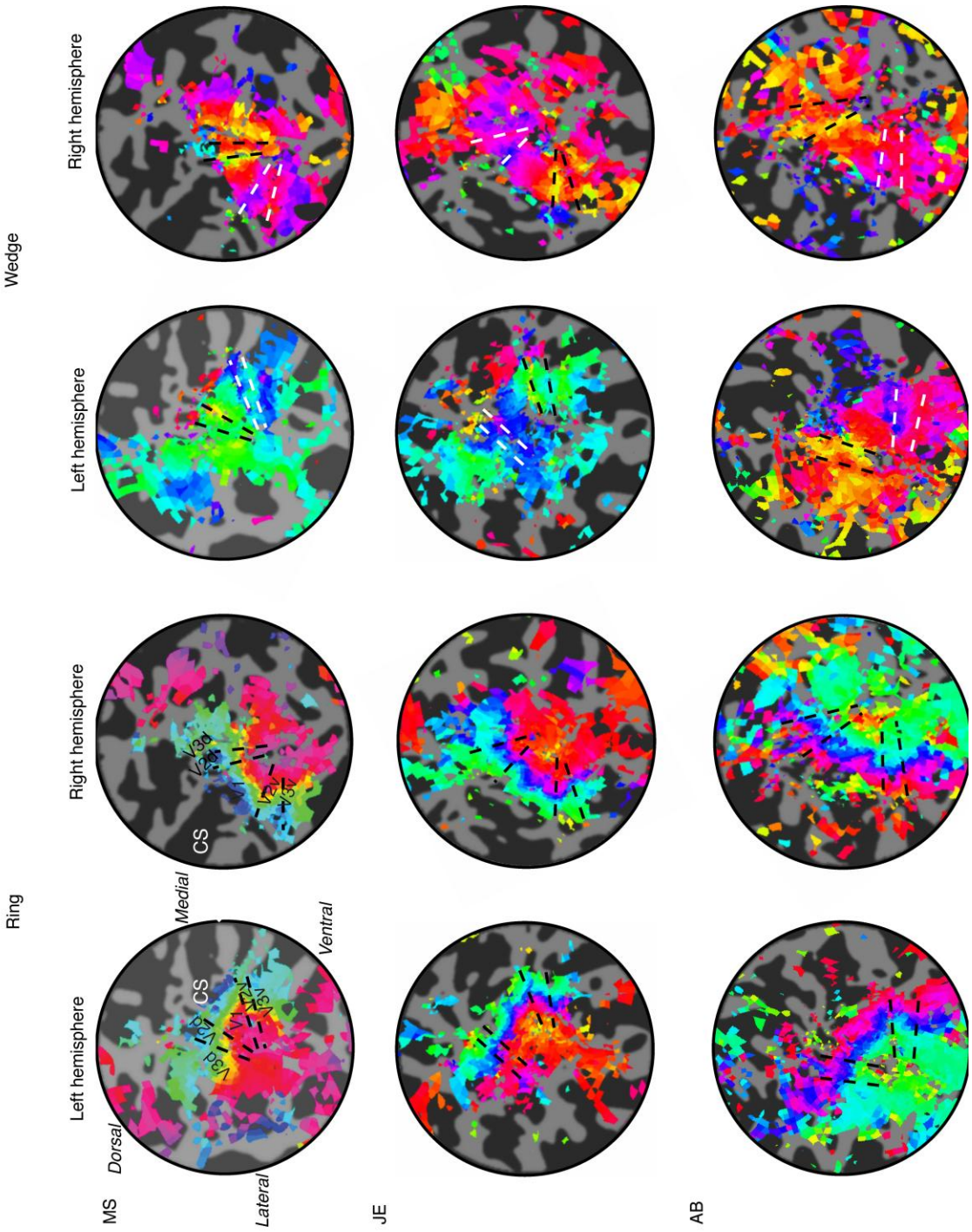

Figure 2.27: Retinotopic maps overlaid by flattened structural maps of early visual areas in both hemispheres for all subjects (n=6). The eccentricity representation computed from the colour-coded response phase of the fMRI signal, using the ring stimulus. The first column, left hemisphere; the second column, right hemisphere. From centre (dashed circle) to the periphery of visual areas, with colour changing from 0 to 6.28 (2π) in the colour spectrum. The angular representation is also computed from the colour-coded response phase of the fMRI signal, using the wedge stimulus. The third column, left hemisphere; the fourth column. right hemisphere. Dashed lines: boundaries of different visual areas in the both hemisphere. CS, calcarine sulcus.

2.3.5 Data Analysis methods

2.3.5.1 General Linear Model Analysis

To gain useful information from functional MRI experiments (from the point of view of neuroscience), we should not only look for voxels that are significantly more activated by certain kinds of stimuli than others, but also try to use the data that we observed to make further inferences about the underlying neuronal processes. Thus, it is necessary to first establish a model of the underlying experimental hypothesis, how fMRI responses are linked to the presentation of stimuli and the subjects' behaviour, and then to use inferential statistics to check the reliability of measured responses. The traditional and most commonly used approach to analyse fMRI data is based on the General Linear Model, which is summarized by the following equation:

$$Y = A_0 + A_1X_1 + A_2X_2 + \ldots + A_nX_n + e \qquad \text{(Eq. 5)}$$

Under the assumptions of the General Linear Model, the observed time course Y at each voxel is equal to a weighted linear combination of several modelled factors (X_i) plus an additive error term (e). Factors X_i comprise regressors that are related to either experimental (functional) or nuisance factors affecting the data. Nuisance factors may include, e.g. linear drift and physiological noise. The parameter weights (A_i) indicate how much each factor contributes to the overall data, and A_0 reflects the total contribution of all factors that are constant throughout the whole experiment. To simplify the presentation, the BOLD general linear model can be re-written in matrix form as

$$\mathbf{Y} = \mathbf{XA} + \mathbf{e}, \qquad \text{(Eq. 6)}$$

where **Y** is the measured fMRI data, the matrix **X** represents the design matrix containing the idealized fMRI responses for different stimulus conditions in the scan, and the vector **A** quantifies the contribution of the time course of each condition in explaining the obtained BOLD signal. The matrix **A** is also often referred to as the beta weights associated with each

volume in the design matrix **X. XA** indicates the multiplication of the design matrix and a weight vector. Figure 2.28 illustrates a diagram form of the GML model.

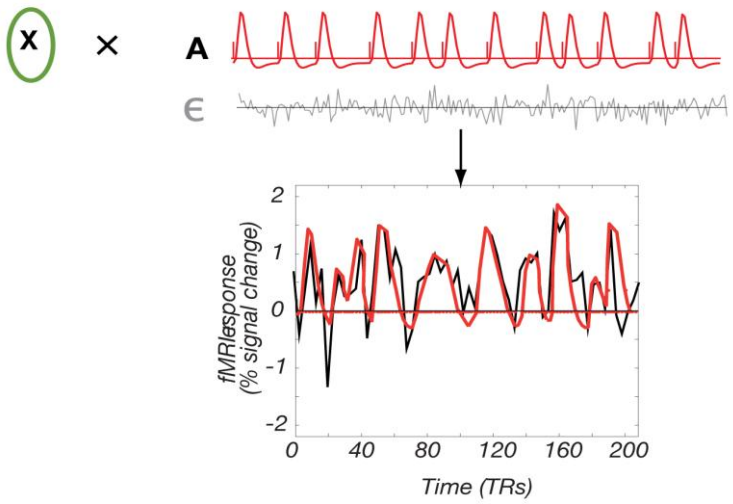

Figure 2.28: A diagram form of the GML model. Black curve, the measured fMRI data of one voxel. The predicted fMRI data (red curves) can be represents by the multiplication of the design matrix **X** and beta value **A**. **Є** represents the error values (grey curve) that quantify the deviation of the measured voxel time course and this predicted time course.

The Design Matrix

The design matrix **X** is constructed under the assumption that the fMRI responses to the stimulus act in an approximately linear, time-invariant manner (Huettel et al., 2009). Its columns contain time courses of regressors for a voxel, and its number of rows corresponds to the number of time points in a scan that is being modelled (see the design matrix in Figure 2.29).

To obtain a set of $\hat{\mathbf{A}}$ that best fit the measured data given **Y**, the fMRI data and **X** the design matrix, often the ordinary least squares solution, which minimizes the sum of squared error (Σe^2) is sought:

$$\hat{\mathbf{A}} = (X^T X)^{\dagger} \mathbf{X}^T Y, \qquad \text{(Eq. 7)}$$

where $()^T$ is matrix transpose and $()^{\dagger}$ is the pseudoinverse (Dale & Buckner, 1997; Schluppeck, et al. 2006).

Nuisance Factors, including physiological motion and other low-frequency disturbances, are often explicitly modelled in the GLM analysis. Because they can substantially reduce the power of statistical tests, it is usually advised to remove these experimental-irrelevant components. This can be done either by preprocessing or modelling noise explicitly as regressors in the design matrix. In this thesis, the time series were high-pass filtered during pre-processing and no further explicit modelling of noise sources was included (Offen et al., 2009; Sapountzis et al., 2010; Sapountzis et al., 2008; Larsson et al., 2003).

Estimation of fMRI response amplitudes

To quantify the activity during different events, we estimated the average amplitude of the fMRI responses in each ROI by multiple linear regressions. There are two different, but related ways to analyze data in this context: (1) assuming a fixed/canonical hemodynamic response function, and (2) assuming nothing about the particular shape of the HRF and only that the response to repeated stimulus presentations is the same (the so-called *deconvolution approach*) (Glover, 1999). To construct a linear model of the underlying neuronal activity during a scan: the onset of each trial / repeat of an event was modelled by placing a '1' at the appropriate time point in that regressor (Dale, 1999). Each regressor (column) in the neuronal response model was convolved with a HRF to yield the corresponding component of the fMRI measurements (Figure 2.29). To sum up, linear regression was used to estimate the desired response amplitudes, i.e. the parameter weight $\hat{\mathbf{A}}$ for each column in the design matrix.

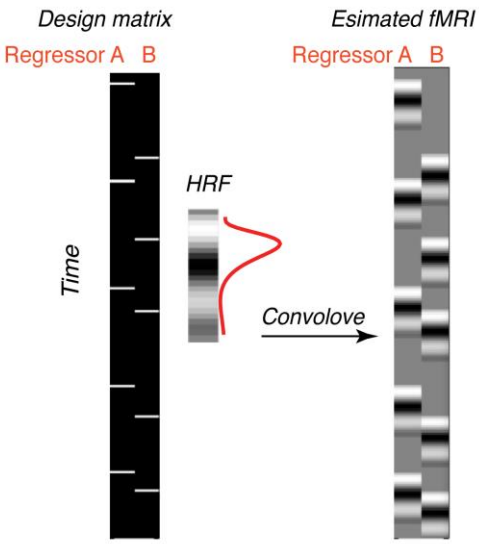

Figure 2.29 Estimation of fMRI response with a design matrix and HRF. A and B are two regressors (event types) separated in two columns. The white thin lines in the design matrix (left) demonstrate the onset of each event in different trials over time. fMRI response (right) can be estimated by summarizing the convolution of functional impulse function (FIR) with the design matrix of both regressors.

Note that the inter-trial intervals in our experiments were randomized because analysis shows that if the inter-stimulus interval (ISI) is properly jittered or randomized from trial to trial, the statistical efficiency afforded by such variable ISI designs can be more than 10 times sufficient than fixed ISI designs (Dale, 1999). However, the randomization of inter-trial intervals and the sequence of different trials with variable intervals may increase the variability of estimated response amplitudes.

To quantify the quality of the model fit for the time courses of individual voxels or across ROIs, we calculated the proportion of variance accounted for by the linear model in the observed fMRI responses (r^2):

$$r^2 = 1 - \frac{var_{residual}}{var_{observed}} \qquad \text{(Eq. 8)}$$

Estimation of Hemodynamic Impulse Response Function

If the functional responses measured by MRI behave like a linear system, the output fMRI response of an arbitrary experimental design can be predicted by convolution of a

hemodynamic response function (HRF) with the design matrix in time courses. The HRF describes the BOLD response to a transient stimulus (also called the "impulse response") (Rosen et al., 1998; Buckner et al., 1996; Blamire et al., 1992).

The shape of the HRF can be divided into three main epochs, which reflect the underlying physiological changes (Blamire et al., 1992; Friston et al., 2002; Dale 1997; Boynton et al., 1996) (see Figure 2.30). The first epoch, reported by some researchers, is termed an "initial dip". It is a period of relatively small signal decrease after the stimulus onset and lasts for about 0.5-1s. The second epoch is the subsequent increase in the BOLD signal, which peaks at 5-8s after stimulus onset. There are mainly two factors explaining this signal increase following the brief decrease of local oxygenation. One is based on the view of metabolism and the other is from the perspective of blood flow kinetics. The first theory links the increased BOLD response to compensational need of glucose, whereas the latter statement emphasizes that increased blood flow is supplied to the cortical areas with activated neurons. The last epoch is a "post-stimulus undershoot" and the final return of the BOLD response to the baseline, occurring 24-30s after the start of the stimulus (Glover, 1999; Heeger & Ress 2002; Duyn et al., 2003).

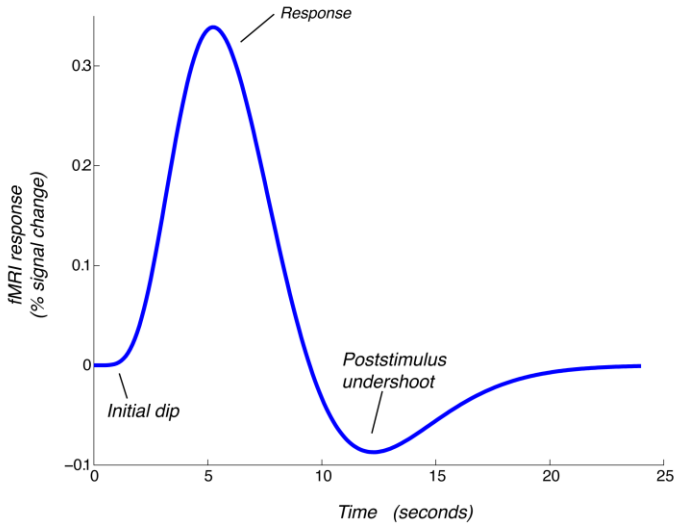

Figure 2.30, Hemodynamic response function (HRF) to an event, approximated by the Glover function with a time to peak of 5.4s (see the value of parameters in the text).

In our last fMRI experiment in this thesis, we used one widespread model of the HRF, a double-Gamma function to estimate the response amplitude for each event (i.e. stimulus 1, delay and stimulus 2 in an delayed orientation discrimination task, see Figure 2.31) (Friston et al., 1998; Glover, 1999; Jezzard, et al., 2003). Specifically, the HRF is modelled as the difference of two gamma density functions (Glover, 1999), which can be modified with five parameters. The following values were used to construct the HRF (Figure 2.30) in the piloting fMRI experiment in Chapter 4. Time to the peak of the first and second gamma density, 5.4 and 10.8, respectively; approximate full width at half maximum (FWHM) of the first and second gamma density 5.2 and 7.35, respectively; coefficient of the second gamma density, which determines the dip of the HRF is 0.35.

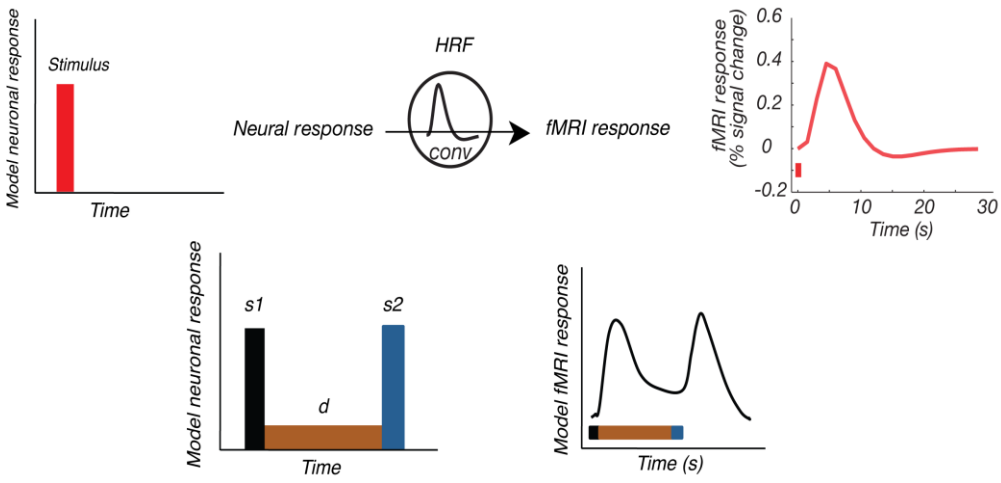

Figure 2.31, Upper panel, the modelled BOLD response (solid red curve) is obtained by convolving the stimulus input (solid red bar) with the HRF. Lower panel, the modeled fMRI responses acquired in the similar way to the result showed in the upper panel when there were three events in a trial of an motion coherence memory task instead. The stimulus input (stimulus 1- S1 [black bar], delay-d [brown bar], and stimulus 2-S2 [blue bar]) were convolved with the HRF.

Deconvolution

Using this double-gamma function as a model to estimate the HRF is preferable when the shape of the actual response is comprised of a gamma-variant. However, if the experiment design and stimulus are more complicated and include more than presentation of simple and

short stimuli, we might expect different shapes of BOLD response across various kinds of task requirements, brain regions and/or subjects. Deconvolution is an approach that allows more flexibility to model the HRF for each condition when various areas in the brain are involved. Instead of explicitly modelling the shape of the HRF, and then using GLM to estimate the amplitude of fMRI response for various events, it estimates not only the amplitude but also the shape of the response. It assumes that the HRF is a weighted linear sum of a set of basis functions. In the experiment for studying the spatial characteristic of working memory with an event-related design (Chapter 8), we estimated the hemodynamic response using this deconvolution method, in order to have a more refined observation of the responses during different trials in each voxel that are distributed across the brain.

Despite the fact that deconvolution analysis is model-independent, it shares a similarity with the synthetic response function composed of two gamma-variants in that both of them are based on the assumption that the hemodynamic responses superimpose linearly over time (Boynton et al., 1996). And with either of them, we can then compute ordinary least-squares estimates of the mean fMRI response time course for our experimental conditions (see Chapters using fMRI methods in this thesis) according to the above Eq. 6.

2.3.5.2 Multivariate pattern analysis

During the last decade, a growing number of studies have shown interest in the use of machine learning classifiers for analyzing BOLD fMRI data and have bore impressive fruits (see review Haxby, 2012 and Norman et al., 2006). Early experiments demonstrated that MVPA could determine the category of object the participant was viewing (Spiridon & Kanwisher, 2002; Tsao et al., 2003; Carlson et al., 2003; Cox & Savoy, 2003; Haxby et al., 2001; Kay et al., 2008; O'Toole et al., 2005), as well as orientation of lines and colours (Freeman et al., 2011; Kamitani & Tong, 2005b; Haynes & Rees, 2005).

Following these initial demonstrations in the visual (sensory) domain, it has even been used as a "mind-reading" tool to reveal which orientation was maintained in the memory (Harrison &

Tong 2009), to predict the participant's intention for the following action (Haynes et al., 2007), and even to differentiate between truth telling and speaking lies (Davatzikos, 2005). In this thesis, we applied multivariate pattern analysis (MVPA) to decode whether early visual areas are also involved in remembering the contrast of a visual stimulus. The following sections provide an overview of some relevant information about MVPA.

The differences between univariate analysis and MVPA

Conventional fMRI analysis detects individual voxels or time courses that significantly respond to the experimental stimuli. The general linear model (GLM) is the most common model used in this univariate analysis of neuroimaging; it is based on multiple linear regressions and has been extended to take into account different properties of the fMRI signals that are analyzed with the technique. The result of a GLM analysis is a set of estimated weights, which reflect the effect size of an event (i.e. stimulus) on each voxel. Then through a statistical inference stage, GLM assesses which voxels are significantly activated by the event. To increase the sensitivity to a specific condition, it averages across those activated voxels within ROIs (Friston et al., 1994, 1995; Worsley and Friston, 1995). However, this traditional approach does not only reduce noise, but may also skip some voxels with relevant cognitive information yet are not statistically significant. Moreover, it inevitably losses the information that spatial patterns may present under different experimental circumstances (Kriegeskorte et al., 2006).

Alternatively, instead of focusing on the response of individual voxels, MVPA methods take advantage of the pattern of activity corresponding to the stimulus conditions. Rather than fitting a particular model to data, these methods essentially work 'backwards' from the data, which is why they are sometimes referred to as *decoding* techniques. Specifically, they try to assign data points to one of two (or more) classes based on the pattern across multiple voxels. Since MVPA exploits the pattern differences in voxels within a ROI, it is more sensitive than

the outlined univariate analysis that spatially averages activity (Kriegeskorte & Bandettni, 2007) (see Figure 2.32).

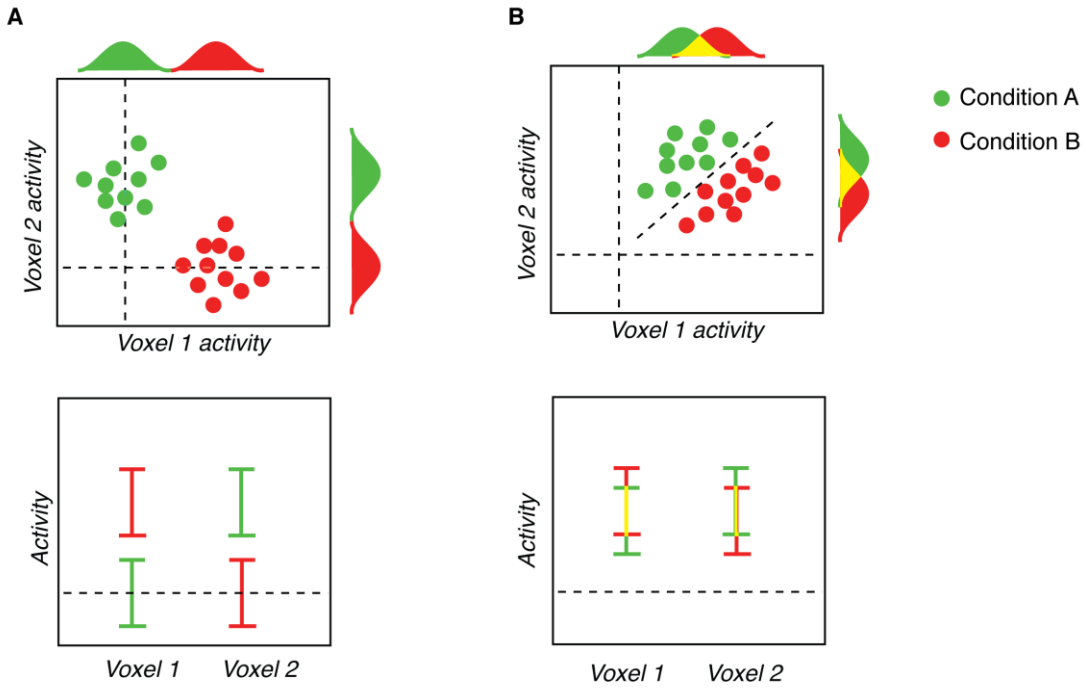

Figure 2.32: Multivariate analysis basics. Most fMRI studies use univariate analyses, in which the data at each voxel (across the many image acquisitions in a given run or session) are treated independently from the data at other voxels. In **A**, Above, the activity for voxel 1 is plotted against the activity for voxel 2, and each circle corresponds to one acquisition, with the colour indicating to which condition each acquisition corresponds. The coloured, filled curves on the right and above this plot represent projections of the distribution of the data onto the vertical (voxel 2) and horizontal (voxel 1) axes, respectively. Note that these projected distributions do not overlap, and thus a univariate analysis discriminates between the two conditions perfectly. Below, the same data are summarized in a traditional univariate manner, with the activity at each voxel plotted. Error bars indicate some measure of the spread of the data in this hypothetical example. Voxel 1 is significantly more active during Condition A than baseline, but is not active during Condition B. Similarly, Voxel 2 is active during Condition B, but not during Condition A. There is a clear mapping between location (voxel) and condition, and if one looks at the distributions of the data from each condition at either voxel (depicted in green and red at the margins of the left plot), they are clearly separable. However, in **B** the situation is slightly more complicated. Both voxels are now active relative to baseline during both Condition A and Condition B, and there is no clear mapping between voxel and condition. Furthermore, if one looks at the distributions of data for each condition for each voxel, there is significant overlap, and the conditions might be difficult to distinguish without large amounts of data. However, if one looks at both dimensions simultaneously, it is obvious that the data from each condition occupy a distinct region of the two-dimensional space and that one need only draw a line between the data clouds to distinguish them. Linear classifiers can perform this basic partitioning of space with arbitrarily many dimensions (or in this context, voxels) and arbitrarily many classes of data (in this context, conditions), drawing

hyperplanes between different classes of data. Figure and legends modified based on Cox & Savoy, (2003)

What is classifier?

MVPA learns from the relationships between discrete independent examples (training data) and a dependent variable for predicting the unknown variable for testing data. In the context of functional MRI in neuroscience, both training data and testing data are discrete examples that denote the voxels. The dependent variable could be the stimulus type used in the different experimental conditions, which we often labelled as *class*. A classifier is a function that has a number of parameters obtained from learning the relation between classes and training data. It can be then used to predict the types of stimuli for the testing data set. The extensive use of classifiers in the study of visual neuroscience is a group of linear discriminative functions (Kippenhan et al., 1992; De Martino et al., 2008; Haynes and Rees, 2006; Hansen, 2007; Mitchell et al., 2004; Norman et al., 2006; O'Toole et al., 2007 and Pereira et al., 2009 for reviews). They can be written in the form of:

$$g(x) = w_i \times x_i + w_o \qquad \text{(Eq. 9)}$$

where vector x_i represents the amplitude of fMRI response from voxel i, w_i is a vector of weights acquired during training process for each i, and w_o is the overall bias. If $g(x) > 0$, then the stimulus type of that corresponding voxel will be labelled as class A, and if $g(x) < 0$, it will be class B. This formula shows that each voxel affects the predictive result solely via weight without interaction between each other, providing a direct measure of influence on prediction for each voxel (Figure 2.33). The measure used for performance evaluation of a classifier is *accuracy*, which counts the proportion of correctly predicted trials out of the total number of examples in the testing dataset.

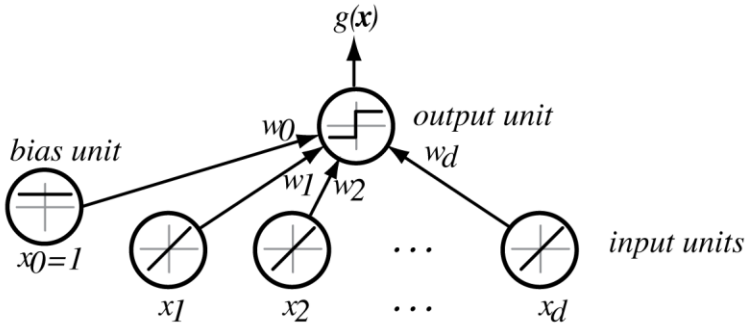

Figure 2.33: A simple linear classifier having d input units, each corresponding to the values of the components of an input vector. Each input feature value x_i is multiplied by its corresponding weight w_i; the effective input at the output unit is the sum all these products, $\Sigma w_i x_i$. We show in each unit its effective input-output function. Thus each of the d input units are linear, emitting exactly the value of its corresponding feature value. The single bias unit always emits the constant value 1. Adapted figure and legends from: Duda et al. (2001)

Commonalities and differences between classifiers

Besides the linear classifiers mentioned above, there are other more sophisticated classification functions, such as nonlinear classifiers with different kernels and neural networks (Cox and Savoy, 2003; Davatzikos et al., 2005; Hanson et al., 2001). However, the application of nonlinear approaches has not become a focus in the fMRI data analysis since past evidence showed that they have not outperformed the former group of classifiers (Kamitani & Tong, 2005b; Cox & Savoy, 2003). And it potentially has a problem of overfitting, which can be alleviated to some extent by linear methods. Therefore, in this section, we will only review and compare two popular linear classifiers, which are Fisher's linear discriminate analysis (LDA) and Linear Support Vector Machine (SVM).

The techniques have commonalities in that both LDA and SVM have parameters containing a set of weights of activity for voxels in the region of interest in different experimental conditions (Misaki et al., 2010; Mur et al., 2009; Pereira et al., 2009). These weights are summed and then feed into a decision function (a hyperplane in multidimensional space), which generates a threshold to judge the presence/absence of the stimulus or a cognitive state.

They also possess distinct features of their own. LDA determines the discriminant dimension that maximizes the ratio of between- and within-class variance. There is an analytic solution

for LDA, which can be written as a matrix equation and solved efficiently using standard linear algebra methods – it is therefore associated with less computational cost than SVM. However, computational cost grows as the dimensionality of data increases, particular for estimating the data covariance-matrix and matrix inversion at different steps. Thus, it is often used in conjunction with voxel selection to reduce dimensionality. More importantly, the use of LDA is based on the assumption that the distribution of response from each class is *multinormal* with equal-covariance and statistically independent across voxels (Hastie & Zhu, 2001; Carlson et al., 2003) (Figure 2.34). However, for many data sets, the performance of LDA is degraded due to violation of this assumption, because the inversion of the covariance matrix is unstable. One means for alleviating this problem is to neglect covariance between voxels by setting the off-diagonal element in the covariance matrix to zero and using the vector orthogonal to the hyperplane instead (Dinstein et al., 2007). Meanwhile, LDA demands large enough examples to estimate its covariance matrix, therefore requires using methods to generate more examples, such as extreme voxel selection or nested-cross-validation.

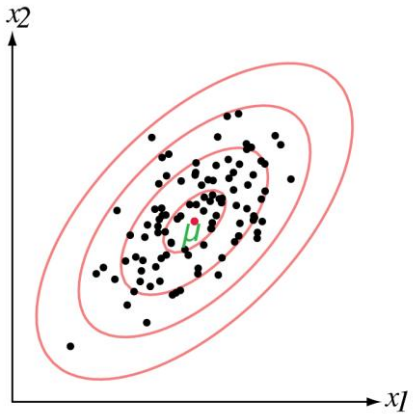

Figure 2.34: Samples drawn from a two-dimensional Gaussian lie in a cloud centered on the mean μ. The ellipses show lines of equal probability density of the Gaussian. Figure and legends from: Duda et al. (2001).

Like LDA, a linear-SVM also needs to draw a decision boundary to separate different classes (Cox and Savoy, 2003; Hastie & Zhu, 2001). However, unlike the former method, the

hyperplane selected by a SVM is controlled by a variable called the *functional margin*, which is a quantity that reflects how well the classifier can discriminate between classes (see Mur et al., 2009 for review). The geometric margin is a measure of distance from the hyperplane to the *support vectors*: the support vectors of the hyperplane are the nearest training data points at the edge of the margins. An optimal separating boundary is found to maximize this distance and, in practice, is capable to generalize well for unseen testing examples. In other words, linear-SVM chooses a classifier that maximizes the margin to obtain highest accuracy for classification. Figure 2.35 is an illustrative linear-SVM classifier with two voxels represented in a two dimensional space. Another characteristic of SVM is that it is more robust to different distributions of data, which is ideal for data sets that do not follow a Gaussian distribution (note that for LDA, this is an important assumption).

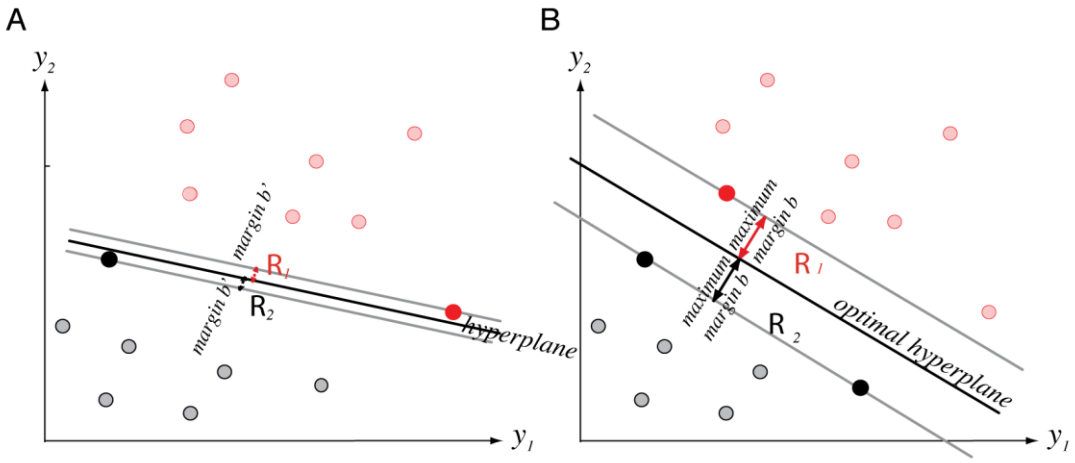

Figure 2.35: Training a support vector machine consists of finding the optimal hyper-plane, that is, the one with the maximum distance from the nearest training patterns. The support vectors are those (nearest) patterns, a distance *b* from the hyperplane. In **B**, the three support vectors are shown as solid dots. Compared to the margins *b'* in **A**, the optimal margins are larger. Figure and legends modified based on Duda et al. (2001)

Framework of classification

In this thesis, MVPA was used following some basic pre-processing steps that are summarized into a framework shown in Figure 2.36.

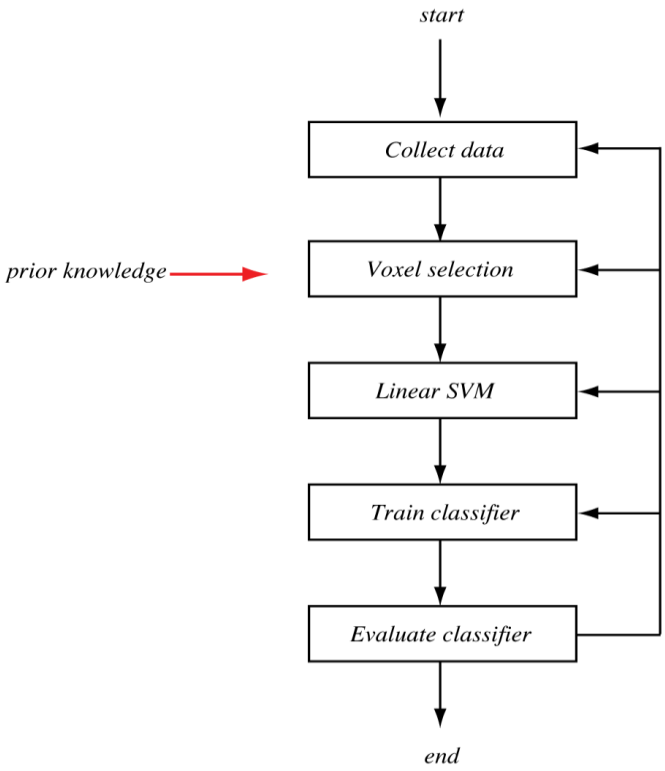

Figure 2.36: the framework of MVPA. Figure and legends modified based on Duda et al. (2001).

Voxel selection

Voxel selection refers to the fact that we need to decide which voxels would be included in the classification. For the experiments in this thesis, it is based on the visual responsiveness for the purpose of catching voxels with discriminative information. Most studies used traditional univariate analysis to localize the voxels in the anatomical ROI with a statistically larger response to the stimulus compared with baseline (Cox and Savoy, 2003). The voxel selection approach we employed is that we computed the coherence values (the ratio between the amplitude at the stimulus frequency and the square root of the sum of squares of the amplitudes at all frequencies) for all voxels and then selected those above a given threshold. This dimensionality reduction procedure yields a new data matrix with a reduced number of rows (number of voxels) while keeping the columns the same (i.e. number of trials).

In addition to the question of how to select the voxels to be used in the classification, another question that needs to be answered is *how many voxels* should be included in the final

analysis? Several studies have investigated the effect of voxel numbers on classification accuracy (Mitchell et al., 2004, Guyon & Elisseeff, 2003; De Martino et al., 2008). It was found that for linear SVM, in general, that the performance improved as more voxels are included and that the accuracy levelled off usually above 100-150 voxels. Nevertheless, other experiments (i.e. Kamitani & Tong, 2005b) used more voxels, sometimes 400 and more, to run the classification, and it has been shown that 500 may be a reasonable upper limit where there were only 10 examples / trials.

An important consideration is that the decision concerning voxel numbers needs to be a compromise between including more informative voxels and excluding more noisy ones (Pereira et al., 2009). As more voxels are selected, the performance of classification increases until it reaches an asymptote. If the number of voxels is increased beyond reasonable limits, more dimensions will be added in, which has been observed in some cases to degenerate the performance of machine learning due to increase of noise and overfitting (refer to the following section). Therefore, the number of voxels included can vary as number of examples is concerned, as well as the approaches of classification, kernel / classifier, amplitude of signal and the difference between the examples.

Creating examples

After the step of voxel selection, time series were rearranged into a matrix: the number of voxels selected from a 3D brain volume was organized as row vectors with properties from each trial in the different columns. Different approaches have been used to summarize the responses in voxels to be put into the different columns. Some studies addressed this issue with the beta weights obtained for each trial using GLM (Haxby et al., 2001; De Martino et al., 2008). Other recent reports employed MVPA with raw fMRI data (% signal change), including individual time points or after averaging the response within a given period of time as examples (Cox & Savoy, 2003; Mitchell et al., 2004; Haynes & Rees, 2005; Kamitani & Tong, 2005a; LaConte et al., 2005). These temporal intervals contain the expected signals that

represent the cognitive process of interest during each trial. In our present work, we adopted the last method: calculating the average response from each selected voxel over a given number of time points as input for MVPA.

Splitting data and Cross-validation

Since the collected signal response was confounded by noise, there is potentially a problem of over-fitting the data by fitting not only the information related to the signal of interest but also noise. In order to limit the influence of noise, and further, to avoid circularity of reasoning, we need to train a classifier to be robust to the noise with sufficient examples whilst detecting the different patterns in the datasets. Because discriminating 'authentic' information variability from noise is often difficult, different procedures are used for fMRI data analysis. Besides the aforementioned voxel selection procedure, a variety of options exists to avoid over-fitting, among which is the widely used cross-validation approach. This provides a method for finding more reliable parameters of the discriminative function.

The performance of a classifier learned from *training examples* is assessed by the accuracy of generalization to classifying *testing examples*. This involves a step of splitting examples in the dataset into two parts in one of several possible ways, which have variously been used in fMRI studies.

One extreme instance is called leave-one-out cross-validation. This method trains the classifier on all examples except one, whose label will be predicted. The same procedure is then repeated for each example in the matrix. The prediction accuracy depends on whether the new labels for each trial match the actual type in the testing set.

The set of all examples can also be divided for the purpose of training and testing (Figure 2.37). This is one special instance of another procedure denoted as a k-fold cross-validation, where k is the number of partitions into which the data set is separated. fMRI experiments often set k to be 2, 5 or 10, corresponding to leaving out 50%, 20% and 10% of examples in each fold, respectively. With enough runs, the whole MRI data set can be also be divided

based on these natural data units. For example, by leaving out one run for testing, and use the remaining runs for classifier training. During data splitting, it is important to check whether each fold contains balanced examples from every sort of experimental conditions. This measure assures that classifiers learn data distribution with sufficient information, thereby providing more accurate prediction performance.

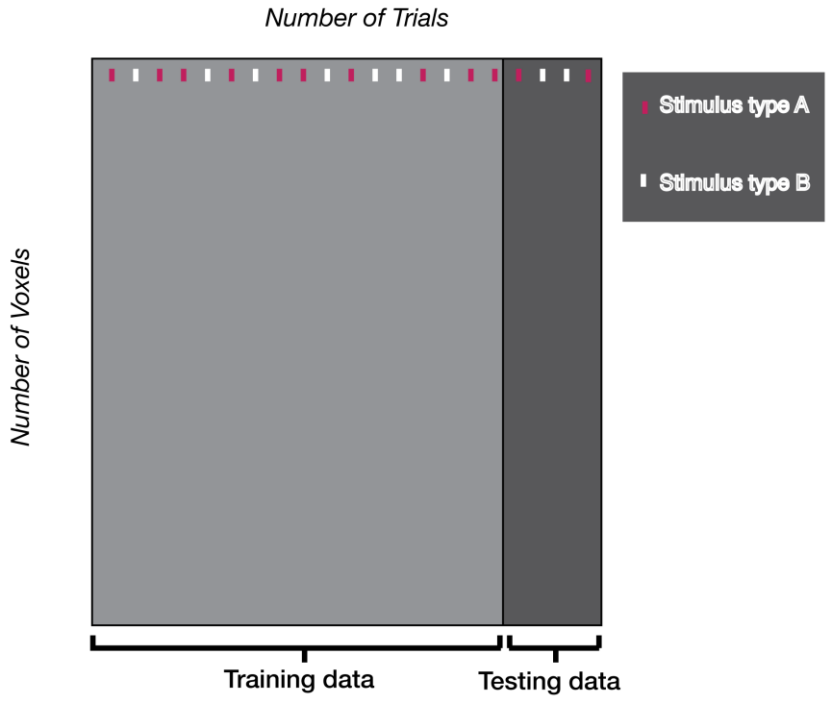

Figure 2.37 is an illustration of dividing the data set into training and test data for classification. The performance was repeated for k-fold cross-validation.

Which voxels drive the classifier?

If the classification analysis shows that there are reliable patterns of activity in the ROIs for different experimental conditions, we can also access which voxels have more of a crucial role in driving the classifier. The absolute value of the weights from linear classifiers in Eq. 9 directly reflects how each voxel affects the decision of drawing the hyper-planes with no interaction with other voxels (Kamitani & Tong, 2005b). For example, voxels that responded similarly to the two experimental conditions being compared would have a weight value near 0, whereas more informative voxels that responded differentially would have a high absolute weight value, indicating that they are more important in contributing to the overall

classification. This straightforwardness allows us to visualize the weight of voxels in the ROIs in an analogous way as statistical maps. Some investigators have used it to evaluate whether the same set of voxels contributed to the decoding of two or more categories (Clithero et al., 2011; Liu et al., 2011; Nichols et al., 2010; Kaplan & Meyer, 2012). However, though larger weights imply more decisive voxels, recently researchers indicated a caveat that linear SVM picks up on correlated changes in activation across voxels, which cause their weights to decrease proportionally (Nichols et al., 2010). A possible consequence could be that these correlated voxels with smaller weights also play an important role in deciding the discriminating hyperplane (Pereira et al., 2009; Clithero et al., 2011).

Effect of fMRI study design on classification performance

Although block designs and event-related designs can both be used with MVPA, block designs often achieve higher accuracy because they yield a higher functional contrast-to-noise ratio, and thus estimates of the response patterns are better with less noise interference. On the other hand, event-related designs can be subject to interaction between the rapid successions of stimulus events and affected by the sluggish hemodynamic response in the time domain (Mur et al., 2009). Despite these drawbacks, event-related designs have their own advantages for both experimental design (cognitive neuroscience) and statistical reasons, which have been presented in the section on fMRI design methods in this chapter. For our work in the temporal domain with MVPA, we used an event-related design because it reduces predictability for the subjects in the experiment, and it is less susceptible to habituation effects. Furthermore, it provides with us an opportunity to observe either transient or delayed activity during consecutive occurring events in time more readily than a block design is capable of (Kriegeskorte et al., 2006).

Chapter 3: Aims and introduction to the experiments

The purpose of this Ph.d. project is to investigate the role of early visual cortex in the process of working memory (WM). Previous studies suggest that some elementary visual features are represented in working memory at the sensory level. In this present work, visual stimuli with three different attributes were used: (1) coherence of random dot kinematograms (RDK), (2) the contrast of gratings and pixel noise patterns (3) orientation of gratings.

In the first part of my thesis (Chapter 4), I used RDKs with different levels of coherence to examine the temporal properties of working memory for motion. A two-interval forced-choice procedure with different delay durations was used to measure the psychophysical threshold. By introducing 2 types of masks separately into 4 phases of the retention interval, respectively, we further investigated which temporal phase is crucial for visual short-term memory, and whether information is selectively retained in early visual cortex. We also assessed the suitability of these kinds of stimuli for probing the neural correlates of working memory for motion with brain imaging.

The next set of experiments (Chapter 5) focused on different stimulus attributes, especially contrast. The properties of early visual areas (V1, V2 and V3) in processing information on perceived contrast and orientation of stimuli have been well established, especially for V1 (see relevant section in the chapter of Introduction), yet the role of early visual cortex in visual working memory is still unclear. We approached the temporal and spatial aspects of this question with psychophysics as well as brain imaging (fMRI).

In terms of temporal characteristics, the ability to remember contrast (up to 5s duration) was assessed using sinusoidal gratings. This brought about an important question of what information contained in a grating stimulus is actually encoded and retained? A spatial pattern (pictorial representation) with different contrasts, such as a sine-wave luminance profile or a more abstracted representation of contrast (possibly even on a segment within a stimulus)?

Using random pixel noise patterns enabled us to resolve this question. This answer is crucial for the understanding of representation of contrast in the early visual cortex. Results from this behavioural experiment also provide fundamental evidence for our subsequent fMRI experiments.

As reviewed in Chapter 2, one of the strengths of fMRI is that it allows researchers to connect function and anatomical structure in the human brain with sensation, perception and different kinds of behaviour. Here, we used BOLD MRI to establish the neural correlates of WM for stimulus contrast in early cortex. However, the spatial resolution of BOLD fMRI makes it impossible to distinguish the activities evoked by the many stimulus types that we used for the psychophysical experiments: e.g. cortical responses will be very similar for a particular pixel noise pattern and its contrast-reversed version. The results from psychophysics strongly suggested that it is indeed the contrast information rather than an iconic representation that was held in working memory. We therefore chose to use sinusoidal gratings to study the correlation between our behavioural results obtained from psychophysical measures and fMRI responses, as this opened up the possibility of using well-established advanced analysis techniques, such as multivariate classification / pattern analysis (MVPA) on our data. A growing number of studies have shown that patterns of activation may offer substantial extra information related to distinct stimuli other than the averaged activity. Recently, Harrison and Tong successfully decoded working memory of stimulus orientations in early visual cortex using this multivariate pattern classification analysis. Using similar methods, two fMRI experiments described in Chapter 6 and 7 were conducted to investigate whether classifiers are also able to decode perceived and remembered contrasts and orientations in early visual cortex, respectively.

Finally, to tease apart different spatial aspects of visual working memory, we designed a psychophysical experiment (second part of Chapter 5) in which subjects had to transfer visual information between the left and right visual fields; the aim of this experiment was to probe whether contrast information is spatially localized (to the corresponding cortical hemisphere)

in a visual working memory task or whether information is encoded in a more abstract representation.

Building on this behavioural evidence, an fMRI experiment comprising 3 different tasks was designed to explore possible neural mechanisms underlying working memory in the human brain (mainly primary visual cortex) in Chapter 8.

Chapter 4: The role of early visual areas in working Memory for Motion Coherence

Abstract

Several psychophysical studies of visual short-term memory (VSTM) have shown that different motion attributes, such as direction and speed can be stored in memory with a high level of precision. We reported three psychophysical experiments and one pilot fMRI experiment in which we investigated the nature of the representation of stimulus *coherence* in VSTM. In the section for psychophysical experiments, we first examined the ability of storing motion coherence using a delayed discrimination procedure. Next, we introduced a mask right after the offset of the first stimulus to examine its influence on VSTM. To further explore the temporal characteristics of VSTM and to determine whether the memory representation of motion coherence is selectively retained, we displayed the mask with two types of coherence levels at different time points during the memory interval. During the delay period, a random- or directional-motion with mean coherence (definition explained in Experiment 3) was presented briefly either at the beginning, in the middle or at the end of the delay period. The results showed that the motion coherence could be stored with a high accuracy. We also found that discrimination thresholds increased significantly when a mask was presented regardless of the masking timing. Further, the mask is more effective when its coherence is similar to the stimulus intensity of the remembered feature. These results suggest that VSTM for motion coherence is represented selectively rather than distraction. Moreover, this selectivity supports the sensory recruitment model that the same neural mechanisms involved in the processing of motion coherence may be recruited for its memorization.

In the section of fMRI experiment, we performed a pilot fMRI experiment to measure the response in V1 and V5/MT to probe the effect of VSTM and visual attention on these two cortical areas that are sensitive to motion. A coherent motion detection task and a delayed coherence discrimination task were included in this experiment to set differential demands of memory and attention and the responses during the delay intervals were measured. Our result

illustrated that both regions exhibited sustained responses throughout the delay period in detection task where attention is highly required. For the coherence discrimination task when subjects were asked to remember the coherence of the first stimulus, only V1 but not V5/MT showed comparable response. These piloting results may reveal different neuronal representations of motion coherence in V1 and V5/MT as well as possible distinguished mechanisms underlying VSTM and attention. Succeeding fMRI experiments with more advanced analyzing method were executed to further investigate the characteristics of these two cognitive processes.

4.1 Psychophysical evidence

4.1.1 Introduction

Psychophysical measurements provide a powerful approach to investigate the internal representation of different stimulus dimensions behaviourally. As discussed in chapter 2, psychophysics can also be used to probe the mechanisms underlying the *encoding* and *storage* of visual stimulus information. Several previous studies have demonstrated that visual memory has very good fidelity over time, for different visual attributes (summarized in Magnussen & Greenlee, 1999). For example, they reported a study for remembering spatial frequency of simple gratings, which showed that this feature could be perfectly retained for up to 30s. Compared to the extensive studies using orientation, spatial frequency and colour, much less is known about motion coherence. Therefore, in the first experiment of this chapter, we examined the memory storage of motion coherence.

In addition to measuring memory performance with a delayed discrimination paradigm as in some previous reports, many other studies used 'memory masks' to further explore the characteristic of working memory for a variety of visual features. It was suggested that when a task-irrelevant stimulus is displayed at different time points during the retention period but beyond the time window of masking sensory input, subjects' performance was impaired. The majority of these experiments presented the mask stimulus halfway through the delay period.

In our second experiment, the mask was immediately presented after the offset of the first stimulus in each trial, in order to test interference with the encoding stage. In particular, this early time window is assumed to be essential for transforming the iconic representation to a more durable representation in working memory, which is conceptualized as consolidation (Chun & Potter, 1995). It has been estimated that this process is accomplished approximately within 500ms, but some of the studies showed even briefer duration for consolidation of one single item. For instance, Vogel and colleagues sought for the length of consolidation period by varying the interval between the mask stimulus and the first stimulus (Vogel, Woodman & Luck, 2006). They claimed that memory performance improved as the stimulus onset asynchrony (SOA) increased and gradually reached an asymptote. They concluded that consolidation for one item ends by as little as 50ms. Despite this slight discrepancy of time course among the previous studies, they uniformly performed a change detection task with an array of stimuli to observe the role of consolidation in the capacity of working memory. However, this thesis focuses on the memory precision of detailed visual features, rather than the storage limits for arrays of stimuli. Therefore, the second experiment of this chapter was designed to see whether the robust maintenance of motion coherence could be masked at the initial stage of the retention period.

Beyond the early encoding stage during the memory interval in Experiment 2, we also investigated other phases within the interval of maintenance in Experiment 3. By varying the time point at which the mask was presented, we examined the temporal dynamics of holding information for motion coherence in memory. These temporal characteristics may further indicate the role of sensory visual areas in working memory.

One common approach in the literature for investigating the represented visual information in the early visual areas is to manipulate the property of the mask. The influence of a memory-irrelevant visual stimulus (mask) often indicates that areas which are responsible for processing sensory information are also engaged in the working memory of visual information, because encoding an irrelevant stimulus disrupts the maintained representation

within their shared functional areas. However, it does not provide evidence of whether the mask interferes with the representation of the remembered stimulus or not. By varying the mask's property along the dimension of interest, investigators can discover the nature of the masking effect in more detail. For instance, it was found that a mask stimulus had its maximal disruptive effect when it shares visual features and/or spatially overlaps with the stimuli maintained in memory (Pasternak & Zaksas, 2003). This result has been thought to support the idea that the corresponding perceptual and memory coding share a common representation. Some studies further scrutinized the degree of similarity in association with the masking effect (Magnussen, et al., 1991; Mckeefry et al., 2007; Nemes, et al., 2011). They found that within a certain range, the masking effect is reversely proportional to the resemblance of the target stimuli. This result has been interpreted to be analogous to the model of lateral inhibition for processing sensory information. Figure 4.1 presents a brief scheme of this mechanism. It illustrates that the mask activates neurons that are selectively tuned for its (preferred) visual feature, and consequently suppresses the activity of other nearby channels, which are involved in retaining the stimulus feature. Here in this experiment, we exploited two particular coherence types (0% and mean coherence) of a memory-masking stimulus that were presented at different time-points during the delay interval to access the characteristics and the selectivity of the WM for motion coherence.

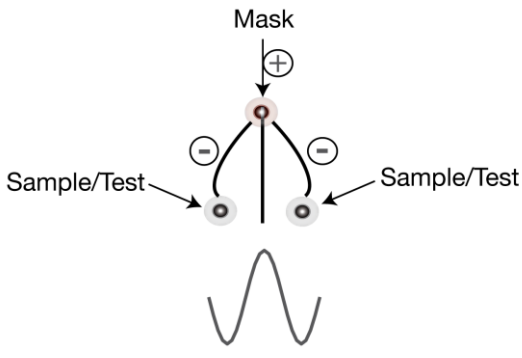

Figure 4.1: A possible model of lateral inhibition underpinning memory masking. The masking stimulus selectively activates a narrowly tuned feature specific channel, which inhibits the neighboring channels for maintaining stimulus features.

4.1.2 Experiment 1: The storage of motion coherence in short-term memory

Previous psychophysical studies have shown that representation of elemental visual features, such as colour and spatial frequency, can be sustained in memory almost without loss of information, whereas others (i.e. contrast and orientation) decay over time (see review Pasternak & Greenlee, 2005). In contrast to these spatial features of gratings, which were commonly used to test limits of short-term memory, it is not clear whether motion coherence information can be maintained in memory. Therefore, in this experiment, we assessed the mnemonic characteristic for coherence of random moving dots using the conventional two-alternative-forced-choice paradigm of a delayed discrimination task. Thresholds were measured for conditions with delay intervals of either 2s or 8s, which represented the "short" and "long" retention periods, respectively. These measurements also provided a fundamental behavioural reference for the planned fMRI experiments.

4.1.2.1 Methods

Observers

Three participants with normal or correction-to-normal vision participated in the task. One participant was experienced in the psychophysical experiment, and the others were naïve with respect to the purpose of this task.

Visual stimuli and Procedure

Stimuli for the experiment were generated using MATLAB and MGL software (for more details see Chapter 2). The observers sat in the dark room, were instructed to fixate at a fixation cross presented at the centre at the screen throughout each block of the experiment. They viewed the stimuli binocularly at a viewing distance of 57 cm.

Subjects performed a two-alternative interval forced choice procedure (2IFC) to measure the discrimination threshold in different conditions. In each trial of this psychophysical experiment, a fixed stimulus and a test stimulus were sequentially presented within one of the two inter-stimulus intervals (ISIs): either 2s or 8s. The stimuli and experimental procedure are schematically described in Figure 4.2. The stimuli were moving dots with different levels of

coherence. They were displayed on a black background. All the dots presented during the stimulus intervals moved at a speed of 3 degree/second. 50 white dots were presented within the circular stencil (radius 5°). The direction of motion was kept constant as 0°, meaning that the dots always moved to the right-hand side of the observers.

As outlined in Chapter 2, we used the method of constant stimuli and implemented two different fixed coherences (30% coherence and 40% coherence) to increase variability and prevent predictability and the formation of a long-term memory of the standard. During each stimulus interval (500ms), a proportion of dots moved coherently (coherence level) to right, and the rest of them (noise dots) moved stochastically to any direction, which were randomly redrawn on each frame. Five different levels of coherence increment were selected based on the pilot data for each participant. This ensured that all the stimulus levels contribute to a usable portion of the psychometric function. Within each trial, one of these five increments was randomly chosen and was added to one of the fixed coherences. This summed coherence and one of the fixed coherence (30% or 40% coherence) were then randomly assigned to the two stimulus intervals. The blocks of trials with 2s ISI were interleaved with 8s ISI to minimize any learning effect. Subjects were asked to make a choice between these two stimuli, and to report which interval contained the moving dot stimuli with a higher coherence level. Their response had to be given within a 1s response window, otherwise it was regarded as an incorrect response. Feedback was signalled at the end of each trial. The gap between each trial was 1 second (Figure 4.3).

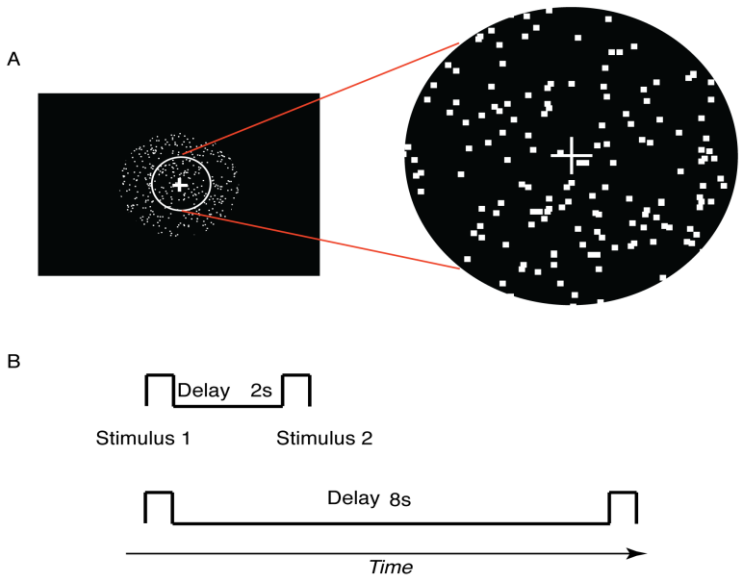

Figure 4.2: **A.** An example of the stimulus used in the delayed motion coherence discrimination experiment. **B.** Scheme of 2IFC with 2s and 8s delay duration; stimulus 1 and 2 lasted 500ms.

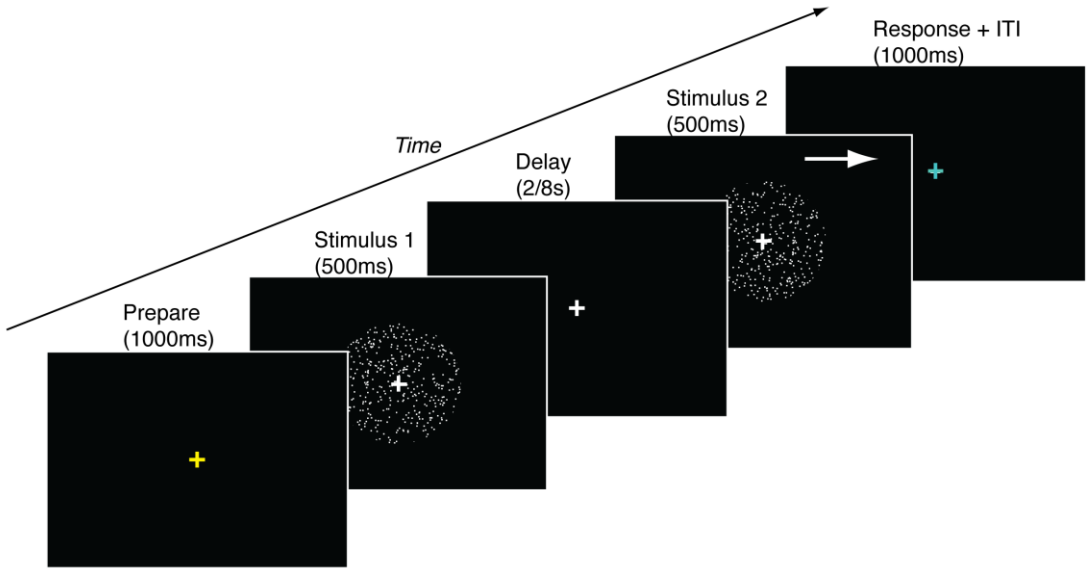

Figure 4.3: A trial in experiment 1. The delay was either 2s or 8s between stimulus 1 (500ms) and stimulus 2 (500ms). The fixed coherence was randomly chosen to be either 30% or 40% coherence level, which was assigned to either the first stimulus period or the second. The coherence of the other stimulus was a summation of one of these fixed coherence level and one of the five stimulus increments. The direction of the coherent motion was 0°, symbolized by the white arrow. When the fixation cross changed colour to cyan, subjects gave their responses.

Psychometric function

Though both fixed coherences were used to present stimulus levels in single blocks, we separated the trials across all blocks based on the fixed level (30% or 40% coherence). Psychometric functions were generated from each condition (2s and 8s ISI, respectively). We plotted "percent correct discrimination performance" against a set of coherence increment values. Discrimination was performed in pairs and thus, chance performance was 50% and we defined 75% correct as the threshold criterion. When the coherence difference is large enough, the observers achieved perfect judgments (100% correct responses), whereas for small differences (near the threshold), performance would be at chance-level. The corresponding performances between these two extremes are reflected in a gradual change that can be described by a sigmoidal curve (see chapter 2 for more details). Figure 4.4 shows a psychometric function that relates the "percent correct response rate" to the level of coherence increment in our delayed motion coherence experiment for 2s (Left panel) and 8s (Right panel), respectively. A sigmoidal function is fitted to the five levels of coherence increment to derive threshold value at the level of 75% correct with its upper and lower boundary of 95% confidence intervals (red dashed horizontal line). A single block in this experiment consisted of 40 trials, and the following results were based on 5 blocks for each participant. There were therefore 40 data points per increment level in each psychometric function.

In order to estimate the fractional increase for each corresponding fixed coherence (30% and 40%), we calculated the Weber constant using the following equation: $K=\frac{\Delta I}{I}$, which can be translated into $Weber\ Fraction = \frac{Threshold\ difference}{Fixed\ coherence}$. This fraction reveals the coherence difference needed to discriminate from the fixed coherence for each subject more directly, and reflects how sensitive the visual system is to coherence discrimination. The data presented in this chapter are all in the form of Weber fractions.

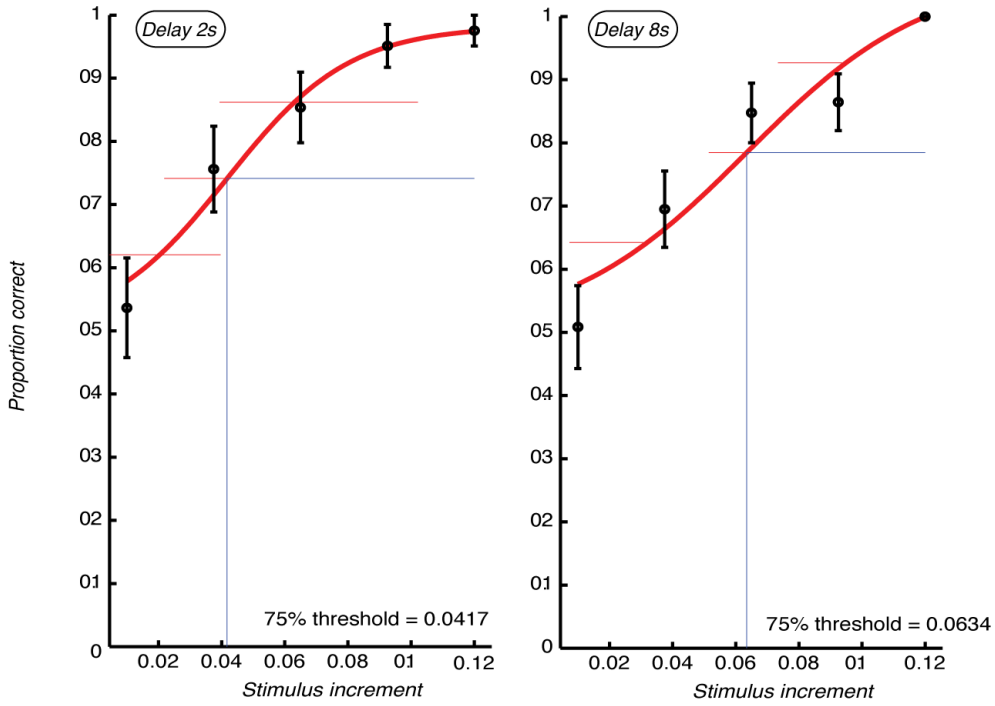

Figure 4.4: An example of psychometric function for the delayed coherence experiment. The points show the average performance at five levels of coherence increment. Error bars: ±1 SEM. A sigmoidal function is fitted to these points to derive threshold value at the level of 75% correct with its upper and lower boundary of 95% confidence intervals (red dashed horizontal line). Left panel shows the psychometric curve with 2s ISI, and right with 8s ISI.

4.1.2.2 Results

Figure 4.5 illustrates the Weber fractions as a function of ISI (2 and 8-second) for the two fixed coherences (30% and 40%), respectively. Three observers' data was plotted individually, and the bottom-right quadrant shows the average proportions across these subjects. A 2×2 analysis of variance (ANOVA) on the discrimination thresholds showed that observers had similar performance when they were asked to remember two levels of the motion coherences over short (2s) and long (8s) duration ($F(1,13) = 0.47$, $p = 0.509$). In addition, thresholds of group data between the two fixed coherences was no statistically significant ($F(1,13) = 0.2$, $p = 0.6639$) and no interaction between fixed coherence and delay duration was found ($F(1,13) = 0.65$, $p = 0.4405$). Clearly these results demonstrate that information of motion coherence can be maintained well over a short period of time, at least for up to 8s. The two fixed coherence we used in the experiment is not a influential factor for the change of discrimination threshold, but rather a varying parameter that weakened the

confusing effect of predictability, adaptation and the establishment of long-term memory, which increased the design efficiency of this experiment.

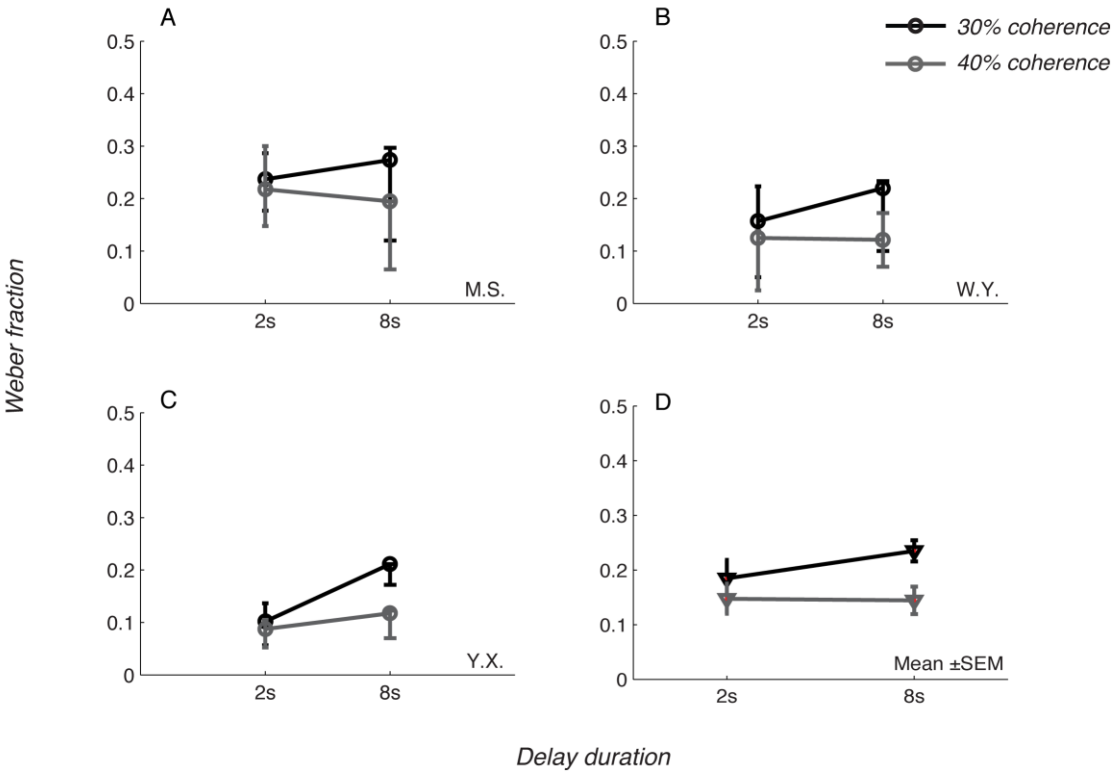

Figure 4.5: **A-C**, the performance of delayed coherence discrimination for each observer. The error bar represented the 95% confidence interval at the 75% correct level of the psychometric curve. **D**, The bottom right panel shows the average weber fraction across these participants. No significant elevation of Weber fraction is observed, indicating that subjects maintained motion coherence robustly over time. Error bar: ±1 standard error of the mean. Darker line, 30% fixed coherence level; Lighter line, 40% fixed coherence level.

4.1.2.3 Discussion

To examine the characteristics of visual working memory for motion coherence in a random dot display, we utilized psychophysical discrimination measurements of two sequentially presented stimuli. Discrimination thresholds were measured and converted to their corresponding Weber fractions for delay durations of 2s and 8s. We found a robust maintenance of motion coherence, revealing results similar to a previous experiment (Blake, Cepeda & Hiris, 1997). Blake and his colleagues found that coherence of moving dots could be perfectly retained for up to 30 seconds, although their definition of motion coherence was

different. Crucially, coupled with their data, our results serve as the baseline for subsequent experiments where we looked further into the temporal and functional characteristics of motion coherence during the retention process with different masks.

4.1.3 Experiment 2: Working memory of motion coherence with memory masking

Experiment 1 showed that motion coherence could be maintained over a relatively long duration (8s) with almost no decay over time. In experiment 2, we tested whether this well maintained memory could be influenced by a task-irrelevant, but feature-similar visual stimulus appearing during the retention period. The majority of preceding studies on consolidation of working memory suggest that the establishment of durable storage of the sample stimulus takes a short amount of time after encoding. Considering the importance of this process in short-term visual memory, we also post-exposed a mask shortly after the onset of the coherence memory period, to examine whether the interference effect found previously for memory capacity was replicable for remembering detailed stimulus attributes.

It should be noted that there are a few factors that may potentially influence memory precision to be different from memory capacity. First, most previous visual working memory experiments limited the stimulus interval to a brief duration (no more than 200ms). Here, the stimuli lasted 500ms. One of the reasons for this difference was that our stimuli were not static but random moving dots, which require some integration time to process. Thus, this duration made it possible to complete the earlier encoding process, assuring that any deterioration of performance was not due to the disruption of perceptual processes. Second, earlier relevant studies used different presentation times for the mask stimulus. For example, the consolidating process has been assumed to be relatively slow (~500ms) for the storage of a single item (Chun & Potter, 1995; Jolicoeur & Dell' Acqua, 1998; Ward et al., 1996), but their results were based on dual tasks, which might overestimate the time used for consolidation. With a simple object detection task, Vogel et al., (2006) pointed out that a much shorter time (~50ms) is actually used to construct a durable WM representation. Our

mask appeared 125ms into the retention window. This time point was selected for two reasons. (1) We assumed that earlier object identification tasks that memorized arrays of objects were more time-consuming in contrast to our task of one single elementary stimulus feature, and thus we used shorter SOA. (2) 125ms is far longer than the period of sensory storage of a visual image, such as iconic memory (Phillips & Christie, 1977a, 1977b; Sperling, 1963). Therefore, we would not impair the encoding processes before visual information enters into the stage of maintenance.

4.1.3.1 Methods

Observer

Four observers participated in this experiment with normal or correction-to-normal vision. Among them were three participants (Y.X., Y.W., and M.S.) who took part in the previous experiment.

Visual stimuli and Procedure

The structure of this experiment were similar to the two interval forced choice procedure used in Experiment 1 and the parameters of stimuli used in each trial of the discrimination task followed the same design of the first experiment: one of the fixed coherence (30% or 40% coherence) and one of the fixed coherence added to one of the five stimulus increments were then randomly assigned to the two stimulus intervals. Different from Experiment 1, there was another stimulus (mask stimulus) presented during the 2s ISI, which consisted of moving dots with coherence levels that were presented at the same location as stimulus 1 and 2. Observers were instructed not to explicitly remember these masks but only to maintain viewing and fixation. Because the ISI was relatively short, we used a brief mask duration (250ms), equivalent to 1/8 of the retention duration. Though the duration of the masking was short, observers reported during de-briefing that they were able to perceive the mask. Another reason to keep mask duration short was to rule out the influence of motion adaptation. One of five levels of stimulus coherence was randomly assigned to be the mask coherence, ranging from 35% to 55% with increments of 5%. The mask was presented at the early time point

during the ISI - the interval between the appearance of this mask and the offset of the first stimulus was 125ms. Subjects needed to be attentive throughout the task and make a judgment of which stimulus interval displayed the higher coherence level, and then pressed the corresponding button. There were discrimination 40 trials in one block and thresholds were measured and converted to Weber fractions as in the previous experiment.

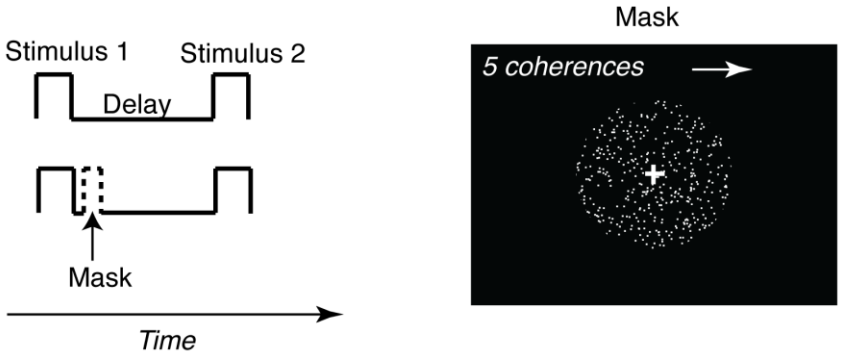

Figure 4.6: Paradigm of 2IFC with a mask stimulus (250ms) that presented 125ms after the offset of stimulus 1 during the 2s-delay duration. Stimulus 1 (500ms) and stimulus 2 (500ms) were identical to those presented in Experiment 1 with two fixed coherences: 30% and 40% (an example is illustrated on the right). One of five levels of stimulus coherence was randomly assigned to be the mask coherence, ranging from 35% to 55% with increments of 5%. The white arrow indicates the direction of coherent motion of stimulus dots.

4.1.3.2 Results

In our second experiment, we investigated whether the robustly preserved motion coherence information (revealed in Experiment 1) would be influenced by another task-irrelevant coherence stimulus when it was added at the beginning of ISI. Figure 4.7 A-D illustrate individually for both 30% and 40% coherence fixed levels. For all observers, the Weber fractions evidently increase when a mask appears at the initial stage of the delay period compared to the no masking condition (data was derived from Experiment 1 for three participants). Since the individual patterns were comparable, we calculated the mean Weber fractions across observers for the two conditions at each coherence level separately in Figure 4.7 E. The results from our 2×2 ANOVA were consistent with the graphical demonstration showing that performance was significantly degraded by the presence of the mask ($F(1,15) = 11.35$, $p = 0.005$), but not caused by the effect of two different fixed coherences ($F(1, 15) =$

0.52, p = 0.4835) nor the interaction between mask presence and fixed coherence (F(1,15) = 1.21, p = 0.293). These results demonstrate that the robust memory performance showed in Experiment 1 is interfered by the display of another task-irrelevant stimulus during the memory period, indicating that the areas that are processing the motion coherence (masking stimulus) is also involved in the information storage.

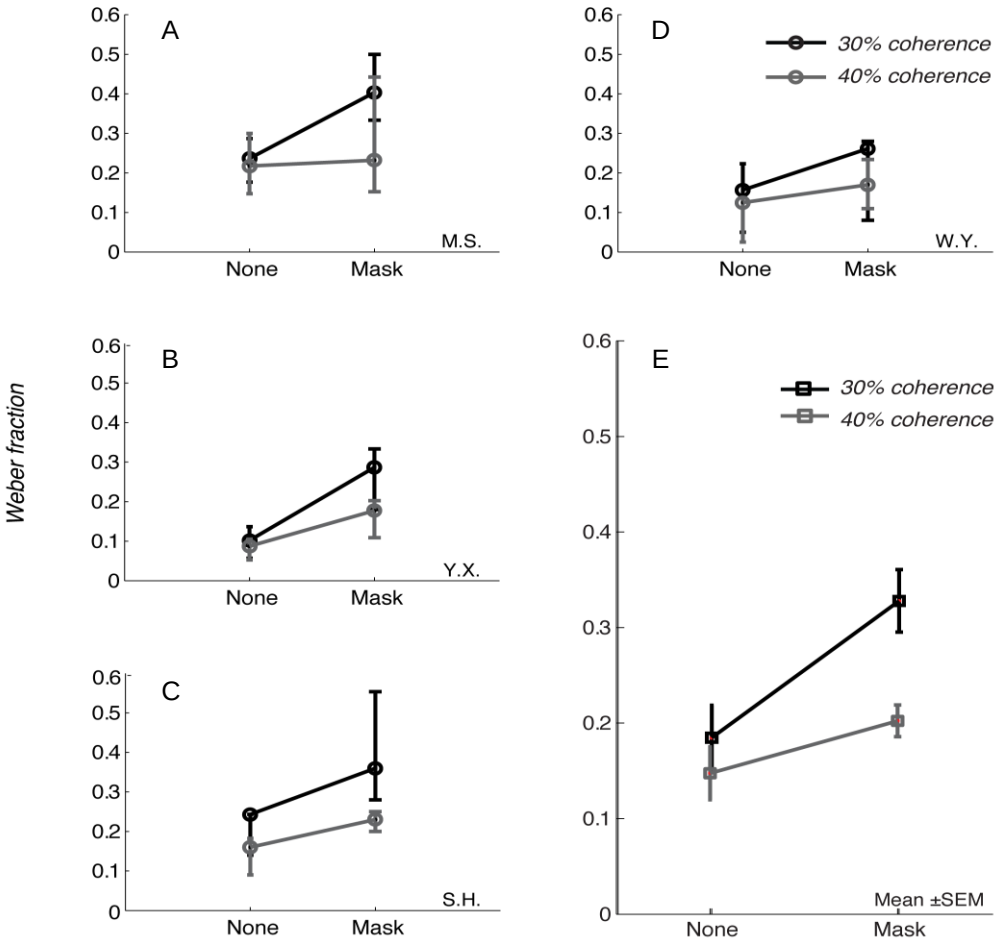

Figure 4.7: **A**-**D**, the degraded performance of delayed coherence discrimination task of 'mask condition' for each observer compared to the 'no-mask condition'. The error bars represent the 95% confidence interval at the 75% correct level of the psychometric function. Darker line is a fixed coherence level of 30% and the lighter line, a coherence level of 40%. **E** shows the mean performance for coherence discrimination across these participants. Error bar: ±1 standard error of the mean.

4.1.3.3 Discussion

The results of this study show that when the masks were presented with a small SOA, performance on delayed discrimination of motion coherence was poor compared to the no-

mask condition (with a 2s ISI). Similar findings come from a visual motion experiment in which the interfering stimulus was most effective in the early phase of the retention period (Pasternak & Greenlee, 2005; Pavan et al., 2013). Analogously to these findings with moving stimuli, recent behavioral experiments also found evidence for masking of static stimulus features, such as spatial frequency and orientation, when interference stimulus masks were presented shortly after the offset of the memory stimulus (Magnussen et al., 1996; Vogel et al., 2006). Taken together, we think that this masking effect occurs within the window of consolidation and acts on the perceptual representation of the low-level visual information, which is fragile and vulnerable to disruption.

Another question we addressed in this experiment was the likely anatomical level of neural correlates of memory masking. Past neurophysiological and brain-imaging studies attributed the consolidation process to the higher-level cortex, including prefrontal areas and parietal regions (Goldman-Rakic, 1995; Miller et al. 1996; Courtney et al., 1997; D'Esposito et al., 2000; Munk et al., 2002; Linden et al., 2003). In Experiment 2, we probed the process of consolidation in VSTM and suggested that the interfering stimulus disrupts the memory representation of the target stimulus at an initial short-lived perceptual stage. What is more, we assume that if the visual areas for processing sensory information were also involved in working memory, then the process of sustaining information would be interrupted by an additional visual stimulus when it activates sensory-encoding regions. Therefore, this experiment provides further evidence supporting the importance of early visual cortex in the process of consolidation of WM. Another bit of supporting evidence comes from the external disruption to neuronal activity (van de Ven et al., 2012). Investigators delivered transcranial magnetic stimulation (TMS) to occipital cortex at 400ms into the retention phase to investigate the functional relevance and temporal characteristics of early visual cortex in VSTM. They found a very strong correspondence in memory interference between TMS and visual memory masking, which suggested that the visual cortex contributes to the process of consolidation during initial stage in VSTM.

Besides external interference (e.g. TMS- induced), there have been studies using feature-interference-selectivity in delayed discrimination tasks to show the similarity between lower-order visual activity and memory (Magnussen & Greenlee, 1999; Pasternak & Zaksas, 2003; Pavan et al., 2013; Magnussen et al., 1996). In this experiment, we focused on the question of whether a task-irrelevant mask could interfere with the memory. But we did not design the variation of mask coherences in Experiment 2 for the question of whether there was selectivity of coherence maintenance. Therefore, we performed another experiment (Experiment 3) to examine whether different levels of mask stimulus have different masking effects.

4.1.4 Experiment 3: Stimulus specificity of visual motion coherence in working memory

We examined memory of visual information as a function of time in the first experiment. Experiment 2 showed an interference effect of a moving RDK stimulus at the very early stage during the retention period in the lower-level visual areas. Here, we address the selectivity of mask interference for coherence judgments in RDKs.

Over the last decade, many studies have revealed stimulus selectivity of interference using a range of mask properties. For instance, some studies provide evidence for channels tuned for specific spatial frequencies. Magnussen et al. (1991) found that the memory effect varies with the spatial frequency of the mask. They showed that discrimination thresholds were not elevated when mask and test frequencies were identical, but the opposite result when they were different, suggesting that the memory array of spatial frequency operates in a similar framework to its sensory processing in the early stages of visual processing. Based on the important groundwork provided by Experiment 2, here in Experiment 3 we specified two kinds of mask coherence levels - one is a masking stimulus of random moving dots with no ‘useful signal’, while the other mask presented the mean level of coherence used in the

experiment for each subject. Our aims were to examine: (1) whether both types of mask evoke a masking effect on the memory of motion coherence and (2) whether there is any differential interference effect between them? By answering the second question, we may further infer some characteristics of the memory mechanism for motion coherence. Furthermore, in order to gain more insights into the temporal property of short-term memory, we also presented the mask stimulus at three different time points during a 4-s delay.

The duration of the mask was increased slightly from Experiment 2. Though studies have shown that even almost-invisible stimuli would exert in interference effect on the capacity of working memory, we wanted to maximise any potential interference. In experiment 2, as the masking duration was short (250ms) and our focus is now on detailed visual features, the masking stimulus used might not have been sufficiently encoded as stimulus (which were presented for 500ms each). A similar point was raised in a previous experiment, in their case about the target stimulus duration (Luck & Vogel, 1997). In their visual storage capacity experiment, the investigators assumed that if the duration of sample stimulus was an influential factor, then a longer stimulus interval should improve the memory performance, because longer duration allows the first stimulus to be encoded adequately. Inspired by their design choices, we made the masking duration in Experiment 3 as long as the stimulus interval (500ms) to offer an equal chance for encoding of mask and target stimuli. In this sense, by comparing results between experiments 2 and 3, we may also able to examine whether a longer mask duration would induce more disruption to memory of coherence.

4.1.4.1 Methods

Observers, Visual stimuli and Procedure

The same four participants took part in this experiment. The stimuli were generated using the same programming software, computer and display as in Experiment 1 and 2. The parameters for generating the moving dots were all identical as well. But in this experiment, the mask coherence only had two levels (0% and mean). The mean coherence was calculated as the mean value of the range of coherences used in this experiment for each individual. The

masking stimulus (coherently moving dots) could appear at the three possible time points: early, middle or late in the delay period (4-second). Its duration was 500ms, which was equivalent to the two stimulus durations. The relationship between the onset and offset of the stimulus interval and the masking interval is illustrated in Table 4.1.

Observers still needed to discriminate coherence levels between fixed and test stimulus, and to press the button corresponding to the stimulus interval that contained a higher proportion of coherently moving dots. In the pilot experiments, we found that combining trials, in which stimulus of different masking timings was presented, caused some confusion and uncertainty, because subjects could not easily determine whether the second occurrence of random dots in each trial was a mask or a comparison stimulus. In order to avoid this confusion, we collected data for different conditions of mask timing and the no-mask condition in separate blocks. The purpose of this experiment is to see whether performance could be disrupted by a mask introduced beyond the consolidation period; and second, to examine whether the exact timing of the mask produced different effects on the memory of motion coherence. Three kinds of masking conditions were alternated with the no-mask condition to prevent the build-up of long-term memory. Figure 4.8 shows a schematic of the experiment for different mask timing conditions with two options of mask coherence.

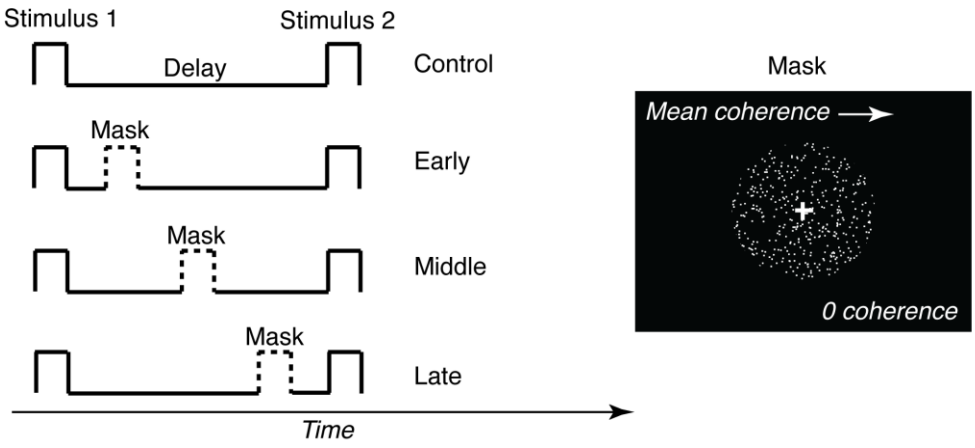

Figure 4.8: Paradigm of 2IFC task for coherence memory masking experiment (solid lines represent stimulus intervals that lasted 500ms). The dashed lines represent different mask intervals: either at early, middle or late time points during the delay interval (3s) (see Table

4.1 for the specific time of different conditions). The mask coherence could be either 0% coherence or the mean coherence level. White arrow in the right graph indicates the direction of coherent motion during the mask duration. These mask conditions were contrasted with a control condition, where no mask stimulus was presented during the delay period (first row on the left).

Table 4.1: Parameters for the timing of different events in one trial

Masking time	**Duration A (seconds)**	**Duration B (seconds)**
Early	1	2.5
Middle	1.75	1.75
Late	2.5	1

Duration A: offset of first stimulus to the onset of masking stimulus

Duration B: offset of masking stimulus to the onset of second stimulus

4.1.4.2 Results

From our data sets, we calculated proportion of correct responses at each coherence level for two types of mask and three possible mask onsets. Then we fitted a psychometric function to each subgroup. The coherence difference at the 75% correct level was estimated, with a procedure similar to that illustrated in the previous experiment. Figure 4.9 shows examples of deriving thresholds from the psychometric curves for two different mask types in a single subject. Based on these values, we then computed the Weber fraction. Figure 4.10 shows the results plotted as a function of three mask timings for each observer. Masks that appeared at three different time points within the delay interval, all significantly affect the performance of working memory compared to the no-mask condition. Weber fractions are approximately doubled, indicating performance was affected by maskers even after the process of consolidation, and these disruptive effects are similar across different conditions with no statistical significance between them. The averaged values are plotted as a function of masking time for both fixed coherences (Figure 4.11).

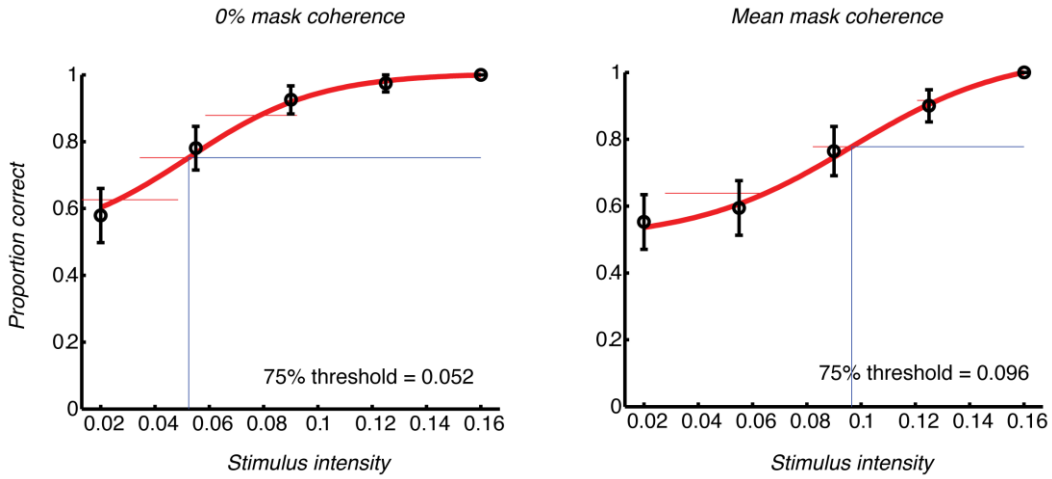

Figure 4.9: An example of psychometric function for the delayed coherence experiment when two different mask coherences were used. Left panel shows the psychometric curve with 0% mask stimulus, and right panel illustrates the condition when mask had mean coherence level.

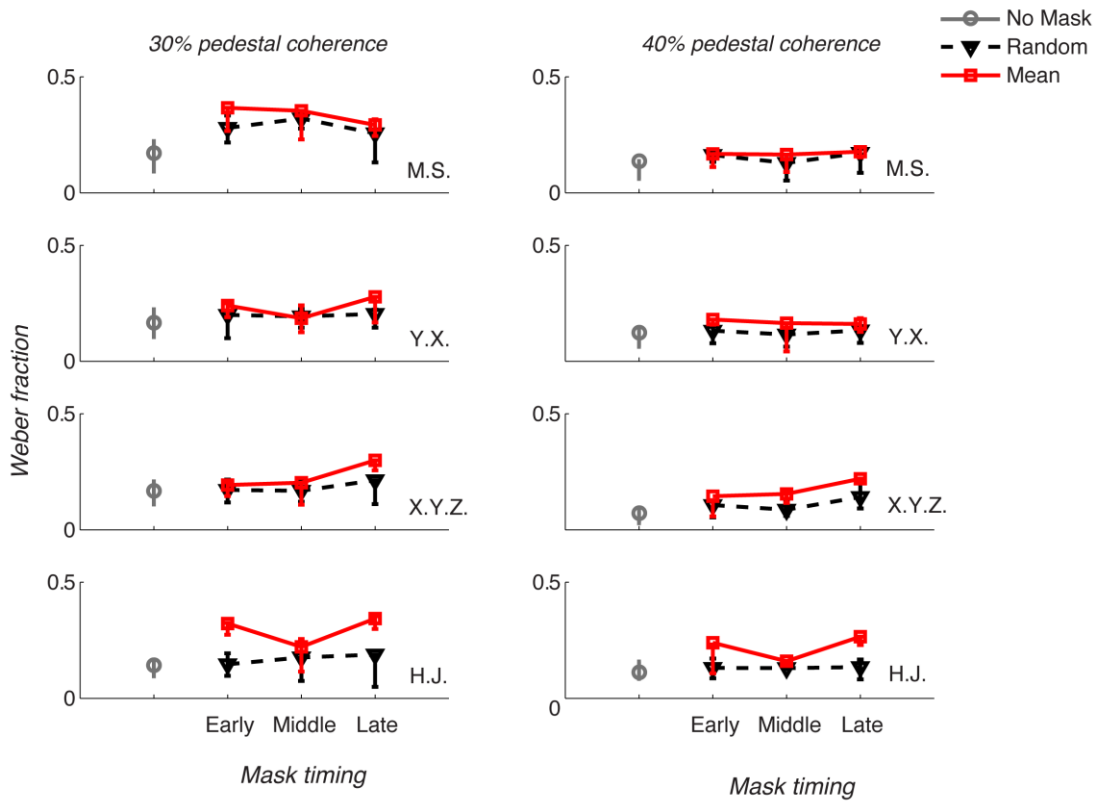

Figure 4.10: The individual Weber fractions plotted as a function of three mask timings for both mask type based on 30% (left) and 40% (Right) fixed coherence, respectively. Dashed black line: 0% coherence mask. Red solid lines: mean coherence mask. Grey single point: the baseline when no mask was presented during the ISI. Error bar represent the 95% confidence interval at the 75% correct level of the psychometric curve.

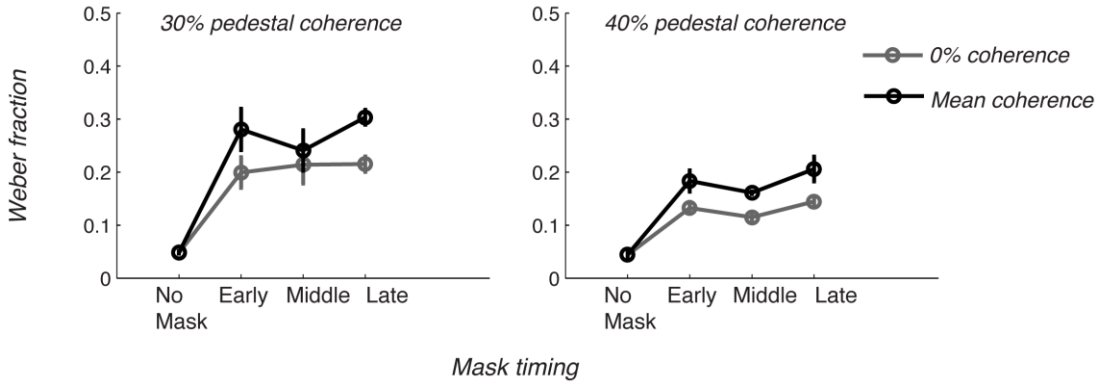

Figure 4.11: Weber fraction plotted as a function of three mask timings for both fixed coherence levels across observers. Left and right represent 30% and 40% base-coherence, respectively. Lighter line, 0% coherence mask and darker line, mean coherence condition (see following section). Error bar: ±1 standard error of the mean. Masking stimulus displayed in the middle of the delay interval significantly increase the weber fraction for both fixed coherences. Mask with mean coherence has more disruptive effect on memory than mask with random motion, regardless of the masking time points.

This experiment also examined whether coherence information is selectively maintained in working memory. To address this question, we assessed the influence of two types of mask coherence: 0% coherence of moving dots or the mean value of the five coherence levels used in the target stimulus intervals. The conditions were randomly interleaved for each trial. Figure 4.10 also displays the Weber fraction for two coherence masks for each individual observer. Figure 4.12 shows the averaged values across all observers in both conditions for different masking times. As demonstrated above, both types of mask (0% and mean coherence) elevated the discrimination threshold significantly compared to the no-masking condition, but the mask with the mean coherence degraded the memory performance more severely than the random coherence mask. An ANOVA confirms a significant main effect of mask coherence (coherence: $F(1, 47) = 19.12$, $p < 0.05$), suggesting that the masking effect of stimulus with random motion is different from the one with certain level of similarity of stimulus feature (mean coherence in our case). But there is no differential effect for the three mask onset timing ($F(2,47) = 2.67$, $p = 0.082$) on memory performance. As shown, this pattern is consistent for both fixed coherences. However, our ANOVA shows that the use of two fixed coherences is also a reason of the difference of discrimination thresholds ($F(1,47) =$

5.2, p = 0.0283). No interaction was observed between masking timing and mask coherence type (F(2,47) = 0.71, p = 0.4965), masking timing and fixed coherence (F(2,47) = 0.14, p = 0.8681), or mask coherence type and fixed coherence (F(1,47) = 0.03, p = 0.8737).

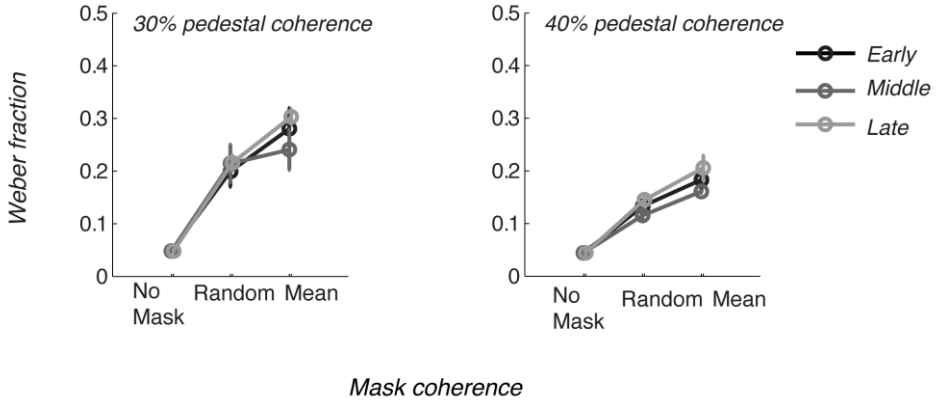

Figure 4.12: Weber fraction replotted as a function of mask type for both fixed coherences across observers. The darkness of the line specifies the Weber fractions for different masking times. Error bar: ±1 standard error of the mean.

4.1.4.3 Discussion

No decay in performance was observed in this experiment when the delay duration was 4 seconds, which confirms the results from Experiment 1. Compared to the no-mask control condition, all mask manipulations in this experiment had a considerable effect on coherence memory. This suggests that the degradation of performance is mainly caused by exogenous interference rather than spontaneous information decay. Moreover, the significant masking effects from both 0% coherence and mean coherence level (definition explanined in Experiment 3) masks suggest that memory masking could be induced with masks that were 'related information' as well as what might be considered 'random noise'.

Beyond this similarity in the masking effect, Experiment 3 also shows that the masks containing relevant stimulus information have a differential interference on memory. We manipulated the mask coherence to examine whether selective representation of motion coherence is held in working memory. If no selective masking was taking place, then 0% coherence mask and mean coherence mask at the same time point would have a similar effect

on the memory representation. This was not the case. Consistent with previous evidence (Intraub, 1981; Pasternak & Zaksas, 2003; Pavan et al., 2013; Magnussen et al., 1996), our data shows that the mask has more powerful disruptive effect on mnemonic representation when it has a certain level of similarity (signal) pertaining to the remembered feature, supporting the mechanism of stimuli-similarity interference effect (cf. lateral inhibition model introduced above) along the task-relevant dimension. Slightly different from those reports investigating the selectivity of masking on a trial-by-trial basis, we addressed the masking characteristics from an overall perspective of feature similarity, adding to the previous studies of interference selectivity, which have shown that the effect is weaker when there is no signal compared with masks that were certain similarities (but not completely identical).

It is noticeable that although it was smaller effect, our data also showed that a 0% coherence mask impaired WM. We may interpret this result from another point of view. To some extent, the random motion in a 0% coherence stimulus may be considered a task-irrelevant mask, compared to a blank grey screen, white noise mask or other unstructured images. It is possible that the random motion of dots interferes by wiping out the trace of memory, whereas a task-relevant stimulus mask (mean coherence) may actually *overwrite* the common features since the neuronal substrates for encoding the mask are partially overlapped with those represented in memory.

Beside the explanations relating to WM, there are other hypotheses for how memory masking may occur, among which attentional explanations are a major focus. A number of studies have explored the relationship between attention and WM. Many of them discussed the role of attention on task-relevant information. Some neuroimaging studies found that the sensory representation of task-relevant information can be amplified by attention at the encoding stage (Egner & Hirsch, 2005; Awh & Jonides, 2001; Broadbent, 1958; Deutsch & Deutsch, 1963). Is it likely that the mask with the mean coherence level was also modulated by attention due to its similarity with target stimuli, causing a more pronounced interference, while the attention did not promote the representation for the random moving dots. In the next part of

this chapter, I present our investigation into the relationship between attention and WM with evidence from fMRI measurements.

Up to this point, all the results support the 'sensory recruitment model', which assumes that the neuronal substrates for working memory of sensory visual information overlaps with those that encode and store these features in WM. However, it is not clear how and to what extent the early visual areas are involved in WM. It may operate through two possible approaches: first, early visual cortex is involved throughout the retention period, which may be evident as a sustained neuronal activity. Alternatively, the recruitment of neurons in primary visual cortex and extrastriate visual cortex only occurs at the retrieval stage when the memory representation is reclaimed from these areas via top-down processing. Experiment 3 takes advantage of the possible time courses of WM to investigate how V1 is recruited. Masks were presented at early, middle or late stages during the retention interval, respectively. If the mnemonic representation is formed and retained in the early stage of visual stream throughout the storage process, then the masks should have a similar effect on retention, regardless at which time point they were introduced. On the contrary, if signal was forwarded to higher-level areas and then 'returns' during the retrieval of the mnemonic representation, then masks displayed at a later stage during the delay period may not exert as much influence as at earlier times. In the present experiment, our data reveals no significant difference between the performances for the three points within the retention period, suggesting the possibility that early visual areas is involved throughout all of the retention period.

4.1.5 General Discussion

In the first experiments, we conducted a simple short-term working memory experiment using a 2IFC discrimination procedure and found that the information about the motion coherence of a stimulus could be well maintained for at least 8 seconds. Experiment 1 provides an important control condition for other measures in later experiments.

The second experiment aimed to investigate whether this robustly sustained memory of motion coherence could be affected by a 'memory mask'. One interference stimulus of motion with a certain level coherence was presented at the initial stage of the retention period. If the mask deteriorated memory performance, we would expect a greater elevation of threshold. Our result shows pronounced degradation of performance with the presence of a mask compared a no-mask condition with a 2s ISI. In agreement with other experiments about the role of consolidation in memory, we concluded that robust maintenance of information about motion coherence is dependent on the accurate encoding of the target stimulus during the process of consolidation, which occurs at the very early stage of memory formation.

After the consolidation is complete, the memory of visual information is relatively better protected from incoming sensory input, which may corrupt the stored information. In order to determine the point in time when the representation of coherence is most susceptible to disruption beyond the initial phase of retention, we introduced a task-irrelevant mask at three different time points during the delay interval in Experiment 3. However, no substantial difference was found between the three time points, which indicate that all phases throughout the delay duration are important to the precision of WM.

Since the same observers participated in Experiment 2 and 3, and all the other parameters were comparable, we could make direct comparisons between their data. It should be noted that both experiments examined different phases within the retention interval with a memory mask procedure, and the mask duration was increased from half of the duration in Experiment 2 to the same duration as the target intervals in Experiment 3. In this sense, we assessed the factors that may impair the WM of motion coherence, including different time points of masking and the length of mask interval. Presumably, if the duration of mask were one of the influential factors, then the results of Experiment 3 would become worse because there is more time to allow encoding of the mask stimulus. On the other hand, if the phase of retention is predominant, then there might be a difference when the mask was administered during the period of consolidation, rather than later phases within the ISI. Compared to the results of

Experiment 3, the Weber fractions for each observer in Experiment 2 were larger, suggesting that the mask duration is not a major factor. Instead, our result shows that the initial phase of the memory process plays a more prominent role. Analogous results, showing that the early stage of the memory interval is sensitive to disruptions, were also found in experiments with small SOA for storage of speed (Pasternak & Zaksas, 2003) and direction (Pavan et al., 2013) of motion. Together, this evidence supports the idea that the retention process may have two distinct phases: the first part corresponds to the process of consolidation, during which the mask itself could lead to more impairment to memory maintenance; whereas the information passed to the second phase is less susceptible to interference (Pasternak & Greenlee, 2005).

In addition to the memory selectivity of motion coherence stored in early visual areas (see Discussion in Experiment 3), our last two experiments also addressed the role of early visual cortex in the process of WM in terms of timing. Experiment 2 points out that the incoming stimulus that is irrelevant to the memory task follows the same neural pathways from the retina through the visual processing hierarchy as a remembered stimulus. The mask can therefore compete with the maintained mnemonic representation in the regions responsible for visual encoding at the initial stage of memory, and as a consequence, degrades the performance. Built on this result, Experiment 3 further explores how these areas are recruited in the memory process by presenting masks at different phases during the retention period. We conclude that there may be an on-going neural process in these early visual regions. fMRI experiments have been used to tap into this question for more than a decade and a sustained BOLD signal during the memory period was regarded as the symbol of functional-relevance for any involved areas. Most of the earlier evidence did not show overall changes of activity in occipital cortex (Offen et al., 2009; Harrison & Tong, 2009). Recently, however, the introduction of multivariate decoding has allowed investigators to look at whether early visual cortex exhibits differential activity patterns that represent the content of WM even though no increase of overall activity was detected (Sperling, 1960; Oberauer & Kliegl, 2001; Lepsien et al., 2005; Harrison & Tong, 2009).

In general, our psychophysical evidence in this chapter illustrates that the memory representation of motion coherence appears to rely on early visual areas. However, psychophysics provides relatively indirect support. In the following part, I will describe a pilot fMRI experiment in which we performed similar psychophysical experiments while we scanned subjects' brains to see whether there is active storage in the neural populations in the early visual areas during the process of working memory for motion coherence.

4.2 Piloting fMRI experiment for working memory of motion coherence

Besides psychophysical evidence obtained using its methods described in the previous part, there is a growing number of neuroimaging studies investigating the role of early visual areas in higher-order cognitive processes. This includes studies of working memory of detailed visual information and attention. We attempted one fMRI experiment to search for the characteristics of both processes when observers performed tasks based on the coherence feature of motion.

4.2.1 Introduction

Working memory often refers to the maintenance of visual input for a short period of time, making efficient information access and manipulation possible. The information is held in a highly active/accessible state, which is often reflected by persistent activity in those areas that are involved in this process. Physiological and imaging studies have shown that sustained activity was present in parietal and/or prefrontal areas during the working memory process without the presence of any visual information (Haenny, Maunsell and Schiller 1988). From this point of view, the process of *attention* shares a similarity with WM because of its ability to modulate neuronal activity when a stimulus is not in view. Evidence from both neuroimaging and single-neuron studies have also demonstrated that visual attention affects brain activity in a number of areas. However, whether such attentional modulation of

responses occurs in primary visual cortex has been a controversy issue. It was assumed that attention exerts influence only at the highest levels of the visual pathway (Corbetta, et al., 1991; Heinze, et al., 1994). Until recently, the view that early visual areas exclusively perform sensory analysis of visual information had to be abandoned in light of studies in the last decade. A few neuroimaging studies have clearly illustrated the effect of attention in V1 (Cook and Maunsell 2002; Somers et al., 1999; Gandhi, et al., 1999). But the overlap of functional-relevance in primary visual cortex complicated the relationship between WM and attention, which was reported as two intertwined constructs.

However, one recent fMRI experiment has yielded an important approach to address these two processes individually (Offen, Schluppeck, & Heeger, 2009). They employed a detection task to highlight the process of attention. In order to detect a low-contrast grating at threshold, subjects needed to pay close visuospatial attention to the possible incoming stimulus. Yet, this task did not involve any maintenance of visual information over time, since the first stimulus only served as a cue of the onset of each trial. In contrast to this task, their discrimination task emphasized the need of retaining information in a mental workspace during the delay interval and being available for other cognitive processes (Baddeley & Hitch, 1974). This condition did not require a high level of attention. Therefore, the difference between these two tasks lies in the requirement of attention and the application of memory during the delay interval. With these paradigms, Offen et al. (2009) found that the early visual cortex exhibited sustained responses throughout the interstimulus interval when subjects performed attention-demanding task, whereas the delay-period activity was not distinguishable from zero in the short-term memory task. They suggested that the sustained activity might be the result of attentional modulation, or other contextual modulating cognitive processes rather than working memory. Inspired by this study, we used similar kinds of tasks to assess whether their result is replicable for visual motion coherence in two crucial sensory visual areas. V1 was included because neurons in this area appear to be responsive to motion coherence (see Chapter 1 for

more details). We also looked at the responses in V5/MT, where neurons are extremely sensitive to motion coherence.

4.2.2 Methods

4.2.2.1 Subject

In this pilot experiment we only scanned one subject, who signed informed written consent before scanning. The scanning was approved by the Medical School Research Ethics Committee, University of Nottingham.

4.2.2.2 Visual stimuli and procedure

A projector was positioned outside the scanning room. Stimuli were then projected onto a display screen located at the subjects' feet outside the magnet. Stimuli were presented by an Apple MacBook Pro running Matlab and MGL (a Matlab wrapper for OpenGL) with related tools (http://gu.brain.riken.jp/doku.php/mgl/overview). Subjects were instructed to maintain fixation at a cross at the centre of the screen while stimuli were displayed.

Common properties of the detection task and discrimination task

There are some shared properties between the two tasks we used here. I will outline the similarities and then discuss particular aspects of each task. First, both of the tasks in this pilot fMRI experiment were based on a two-interval procedure, and stimuli were displayed in a circular aperture around fixation. All the stimulus parameters used in this functional imaging experiment were identical to those employed in the psychophysical experiment. Second, a proportion of dots was randomly chosen to move coherently in one of six directions (0, 60, 120, 180, 240 and 300º) and was renewed on each frame. Each direction had equal probability to be selected in a particular trial. In each trial, the directions for the two stimulus-intervals were kept the same if there was any coherent movement in the second interval. This ensured that there was no uncertainty about the direction of motion, because the direction in each trial is known after the presentation of the first stimulus. More importantly, it is feature-irrelevant to the task. The third similarity of the two tasks is that the delay duration was randomly chosen from 2.5s to 11.5s (in increments of 3s). The randomization of both tasks limits

subjects' anticipation of the second stimulus, and it also provided enough longer-duration delays to disambiguate the BOLD response during the delay period from the responses evoked by the target stimuli. The final common parameter is that the inter-trial interval was varied over trials in both tasks (randomly selected from 4.5s, 6s and 7.5s), and random dots were presented during these ISIs.

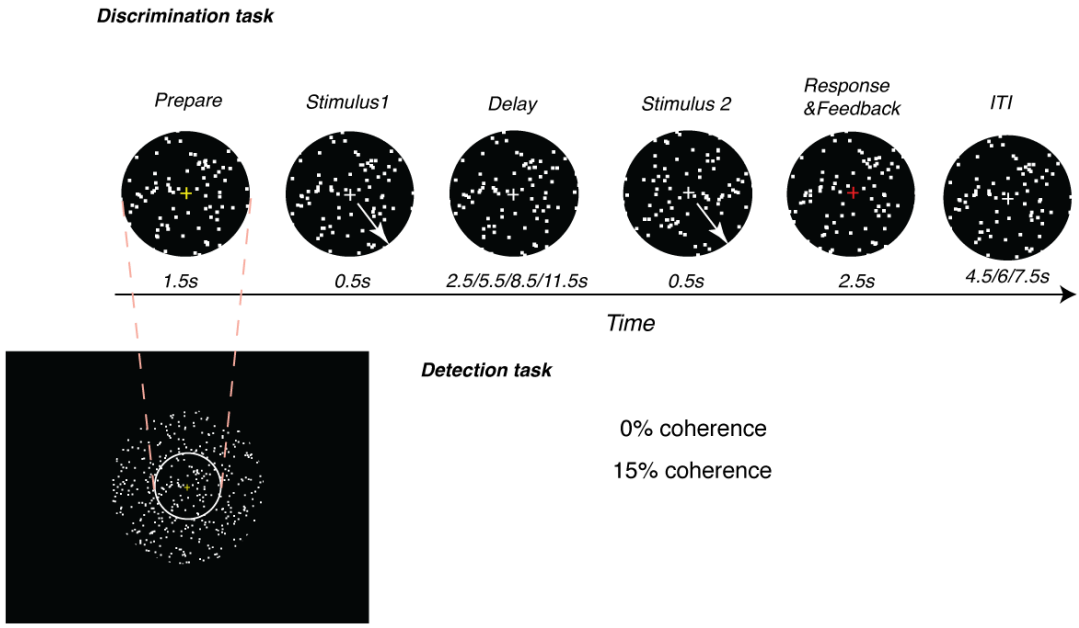

Figure 4.13: Outline of the discrimination and detection tasks. Stimuli were white pixel dots displayed on the black background throughout each trial. The stimulus shown in the circle is a zoomed-in version of the actual stimulus used in the experiments. Following the presentation of the first visual target stimulus that had a certain level of coherent motion (500ms) and the variable delay period (stimulus with random coherence), the second target stimulus was displayed briefly for 500ms. In the discrimination task, the coherent motion in the second stimulus interval could be easily identified, and the subject was asked to discriminate which stimulus interval contained higher coherence; whereas in the detection task (lower panel), observers had to be highly attentive to judge whether any near-threshold coherent motion (15% coherence) was present or not (0% coherence). In addition, the first stimulus in the detection task was used to simply indicate the onset of a new trial. The colour of the fixation was yellow at trial onset and remained white during the stimuli intervals and delay interval. After participants responded, it changed colour to give feedback (red, incorrect answer; green, correct answer).

Differences between the detection task and discrimination task

(i) Detection task:

In this task, each trial started when the colour of the fixation crossing turned yellow. 500ms after the trial onset, the first target stimulus with coherent motion (30%) was presented for 500ms. During the delay interval, the stimulus remained on the screen with the fixation cross. After a variable delay period came the second stimulus, which had a low coherence (at threshold). Outside the scanner, we used a Yes-No detection procedure to find the 75% threshold of the subject's detection level for coherence, and employed it (15% for this subject) as the strength of coherence in the second stimulus interval. These periods were in alternation with random motion (0% coherence). The target probability was 50% and subjects made a judgment of whether a coherent stimulus was present or not. A response had to be given within 1.5s (indicated by the colour of fixation cross turning to cyan; response interval). There was feedback (colour of the fixation changed) afterwards depending on the response. Note that the observer did not need to remember the first stimulus. It simply symbolized the start of each trial, which cued the subject to be attentive to the incoming stimulus. The paradigm for the task is shown in Figure 4.13.

(ii) Discrimination task:
The timing of the discrimination task, including the first interval and delay period was similar to the detection task, except that the motion coherence level of the target stimuli were different. During the first target interval, 60% of the dots moved coherently in one of the six directions. This level of coherence was used because previous evidence has demonstrated that MT responds more strongly to higher proportions of coherent moving dots, and 60% coherence enabled us to record a stronger BOLD signal. The second stimulus interval contained a coherence level that was differed by $\pm$25% from the first stimulus. These two possible coherence levels had equal chance. Subjects needed to discriminate whether the second stimulus had higher coherence than the preceding stimulus in the same trial. The paradigm is shown in Figure 4.13:

MT/V5 localizer stimulus

Area MT/V5 is well known for its selectivity of motion, and the neurons in this area respond strongly to different directions of motion, especially coherent movement. Slightly different from the conventional approaches (Zeki et al., 1991; Watson et al., 1993; Tootell et al., 1995, Huk, et al., 2002), we used stimuli that alternated in time between blocks of coherent movement (100% coherence) and a blank screen in order to localize MT/V5. Within a 17° annular aperture (central 3° removed), 2000 white square dots with size of 0.26° travelled consistently at the speed of 5°/s in a random direction selected from a uniform distribution of 0° to 359° on a black background. This moving-dot field was alternated with a blank screen every 12 seconds. The cycle was repeated approximately twelve times during each fMRI scan.

Retinotopy stimulus

We used counter-clockwise / clockwise rotating wedges and contracting / expanding rings of checkerboard, respectively, to localize the retinotopic organization in the visual areas (see more detail in the corresponding sections in the General method chapter).

fMRI methods

We performed functional MRI at 3T (Philips 3T Intera Achieva) using an eight-channel SENSE head coil. Subjects lay in the scanning bore supine. Foam padding was used to minimize head movements. The fMRI scanning was performed over 2-3 scanning sessions. Session One: An anatomical scan provided a 1 mm^3 resolution image of the brain and covered a 256 × 256 matrix in axial slices. Session two: The "inplane" slices were oriented approximately perpendicular to the calcarine sulcus, with a slice thickness of 3mm (1.5mm inplane resolution). They were T1-weighted images obtained using a 2-D MPRAGE pulse sequence with phase encoding direction of right-left. Functional scans, included one for MT/V5 localization and three for each of the two main tasks (7 in total). The scans of the detection and discrimination tasks were completed with the usual T2*-sensitive echo planar imaging pulse sequence (EPI) (64 × 64 matrix, TE = 30 ms, TR = 1500 ms, flip angle 75°).

The same slice prescription was taken as the inplane image. We scanned 32 slices in an oblique-axial plane with a voxel size of $3 \times 3 \times 3$ mm^3. A SENSE factor of 2 was used to accelerate imaging, which helps reduce image distortions. Data for these two main tasks were obtained in interleaved order. After each scan (lasting ~300s), the subject was allowed to rest for a minute.

fMRI data analysis

We used standard event-related methods to estimate the fMRI response time course for variable conditions with different delay intervals. Four delay durations ranged from 2.5s to 11.5s were included in this experiment. As indicated in Chapter 2, the measured fMRI data of each voxel (Y) can be fitted with general linear model with four regressors, corresponding to different delay conditions. **A** denotes the design matrix that characterizes the order of those four conditions. Each regressor contains 15 columns of time-shifted 1's, which signified the onset of each trial. By solving the ordinary least squares $X = (A^TA)\dagger A^TY$, where $()^T$ is matrix transpose and $()\dagger$ is pseudoinverse, we estimated the time response (X) for conditions with different delay intervals (Schluppeck, et al. 2006). This deconvolution assumes no particular shape of the hemodynamic response, but linearity in temporal summation (Boynton et al., 1996; Dale, 1999). Then the deconvolved responses of all the voxels in the ROI were averaged to obtain the mean fMRI response.

4.2.3 Results

Identifying V1 and MT/V5

According to the traveling wave method, we derived the polar angle and eccentricity maps of retinotopy. Based on these maps, we defined the retinotopic boundaries between V1 and V2 on both hemispheres (More details in Chapter 2).

MT/V5 was localized for our participant by combining information from the anatomical and functional images. Similar to delineating the retinotopic areas such as V1, V2 and V3, we manually defined MT/V5 by including voxels located in the lateral surface of the occipital lobe. The stimulus-response correlation value was thresholded to ~0.5 to ensure the response was elicited correspondingly by the moving-dots versus blank localizing stimulus. Figure 4.14 shows a demonstration of MT/V5 in both hemispheres in inflated cortical surface. Consistent with other reports, we found that MT/V5 in this participant was far anterior to the early visual areas.

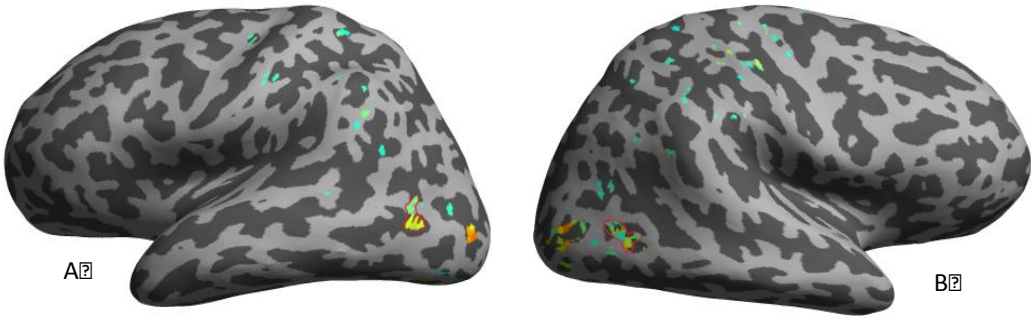

Figure 4.14 shows a demonstration of MT/V5 (within red circumscribed curve) in both hemispheres in unfolded surface (Subject Y.X.): A. Left hemisphere and B. Right hemisphere.

Result for two main tasks
(i) Detection task (Attention)
The subject performed a visual detection task in which the second stimulus consisting of coherently moving dots close to the coherence threshold level. It was presented after a variable delay period (2.5s—11.5s) followed by the first stimulus at 30% coherence. Since there is no significant difference in the fMRI responses between the left and right V1, and neither the MT/V5 in each hemisphere, we combined these bilateral results for both regions (Figure 4.15 and Figure 4.16). Figure 4.15 shows the average fMRI responses of V1 for different delay periods. Results demonstrated a sustained activity in V1 when attention is highly required. As the delay duration increased, the separation between the first stimulus and second stimulus became more pronounced. We also plotted the response of MT/V5 as a function of different ISIs in Figure 4.16, which also shows a sustained activity during the delay interval (see Table 4.2 for the statistical result), replicating previous other results

(Kastner et al. 1999, Silver, Ress and Heeger 2007). Table 4.2 list the results of *t* statistics and *p* values of each task for the subject. The data that fed into these statistical analyses was each voxel's (thresholded r^2 at 0.2) average response across the time points of the delay interval for each task. The sixth time point was chosen to be the starting point of this period, but different ending time points were selected considering the lengths of delay interval and possible contamination of the first visual stimulus due to the sluggishness of hemodynamic response.

Table 4.2 Statistical significance of response during the delay interval

	Detection Task (Attention)		Discrimination Task (Working memory)	
Delay	*V1*	*V5/MT*	*V1*	*V5/MT*
3.5s	**t: 12.0984 (2.0851e-24)**	**9.5777 (1.3156e-09)**	**9.6339 (3.6396e-14)**	**3.6343 (0.0027)**
5.5s	**9.3026 (6.4781e-17)**	**8.4904 (1.0840e-08)**	**9.8415 (1.6366e-14)**	**3.6207 (0.0028)**
8.5s	**9.0194 (3.5415e-16)**	**6.9825 (2.6130e-07)**	**9.3005 (1.3245e-13)**	1.6150 (0.0704)
11.5s	**9.5103 (1.8482e-17)**	**8.5033 (1.0563e-08)**	**8.3505 (5.4964e-12)**	0.9611 (0.1808)

Entries in boldface indicate statistical significance at $p < 0.05$, one-tailed *t* test (null hypothesis, mean of 0).

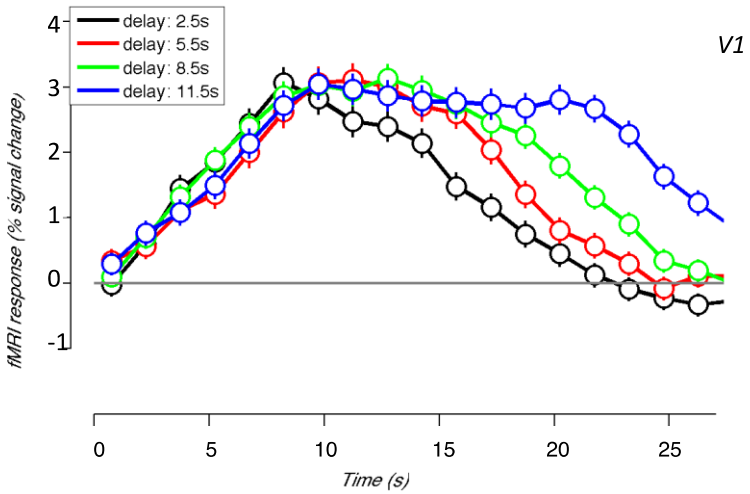

Figure 4.15: Sustained fMRI responses (% signal change) during the delay intervals in V1 in the detection task where subjects attended to the presence of any possible coherent motion

during the second stimulus interval. Colours represent different delay period durations. Lines, mean responses; Error bars, ±1 SEM across trials.

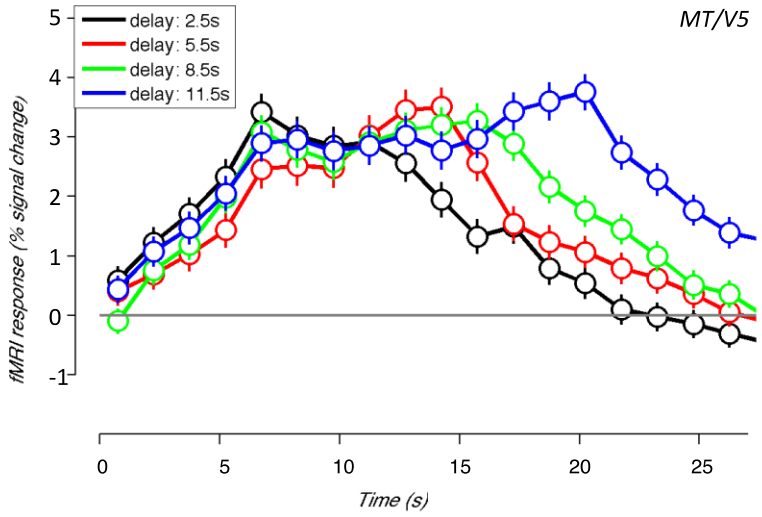

Figure 4.16: Sustained fMRI responses (% signal change) during the delay intervals in area MT/V5 for the detection task (high-level attention required). The average responses evoked by the stimuli presented in the stimulus intervals are also illustrated. Colours represent different delay period durations. Lines, mean responses; Error bars, ±1 SEM across trials.

(ii) Discrimination task (working memory)
Similar to the trend seen in the detection task, the transient activities corresponding to the first and second stimulus gradually separated as the delay duration increased (compare the transient responses in Figure 4.17 and Figure 4.18). For the discrimination data, they appeared segregated when the delay duration was 11.5s, especially true for MT/V5.

However, completely different fMRI activities during the variable delay periods were found for MT/V5 and V1 in this task (see the contrasting delayed response illustrated in Figure 4.17 and Figure 4.18). No sustained activity was retained in MT/V5 during the delay period in the discrimination task, whereas the activity in primary visual area (V1) remained (see Table 4.2 for the statistical result).

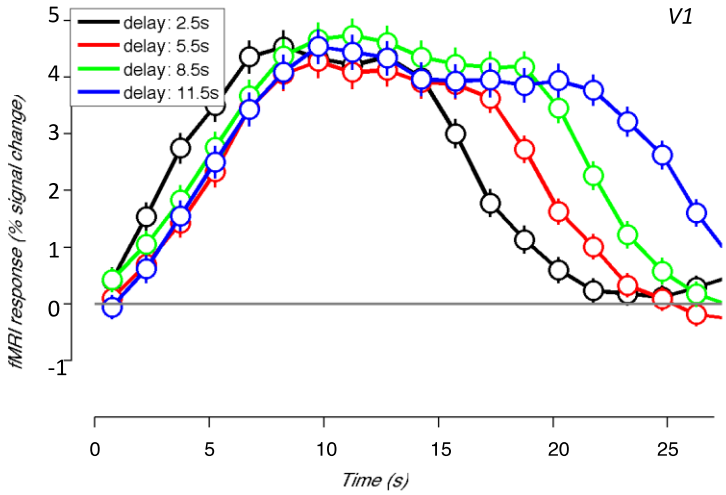

Figure 4.17: Sustained fMRI responses of different delays in V1 during the discrimination task where subjects *memorized* the motion coherence of the first stimulus to compared with the coherence of the second stimulus; abscissa, Time; ordinate, fMRI response (% signal change)

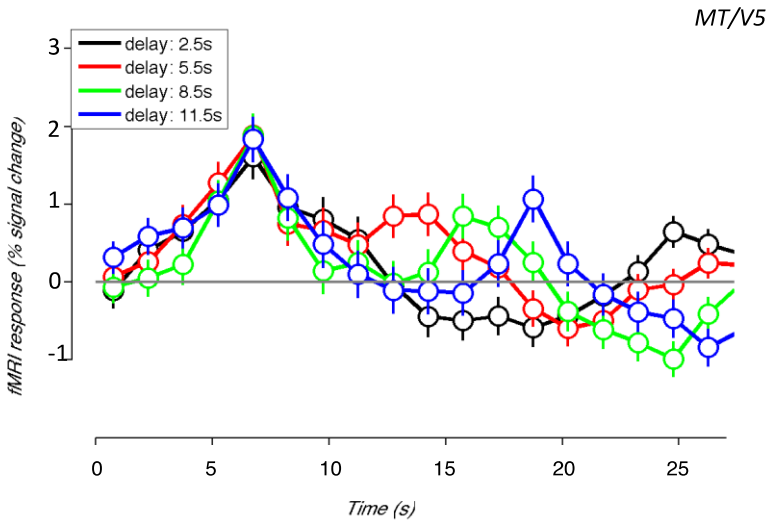

Figure 4.18: fMRI response of different delays in MT/V5 during the discrimination task (WM task) where no sustained activity is shown during the delay interval. abscissa, Time; ordinate, fMRI response (% signal change).

4.2.4 Discussion

In this pilot experiment, we used two-interval detection task and a delayed discrimination task to distinguish the processes of attention and working memory. Our aim was to separate the roles of attention and WM on motion information processing.

The role of attention in modulating the activity in MT/V5 and V1 (detection task)

Sustained activity was found in the detection task during the delay interval in both V1 and MT/V5 when attention was required. Many experiments have shown that the role of attention depends on the requirement of the specific task, including the location where stimuli are presented (foveal or non-foveal), the number of items displayed in the field and task difficulty. In this experiment, we fixed the task difficulty by alternating between coherence at threshold and 0% coherence to increase the requirement of attention. Our data is consistent with the majority of recent studies, although there is debate about the level in the processing hierarchy at which attentional signals arise. It was held for a long time that the earliest region an attentional effect could influence was medial superior temporal area (MST). And it was assumed that the strength of the influence decreased as one moved down the cortical pathways. However, evidences from electrophysiological studies have shown that activity changes in several sensory areas, such as hMT and V1, also depend on attentional state (Treue & Maunsell, 1996, 1999; Seidemann & Newsome, 1999). In addition, imaging and bilateral lesion studies on the human MT homolog, uniformly found a specific attentional effect at the earliest stages along the human dorsal visual pathway (Corbetta et al., 1990; Corbetta et al., 1991; Mcleod et al., 1989). Moreover, a study of speed discrimination of moving gratings revealed that the extent of attentional modulation on signals in V1 is comparable to that in MT/V5, an area known to specialize in motion (Gandhi et al, 1999). These studies combined with our results all corroborate the attentional top-down modulation model, indicating that higher-order cortices send extensive feedback resulting in changes in the response amplitude or response rate of neurons throughout the visual cortex.

It should be noted that our observations on the level of sustained activity is not due to the hemodynamic lag of the first target stimulus. In both tasks, variable delays were used to allow us to distinguish between the fMRI responses of visual target stimuli from the activity during the delay interval. It is indeed the case that when the delay period was short, the responses to the stimuli could not be discriminated from each other because of the hemodynamic sluggishness. However, for long delay periods, the activity peaked in response to the initial

visual stimulus and then fell to a lower level. Following the long ISIs, the response rose again in response to the second stimulus. Even in the case when the response to a visual stimulus was unlikely to confound the delay activity, V1 and MT/V5 still exhibited strong signals. In addition, the sustained activity is not simply the consequence of random motion during the delay interval. This is particularly true for MT/V5 because it does not display delay period activity with the presence of the same random dots in the discrimination task (see the result of discrimination task), indicating that it was genuinely modulated by attention. Therefore, our results assertively suggest that the attention strengthened the neuronal response in early sensory regions.

The role of visual cortex in WM of motion coherence (discrimination task)

- *MT/V5*

Previous studies have shown that area MT/V5 (in monkey) is sensitive to coherent motion (see Chapter 1), but is this area also activated when information about motion coherence has to be maintained in memory? In this experiment, we found that the discrimination task did not show any significant activity during the delay period in hMT. Many physiological studies have provided evidence that a subset of neurons in a relatively advanced stage of the hierarchy fired constantly at an elevated rate after a specific feature was presented, but not the early visual cortex. For instance, Ferrera et al. (1994) used a similar delayed match-to-sample discrimination task of motion direction and found no sustained pattern carrying information about motion direction in MT/V5. Since neurons in area MT/V5 are directionally selective (Zeki, 1974; Maunsell & Van Essen, 1983; Albright, 1984), we expect similarties between direction and coherence of motion. Indeed, we found no enhancement of overall activity in MT/V5 during the retention duration. However, contrary to our findings in human MT, one study using monkeys with unilateral lesions in MT/MST claimed that this area is also involved in maintenance of motion information (Bisley & Pasternak, 2000). There are a few

possible explanations for this discrepancy. First, as the authors of that monkey study pointed out, it is likely that the humans and monkeys applied different strategies in remembering information about stimulus direction. Since no survey of the strategy used by the animal could be applied, we are not certain whether this disagreement is due to a species difference. Second, our null sustained activity might be influenced by the size of the neural subpopulation involved in the task. However, our results clearly showed that the moving stimulus of dots with 60% coherence can evoke marked response in human MT in another fMRI experiment, and presumably if similar subpopulation of neurons were recruited in the process of memory, the activity should be large enough to be observed. Nevertheless, our result is analogous to those studies that failed to find sustained activity for remembered orientation in V1. It is highly possible that as Offen et al. (2009) suggested, there were some neurons in MT/V5 that increased their activity whereas others did not, and thus when we measured the averaged activity (pooled by the fMRI response), the activity of the excitatory neurons were washed out, leading essentially to a false negative result for delay period activity during the memory period.

- *V1*

Sustained BOLD activity was found in the primary visual cortex in our discrimination task. Despite the fact that attention could modulate the activity at this early stage, considerably less attention was involved in our discrimination task because firstly, both target stimuli were easily perceived and secondly, their difference along the dimension of coherence was above threshold (Zhou & Fuster, 1996, 1997). It seems that our data on sustained activity in V1 provides an indication of its involvement in WM of motion coherence tasks. However, we should be cautious to make this conclusion because of the dissociation of the activity in hMT and V1 during the delay interval. According to previous investigations, neurons in V1 have much less selectivity of the coherence of motion compared to MT/V5, and random-motion can effectively evoke activity in V1. Thus, it is possible that the delayed activity was a result of unselective response to random dots. Yet, we cannot completely exclude the possibility that

a majority of neurons unselectively involved in the maintainance of one level of coherence, contributed to a global increase during the delay interval, whereas the response evoked by the selective neurons in MT/V5, as discussed, might be cancelled by other subpopulations of non-preferred neurons (Offen, et al., 2009).

4.2.5 Limitation and future direction

Here, we discussed whether our measures of averaged response over the whole regions of interest (ROI) indicate V1 and/or MT/V5 is not involved in the process of WM. Other neuroimaging studies repeated some of the delayed memory experiments and with the application of multivariate pattern classification method (MVPA), they found that patterns of fMRI activity were different depending on the maintained visual information (Harrison & Tong, 2009; Serences et al., 2009; Sligte et al., 2013). Therefore, it is possible that the *pattern* of activation in our study was concealed after averaging the activity across all voxels in the ROI.

Additionally, it should be noted that the above inference is only based on a piloting experiment with one participant. In spite of this fact, it lays the foundation for our following fMRI experiments that further address the connection between and distinctness of attention and WM (Chapter 8). In addition, it inspired us to use a more sensitive approach to analyse data in a larger groups of subjects. Accordingly, we therefore conducted MVPA analysis on data from the fMRI experiments that followed. Additionally, we focused on the primary visual cortex (V1) and extrastriate areas (V2 and V3) since their tuning features for spatial frequency, orientation and contrast are clearer than the evidence for coherence tuning in MT/V5 (Beckett et al., 2012; Schwarzkopf, et al., 2011). Compared to the visual attributes of spatial frequency and orientation, the mechanism of remembering visual contrast has been more elusive. Therefore, we mainly concentrated on the memory characteristics for the *contrast* of visual information with fMRI in the following chapters.

Chapter 5: Temporal and Spatial characteristics of working memory of stimulus contrast

Abstract

Differential abilities of maintaining visual information have been revealed in studies of visual short-term memory (VSTM). Some evidence has shown that human have high-fidelity storage capacity for many properties of visual stimuli. On judgments of spatial frequency of gratings, for example, discrimination performance does not decrease significantly even for memory intervals of up to 30s. For other properties such as stimulus orientation and contrast, however, such "perfect storage" behavior is not found although the reasons for this difference remain unresolved. Here, we report three experiments in which we investigated the nature of the representation of stimulus *contrast* in VSTM using simple drifting grating as well as more complex noise patterns. We addressed whether information about the contrast *per se* is retained during the memory interval by using a complex 2-D stimulus with the same spatial structure but either the same or opposite local contrast polarity. Next, we introduced a mask during the memory interval and examined the influence of its spatial structure on memory representation. We found that discrimination thresholds got steadily worse with increasing duration of the memory interval for both simple gratings, as well as the binary noise stimuli. Further, for noise patterns, performance was better when test and comparison stimuli had the *same* local contrast polarity, than when they were contrast-reversed. Finally, when a mask was introduced during the memory interval, its disruptive effect was maximal when the mask had a higher contrast and differed spatially. These results suggest that VSTM for contrast is closely tied to the spatial configuration of stimuli and not transformed into a more abstract representation.

In addition to investigating the characteristics of contrast representation along the temporal domain, we also studied the spatial properties of VSTM by performing contrast discrimination task with pixel noise patterns displayed at either same (intrahemispheric) or different (interhemispheric) sides of the visual field. Two delay intervals (0.3s and 3s) between the first

stimulus and the second stimulus were used to observe the difference between the process of perception and VSTM, respectively. Discrimination thresholds for the intra- and interhemispheric condition were similar when the delay interval was short, but they became significantly different when the process of memory was involved. This result in addition to the increased reaction time in the interhemispheric condition indicates that there is an extra loss when information was transmitted across hemispheres, suggesting that the contrast representation is not localized. It is likely that a higher-level feedback signal was sent to retrieve and transfer information across hemispheres, making contrast comparsion at different spatial locations possible.

5.1 Temporal characteristics: What information is crucial for working memory of stimulus contrast? Evidence from psychophysical experiments

5.1.1 Introduction

Results from the experiments in chapter 4 suggest that the level of motion strength in a RDK stimulus (its coherence) can be stored selectively and robustly over several seconds in a two-interval forced choice task. Similarly, previous studies have shown that for other properties of visual stimuli, such as the spatial frequency of a grating, discrimination performance on a trial-by-trial basis did not decrease significantly even for delay intervals of 30 sec (Magnussen & Greenlee, 1992). Contrary to these results, however, earlier psychophysical evidence illustrated that the memory for contrast of single gratings (Magnussen et al., 1996) and orientation of single bars (Magnussen & Greenlee, 1985; Vogels & Orban, 1986) did not show such "perfect storage" behaviour. These differential characteristics of working memory for various visual features are consistent with the view that they are processed in parallel. It has been pointed out that the neural representations of different stimulus dimensions in early visual cortex are independent from each other, allowing for only limited interaction across domains (Magnussen et al., 1996). Moreover, neuroimaging experiments have found sustained activity in early visual cortex during the retention interval, suggesting that neurons in these areas are recruited for maintenance in short-term memory tasks (see e.g. Bisley, et al.,

2004; Zaksas & Pasternak, 2006). All of these findings were interpreted in support of the view that the same cortical areas / neural circuitry are used during the *processing* of visual stimuli as well as their *maintenance in working memory*. This view has been termed the 'sensory recruitment hypothesis'. However, most of the previous experiments have focussed on the features of spatial frequency or orientation. Less is known about the characteristics of working memory for stimulus contrast. Therefore, we investigated how perceptual information about stimulus contrast is maintained in memory and how early visual areas may participate in this process. We used both psychophysical and fMRI approaches. Prior to the neuroimaging study, which will be presented in the next chapter, we first examined the properties of visual working memory for contrast using behavioural measures. The results of these experiments are described in this chapter.

Definition of Stimulus contrast

There are several ways to calculate and report the contrast of a visual pattern. The specific choice usually depends on the stimuli used in experiments. *Michelson contrast* is often used to report the contrast for periodic stimuli, such as sine-wave gratings. It is calculated as $(L_{max} - L_{min})/ (L_{max} + L_{min})$, where L_{max} and L_{min} are the maximum and minimum luminance of the sinusoidal luminance distribution. On the other hand, for irregular pattern stimuli, root mean square (RMS) contrast and contrast energy are better metrics though Michelson contrast can still be calculated. In this chapter, we used *Michelson* contrast in all experiments in order to compare the memory characteristics across two stimulus types on an equivalent basis.

In the first experiment of this chapter, we examined how an elementary visual attribute of a simple sinusoidal grating, its contrast, is kept in memory. The performance in a two-interval contrast discrimination task was measured with a variety of stimulus parameters and retention durations, including three different levels of Michelson contrast (see Figure 5.1 for the experimental scheme). In Experiment 1, we also tested the effect of spatial frequency on contrast discrimination with three different values for each of the three Michelson contrasts. We explored these properties to guide the choice of parameters in our fMRI experiment,

which followed the initial psychophysical study. For this reason we did not include very low contrasts as such stimuli induce low BOLD signal changes, which in turn leads to lower signal to noise ratio in the measurements.

Experiment 2 and 3 focused on some additionally interesting questions about contrast perception and memory. As it is defined, contrast is the disparity of absolute luminance between spatially neighboring elements in an image, to which the human visual system is sensitive. But how does visual system maintain information of contrast presented by these elements? There are at least two possible strategies to remember contrast. One possible means is to encode and retain contrast of a number of small sub-regions of a stimulus as an iconic representation or "image". Along the same lines, subjects may even use very localised profiles in the change of luminance to facilitate their perception and memory of contrast rather than the entire stimulus. Another alternative might be that the visual system extracts a more abstracted representation of stimulus contrast irrespective of the distribution of the stimulus components and represents it on a one-dimensional scale. To our knowledge, no previous study so far has addressed this question.

Grating stimuli – usually with a sine- or square-wave luminance profile, are typically used spatial patterns in psychophysics experiments but the use of such a regular pattern does not allow us to untangle the two possible outlined above strategies. With the use of random pixel noise patterns, however, we may be able to, because they allow the independent control of local and global contrast characteristics. A large number of previous studies have provided some related evidence on the perceptual characteristics of these noise patterns, including how human vision identifies or segments textures (Bergen & Adelson, 1988; Bergen & Landy, 1991; Fogel & Sagi, 1989; Graham, 1991). A common stimulus used in these experiments is an independent, identically distributed (IID) texture, whose contrasts values of elements are identically distributed as a histogram. With these images, some of the pioneering reports have demonstrated that the visual system segregates the visual field depending on the differences of texture (Julesz & Oswald, 1978; Julesz, 1965, 1975; Beck, 1983). It was suggested that the

visual system uses the difference of average response over space to draw discrimination between two textures (Chubb et al., 1994). A more recent study further explored the mechanism of preattentive discrimination of achromatic texture with random mixtures of a range of linear Weber contrast (-1~1). They observed that the judgments of texture contrast were mainly influenced by the distribution of elements whose contrasts were below the mean value (Chubb & Nam, 2000). Additionally, it was illustrated that visual system may group the darkest pixels in random textures to facilitate the fine discrimination of these noise pixel patterns (Chubb et al., 2004; Whittle, 1986; Frisch & Julesz, 1966). Based on these studies, investigators proposed a "blockshot model", which emphasizes sensitivity to the sparse elements with the lowest luminance in the pixel noise texture, regardless of the overall luminance of the background (Chubb et al., 2004). In this study, we investigated whether subjects also made use of certain distinctive information when they remembered contrast of similar random noise patterns. Another benefit of using these stimuli is that their configurations are randomly determined, and they are thus less likely to allow for any simple schemes of semantic representation, which makes them suitable candidate stimuli to study visual working memory. Taking the grating stimuli and the pixel noise patterns with their advantages together, we tested how contrast information is actually encoded and stored in working memory.

5.1.2 Experiment 1: Working memory for the contrast of simple grating stimuli

In this first experiment, we aimed to replicate and extend previous studies, to examine to what extent the memory for the contrast of simple grating stimuli decays over time (Legge, 1981; Pantle, 1983; Magnussen et al., 1996; Lee & Harris, 1996). A standard two-interval forced-choice (2IFC) contrast discrimination task with different interstimulus intervals was used with stimuli at three fixed contrasts.

In addition, we also measured the contrast discrimination thresholds at different spatial frequencies. Previous psychophysical experiments have explored the interaction between

multiple channels of visual features, such as the processing of spatial frequency in relation to contrast detection or discrimination in detail (Virsu & Rovamo, 1979; Barlow et al., 1987; Geisler & Albrecht, 1997; Boynton et al., 1999; Goris et al., 2009; Meng et al., 2013). For example, studies have shown that visual contrast sensitivity depends markedly on spatial frequency (Bisti & Maffei, 1974; Uhlrich et al., 1981; Hodos et al., 2002; Sowden et al., 2002; Jarvis & Wathes, 2008), which is described as contrast sensitivity function (see Figure 5.1). Moreover, electrophysiological and neuroimaging evidences suggested that visual contrast sensitivities at different spatial frequencies are closely related to neuronal activity in early visual cortex (Berkley & Watkins, 1973; Campbell et al., 1973; Boynton et al., 1999). Since our result from psychophysics will serve the upcoming fMRI experiment as behavioral piloting (Section two), we also tested with three spatial frequencies to see if they would significantly change the performance of contrast discrimination in this psychophysical experiment.

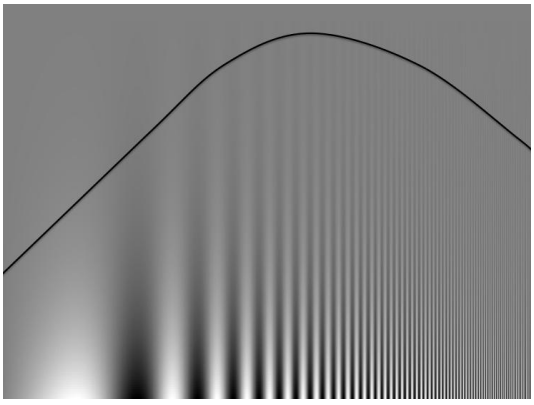

Figure 5.1: An illustration of contrast sensitivity function. Contrast sensitivity reaches a maximum at intermediate range of spatial frequencies, approximately 2-6 cycles/degree. Visual system becomes less sensitive to both lower and higher spatial frequencies (shown by the black curve). (Adapted from http://en.wikipedia.org/wiki/File:SinVibr.png).

5.1.2.1 Methods

Subjects

Four observers consented to participate in this experiment, including two experienced and two naïve participants. Three of them also took part in the contrast discrimination task with different spatial frequencies. Subjects all had normal or corrected-to-normal vision.

Apparatus

All stimuli in the psychophysical experiments reported in this chapter were generated on a Macintosh computer (MacPro, 2.66 GHz Dural-Core Intel Xeon) using custom software written for the stimulus generation tools MGL (http://gru.brain.riken.jp/doku.php/mgl/overview**)** in MATLAB (MathWorks). A CRT monitor (DiamondPlus73, 1024 × 768 pixels, 85 Hz) placed at a viewing distance of 57 cm was used for displaying the visual stimuli. The monitor's gamma nonlinearity was assessed (see details in Chapter 2) and corrected with inverse lookup tables.

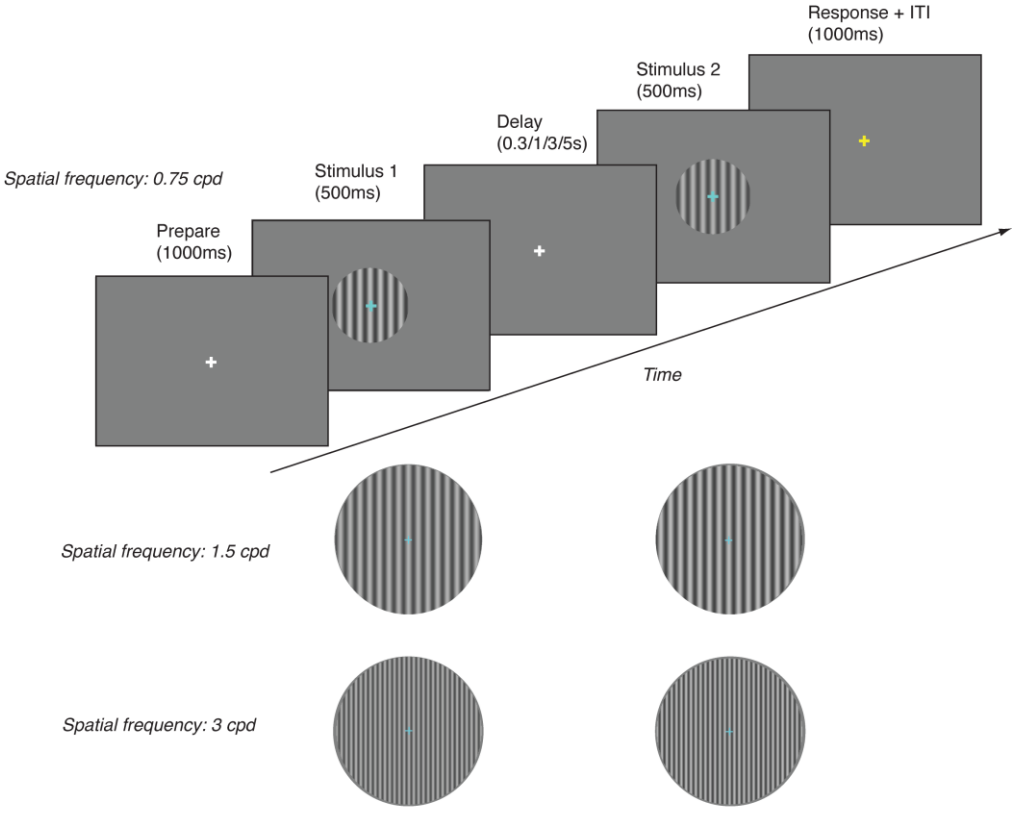

Figure 5.2. Examples of gratings with different contrasts used in Experiment 1. In each trial, observers judged which grating contained a higher contrast level at a fixed spatial frequency.

The first row illustrates the stimuli and time relations when the spatial frequency was 0.75 cycles/degree. Subjects were instructed to fixate centrally, and maintain the contrast of a drifting grating (40% contrast) that was presented during the first stimulus during a variety of delay intervals (0.3s, 1s, 3s and 5s). After the offset of the second stimulus with a different contrast, subjects pressed a button to indicate which stimulus interval contained a higher level of contrast. Feedback was given based on the answer. The two lower rows show two other spatial frequencies of gratings while the experimental paradigm was kept the same.

Visual Stimuli

The stimuli in the experiments were sinusoidal drifting gratings (spatial frequency, 0.75 cycles/°; temporal frequency, 2 Hz) that were presented in a circular aperture, centered at fixation) with diameter of 10° of visual angle. Three Michelson contrasts of gratings were used as fixed contrast (Michelson contrast 20%, 40% and 70%) respectively.

For the examination of spatial frequency effect on contrast discrimination, three different spatial frequencies (0.75 cycles/°, 1.5 cycles/° and 3 cycles/°) were employed while other parameters of the grating remained the same as in the other task (Figure 5.2 lower rows).

Procedure

The psychophysical thresholds for these contrast discrimination tasks were measured with the method of constant stimuli using a two-alternative-forced-choice procedure. Each trial consisted of two 500ms stimulus intervals separated by different delay intervals during which we displayed a blank grey screen with a fixation cross. One of the two stimulus intervals contained a lower contrast that was referred to as a fixed, and we added a signal randomly chosen from seven different contrast increments to this fixed to produce the contrast in the other stimulus interval. The two gratings were in sinusoidal phase, and the order of contrast pairs (and signal interval) was chosen randomly. Observers were asked to fixate on a central cross throughout each block. At the end of each trial, observers were required to choose the interval containing higher contrast. Feedback (color change of fixation) was given to indicate whether the answer was right (green) or wrong (red). Each trial was separated by a 1000ms inter-trial interval. Each run (block) contained 40 discrimination trials and seven blocks were collected for every fixed contrast (20%, 40% and 70%). The blocks for these fixed contrasts

were interleaved. Randomization, interleaving and variation of contrast increments were used to prevent learning and predictability of trial sequences.

In the experiments in which we tested contrast discrimination with various spatial frequencies, we were not concerned with the effects of changing delay period, so both stimuli were presented for 500ms and separated by a fixed 300ms interval of a blank grey screen. The other stimulus parameters remained the same and the procedure was identical to the memorized contrast discrimination task with one fixed spatial frequency. Figure 5.2 illustrates the experimental scheme used in this experiment and it also shows the stimuli with different spatial frequencies.

Similar to the method used in the last chapter, a sigmoid (Weibull) function was fit to the psychophysical data using non-linear regressions, (psignifit toolbox, version 2.5.6 for Matlab http://bootstrap-software.org/psignifit), and the corresponding value of contrast increment at 75% correct performance level was defined as the discrimination threshold. Figure 5.3 shows an example of how we obtained the discrimination threshold from a psychometric curve for contrast discrimination of sinusoidal gratings. All the thresholds in the following experiments in this chapter were calculated with the same method.

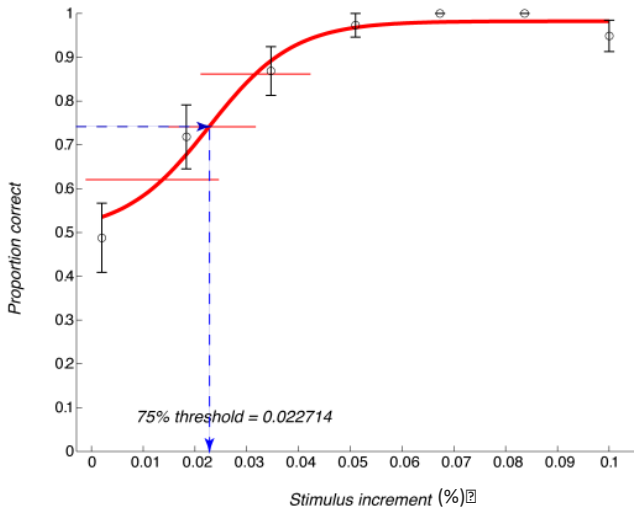

Figure 5.3: An example of a psychometric curve for contrast discrimination obtained with a fixed Michelson contrast of 30% (spatial frequency, 0.75 cycle/degree). Proportion of correct response is plotted as a function of contrast increments (7 levels). Symbols: each point on the

curve is based on at least 40 observations. The smooth red curve is the best-fitting Weibull function through these points. For details on the procedure see the chapter 2 on General Methods. The red horizontal lines at 60%, 75%, and 90% correct indicate the 95% upper and lower confidence intervals for their corresponding proportion correct, respectively. Dashed blue lines pointed at the stimulus increment (X-dimension) at 75% correct (Y-dimension), which we used as the value of discrimination threshold.

5.1.2.2 Result

To assess the dependence of contrast discrimination thresholds on memory interval duration we performed a 4×3 ANOVA (with four memory interval durations and three contrasts). The main effect of memory interval duration and fixed contrast was significant ($F(3,47) = 5.26$, $p < 0.05$ and $F(2,47) = 12.85$, $p<0.05$), but there was no interaction between these two factors ($F(6,47) = 0.15$, $p=0.99$).

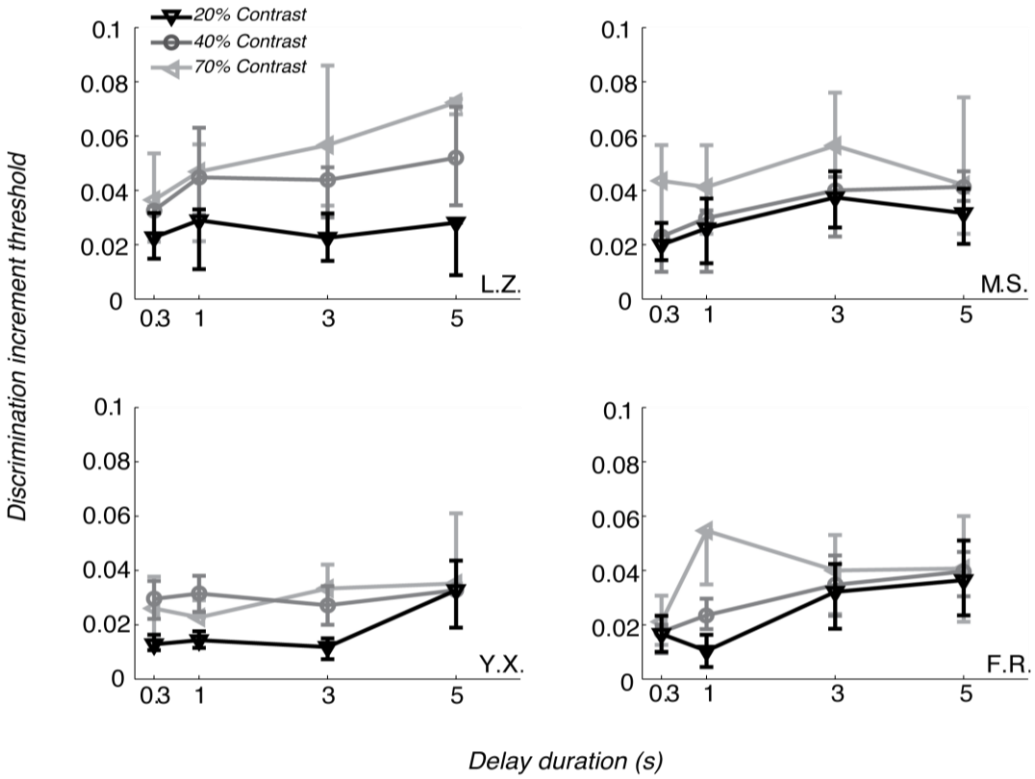

Figure 5.4: Increment thresholds of the delayed contrast discrimination using gratings (spatial frequency: 0.75 cycle/deg) for each observer at different fixed contrasts. Measured discrimination thresholds are plotted against the delay period. Error bars: 95% CIs at the 75% correct level obtained from the psychometric curve.

To compare our results at different fixed Michelson contrasts, we transformed these discrimination thresholds to Weber fractions (ΔS/S, or threshold/fixed contrast) as we did in Chapter 4. The results for 20%, 40% and 70% contrast are displayed in one panel for each observer (Figure 5.5). In each panel, the Weber fractions are plotted against different interstimulus intervals for each fixed contrast. All subjects showed comparable patterns of results. The results in the Figure 5.5 (for 20% fixed contrast) show more variation, but all illustrate a moderate upward shift of the fractions as ISI increases, indicating that memory of contrast decays over time.

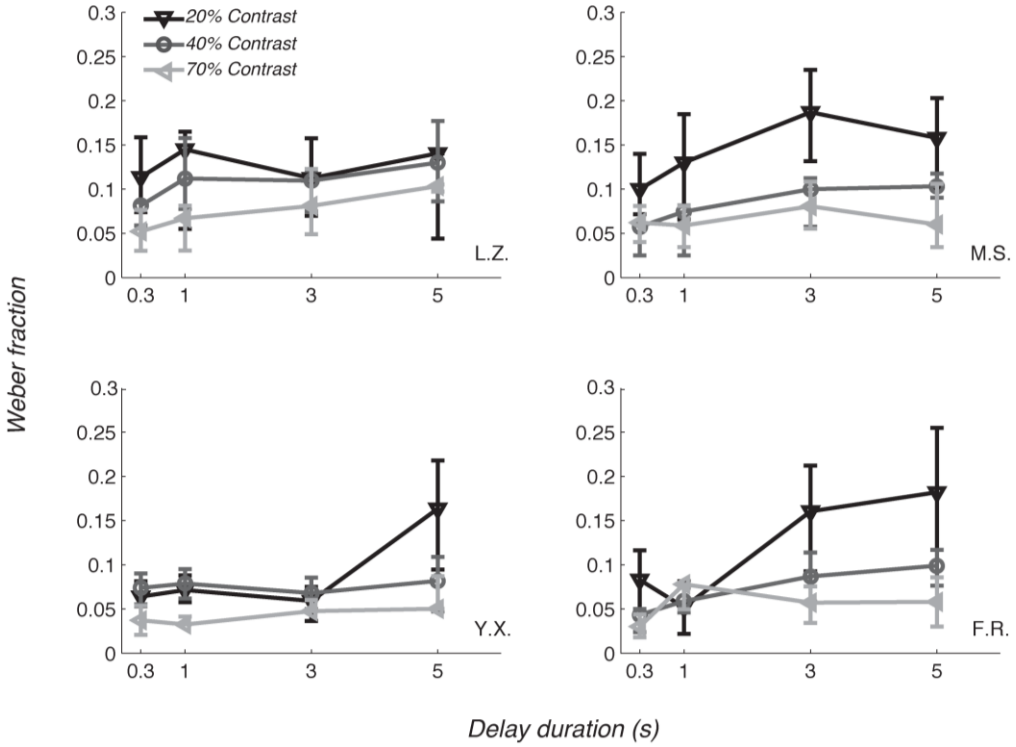

Figure 5.5: Weber fractions for the contrast discrimination experiment using gratings with three contrasts (spatial frequency, 0.75cycle/degree) for individual subjects. Symbols show the discrimination performance for different fixed contrasts. In each panel, Weber fractions are plotted as a function of ISI. Error bars are 95% CIs at the 75% correct level obtained from the psychometric curve.

For the sake of visualization, we combined the discrimination thresholds and Weber fractions of all contrasts into single graphs of Figure 5.6 and Figure 5.7, respectively. Both show mean

values across all subjects as a function of retention duration for the 0.75cpd gratings. It is noticeable that the thresholds increase as the fixed changes from 20% to 70% (see inset of Figure 5.7), but when they are expressed as Weber fractions (Figure 5.7), the trend is reversed. The values become smallest for the highest contrast (70% contrast), and biggest for the lowest level (20% contrast). To avoid this demonstration effect, we present the average results in this experiment in the format of threshold-versus-contrast (TvC) function (see Figure 5.8 for example). The axis of its ordinate describes the discrimination threshold and the axis of abscissa is the fixed contrast, in our case the three fixed contrasts. The oblique lines through the data are best fitting straight lines. These lines exhibit how contrast threshold changes as a function of the fixed contrast. The slopes of the fitted lines were measured to quantify our comparison of performance for various ISIs. They represent the exponent of a power relation between the variables in both axes. If ΔC denotes the contrast increment, and C is the fixed contrast, then the slope can be calculated with the formula $N = \log(\Delta C)/\log(kC)$, where k is a sensitivity parameter. Figure 5.8 shows within the contrast range used in our experiment, the contrast discrimination thresholds increase with increasing contrast level. And the vertical shift of the TvC function illustrates the decay of memory over time at each fixed contrasts. The slopes for different ISI are 0.4546, 0.5874, 0.4686 and 0.3136, respectively. On one hand, these values demonstrate that discrimination performance is a monotonic increasing function of fixed contrast. And on the other hand, they also reflect that the contrast increment threshold rises more slowly than the fixed contrast for all ISIs, with the shallowest for the longest retention duration.

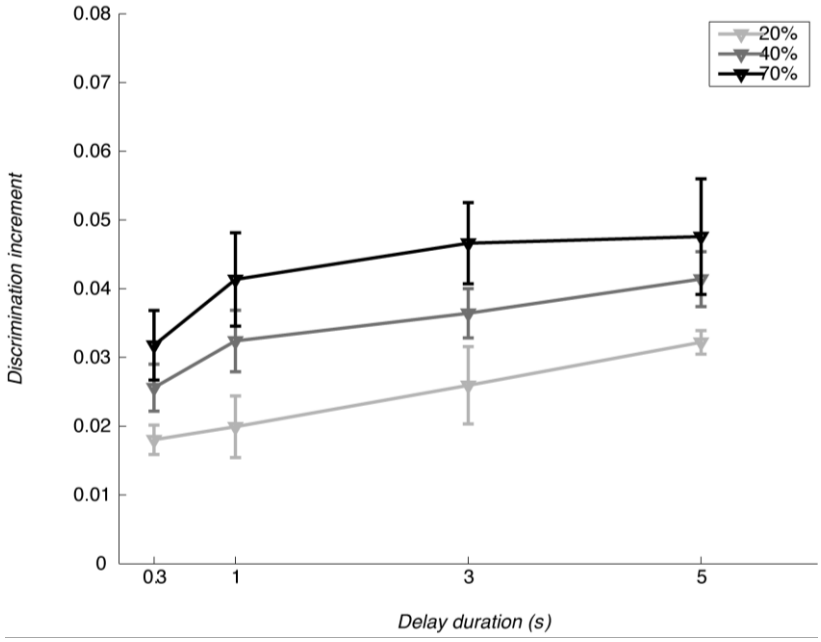

Figure 5.6: Elevated discrimination thresholds as a function of ISI across all subjects in the delayed contrast discrimination task for the three fixed contrasts (20%, 40% and 70%). Colour of the solid lines, data for different fixed contrasts. Error bars: ±1 standard error of the mean.

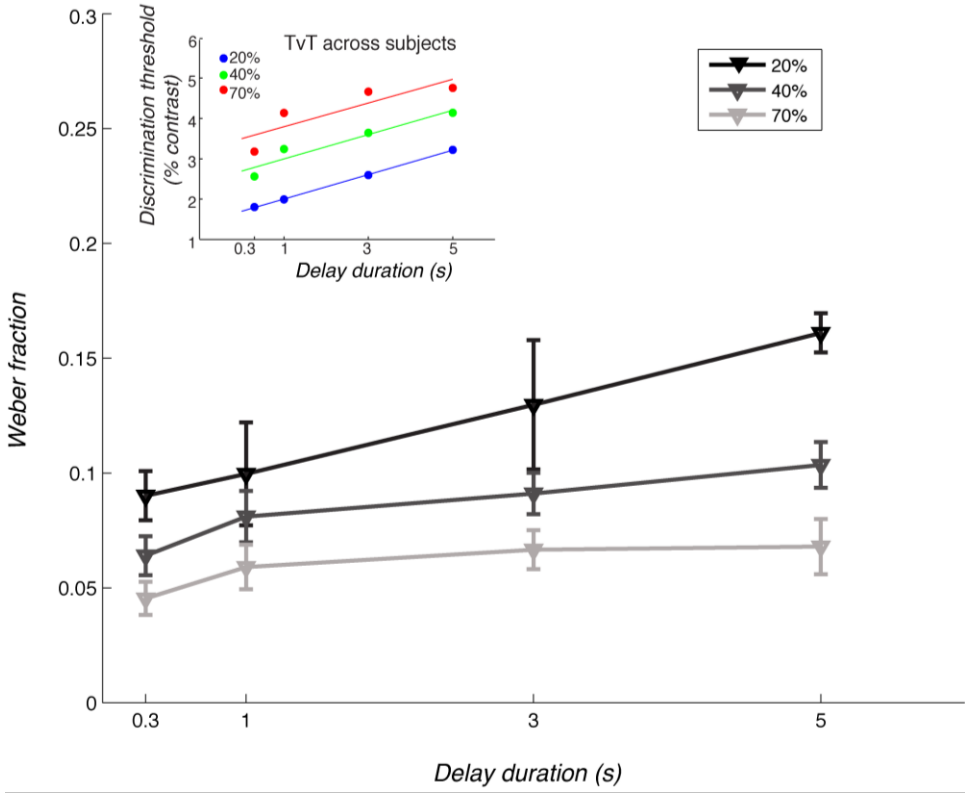

Figure 5.7: Increased weber fraction as the ISI increased from 0.3s to 5s. Colour of the solid lines, data across different fixed contrasts. Error bars: ±1 standard error of the mean. Inset illustrates the average increment threshold against ISI (delay duration). Notice the trend of

Weber fractions is reversed version for the discrimination threshold for different fixed contrasts compared to the one showed in the inset.

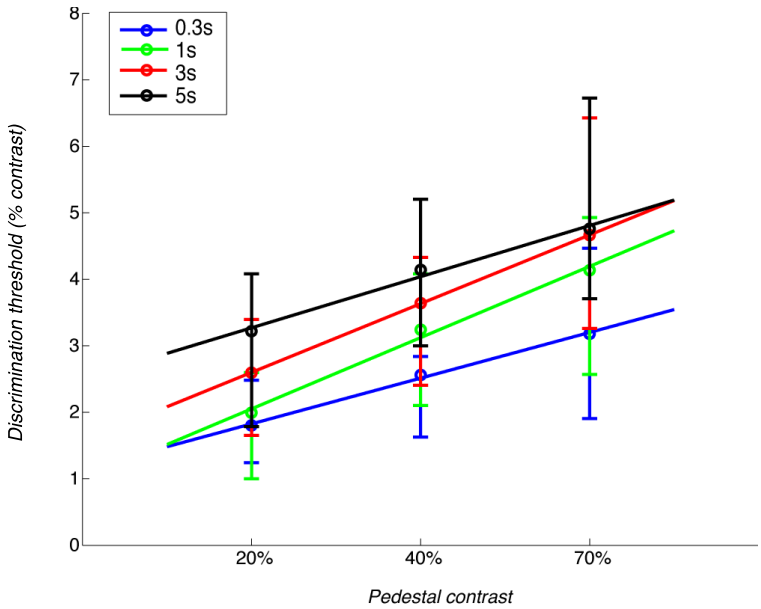

Figure 5.8: Threshold increments replotted as a function of fixed contrast (TvC curve). Data points are the means of discrimination thresholds across four subjects, which increased as the fixed contrast increased. Coloured lines are linear fits through the points.

The effect of spatial frequency on contrast discrimination task

Panel A, B and C in Figure 5.9 and Figure 5.10 show each subject's discrimination thresholds and Weber fractions for different spatial frequencies and a 0.3s ISI for the three fixed contrasts. The discrimination thresholds from each individual showed similar trends and were thus combined. Each data point in Panel D of these two figures represents the mean value across the three observers. Our data confirms previous reports that spatial frequency has an effect on contrast discrimination; however, in our data, the particular choice of spatial frequency was less influencial on the performance for 20% and 40% than for 70% fixed contrast.

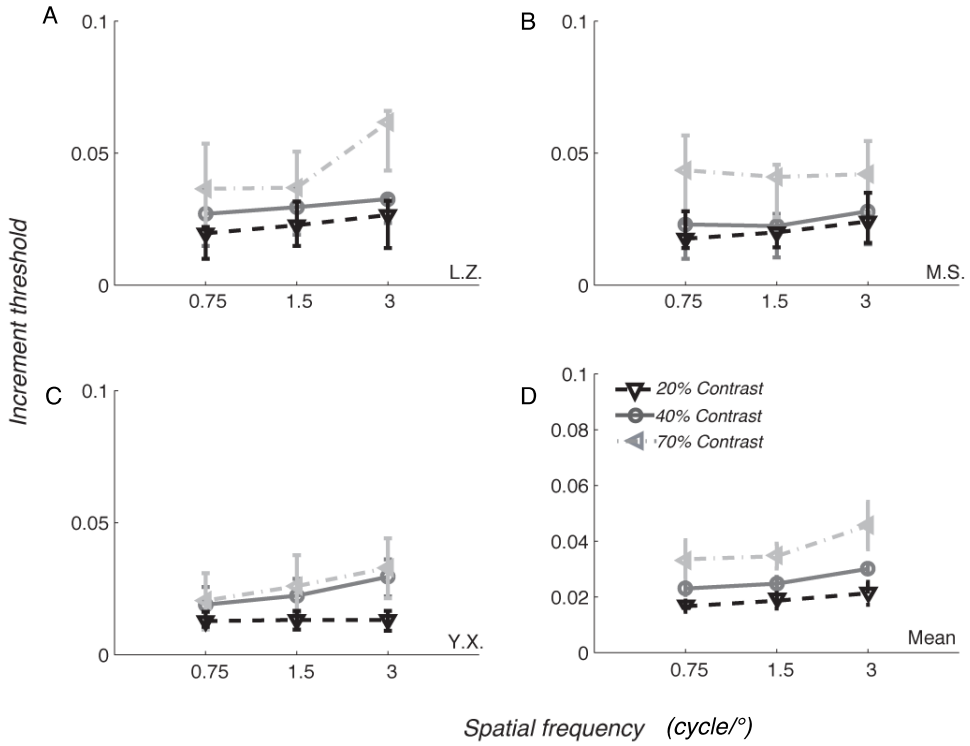

Figure 5.9: A-C: Results of the effect of spatial frequency on contrast discrimination using grating stimuli for each observer at different fixed contrasts. Discrimination thresholds are plotted against spatial frequency. Error bars: 95% CIs at the 75% correct level obtained from the psychometric curve. D: Averaged thresholds as the function of fixed contrasts across 3 subjects for different spatial frequencies.

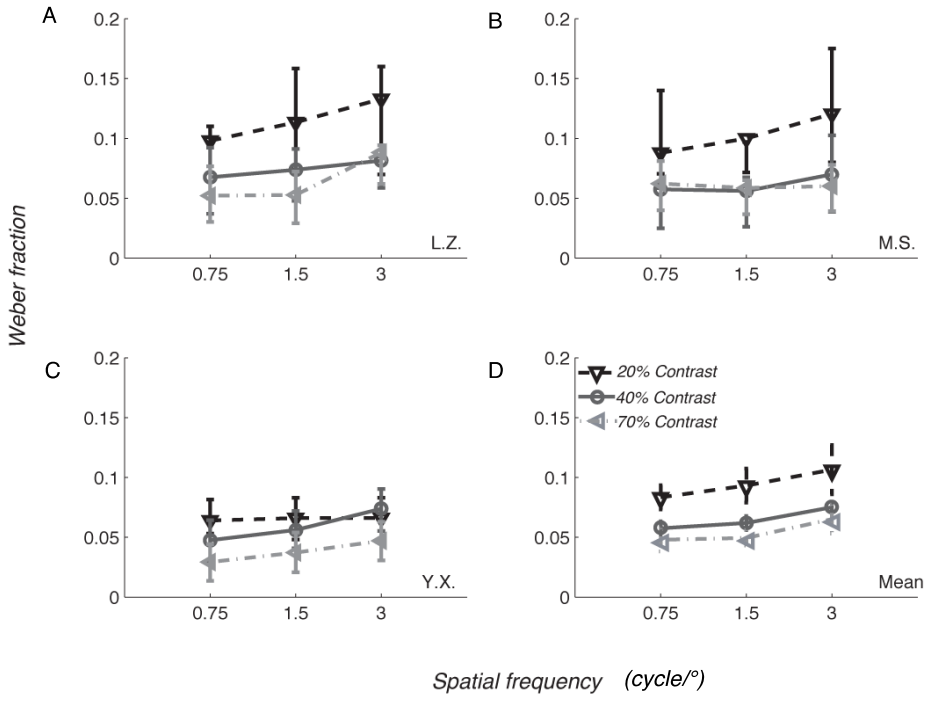

Figure 5.10: A-C: Weber fractions of spatial frequency on contrast discrimination using grating stimuli for each observer at different fixed contrasts. Error bars: 95% CIs at the 75%

correct level obtained from the psychometric curve. D: Averaged fractions as the function of fixed contrasts across 3 subjects for different spatial frequencies.

This relationship is represented in TvC function (Figure 5.11), and also quantitatively demonstrated by the slopes of the fitted lines for the three spatial frequencies: 0.1944, 0.2089 and 0.2378, respectively. These values are comparable across different spatial frequencies, and no statistical difference was detected ($F(2,26) = 2.62$, $p = 0.1006$, 3x3 ANOVA). And our statistical analysis confirmed that the increase of discrimination thresholds as it is shown in Figure 5.11 is a consequence of contrast difference (20%, 40% and 70%) ($F(2,26) = 13.87$, $p = 0.0002$). No interaction was found between contrast and spatial frequency ($F(2,26) = 0.27$, $p = 0.8934$).

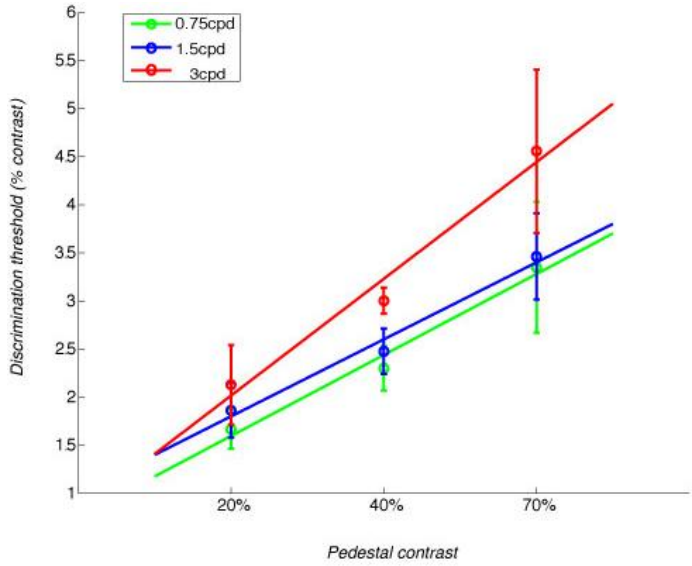

Figure 5.11: TvC function for effect of spatial frequency on contrast discrimination experiment. The average discrimination thresholds are plotted against three fixed contrasts across three observers. The manipulation of spatial frequency has a marginal effect on discrimination thresholds for relatively lower contrasts (20% and 40%) at lower spatial frequency, but bigger effect for higher contrast (70%) especially when spatial frequency was 3 cycles/deg.

5.1.2.3 Discussion

In this experiment, we first measured discrimination thresholds for various lengths of delay duration, including 0.3s, 1s, 3s and 5s, but with one fixed spatial frequency (0.75

cycle/degree). Significant statistical difference of threshold is found as ISI increases, which indicates that retention of stimulus contrast in working memory degrades over time, suggesting a decay of contrast information in short-term memory as it was reported in previous studies (Greenlee & Thomas, 1993; Lee & Harris, 1996; Magnussen & Thomas, 1992). More discussion was described in the General Discussion of this Chapter.

Another aspect of the data is also consistent with a majority of earlier reports that increment thresholds rise steadily with background contrast using sine-wave gratings. Here, we used both Weber fraction and contrast discrimination function (TvC) as approaches to demonstrate our results. For Weber fraction, similar to most studies of contrast discrimination (Nachmias & Sansbury, 1974; Kulikowski, 1976; Legge, 1981; Pantle, 1983), our data show that the size of fractions decreases as the fixed contrast increases over a large range of suprathreshold contrast (Figure 5.7).

The threshold versus contrast functions (TvC) for our discrimination data was also plotted (Figure 5.8). Straight lines fit in such plots allow the estimation of the exponent N in $\Delta C = kC^N$ for different retention durations. If the value of N equals to 1.0, then the contrast discrimination obeys Weber's Law, i.e. the threshold contrast is a fixed proportion of the fixed contrast. However, the slopes of best-fitting lines in our experiment are all less than 1.0, indicating that the increment of thresholds are progressively smaller as the fixed contrasts increase. This tendency was present for all ISIs, including the longest ones. It is noticeable that the exponents of longer ISI durations have smaller values, which may imply that the contrast memory in relation to fixed contrasts becomes less sensitive as time elapses.

Debates as to whether Weber's law accommodates the results from various studies on the perceived contrast of sinusoidal gratings have carried on for more than three decades. These reports suggest that Weber's Law does not apply, and that contrast discrimination instead follows a Power law over the rising segment of the TvC function where the slope is less than 1 (see review in Swift & Smith, 1983; and Bird et al., 2002). Such evidence was based on wider ranges of spatial frequencies and background contrasts, some of which matched our

variables. For example, Pantle (1974) found a value of 0.47 for contrast discrimination at 2 cycles/deg. Legge (1980) derived an exponent near 0.6 for a 2cpd grating with low and middle fixed contrasts at a fixed ISI of 600 msec. Another study on contrast characteristics in working memory also reported that their results for gratings with a 1cpd spatial frequency followed a power law relationship between ΔC and C (5%, 15% and 60% contrast) with 1, 3 or 10 sec ISIs (Lee & Harris, 1996). Slightly different from these parameters, we mainly focus on three suprathreshold contrasts (middle and high levels) with one relatively low spatial frequency (0.75 cycle/degree). Despite these dissimilarities, we find that the exponents of the power function for different retention periods are also around 0.45, leading to the conclusion that present findings do not support Weber's Law for contrast discrimination, and contrast memory in particular since the exponent values for longer ISIs are even smaller.

To examine whether spatial frequency is a factor that influences contrast discrimination (ISI: 0.3s) in the range of parameters we were planning to use in the imaging study, we performed the task with different spatial frequencies. From the graph of thresholds, we can see that contrast discrimination becomes elevate as spatial frequency increases within the studied range (Figure 5.9). The manipulation of spatial frequency has a marginal effect on discrimination thresholds for relatively lower contrasts (20% and 40%) at lower spatial frequency, but bigger effect for higher contrast (70%) especially when spatial frequency was 3 cycles/deg. However, when the TvC are plotted on the usual logarithmic scales, the discrepancies between these middle and high contrasts and the selective loss of contrast information at higher spatial frequency is much less apparent. Furthermore, the 95% CI overlap with each other, and statistical analysis showed no clear evidence for consistent differences. This mirrors findings in Legge and Foley's (1980) investigation of the relation between ΔC and C with gratings that differed in spatial frequency. Others did not only find that the threshold function was invariant with spatial frequency (1, 2.5 4 8 cycles/deg) for brief durations, as used here, but also suggested that the ability of contrast memory is not

systemically dependent on the spatial frequency component (Lee & Harris, 1996; Harvey et al., 1986).

5.1.3 Experiment 2: Working memory of contrast with random noise pattern stimulus

Experiment 1 showed that contrast information relating to periodic stimuli, like sinusoidal gratings was maintained but decayed to some extent over time. The purpose of Experiment 2 was to see if the characteristics of retention in memory would be similar for the contrast of more complex stimuli. A range of ISIs was implemented to specify the fidelity of retention of contrast information over time using a pixel noise stimulus. The aim was to examine whether the contrast signal is extracted independently from the reference of the representation of internal features of the stimulus (e.g. the arrangement of black and white elements). Two experimental conditions were designed for this purpose. In one condition that is referred to as the 'identical-pattern condition', the same pixel noise pattern was displayed in the two stimulus intervals of a trial. In contrast to this condition, the 'reversed-pattern condition' made use of two stimuli in each trial reversed luminance distributions, i.e. white was inverted to black and vice versa. Therefore the same contrast energy was maintained in the paralleling contrast levels in 'identical condition' and 'reversed condition' but the spatial pattern and the polarity of local edges were reversed in each of the trials in the second condition. Presumably, if the performance in the contrast discrimination task were independent of the distribution of the pixels that convey the contrast, then the thresholds of these two conditions would be similar regardless of the stimulus profile. Otherwise, we might expect differences in performance. We examined more than one delay duration with this paradigm. This temporal extension did not only answer our question of what information of contrast is encoded, but also what is retained and represented in visual system.

5.1.3.1 Methods

Observers

Four subjects performed a contrast discrimination task using the random pixel noise stimulus patterns.

Visual stimuli

The stimuli were generated and displayed by a Macintosh computer (See details in Chapter 2). All the other details of the experiment and environment remained the same as before. For each run, twenty images composed of randomly arranged squares were drawn and stored on disk. This was to ensure that subjects had no specific cue of which random pattern they were going to perceive during a given trial and had little opportunity to develop long-term memory for any particular exemplar. Each random noise pattern consisted of a 10×10 array of square elements and subtended 20°×20° visual angles in total (Figure 5.12).

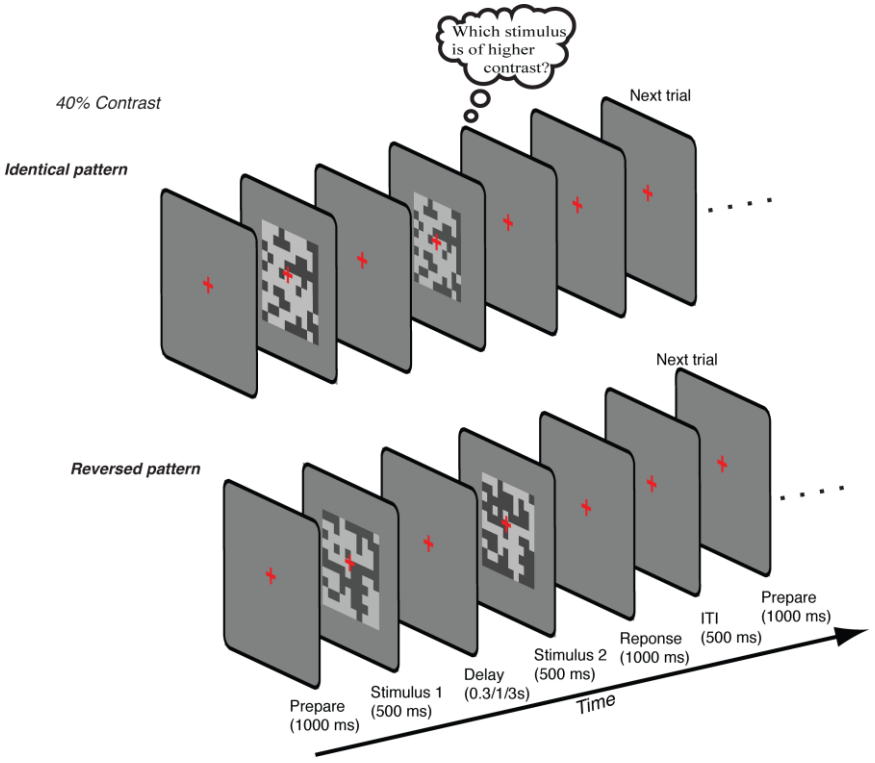

Figure 5.12: Scheme of the contrast discrimination task with a range of delay intervals (0.3s, 1s and 3s) (random pixel noise with 40% contrast). Upper panel, A trial in the identical condition where stimulus 1 (500ms) and stimulus 2 (500ms) have the same spatial pattern. Lower panel, A trial in the reversed condition where the spatial pattern of stimulus 2 is a reversed version of stimulus 1. Subjects need to judge which stimulus interval had higher contrast of stimulus by pressing a corresponding button. A feedback was given based on the answer.

Procedure
Piloting

Contrast discrimination was measured using a 2IFC procedure. Very similar to Experiment 1, following a brief duration of stimulus exposure (500ms), observers viewed a blank screen, which was followed by the second stimulus interval. In this experiment, we first piloted three Michelson contrasts (20%, 40% and 70%) as fixed contrast of the random noise pattern on two observers. Each block had one fixed contrast that was delivered randomly to one of the stimulus intervals. It was coupled with a second noise pattern stimulus, which differed in contrast by a small contrast increment (ΔC). Its value was randomly selected from seven linearly spaced step sizes. For the pilot experiment, the inter-stimulus interval (ISI) between the first and the second stimulus was 300ms. Observers reported in which interval the higher contrast was presented by pressing one of two buttons. Trials in the 'identical-pattern condition' and 'reversed-pattern condition' were conducted in alternating runs.

In the main experiment, to establish the effect of changing the retention period, we then limited the stimuli to a fixed of 70% Michelson contrast. All observers performed the same procedure as in the piloting session, but with four different interstimulus intervals (ISI 0.3s, 1s, 3s and 5s). Figure 5.12 shows the paradigm of this experiment. The upper panel illustrates the ‘identical pattern’ condition at Michelson level 40% in the piloting session, where pairs of binary random noise images were presented in succession, each of which had one unique global Michelson contrast. The lower panel demonstrates the ‘reversed pattern’ condition at fixed contrast 70%.

5.1.3.2 Result

Piloting result
During the piloting of experiment 2, discrimination thresholds for three contrast levels were measured on two observers. TvC function for each subject and their averaged result are displayed in Figure 5.13. Both observers show an increase in threshold as fixed contrast rises

from 20% to 70% in a linear manner though their slopes are different. This trend holds true no matter whether the stimulus pattern is identical or reversed in a trial. The discrimination thresholds in this experiment are in agreement with our result from the last experiment acquired with simple sinusoidal gratings when ISI was also 0.3s. These figures also clearly demonstrate that for all fixed contrasts, the thresholds increase when the stimulus and matching patterns are reversed.

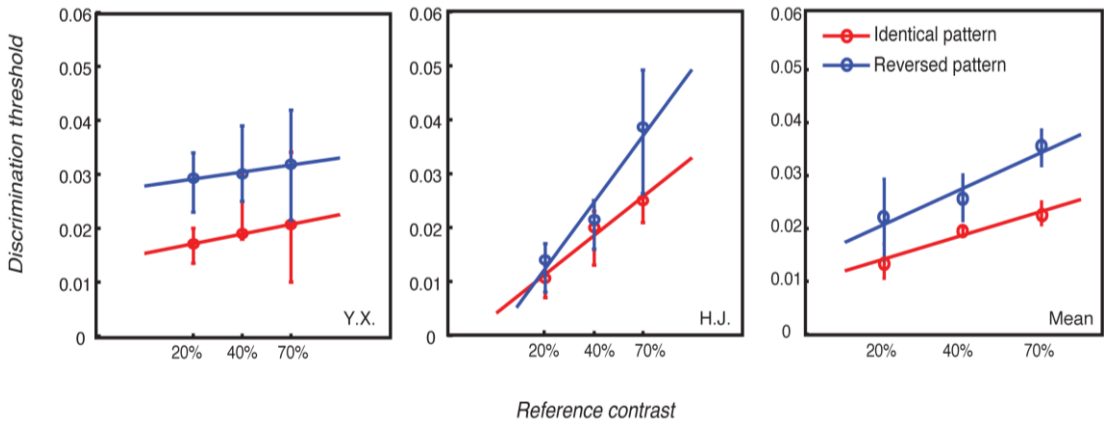

Figure 5.13: Two left graphs, Pilot contrast discriminatin thresholds of two subjects at three different fixed contrasts (20%, 40% and 70%). Random noise pixel pattern was used as visual stimulus. Contrast discrimination results have similar disparities between the 'identical 'and the 'reversed pattern' conditions. Error bar: 95% CI of 75% response accuracy obtained from individual psychometric curve. Right graph, Averaged contrast discrimination thresholds for three fixed contrasts with 0.3s ISI across two subjects who attended the pilot sessions. Error bar: ±1 SEM. Straight lines are lines of best fit through the thresholds data for both 'identical condition' and 'reversed condition'.

Examining working memory

Since the piloting result showed that different fixed contrasts did not cause consistent differences in behaviour, we chose a contrast level of 70% contrast as the only fixed to be examined further with different ISIs. The first question this data can answer is that contrast of this pattern could be stored over different delay durations of the discrimination task. The same 2IFC framework was used to measure discrimination thresholds when the random patterns were memorized. Figure 5.14 illustrates the contrast Weber fraction for each observer at different ISIs for 'identical condition' and 'reversed condition'. As it is shown, the fraction

increases as the delay time becomes longer in both conditions. The trend is more clearly demonstrated in Figure 5.15, where the Weber fractions are averaged over all subjects for the corresponding situation. The results here are similar to those reported earlier in other contrast discrimination studies and consistent with our last experiment using sinusoidal gratings.

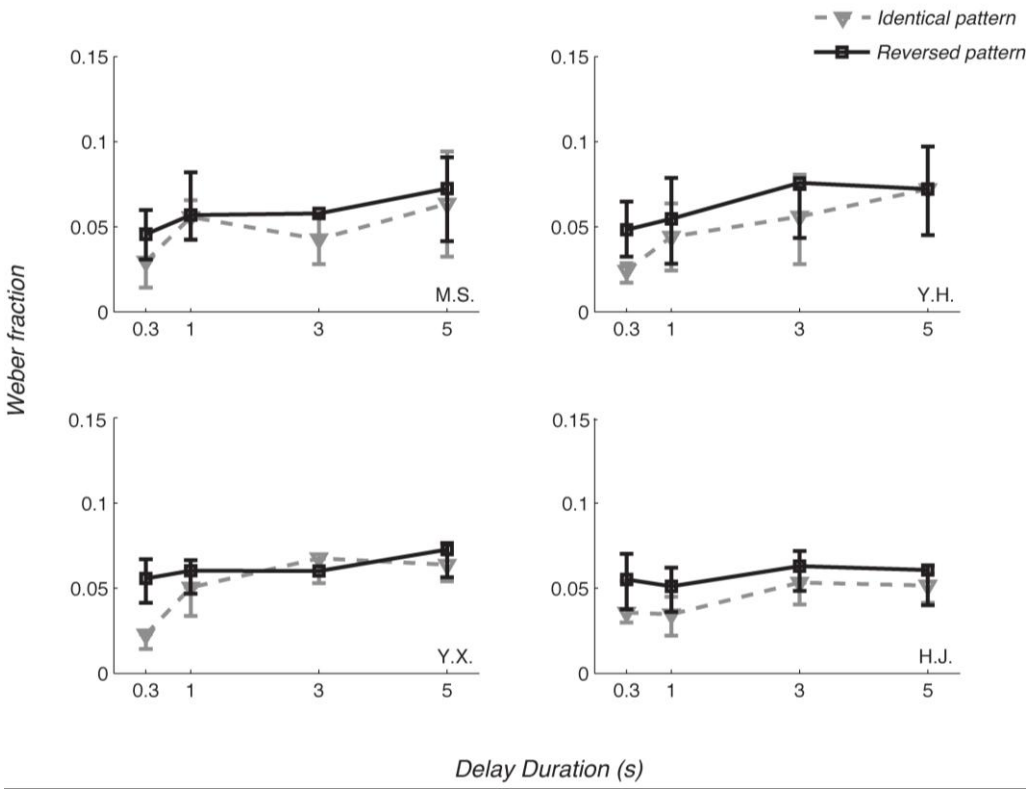

Figure 5.14: The Weber fractions of contrast discrimination task for each observer with different ISIs (at 70% fixed contrast). Colour and line features represent different stimulus conditions used in the experiment.

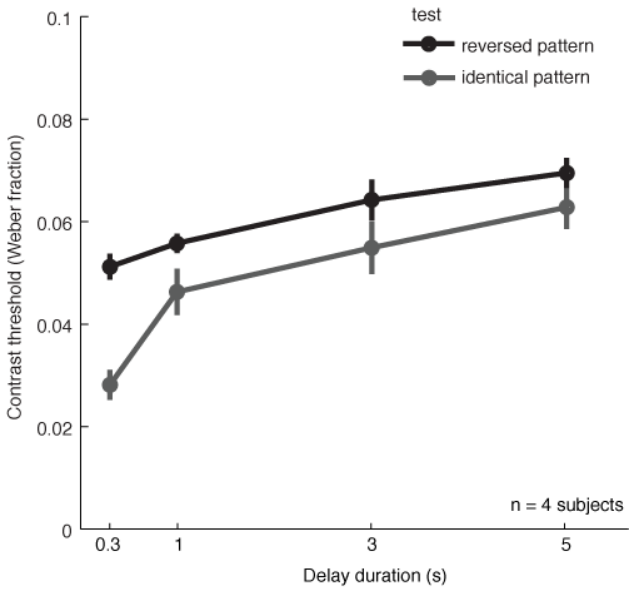

Figure 5.15: The average Weber fractions of contrast discrimination task across four observers with different ISIs (at 70% contrast). For all the delay durations, the performance of contrast memory task is better than that of the reversed pattern condition. Colour represents different stimulus conditions used in the experiment.

The result of this experiment also demonstrates that the Weber fractions of 'reversed pattern' are consistently bigger than the 'identical condition', indicating a cost when the pattern was reversed in comparison of same-pattern condition. To assess statistical significance for the changes in threshold, we conducted a two-way repeated-measures analysis of variance (ANOVA) on retention duration (0.3s, 1s, 3s and 5s) and stimulus pattern type (identical and reversed). The main effect of both memory interval duration and stimulus type were both significant ($F(3,31) = 19.49$, $p < 10e\text{-}9$, and $F(1,31) = 21.94$, $p < 0.001$, respectively). The interaction was not significant ($F(3, 31) = 2.03$, $p = 0.1366$). This result suggests that the visual system may encode and represent the spatial configuration of the stimulus to facilitate the process of VSTM for contrast.

As a subsidiary condition, we also mixed these two conditions in a single block for two subjects (see M.S. and H.J. in Figure 5.14) to discourage observers using possibly different strategies for maintaining contrast information if they were segregated into 'identical' or 'reversed' blocks. Similar result was found even when same and reversed conditions were

presented in single blocks for all the four ISI durations. Hence, we conclude that the difference of contrast memory induced by the two different pattern conditions is a genuine finding.

5.1.3.3 Discussion

Experiment 1 demonstrated that contrast discrimination thresholds increased as the delay duration elongated. In experiment 2, same systematical tendency was exhibited. More importantly, experiment 2 shows thresholds significantly increased when the stimulus pattern was reversed compared to when it was identical. It is worth noting that everything (including the contrast polarity of each element) within the pattern was kept the same in the 'identical condition', and thus observers simply need to detect the increment of contrast across the whole pattern presented by these same patterns. By comparison, for the 'reversed condition', although the overall contrast energy remained comparable to the 'identical condition', many features of the pattern are changed with inversion, which include the location of dark/light and light/dark edges as well as the location of luminance peaks and troughs within the pattern. If subjects used configural or local information as a reference to discrimination contrast, then the performance should become worse under this circumstance. Our data supports this hypothesis. One possible interpretation is that information about the contrast to be remembered is tied to the whole pattern and that when the pattern or *pictorial representation* of contrast differed from that which was coded and stored, the process of working memory becomes more challenging.

An alternative to coding and remembering the holistic stimulus pattern as a reference for contrast is the possiblilty that the visual system only codes a subset of image elements in memory. If this was the case, then, observers could have performed the task by comparing the contrast between corresponding squares in the first and second stimulus patterns. Though the stimulus is a binary image of random pixel noise, the contrast was uniform within any one of the stimuli, and thus the local contrast could be a proxy for the contrast of the entire stimulus. Then, the representation of local contrast between a few adjacent bright and dark square

elements could support correct performance in the delayed contrast discrimination. In an experiment of a delayed pattern discrimination task, Cornelissen and Greenlee (2000) revealed that the contributions of the elements near fixation were greater than those on the perimeter of the pattern. They interpreted their data as the result of an attentional mechanism operating at the encoding stage or during the maintenance and retrieval stages. For our stimuli, it is also possible that the representation of the central regions of stimulus took a more important role in contrast encoding and sustaining the representation in the present experiment.

5.1.4 Experiment 3: Masking effects for the memory of contrast random noise patterns

Both Experiment 1 and Experiment 2 demonstrate that the memory of contrast decays over time. This has been examined using periodic as well as aperiodic stimuli. Moreover, the marked difference between the 'identical condition' and 'reversed condition' in Experiment 2 also supports our hypothesis that the information of contrast, which is encoded and maintained for discrimination, is closely related to a pictorial representation of the pattern. In Experiment 3, we further tested this hypothesis from another point of view by using a 'memory mask'. Different from a mask that is presented simultaneously during a discrimination task, the masks used here were well outside the time window in which masking could affect the initial *perception* or *encoding* of the first or second stimulus (Breitmeyer, 1984). We employed similar random noise patterns as our stimuli but included an additional noise pattern halfway through the ISI in each trial.

Using a memory mask could address whether lower sensory areas are involved in the process of preserving this information? If working memory of contrast is partially held in sensory visual areas, then viewing and encoding a feature of an extra stimulus pattern should interfere with memory performance, given the assumption that feeding in another visual contrast would

interfere with the memory process occurring in the shared functional areas. Moreover, in this memory masking experiment, we applied two types of mask stimulus patterns, which we called 'same pattern mask' and 'different pattern mask', respectively (see details in Stimuli and Procedure section). If indeed there is a pictorial representation with an associated contrast, then a mask image that is substantially different should exert a more disruptive effect than the masking pattern that is identical to the ones displayed in first and second stimulus intervals.

Besides the variation of mask pattern, we also investigated the effect of mask contrast levels on memory interference. Visual short-term memory has been reported to be both dimension-selective (Magnussen & Greenlee, 1992; Blake et al. 1997) and feature-selective to memory interference (Magnussen & Greenlee, 1992). One example of *dimension selectivity* is that the memory masking of spatial frequency is selective along the dimension of the task-relevant visual feature (spatial frequency) but independent from other visual dimensions (i.e. orientation). *Feature-selectivity*, on the other hand, can be demonstrated by the more salient masking effect that occurs when the spatial frequency of mask was similar to the remembered spatial frequency of gratings displayed in stimulus intervals. However, unlike spatial frequency or orientation, the neuronal representation of contrast is not narrowly tuned, so it was an open question: whether masks at different contrasts would show differential effects when they are delivered during the ISI?

5.1.4.1 Methods

Observers, Stimuli and Procedure

Two observers who participated in the contrast memory task with the random pixel noise stimuli were recruited in experiment 3, which also used a 2IFC discrimination task but with different types of masks during the memory interval. Figure 5.16 shows the experimental scheme and stimuli employed in this experiment. The mask stimulus was a noise pattern that was introduced in the middle of the 3s delay period. It lasted as long as the stimulus interval (500ms). The same parameters were used for generating the random pattern displayed during the first and second stimulus intervals on each trial in order to make them always identical to

each other. The mask was also formed by this binary image of random blocks except that its pattern could be either identical to or different from, the pattern presented in the stimulus intervals. 'Same pattern mask' occurred in 50% of trials. In addition, three different levels of contrast for the mask were implemented in each mask pattern condition. One condition of the masker's contrast was the mean of the contrast levels used in the stimulus intervals (mean mask condition). The others were assigned a level +10% higher than the maximum contrast (higher mask condition) or 10% lower than the minimum contrast (lower mask condition). This meant that the minimum value of mask contrasts was 57% contrast. At the end of each trial, feedback was given. Different blocks of these mask contrast conditions were interleaved. In total, there were at least 40 trials for each contrast increment when measuring discrimination thresholds on each subject.

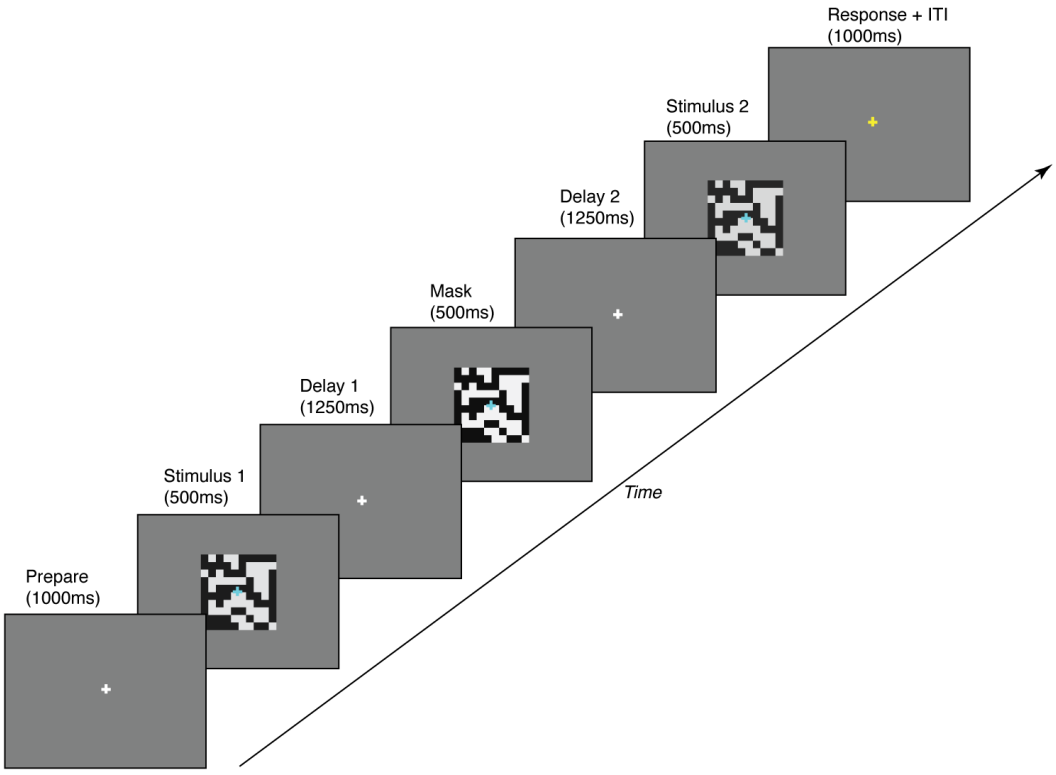

Figure 5.16: Contrast memory masking task of random noise pattern. On each trial, two stimuli of different contrasts were presented for 0.5s each, separated by 3s. While subjects retaining the contrast information of stimulus 1 in working memory, a mask stimulus of different contrast was presented in the middle the delay period. Subjects had to respond by

pressing a button whether the remembered stimulus (stimulus 1) or the test stimulus (stimulus 2) had higher contrast. The mask stimulus at the top represents the condition when the mask stimulus had the same pattern as the stimuli showed in the two stimulus intervals, whereas the mask at the bottom represents a different pattern stimulus from stimulus 1 and 2. The next trial started after an intertribal interval of 1s.

5.1.4.2 Result

Figure 5.17 shows the threshold (75% correct contrast discrimination) for the random noise pattern. One example curve is for a condition without a mask (left panel) and another is with a mask (right panel). It can be seen that the psychometric curve shifts to the right when there was a mask during the ISI, indicating a threshold elevation with the mask.

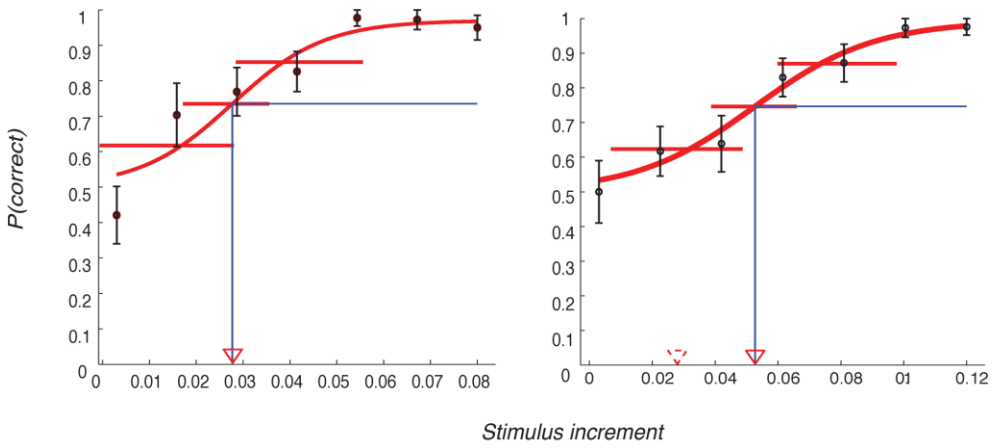

Figure 5.17: Two examples of psychometric curves obtained separately for two conditions from one viewer. Left panel: no mask. Right panel: with a mask of the same pattern as the stimulus at the mean contrast level. Reversed triangle (Solid) illustrates the stimulus increment at 75% correct. Dash triangle in the right panel shows the corresponding value when no mask is displayed.

From the thresholds and their corresponding 95% CI shown in these psychometric curves, we computed the Weber fraction for 70% contrast for different experimental conditions (Shown in Figure 5.18 and Figure 5.19). Compared with the *no-mask* condition, it is clear that the overall performance deteriorated when there was a mask between the stimulus intervals. This disruptive effect exists regardless of what stimulus pattern or mask contrast level was used,

which strongly suggests that the early visual areas are indeed involved in the process of working memory.

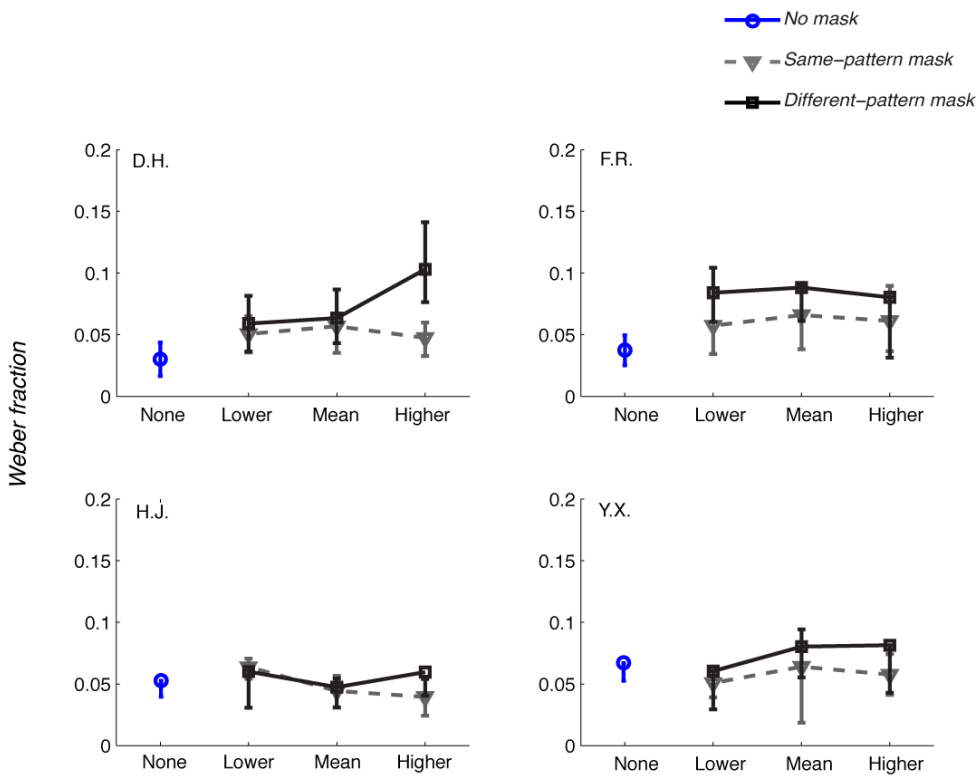

Figure 5.18: The Weber fractions of contrast discrimination task for each observer when different mask contrasts and different mask pattern were used (at 70% fixed contrast). Colour and symbol denotes different mask pattern conditions. Blue dots illustrated the value when no mask stimulus was presented.

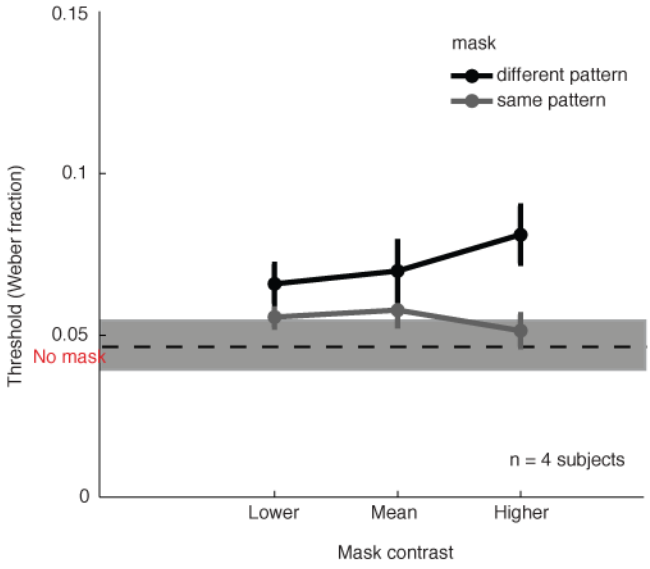

Figure 5.19: Weber fractions in the contrast memory masking task of random noise patterns in the condition when the mask stimulus had a different (black lines, symbols) or identical (light

grey) pattern from those in the stimulus intervals (1 and 2). This illustrates masks with different patterns disrupt the memory of contrast more severely than those with identical patterns. Error bars indicate SEM across (n = 4) subjects. The dashed line and shaded area indicates the threshold and ± 1 SEM across same population of subjects, respectively, when no mask stimulus was presented.

We found that introducing a mask during the memory interval had a deleterious effect on thresholds. The plot in Figure 5.19 shows discrimination thresholds as a function of the masker contrast for trials in which the mask had the same spatial pattern (gray symbols, line) or a different spatial pattern (black symbols, line). Compared with the no-mask condition, which is indicated by the horizontal dashed line, ± 1 SEM across observers in the shaded area, it is clear that the overall performance deteriorated when there was a mask between the stimulus intervals. This disruptive effect was more pronounced when the mask and stimulus pattern were different.

The relative contrast of the mask had relatively little effect on performance. We manipulated mask contrast with three different values (-10%, mean, and +10% of the range of contrasts). On inspection, only the condition with the high mask contrast and a 'different mask pattern' appears to show a clear elevation of threshold. To test statistical significance, we performed a 3×2 ANOVA on changes in the discrimination thresholds for mask contrast (low, mean and high mask contrast) and pattern (same and different stimulus pattern). The main effect of "mask pattern" had a significant effect on discrimination performance ($F(1, 23) = 10.58$, $p < 0.01$), whereas the effect of mask contrast was not statistically significant ($F(2, 23) = 0.36$, $p = 0.70$ [n.s.]), and there is no interaction between the effect of "mask pattern" and mask contrast ($F(2,23)= 1.35$, $p = 0.28$).

5.1.4.3 Discussion

Experiment 2 and its results leave open the possibility that the contrast representation during our memory task might occur at the level of higher-order cognitive areas because they are often delineated as the regions that process integrated features (Pasternak & Greenlee, 2005;

Ranganath, 2006; Ranganath & D'Esposisto, 2005). If contrast and other pattern information, are regarded as separate features, one may argue that early sensory visual cortex is not involved in the process of working memory. To address this issue and bolster the conclusion from last experiment, we performed a 'memory masking' experiment in which we delivered a mask consisting of the same spatial pattern in the middle of the ISI. Different from Experiment 2, the stimulus pattern used in the first and second intervals were always the same, so any threshold elevation should be caused by the extra mask stimulus. Our results provide evidence for the assumption that ongoing working memory processes can be disrupted by disparate sensory input. Masking by a matched pattern profile is only expected if the masker interferes at a level where contrast is processed. As it is shown, the overall Weber fractions increased at the presence of a mask despite the use of different mask contrasts. Therefore, we attribute such a memory-mask-dependent increase in threshold to factors operating on low-level sensory representation.

Previous psychophysical experiments have also explored the memory process of visual features using the method of memory masking (Magnussen & Greenlee, 1992; Magnussen et al., 1991). The additional information gained from the memory mask experiment here, is about the underlying mechanism of contrast representation in the central nervous system. We manipulated the properties of the masker by choosing three levels of mask contrast and two types of masks. First, we compared the masking effects of different contrasts. One of the three levels of contrast was randomly chosen to be the mask contrast for each trial. This randomization was used to minimize the possibility that the mask stimulus might provide extra information to assist this delayed comparison task. The reason for not using very low mask contrasts was to avoid any possible confounding consequence from a facilitation effect. Several previous studies have shown that an additional low contrast stimulus increases the detectability of a signal (Nachmias & Sansbury, 1974; Stromeyer & Klein, 1974). Our result shows no selectivity of contrast interference in this task. This data supported the assumption that the neural representation for contrast is unlike spatial frequency or orientation to which

neurons show specific tuning preferences. According to this hypothesis, the representation of contrast is closely linked to an encoding operation in terms of the overall magnitude of neuronal activity. Related to this, we had expected that a higher contrast mask would bring more interruption to memory task. However, no statistical difference was found even though the higher mask contrast exhibited a moderate increase in one condition. This may be explained by the levels of mask contrast we used in the experiment. Based on the nonlinearity of the contrast response function (CRF), the three values of contrast chosen were within the higher-range, corresponding to the compressive part of response function. Therefore, the neural activity in primary cortex probably does not increase dramatically over the tested range, leading to a constant masking effect.

Experiment 3 also provided supporting evidence for the findings in Experiment 2. By deploying different mask patterns, we once again examined whether contrast is formed on the basis of an image representation. We found that the performance further deteriorated, compared to the condition when the mask pattern is identical to the ones in stimulus intervals. If the pattern information were not an influential factor for contrast memory, we should expect an analogous masking effect, which was clearly not the case. Furthermore, it is very likely that observers also took advantage of the local contrast presented by those squares near the fixation cross in the delayed contrast discrimination (see more on the section of Discussion in Experiment 2).

5.1.5 General Discussion:

5.1.5.1 Comparison of contrast decay between Experiment 1 and Experiment 2

In light of the same logic described in Chapter 4 for studying coherence of random moving dots, we examined the visual memory of grating contrast in this experiment. In the first two experiments, we tested the effects of ISI on contrast memory performance using both periodic stimulus patterns and complex patterns. Similar results were obtained for both stimulus types

in our delayed contrast discrimination task, which strongly suggest that the contrast is not perfectly stored over extended durations. It has been summarized that three causes may lead to the lost of contrast memory as time elapses between the first and second stimulus. (1). The information of contrast fades. (2). The neuronal representation of contrast becomes increasingly noisy even though the contrast storage is still intact. (3). Different contrast levels converge into an average contrast. Lee and Harris (1996) unraveled the possible reason for contrast decay. They performed similar delayed contrast discrimination, but measured the point of subjective equality (PSE) instead. Its value was invariant with the increase of time, which substantiated the mechanism that the memory representation of contrast becomes nosier, leading to higher discrimination thresholds rather than a convergence to a combined contrast level.

In this chapter, however, the disruption of contrast memory in Experiment 2 is larger than in Experiment 1, which is reflected by a slight increase of memory decay rates from gratings to noise patterns. Baddeley (Baddeley & Wilson, 1988) proposed the notion that the nature of a memory task determines the characteristic of the interference. It is likely that the larger deterioration in the second experiment is related to the complexity of the stimulus pattern. Random noise stimuli are more complicated than periodic patterns that have regular phase, orientation and spatial frequency information. Besides, the possibility that a pictorial representation of contrast is retained should also be taken into account. Therefore, we deduce that the greater degradation of contrast information for complex texture is probably the consequence of stimulus complexity, which increases the memory load.

5.1.5.2 Contrast decay due to memory masking

The results in Experiment 3 exhibited decay of contrast information in short-term memory in relation to exogenous interference along the stimulus dimensions. This is not incompatible with the claims of contrast decay from Experiment 1 and the identical condition Experiment 2 in the absence of specific interference factors. The manipulation of the memory mask

elucidates how visual features are held in perceptual memory and whether early visual areas are involved in such a process, and thus further reflects the cognitive mechanisms of working memory. For example, by using an interference method, researchers were able to offer psychophysical evidence that spatial frequency, orientation and velocity are selectively represented in a visually based system (Magnussen et al, 1991; Magnussen & Greenlee, 1992). Contrary to these visual attributes, the representation of visual contrast is not believed to be supported by a spatial map in visual cortex. It has been proposed that the activity ensembles responding to contrast are gathered over the activated neurons distributed across primary visual cortex. Therefore, for contrast, we did not find positive evidence relating to the bandwidth of spatial contrast channels.

5.1.5.3 What is encoded and maintained for contrast memory task

In this chapter, we investigated the representation of contrast in memory with 'identical' and 'reversed' conditions using a contrast discrimination task with noise pattern stimuli (Experiment 2). If subjects could not use the stimulus profile to get additional information about the stimulus contrast, then no difference of discrimination threshold should be observed between these conditions. The visual system discriminates the alteration of contrast depending on the change of overall contrast energy. However, our findings illustrated a different scenario: Observers became poorer at discriminating the contrast of random noise pattern when the second stimulus pattern changed. This result indicates that contrast information was not extracted and coded without referring to the stimulus configuration. Furthermore, the effect of pattern inversion on contrast memory was maintained as ISI increased, suggesting that contrast perception and memory share common representations yielded by similar populations of neurons.

Besides mixing the identical and reversed trials in individual blocks, the use of different patterns in the memory mask experiment (Experiment 3) also discouraged the observers from holding the information of stimulus profile if it is not necessary for memorizing contrast.

Even so, the presence of a mask still showed a clear disruptive effect. Moreover, contrast memory revealed more susceptibility to mask patterns that differed from the memorized item. Therefore, taken together with the evidence from Experiment 2, we conclude that stimulus configuration was necessary for contrast *encoding*, and it has shown that although the task itself did not require the *storage* of the (local) stimulus pattern, the pattern information contained in the luminance profile must have been remembered.

This conclusion is in line with the proposed mechanisms for phase displacement detection, which may be a relevant issue to our study. A phase shift of a harmonic wave can lead to a change in luminance, causing the alteration of local contrast. It has been reported in some studies that observers compared local contrast to perform phase detection tasks (Pollen and Ronner, 1981; Watson & Robson, 1981). These researchers proposed that detecting phase might depend on calculating the phase component relative to a specified retinal location. Others suggested that the gradients of the stimulus pattern contributed to the successful detection of phase change for compound gratings (Stromeyer and Klein, 1974; Lawton, 1982). These hypotheses argue that the encoding of one irrelevant dimension could be used to facilitate the detection of another visual dimension. Analogously, our (delayed) contrast discrimination task requires viewers to detect the change of contrast. Therefore, supported by the results from Experiment 2 and 3, the visual system might benefit from the same representation of stimulus configuration, which expedites the detection of (local) contrast alteration over time (see also the Discussion in Experiment 2).

5.1.5.4 The role of early visual areas in contrast working memory

Another question we addressed with the technique of memory masking in Experiment 3 was whether early areas that process sensory information also participated in working memory. Our data suggested that the visual mnemonic trace is disrupted by another stimulus pattern, which observers were only required to perceive rather than remember. In addition, despite the stimulus pattern being irrelevant to the task *per se*, we still found a disruptive effect on

mnemonic performance. Therefore, visual sensory areas must play a role in the process of working memory for contrast.

5.1.6 Conclusion

We conclude that contrast information and stimulus pattern are not stored independently of each other for making contrast discrimination judgment. Our results, from the perspective of pattern inversion (Experiment 2) as well as memory mask (Experiment 3), support the idea that observers used the configuration of the pattern as an agent to encode and remember contrast information. In addition, we can speculate that early visual cortex is involved in working memory for contrast.

Limited by the spatial resolution of BOLD fMRI that we outlined in Chapter 2, it is impossible to distinguish the similar activities evoked by identical and reversed noise patterns. Considering the strong evidence from our experiments that early visual cortex tends to process the information necessary to remembering and discriminating contrast, we carried on the studies of the neuronal correlates in these areas for sensory and working memory of contrast using a neuroimaging method (fMRI). Sinusoidal gratings were used to exclude confusion caused by different stimulus textures. In the next two chapters, I will explain how we used a well-established technique of pattern classification (MVPA) to analyse data for this type of stimulus.

5.2 Interactions in memory for stimulus contrast *between* and *within* cerebral hemispheres in humans

5.2.1 Introduction

As reviewed in Chapter 1, early visual cortex in the left hemisphere receives input almost exclusively from the right visual field, and vice versa. Similar to the visual pathways and processes, for other systems in the brain – such as the motor system – a multitude of

descending pathways, including pyramidal and extrapyramidal systems, finally target the contralateral muscle to control the movement of the opposite body (Ghez, 1991a; Ghez, 1991b; Ghez, 1991c). Interestingly, lesion evidence from patients or hemispherectomy in intervention animals have shown that each hemisphere alone is sufficient to maintain human consciousness and process sensory information, but also to perform high-level cognitive tasks, including object recognition and memory (Chiarello & Nuding, 1987; Colvin, Funnell & Gazzaniga, 2005; Patterson, et al., 1989b; Zaidel & Peters, 1981; Brainin, Seiser & Matz, 2008; Feinberg, et al., 1992; Suwanwela & Leelacheavasit, 2002).

Despite the fact that each hemisphere can work independently, there are a vast number of visual tasks that rely on communication between them. For example, in the visual domain, if the exchange between two hemispheres were blocked, the visual image across the vertical midline would be viewed like a half-cut picture. Similarly, when sensory signals arrive in the left and right hemisphere representations sequentially, and separately, in the temporal domain, the process of interhemispheric communication is imperative for coherent perception, maintenance of memory and the following motor reaction. The anatomical structure for this left- and right hemispheric transmission mainly consists of the corpus callosum, the anterior commissure, posterior commissure and other connective fibres (Clarke, 2003; Aboitiz et al., 2003; Hoptman & Davidson, 1994). Studies with surgical restrictions and sections of different commissures and decussations have been executed and showed the indispensable role of these connecting structures for processing involving the two hemispheres (Damasio et al., 1980; Pollmann et al, 2002; Risse et al., 1989; Sugishita et al., 1995).

A great number of studies, including behavioral and electrophysiological measures, have investigated the interhemispheric communication of visual information with a comparison task (Chiang, et al., 2004; Lavidor & Walsh, 2004; Reinhard & Trauzettel-Klosinski, 2003; Doty et al., 1988; Eacott & Gaffan, 1989; Ringo 1993). They often assess the performance when two stimuli were displayed to one single visual field versus across the two hemispheres. In the latter condition, it is assumed that the information has to be sent to the other hemisphere

across brain commissures to be compared, which may lead to a loss of information or a delay of reaction during the transmission process. To elucidate whether performance would degrade for contrast across hemispheres in comparison to the within-hemisphere condition, we first measured the discrimination thresholds as well as reaction times under both circumstances in this chapter.

Many studies have shown that interhemispheric interaction starts from the perception of stimuli (Cavina-Pratesi et al., 2004; Marzi, 1986; Marzi et al., 1998; Tootell et al., 1998a) and a great majority of information is transmitted within the first seconds (Doty 1983; Gleissner, et al., 1997; Ringo, 1993). But is there relatively more loss of information when two stimuli are separated over longer time periods and a second stimulus therefore needs to be compared with a potentially decayed *memory* representation of the first stimulus? In other words, when the process of working memory is involved, is the memory representation of contrast different from across-hemispheric perception and within-hemispheric conditions? To address this question, we measured how well stimulus representations in the two hemispheres are maintained over two different interstimulus intervals.

5.2.2 Methods

5.2.2.1 Observers

Four subjects (two experienced observers and two naïve participants) participated in this experiment with written consent. The standard of normal or corrected-to-normal vision was met by all the observers, and all of them were right-handed.

5.2.2.2 Visual stimuli

In the last section, we utilized random noise patterns to investigate the features concerned with contrast memory within stimuli presented at one location on the screen. In the present study, we continued to use the same randomly arranged square fields of binary noise as a stimulus, generated with the same methods and apparatus (first section of this chapter). But

there were two possible positions of the visual stimuli, each located at the corresponding side of the left and right visual field. The stimuli were viewed at a distance of 57 cm, and thus, 1cm on the display is equal to a visual angle of 1°. Each stimulus subtended 10° × 10° visual angle. The distance from the center of each image to the central fixation cross was equally 10° of visual angle. Based on our previous result that the local features of such a stimulus influence contrast discrimination, we used the same stimulus patterns within every trial to avoid confounding results by changing the noise pattern. But in order to minimize the potential effects of (perceptual) learning or adaptation, the patterns changed across trials (patterns for any two consecutive trials were guaranteed to be different).

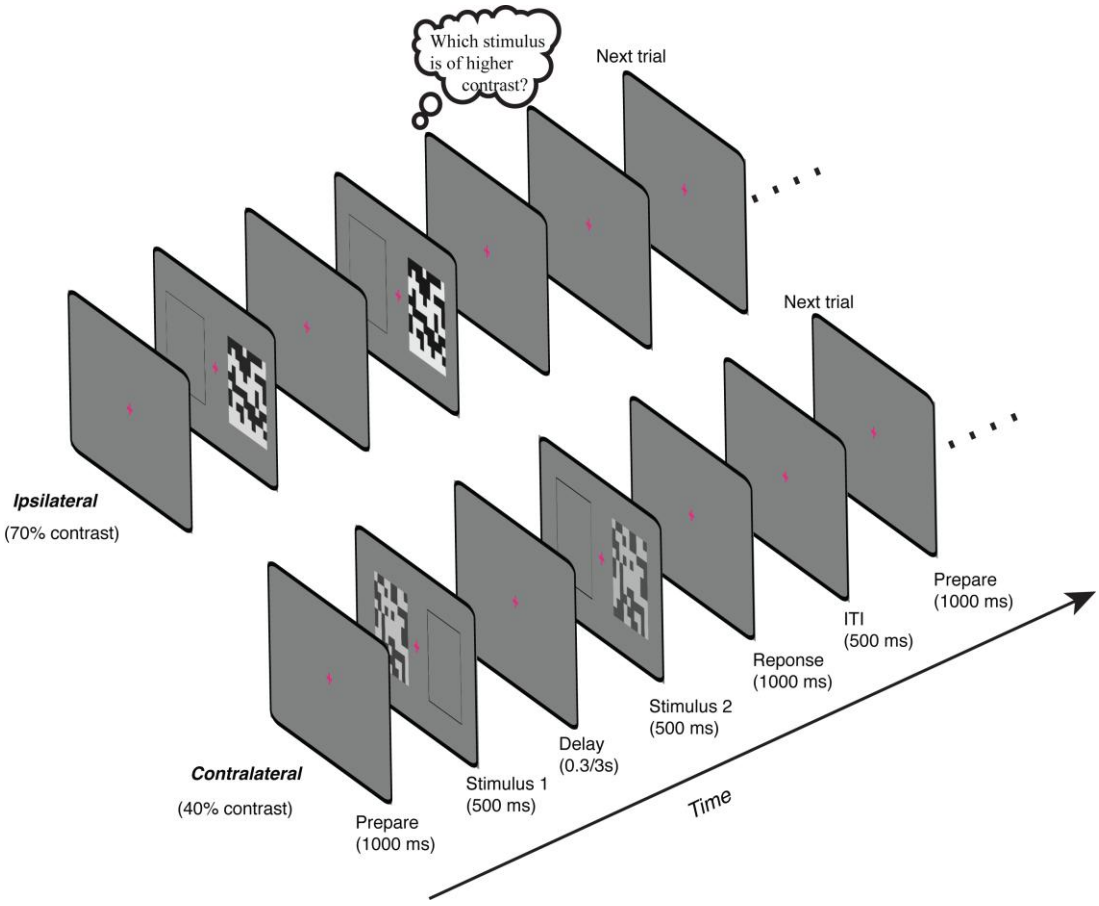

Figure 5.20: Contrast memory masking task of random noise pattern in space. On each trial, two stimuli of different contrasts were presented for 0.5s each, separated by either 0.3s or 3s. Subjects had to respond by pressing a button whether the stimulus 1 or the stimulus 2 had higher contrast. The stimuli at the top represents the ipsilateral condition when first and second stimuli of random pixel noise pattern (70% contrast) were on the same hemifield, whereas the mask at the bottom represents the contralateral condition when first and second

stimuli were displayed to different hemifields (40% contrast). The next trial started after an intertribal interval of 1s.

5.2.2.3 Procedure

To study the characteristics of contrast representation across the visual field, subjects performed a similar contrast discrimination task as in the last chapter. In this study, the locations of first and second stimuli might be separated in two hemifields: from left to right or right to left (contralateral condition, see the lower panel in Figure 5.20). In the control situation, the two stimuli with different contrasts were always rendered on the same side, either left or right of fixation at the same eccentricity, where information did not cross hemisphere (ipsilateral condition, see the upper panel in Figure 5.20). Within each block, the number of trials on the right or left visual field was counterbalanced. Though one of our observers piloted a test with three different fixed contrasts (see data in Result section), only one fixed contrast (70% Michelson contrast) was ultimately employed in the experiment for all observers. As before, using the method of constant stimuli, one of the seven different contrast increments was randomly selected and added to this fixed contrast. Their summation was assigned randomly to one of the two stimulus intervals. At the end of each trial, participants decided whether this contrast level was higher than the contrast in the first presentation and they were instructed to press the corresponding button as fast and accurately as possible with their right hand to give their response. Each condition contained 10 blocks of 40 contrast discrimination trials. The contralateral and ipsilateral conditions were interleaved. Since observers knew the type of each block and these two conditions were disparate in two kinds of blocks, no spatial uncertainty was involved in this study.

Some degree of hemispheric specialization has been reported in several studies (Delis et al., 1986; Kelley et al., 1998; Rogers 2000; Witelson, 1974). There may therefore have been some issues related to hemisphere asymmetries. To avoid a potential bias for one side, we set an equal probability for the visual stimulus to be presented to the left and right hemifields and

mixed them for both ipsilateral and contralateral conditions. Furthermore, this experiment was specifically designed to search for a cost between these two conditions.

To examine the possible interaction between retention duration and discrimination performance, we also instructed the participants to hold the contrast information for 3s in both conditions. Sessions of these memory studies were separated from sessions of pure perceptual tasks by holding them on different days. Discrimination thresholds for the different conditions were estimated using the same method described in previous chapters.

5.2.3 Results

5.2.3.1 Result of discrimination threshold

The data from one subject who was tested for at different contrast levels are displayed in Figure 5.21.

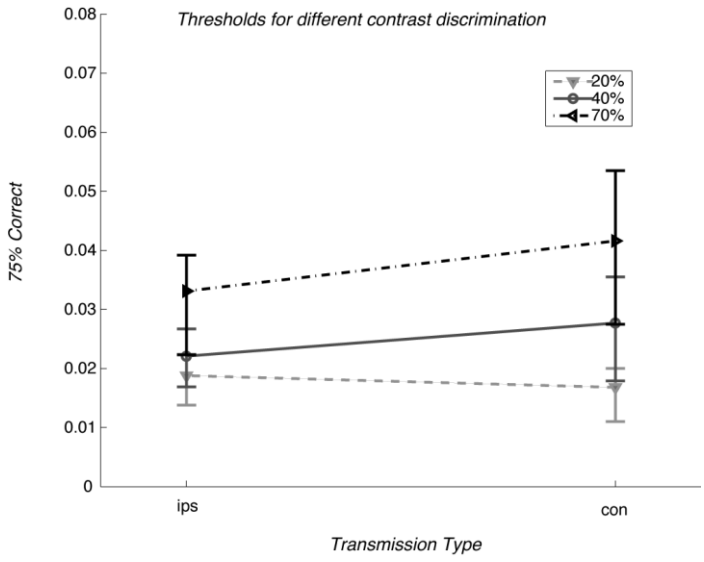

Figure 5.21: Increment thresholds of the contrast discrimination for one observer (Y.X.) at different fixed contrasts. Measured discrimination thresholds are plotted against laterality. Simiilar trends are illustrated for the three fixed contrasts. Error bars: 95% CIs at the 75% correct level obtained from the psychometric curve.

Preceded by two blocks of piloting for each observer, we measured the accuracy (percent correct) of perceiving and remembering contrast with random noise patterns for both ipsilateral and contralateral conditions. Results were converted to Weber fraction for each

subject (Figure 5.22) and the average across our four subjects are shown in Figure 5.23. Each observer in our experiment showed a similar pattern of results: no significant difference between the ipsilateral and contralateral condition in performance when the interstimulus interval was 0.3s. But for the working memory task, their performance in the ipsilateral condition was superior to the contralateral condition. The threshold difference between the ipsilateral and contralateral conditions suggests that interhemsipheric transmission (necessitated by the separation of the visual fields in the two hemispheres) yields more loss. To explore the potential interaction of transmission types (ipsilateral and contralateral) and delay duration (0.3s and 3s), we performed a 2x2 ANOVA. This statistical test revealed a significant main effect of retention duration ($F(1,15)=8.36$, $p=0.0135$), illustrating that the information was lost or degenerated over time. Though the discrimination thresholds increase as the information is transferred across hemispheres, the result of the test did not show significant effect of transmission types ($F(1,15)=3.93$, $p=0.0709$). In addition, no interaction was observed between these two factors ($F(1,15) = 0.9$, $p = 0.3603$).

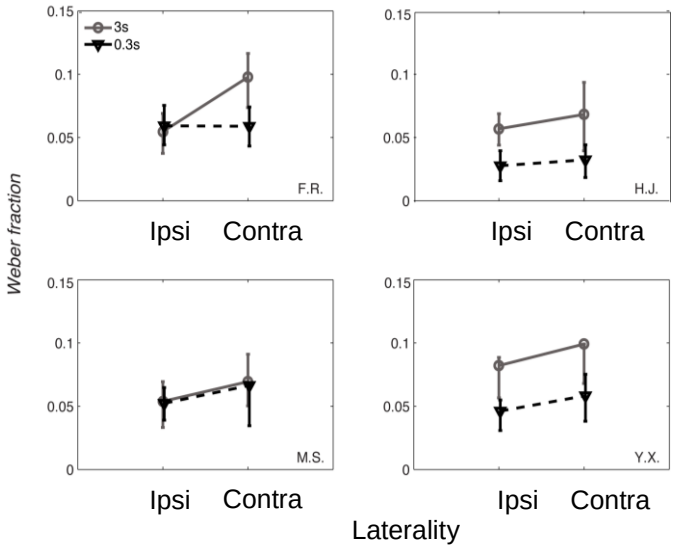

Figure 5.22, Weber fractions for the contrast discrimination experiment with 70% contrasts for individual subjects. Symbols show the discrimination performance for delay durations (0.3s and 3s). In each panel, Weber fractions are plotted as a function of laterality. Error bars are 95% CIs at the 75% correct level obtained from the psychometric curve.

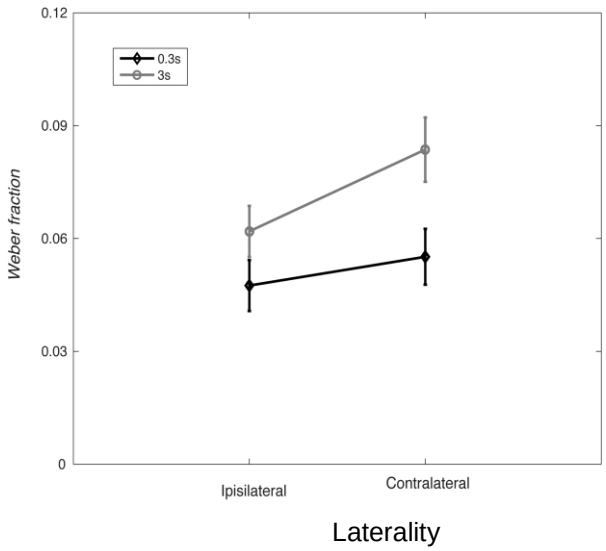

Figure 5.23, Average discrimination thresholds as a function of laterality across all subjects. Colour of the solid lines, data for different delay durations. The duration effect is stronger in the contralateral condition when two stimuli are presented on the different side of visual field compared to the ipsilateral condition. Error bars: ±1 standard error of the mean.

5.2.3.2 Reaction time results:

Most of the available results from other studies measured the reaction time (RT) as an alternative to perceptual accuracy to evaluate the cognitive processes involved. In the present study, we also obtained the RT as a psychophysical gauge of interhemspheric interaction. The distributions of reaction time over all the trials for ipsilateral and contralateral condition were plotted independently. Though observers were asked to press a button as fast and accurately as possible, reaction time is still easily biased by short-latency, fast-guess responses as well as long-latency response. In order to minimize this potential contamination and to correctly reflect the possible latency, we eliminated the values of RT that were three standard deviations beyond the mean for each subject. By doing so, we could transform our RT dstribution to approximately the shape of a Gaussian distribution. Given our response duration was restricted within 1 second, any response input beyond this was excluded from our data automatically. Means of reaction time for correct trials were analyzed and compared across different conditions.

RTs were faster for intrahemisphere condition than the interhemisphere condition in both perceptual and memory tasks. Our 2×2 ANOVA statistical analysis for each subject (p <0.05) confirmed these observations. Figure 5.24 and Figure 5.25 demonstrate each observer's RT and the group result for the two conditions, respectively. This similarity of bilateral and unilateral transmission for perceptual and memorized contrast suggests an analogous pattern underlying two cognitive processes. Our results also show that reaction to memory trials takes 10-20ms longer than that in simple perceptual trials, which may be due to information retention and retrieval.

Table 5.1 Statistic significance of RT difference between intrahemsiphere and interhemisphere condition in each subject

Subject	**F.R**	**H.J.**	**M.S.**	**Y.X.**
0.3s delay	***p* =5.09678e-07**	***p*=5.95755e-06**	***p* = 0.013**	***p*= 4.56115e-07**
3s delay	***p* = 2.69107e-10**	***p* =5.15519e-06**	p = 0.2562	***p* = 5.58311e-24**

Entries in boldface indicate statistical significance at $p < 0.05$.

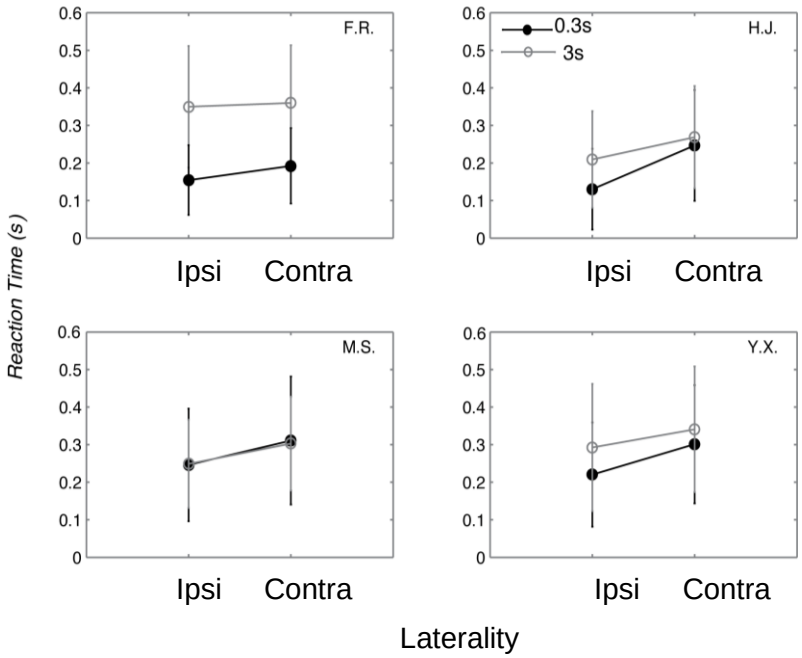

Figure 5.24: Reaction time for each observer. Error bar, ±standard deviation of the mean. Darker line and lighter line represent 3s and 0.3s delay duration, respectively.

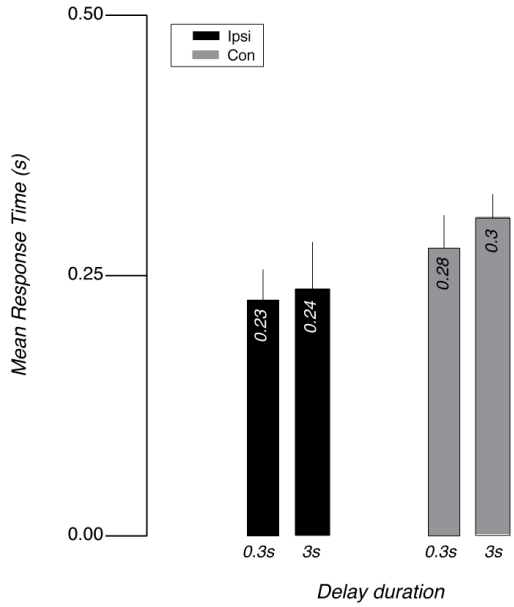

Figure 5.25: Increased mean reaction time for the contralateral condition when contrast discrimination required information transmission across hemispheres. Error bar, ±S.E.M across four observers.

5.2.4 Discussion

Previous chapters mainly focused on studying the characteristic of working memory of contrast in the temporal domain. In this study, we have assessed both visual perceptual and short-term memory for contrast using stimuli split or decoupled in space. Participants were required to discriminate pairs of stimulus patterns made up of random noise viewed in either the opposite or the same visual field. This task structure was used to probe several questions.

5.2.4.1 Intrahemispheric and interhemispheric perception of contrast

Firstly, what is the difference (or cost) for processing information across rather than within visual hemifields/cortical hemispheres? Our data reveals that the discrimination of image contrast was comparable in both conditions. Information transmitted across hemispheres was almost equivalently maintained, as they were transferred within hemisphere. Previous studies indicate that interhemispheric and intrahemispheric transfer of items could be well performed but with some differences in respect of accuracy (Doty, Ringo & Lewine, 1988, 1994; Eacott & Gaffan, 1989; Kavcic & Doty, 2002; Ringo 1993). It has been suggested that results were due to a trade-off between a benefit of distributing information across the two hemispheres

and a transmission cost during the process of interhemispheric communication (Banich & Nicholas, 1998). Findings from both neurophysiological and neuroimaging methods showed that responses from the contralateral side of the visual field, where the visual stimulus was presented, were less strong than the ipsilateral side, indicating that there was some loss of information during the exchange across two hemispheres (Banich & Belger, 1990; Hellige, 1993). On the other hand, there are results illustrating that the benefit outweighed this cost when information is distributed across hemispheres. Since each of the hemispheres has a certain level of capability to process information, when the processing load is distributed, the performance does not deteriorate because of information transmission (Liederman 1986; Liederman et al., 1986; Dimond 1971; Dimond & Beaumont, 1971). Consistent with the second model, our results showed no elevation of discrimination threshold. It may suggest that when contrast information requires interhemispheric interaction, the advantage of distribution balances the cost inccurred during transmission, in keeping with the trade-off between distribution and cost theory. The anatomical explanation for this theory has been attributed to the forebrain commissures, such as corpus callosum and anterior commissure in both humans (Raybaud 2010; Gazzaniga 2000; Buklina 2005; Fabri et al., 2005; Hofer & Frahm, 2006) and animals (Glickstein, 2009; Doty 1983). The intactness of these structures is closely related to the distribution and communication across hemispheres. Disruption of information exchange was found when the forebrain commissures were disrupted (Eacott & Gaffan, 1989; Ringo 1993). Together with this supporting evidence, and our result that the information transmitted across hemispheres is as reliable as that available after intrahemispheric transfer of information for perceived contrast, we therefore think that contrast discrimination is independent of bihemispheric division.

5.2.4.2 Intrahemispheric and interhemispheric memory of contrast

Another question we have addressed is: what is the consequence when the delay between first and second stimuli is increased, and observers had to remember the first stimulus over a slightly longer period in order to compare with the second stimulus? Most of the previous studies on bihemispheric working memory looked at various abnormal conditions in animals

via external intervention (Doty, et al., 1994; Trevarthen, 1972). These reports have strengthened our understanding of mnemonic activity while using interventions that cannot be implemented on human subjects. Furthermore, the animal evidence may not extend to humans completely because of the variation in anatomical structures between different species. Moreover, the majority of human experiments were designed to present stimuli simultaneously to both sides of the visual field, which are more likely to be confounded by attentional factors (Awh & Jonides, 2001). Further, most of the studies used running recognition tasks that tap the mnemonic mechanism in relation to memory load (Griffith & Davidson, 1966; Gazzaniga & Young, 1967; Holtzman & Gazzaniga, 1985). Therefore, in this present study, we utilized a cross- versus within- hemisphere delayed discrimination task to non-invasively address the process of human working memory for contrast when spatial factors were included.

In our study, by discriminating contrast in the ipsilateral or the contralateral visual field (with 3s ISI), we found that performance lag between these two conditions (across-hemisphere and within-hemisphere) became much more apparent, indicating greater cost was paid during the interaction across hemispheres. Previous electrophysiological evidence indicated similar losses during interhemispheric exchange by delivering the disruptive low-level stimulation at different stages (Doty et al., 1994). In their memory load experiment, when six items were stored in memory, their accuracy was reduced by a penalty ranging from 2% to 6%, comparing between interhemsipheric and intrahemispheric conditions.

Several electrophysiological experiments in animals have found bilateral memory formation in both hemispheres, even though information was viewed by only one eye (and therefore the visual cortex in one hemisphere), provided the corpus callosum is intact. This evidence gives support to the hypothesis of bilateral representation. But when and how was the information transferred across hemispheres? There are a few possibilities to establish a mnemonic representation in both hemispheres. It is likely that the contrast information was copied to the opposite hemisphere and retained, ready to be compared with the upcoming stimulus. Another

possibility is that the information rather remains in the stimulated hemisphere and is only available to the other hemisphere at the retrieval stage. It is also possible that more bilateral interactions are invoked between two hemispheres than those distinct unilateral representations. Previous animal experiments investigated this question by using electrical tetanization. Contrary to the prior suggestions that sensory input was conveyed to the non-stimulated hemisphere, their findings demonstrated that the bilateral representation was not achieved by transferring information to the other hemisphere for encoding, but rather during the retention or retrieval stages (Doty et al., 1988; Doty et al., 1973).

To sum up, we could conclude that the visual information was accessible in the other hemisphere despite the fact that it did not encode the stimulus initially, and such interhemispheric mnemonic integration was accomplished via intact commissures.

5.2.4.3 Comparison between intrahemsiperic and interhemispheric perception and memory

As described above, any incongruence between the ipsilateral and contralateral situations is conceived to be the result of interhemispheric transmission, but what led to the significant discrepancy of performance between the perception (0.3s ISI) and memory (3s ISI) trials in our study? For working memory, the initial process of encoding the contrast stimulus in one hemisphere is similar to visual perception. Hence, any mismatch of discrimination threshold and reaction time of visual perception and memory trace of the same image established under the same experimental condition might suggest the characteristics of a bihemispheric mnemonic process.

Figure 5.22 shows a vertical shift of Weber fraction for both interhemispheric condition and intrahemispheric condition, particularly a bigger disparity is found in the former situation. An ANOVA indicates an interaction of delay interval on the discrimination threshold. Our data reveals that the ability to memorize the contrast information is inferior to instantly perceiving contrast within half of the brain. In another animal study, which used a running recognition procedure, accuracy measurers were degraded by 20% when the delay interval lasted 5

seconds (Doty et al., 1988). And the accuracy was halved when three intervening stimuli were displayed. Doty's results indicated that retaining information in working memory was vulnerable to ISI, which was consistent with our result. Other studies with extensive data sets also reported the importance of delay time as a mnemonic factor. One of them showed that prior to any interference, a small (2-3%) but significant deficit was observed in interhemispheric in comparison to intrahemispheric process, implying that the unilateral visual perception is slightly different from mnemonic trace acquired through the opposite visual field in macaque (Lewine, et al, 1994). In one experiment that studied the role of memory load on information maintenance, they pointed out that the intervening delay time should be regarded as an influential parameter for studying bihemispheric integration (Doty, et al., 1994). Our result from the last section of this chapter, using the same stimulus pattern, also demonstrated the decay of contrast information over time. A 20% change in the Weber fraction was noticed when the ISI was 0.3s compared to a 3s ISI in that experiment when stimuli were presented to both hemifields (Figure 5.15). If there were more than this decay factor, we might expect a different proportion of change. Therefore, it seems very likely that our reported difference was due to the information decay over time. However, without further evidence we could not preclude other mechanisms that may participate in this process that might cancel each other out.

Other than memory decay, different theories about interhemisperic communication have been proposed. One example is that the performance for these two conditions is related to the complexity or difficulty of a task (Marsolek et al, 2002). According to this theory, the benefits of distributing may outweigh the cost of interhemispheric transmission, when a task becomes more difficult. However, in the current study, the difficulty of tasks does not correctly predict our result. Task difficulty can be represented by the change in threshold. Though discrimination threshold increased, the difference between perception and memory for interhemispheric condition is not remarkable, which may explain why the beneficial effect of distribution does not compensate the cost during transmission. It is also possible that there is a

more complicated picture when comparing mnemonic perceptual processes, since these cognitive functions involve highly complex mechanisms, including interhemispheric compensation, cooperation, competition and suppression (see review Van der Knaap & Van der Ham, 2011).

Another question that we could address using the observations in our present study is whether division of stimulus first and second between the hemispheres influences the perception as well as the memory of contrast discrimination? The Weber fractions in this current study were greater than the corresponding numbers when the stimuli were presented in one central location (see Figure 5.15 for comparison), which implies that the division of information between hemispheres did introduce an extra cost for both perception and memory.

5.2.4.4 Reaction time

The current task in which subjects viewed stimuli presented to separate visual fields is composed of a sequence of processing stages, including stimulus encoding, transmission, (encoding), retention and retrieval. All require time to complete. But the difference between inter- and intrahemisphere condition mainly relies on the time for information transmission, thus a simple method for estimating the time used for transferring information is to measure reaction time (RT). A longer RT was observed in contralateral conditions for both perceptual and memory tasks, which are in agreement with the majority of previous results (Corballis, 2002). It is well known that visual items are mainly processed in stimulated occipital and temporal structures, and the interhemispheric communication of this information depends predominately on the splenium and posterior body of the corpus callosum (Gott, 1973; Austin et al., 1974; Schepelmann et al., 1976; Sperry et al., 1979; Ogden, 1989; Patterson et al., 1989a). Human electrophysiological studies indicated that some interhemispheric transfer could be finished within 10 msec (Ferbert et al., 1992). Others have reported that this process exceeded 100 msec for some commissural fibres (Liederman, 1998). In our present study, other than the time used for interhemspheric interaction through these connecting fibres, the total reaction time also takes account of the time for sending signals to the arms and hands on

the contralateral side of the body. Early reports also measured the reaction time to study hemispheric specialization and visuo-motor integration (Poffenberger, 1912). They presented a visual stimulus to one hemifield and asked the observers to respond with the hand either on the contralateral side (crossed visuo-motor combination) or ipsilateral side (uncrossed combination). Their findings showed that there is 3-4 msec interhemispheric transfer time in humans. In our study, all subjects used their right hand to press the button, so the motion component of reaction time has little variability. We have four types of visuo-motor communications, clarified in Figure 5.26. As illustrated, the reaction time for the contralateral condition is significantly longer than the ipsilateral case as a result of the time for interhemspheric interaction in addition to the latency from cross visuo-motor combination.

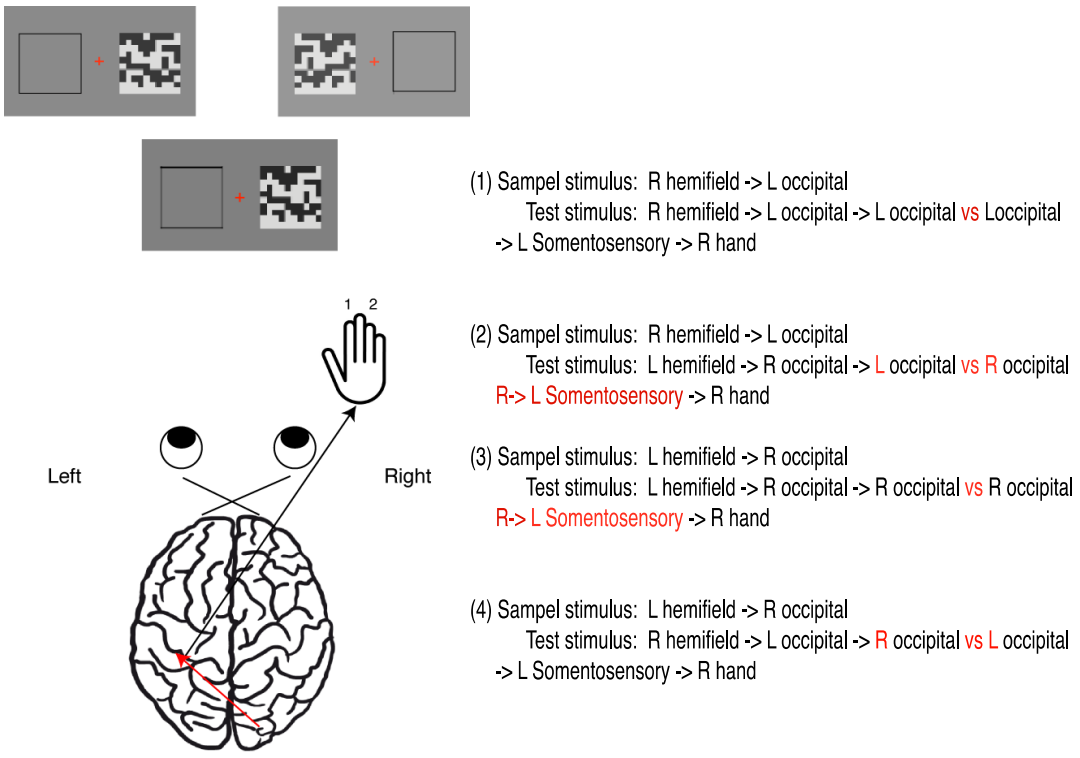

Figure 5.26: Four possible conditions of visuo-motor communications for intrahemispheric and interhemispheric transmission. The time for interhemspheric interaction (L vs R in red) in addition to the latency from cross visuo-motor combination (R->L Somentosensory in red) causes the increased reaction time for the contralateral condition than the ipsilateral case.

For the memory process, by integrating the results of RT and discrimination thresholds, we postulate that the transfer of information, via interhemispheric structures, would cost more time and slightly deteriorate the memory trace, consequently causing increase to reaction time and elevation of threshold values, respectively. This result is not surprising. However, regarding the perception task, a rather different scenario was obtained, because RT does not parallel the result between inter- and intrahemisphere condition as the threshold measurement does. The sensory performance was almost unimpaired but RT increased dramatically. This incongruent result suggests that latency and threshold may not reflect identical factors in our experiment. Elevated RT here represents delay for hemispheric communication rather than the discriminability.

5.2.5 Conclusion

In conclusion, this chapter describes our investigation of the perceptual and memory transfer differences when different cortical hemispheres were engaged in a task. Instead of simple abstract alphabetic letters, objects or faces most commonly used to study memory related processing in different hemispheres, we studied the visual attribute of *contrast* using a random noise pattern. This study revealed that the visual perception of stimuli appears not to differ systematically between across-hemisphere and within-hemisphere conditions. But more advantage was gained in the latter condition for the memory process. We also found a decay of contrast memory in these conditions. Combined with our previous results for contrast processing along the temporal domain, the present chapter improves our understandings of the mechanism for contrast working memory and has elucidated some of its spatial characteristics.

Chapter 6: Decoding stimulus contrast from responses in early visual cortex

Abstract

Previous studies have shown that the perceived orientation of gratings can be decoded from the pattern of fMRI response (Kamitani and Tong, 2005). But the neural representation of stimulus contrast in early visual areas is different from that of orientation, and thus it is unknown whether it is possible to decode contrast from fMRI signal in these early cortical regions. Here, we first used gratings with orientations to see whether we could replicate the successful classification for orientation. Our result in this chapter shows that the stimulus orientation of a *perceived* image can be decoded from event-related BOLD signals in early visual cortex. More importantly, we also found that multivariate algorithm is able to decode the *perceived* contrast of a stimulus from fMRI signals obtained in human visual cortex even when the mean response changes were accounted for, suggesting some consistent spatial pattern for contrast in these areas. In additional analyses, we show that stimulus contrast decoding here is driven by biases depending on stimulus eccentricity. This places important constraints on the interpretation of *decoding* stimulus properties for which cortical processing is known to vary with eccentricity such as contrast, colour, spatial frequency and temporal frequency.

6.1 Introduction

As this thesis described in Chapter 1, the orientation selectivity of neurons in early visual cortex (V1-V3) is well established by electrophysiological and optical imaging studies. Neurons that respond preferentially to the presented orientation are more active than the neurons that tuned away from that orientation. As a consequence, activations across the voxels in MRI images, each of which contains hundreds of thousands of neurons, lead to a differential pattern of representation. MVPA provides a more sensitive tool to identify these activity patterns by sampling small neural regions, as compared to the traditional assessment

of mean amplitude of fMRI response across all the voxels within the interested areas (see Chapter 2 for more details). A recent study (Kamitani & Tong, 2005b) exploited this approach and found the linear classification algorithm can extract and integrate the small irregularities of response across multiple 3-mm cubic fMRI voxels in early visual areas to decode eight different line orientations with statistically above-chance accuracy. Most neurons in visual cortex are distributed in discrete columns, and they exhibit tight tuning for a preferred orientation. Unlike orientation, no evidence so far has shown any orderly map for contrast representation. Additionally, it is not known whether there is a clustered spatial representation for *contrast* (see eg Albrecht and Hamiton, 1982 and Boynton, et al., 1999; Heeger et al., 2000; Kastner et al., 2004) or this stimulus feature can be decoded using multivariate analysis as it is possible for orientation. Therefore, we performed a contrast pattern classification to see whether the result for orientation decoding can be generalized to contrast. Moreover, we also investigated the possible information source that is made use of by the classification.

6.2 Materials and Methods

6.2.1 Subjects

Six observers (5 male, 1 female), experienced in psychophysics and fMRI experiments, with normal or corrected-to-normal vision consented to take part in the second experiment. One of the subjects was scanned for both experiments including contrast and orientation response measure. The procedures were approved by the Medical School Research Ethics Committee at the University of Nottingham.

6.2.2 Functional MRI acquisition

In each of the experiments, subjects participated in at least two scanning sessions. In session one a set of 10-12 functional scans were obtained to measure the retinotopic organisation in early visual cortex allowing us to functionally define V1, V2 and V3 with standard methods; In the same session we also acquired high-resolution anatomical T1-weighted MPRAGE

images of the whole brain for segmentation and cortical flattening. In the second (and later) sessions we obtained fMRI data to perform decoding in the stimulus contrast paradigms. The orientation-perceiving task was repeated in two scanning sessions.

MR imaging was performed at 3 T (Philips Achieva, Philips Healthcare, Best, the Netherlands) using an eight-channel SENSE head coil. Foam padding was used to minimize head movements. During each session we acquired several functional scans, including a scan for localizing regions of early visual cortex representing the stimuli and three to four scans for the main tasks. In those scans, we measured responses to perceived stimuli. For blood-oxygen-level dependent (BOLD) fMRI, we used a standard T2* (gradient-echo) echo planar imaging pulse sequence (voxel size 3×3×3 mm^3, TE = 35 ms, TR = 1500 ms, flip angle 75º, FOV = 192 × 192mm^2). 32 slices were oriented approximately perpendicularly to the calcarine sulcus. We used parallel imaging an acceleration (SENSE) factor 2.

6.2.3 Registration, cortical segmentation and flattening

For flat mapping and visualization, we segmented T1-weighted anatomical images into grey matter, white matter, and cerebro-spinal fluid (CSF), inflated and flattened parts of each hemisphere corresponding to early visual cortex using a combination of tools (FreeSurfer, http://surfer.nmr.mgh.harvard.edu/; mrTools, http://www.cns.nyu.edu/heegerlab/; mrVISTA, http://white.stanford.edu/mrvista.php) and tools included in the FSL distribution (FMRIB Software Library ; Smith et al., 2004).

To register data from each session to the subject-specific, high-resolution T1-weighted image, a set of low-resolution anatomical images that covered the same volume as the functional images was acquired at either the beginning or the end of each scanning session (MPRAGE, 1.5 mm inplane, 3 mm slice thickness). These anatomical images as well as the functional images were then registered to the high-resolution anatomical whole-head volume (T1-weighted, 3D MPRAGE, 1mm isotropic, TE = 3.7 ms, TR = 8.113 ms, FA= 8º, TI=960 ms

and linear phase encoding order) using a robust image registration algorithm (Nestares and Heeger, 2000).

6.2.4 Visual Stimuli

In all experiments, the stimuli were generated on an Apple MacBook Pro running Matlab and the MGL toolbox (http://gru.brain.riken.jp/doku.php/mgl/overview). In the fMRI experiments stimuli on a homogenous grey background were projected from an LCD projector onto a display screen at the feet of our subjects. The display resolution was 1024 × 768 pixels, covering 20.4º (width) × 15.4º (height) of visual angle. Subjects were in the supine position in the scanner bore and viewed the display through an angled mirror. They were asked to maintain fixation at a red cross at the centre of the screen during functional MRI scans and performed a task in all scans to control attention (see below). All the stimuli in the two experiments were moving sinusoidal gratings (spatial frequency, 0.75 cycles/º; temporal frequency, 2 Hz) presented in a circular aperture with radius of 5º, centered at fixation.

6.2.5 Retinotopic mapping session

Early visual areas (V1, V2 and V3) for each subject were identified in a retinotopic mapping session based on the standard travelling-wave method using rotating wedges and expanding rings (Engel et al., 1994; DeYoe, et al., 1996; Engel et al., 1997; for a review see Wandell et al., 2007; also see Chapter 2 General Methods for more details). The responses to the rings and wedges are used to estimate the eccentricity and polar angle of the visual field representation, respectively. Following standard methods, areas V1, V2, and V3 were defined in our subjects using the phase reversals in the polar angle maps to locate the upper, lower and horizontal meridian representations.

6.2.6 Localizer scans

During each functional imaging session of the main experiments, we obtained two brief localizer scans (at the beginning and end of each session) to identify voxels within V1-V3 that were corresponding to the retinotopic stimulus locations. We used these to restrict the V1-V3

regions of interest (ROIs). Each localizer scan lasted 4 minutes (160 time points) and consisted of grating stimuli and grey background alternating in a simple block design between 12 s 'on' and 12 s 'off' (fixation). During the 'on' period in the orientation experiment, we presented eight 1.5 s epochs of moving gratings each with one of the five directions of motion at maximum Michelson contrast (0º to 180º with a increment of 45º). While in the contrast experiment, the gratings were moving to one of the random directions at five contrasts levels (Michelson contrasts of 10%, 30%, 50%, 70%, and 90%) during the 'on' epoch. Gamma correction: we used a psychophysical motion-nulling procedure (eg Ledgeway and Smith, 1994a; Ledgeway and Hess, 2002) to make sure that contrast stimuli would be faithfully reproduced on the LCD projector display at the MRI scanner and on a CRT display in the psychophysics lab (see General Methods).

6.2.7 Orientation response measurements - Experiment 1

Following the localizer scan, one subject participated in this orientation perception task for two sessions to explore the role of early visual areas in orientation decoding. We presented moving gratings (100% Michelson contrast; spatial frequency, 0.75 cycles/º; temporal frequency, 2 Hz; orientations, 45º or 135º) in a randomized event-related procedure. Figure 6.1 illustrates the paradigm for this orientation response experiment. Each stimulus lasted 1.5 s and the subject was asked to respond periodically by pressing a button to maintain a constant attentional state (Figure 6.1).

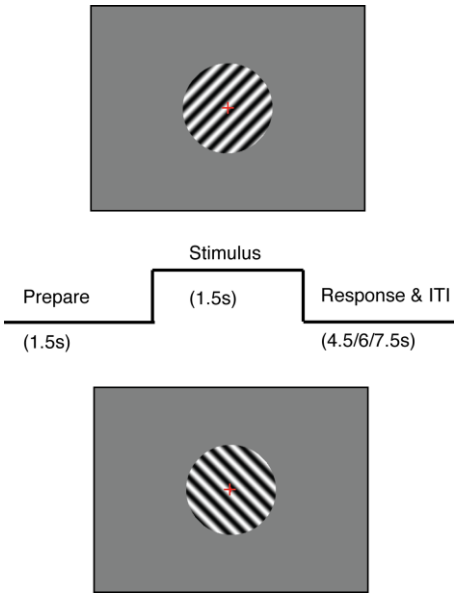

Figure 6.1: Diagram of stimulus in a trial of orientation response measurement. To measure the fMRI response to orientation, we used a block design procedure of stimulus orientations randomly selected and presented to subjects (45° and 135° oriented grating illustrated in the upper row and lower row, respectively).

6.2.8 Contrast response measurements - Experiment 2

Moving gratings with similar properties as in Experiment 1 were employed in this experiment. To measure the responses in early visual cortex to the contrast of stimuli, the same 5 contrast levels used in the corresponding localizer scan were presented in an event-related design. Stimuli were given in random order (preceded by 1.5 s of fixation). Attention state was also controlled. A feedback was given afterwards (colour change of fixation cross).

6.2.9 fMRI response time courses

Imaging data were analyzed using a combination of custom-written software (mrTools, NYU, Heeger lab, NYU; VISTA, Stanford) running in Matlab 7.4 (Mathworks, Natick, MA). First, fMRI data were motion corrected using a robust motion correction algorithm (Nestares and Heeger, 2000), and then high-pass filtered (cut-off, 0.01Hz) to remove slow signal drift. The time course concatenated from the obtained scans of each voxel was divided by its mean

intensity to convert from arbitrary image intensity to percentage signal change. This time series was then used for further analysis (more details in the following sections).

We used standard event-related analysis methods (Burock et al., 1998; Dale, 1999; Burock and Dale, 2000) to reconstruct the time course of fMRI response for each trial type at each voxel in the ROIs with no predefined assumption of the hemodynamic response function. Details of the methodology have been reported in detail in other recent papers (see eg Gardner et al., 2005; Brouwer and Heeger, 2009; Sanchez-Panchuelo et al., 2010). To summarize briefly, we estimated – voxelwise – the best-fitting (least-squares) event-related time course for each stimulus condition. To estimate how good the linear model fit our actual fMRI data, we calculated the amount of variance explained in the original time course for each voxel by our model (r^2) (see General methods for more details). For the sake of visualization, this distribution can also be displayed on a flattened cortical map (Figure 6.2). The averaged fMRI responses across voxels in different ROIs that met a threshold r^2 of 0.3 for contrast and orientation scans are shown in Figure 6.3 and Figure 6.4, respectively.

To measure the response to contrast, we used the maximum values of the average event-related fMRI response for each trial type. We plotted contrast-response curves to estimate the increase in fMRI responses in each ROI with stimulus contrast.

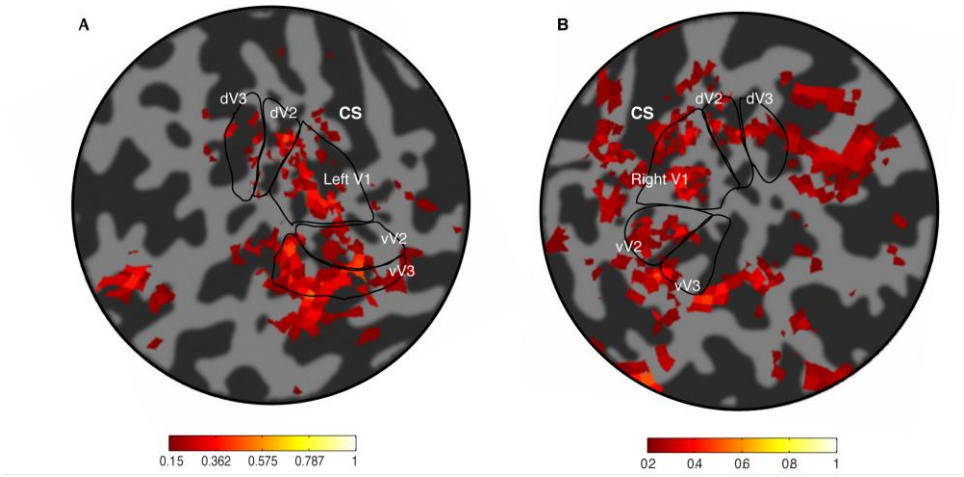

Figure 6.2: r^2 maps illustrated on a flattened cortical surface for contrast (A) and orientation (B) response experiments, respectively. The voxels were selected with a threshold value of r^2 at 0.2 (contrast response measurement) or 0.3 (orientation response measurement), which served to generate the fMRI response.

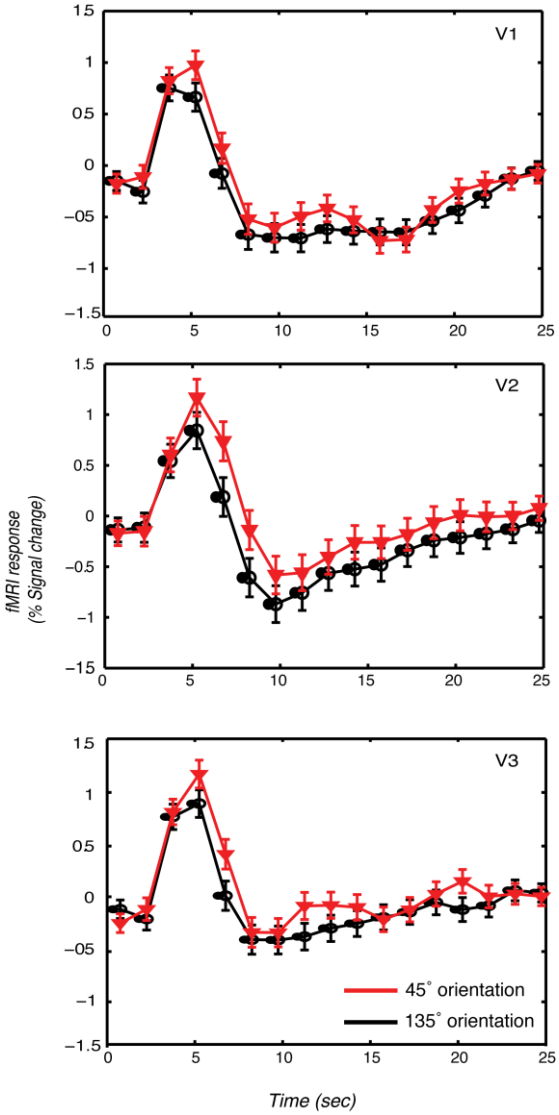

Figure 6.3: The average fMRI time series of orientation response measurement within V1, V2 and V3 (threshold $r^2 > 0.3$).

6.2.10 Multivariate classification

We used linear support vector machine (SVM classification), which is implemented in custom-written Matlab (MathWorks code), to analyze data from both experiments. Each measurement (trial) of fMRI response for a different stimulus condition (class) at different voxels corresponds to a point in a high-dimensional pattern space. In the present study, we obtained each point (which could also be considered a spatial pattern of response) by averaging several time points of the fMRI responses in a single trial, taking into account the sluggishness of the hemodynamic response. Data were sampled and averaged across three

time points (TRs), centred on the peak response in each trial, to deal with variability in the hemodynamic delay for each subject. Therefore, an $m \times n$ matrix served as the input for the classification analysis, where m is the number of trials (rows), and n is the number of voxels (columns) included in the analysis (see more details in General Methods).

A linear SVM provides optimal parameter values (weights and bias) for a hyperplane to categorize two classes of data (orientations) within such a N-dimensional space. To assess how generalisable the classification was, we tested our analysis with a 10-fold cross-validation scheme with the two classes approximately matched in each fold: 90% of data were used to train a classifier and the remaining, hold-out, 10% of data to test. We report the mean classification accuracy across these 10 folds.

For classification of the contrast response data (which had 5 stimulus classes), we trained the model on pairs of stimulus classes using part of the data and then used it to predict one of the two contrast levels with the rest of data. The best-predicted label for each class was chosen by a winner-take-all rule. Trials in which the stimulus type was mislabelled were considered as errors in this particular analysis.

The statistical significance of the observed classification accuracies for each subject was assessed by a binomial test, considering the probability of correctly labelled test examples out of all the independent testing data points is given by the binomial distribution ($p<0.05$; null hypothesis: stimulus class can not be predicted because the classifier was performing at chance, 50%). Statistical significance *across subjects* was assessed with a t-test (two-tailed, $p<0.05$).

6.3 Results

6.3.1 Multivariate classification of stimulus orientation

We first performed a control experiment to test how reliable the information in the human early visual areas is for decoding the orientation of visually presented stimuli. We measured activity in V1, V2 and V3 while subjects passively viewed an obliquely oriented sinusoidal

grating of either 45° or 135° (see Methods and Material). Our classification shows significant performance (above 50% chance level) in all these areas (Average accuracy±standard deviation across two sessions: V1, 0.77±0.01; V2, 0.67±0.04; V3, 0.71±0), which is comparable to the result from Kamitani & Tong's study (2005b). This evidence provided a baseline for our following data when stimulus *contrast* was the visual feature of interest to be classified.

6.3.2 Contrast-response functions

The responses to stimuli with different contrasts were measured and the time courses for these different stimulus conditions (averaged across all voxels in V1, V2 and V3 that met a threshold r^2 of 0.2, respectively) were examined. Figure 6.4 shows the response time courses in V1 of one subject for gratings at five different contrast levels with a systematic increase in the overall fMRI response with increasing contrast. The same pattern of response was found across all the other observers. We obtained contrast-response functions by averaging the peak response amplitude for each contrast level in a time window around the peak response (±1 time point). Figure 6.5 shows contrast curves fitted with standard Naka-Rushton function in three representative subjects. The result also confirmed that for the stimuli we used, the measured fMRI responses were not at floor or ceiling levels.

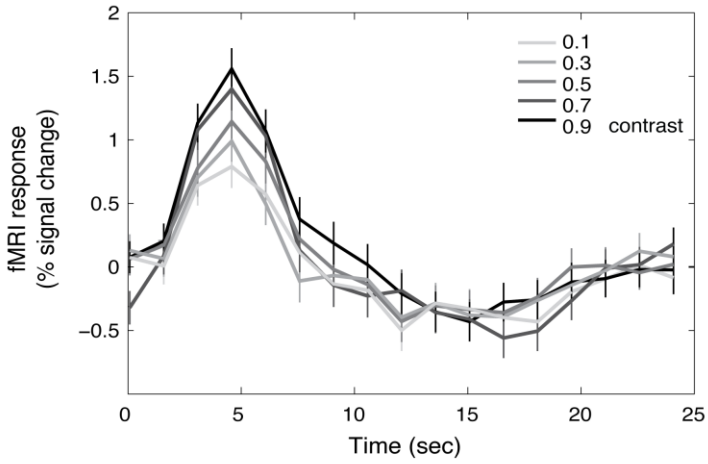

Figure 6.4: Event-related fMRI responses as a function of visual stimulus contrast in V1 of one subject. Grey lines, estimated event-related responses increase as the contrast change

from low (light-grey) to high (dark grey) level. Error bars, standard error of the mean (SEM) across trials.

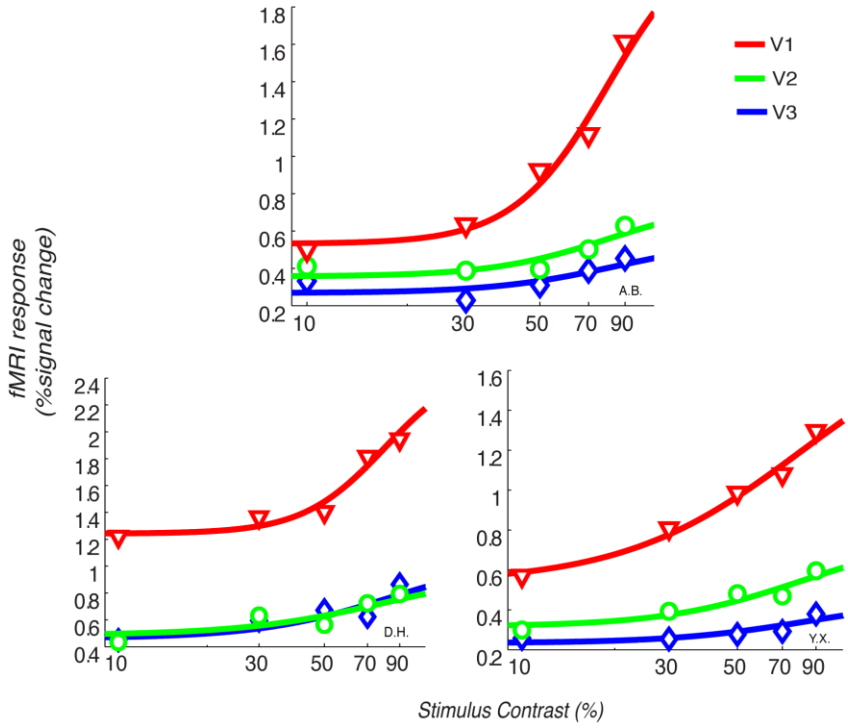

Figure 6.5: fMRI contrast-response curves in V1 (red), V2 (green) and V3 (blue). Symbols, amplitude of measured fMRI response; lines, nonlinear least-squares fit to data (Naka-Rushton).

6.3.3 Multivariate classification of stimulus contrast

To establish whether the fMRI responses in V1-V3 contain consistent information about the contrast of the stimuli, beyond that conveyed in the mean time course across all voxels in the ROI, we studied the pattern of responses using multivariate classification analysis. Classification accuracies in V1 V2 and V3 ROIs were all significantly above chance across our group of subjects (Figure 6.6). To ensure that the pattern of results in the classification accuracies obtained did not depend critically on our choice of voxel number, we performed the following analysis. We randomly selected a range of 2-210 voxels (increments of 15) from the 210 candidate voxels in each V1, V2, and V3 and performed the classification analysis

with this subset of features. We then repeated this analysis in 100 bootstrapped replications for each subject and plotted classification accuracy as a function of the number of voxels included. Figure 6.7 shows the mean (± 1 SEM) for data all three ROIs across 6 subjects, indicating that there are small differences in classification accuracy that depend on voxel number, but importantly the overall pattern of results remained. (The dashed line indicates the classification accuracy for n=180 voxels, the lowest common number of voxels available across ROIs and subjects, rounded down to a multiple of 10). As illustrated in Figure 6.6 and Figure 6.7, the classification accuracies are statistically significant at the group level. But in addition, we also ascertained that the values are robust for each single subject. We include here the graphs in which we show the dependence of classification accuracy on the number of voxels used in the analysis (Figure 6.8).

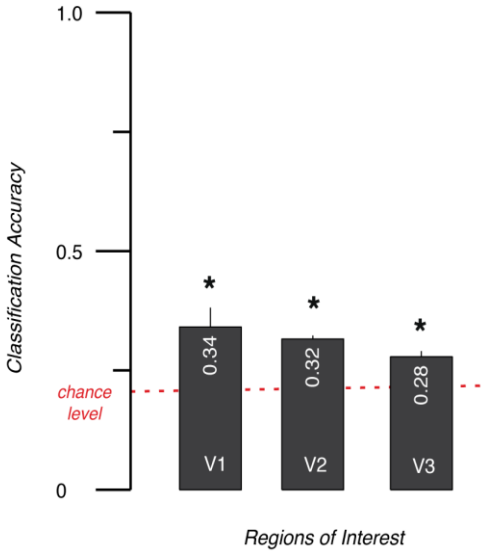

Figure 6.6. Five-way classification for *perceived contrast* data across different regions of interest. Plots show mean ± 1 SEM across subjects. Asterisks demonstrate the ROIs that reach the classification accuracy above 50% chance level ($p < 0.05$, two-tailed t test).

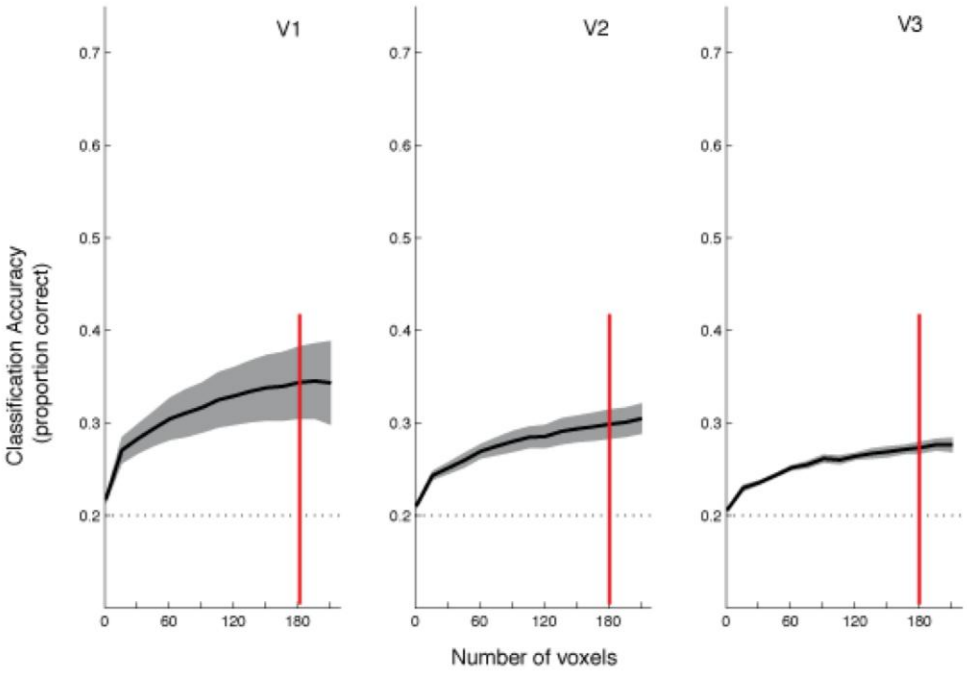

Figure 6.7: Relationship between classification accuracy and the number of voxels included in the MVPA analysis for V1, V2 and V3. The red line indicates the classification accuracy for n = 180 voxels, the lowest common number of voxels available across ROIs and subjects rounded down to a multiple of 10. Shaded areas: standard error of the mean across 6 subjects.

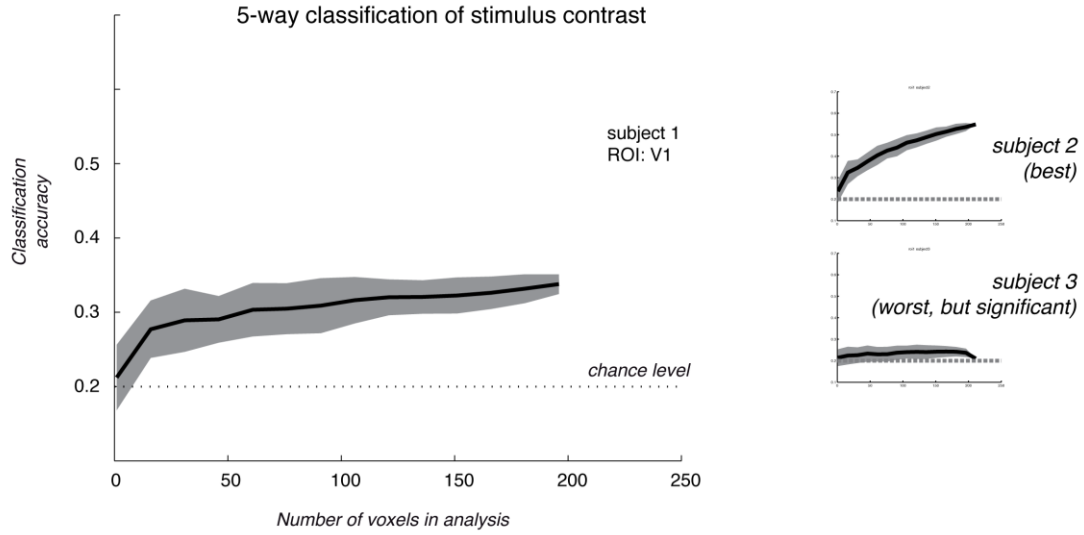

Figure 6.8: Dependence of classification accuracy on the number of voxels included in the MVPA analysis for individual subjects. These plots include data from subject 1 as well as plots for the "best" and "worst" subjects in each case. Even in the worst case, the classification is above chance-level. Shaded areas: standard deviation of the 100 bootstrapped replications.

We expected that correctly classifying trials with large contrast differences should be easier than for small contrast differences. To test this, we performed a finer grained analysis of the pairwise classifications that contributed to the 5-way classification. In four separate analyses, we split trials into groups according to their differences in linear contrast (Δ=0.2, 0.4, 0.6, 0.8). Note that the number of trials that could be included in the analysis therefore differed, ranging from *all trials* for the pairwise analysis of trials with small contrast differences (Δ=0.2) to only the lowest and highest contrast trials for the pairwise analysis with a contrast difference of 0.8. The pattern of prediction accuracies for V1 to V3 is shown in Figure 6.9. Classification accuracies between trials increased with the difference in contrast between the gratings patterns, regardless of the stimulus orientation.

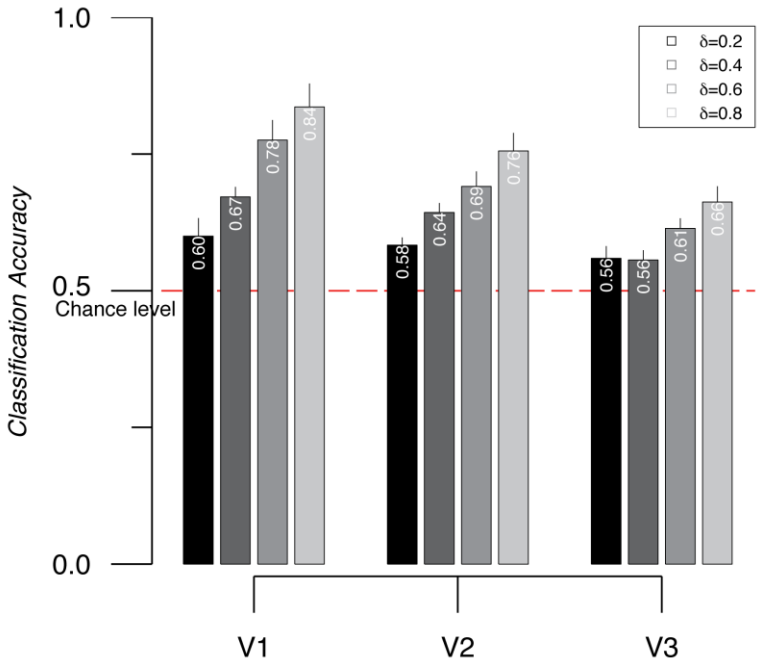

Figure 6.9: Pairwise classification based on the difference of contrast levels in V1-V3, averaged across subjects. Error bars, SEM across subjects. Colours, various contrast differences. Four groups were formed with trials of differences in linear contrast (e.g. Δ=0.8 is composed of the trials when subjects view 90% and 10%). contrast Classification accuracies between trials increased as a function of contrast difference.

Because the classification analysis could potentially have been driven mainly by differences in the mean response level across different stimulus conditions, we also performed a control analysis in which we classified trials using only the mean response level across the ROI. Figure 6.10 illustrates how we calculated the Receiver Operating Characteristic (ROC) and measured the Area Under Curve (AUC) for each of the possible pairwise comparisons. We constructed histograms of the mean fMRI response in the ROI for two classes of trials, which we expected to have a different mean across trials. The left panel in Figure 6.10 e.g. shows the distribution of response amplitudes for trials with 10% contrast (class 1, red line) and 90% contrast (class 2, grey curves). Following the logic of a standard signal-detection theory analysis, we set a criterion level and estimated the proportion of trials from the two distributions that fell above that criterion level. This corresponds to the proportion of 'hits' (or correct labellings) and 'false alarms' (or incorrect labellings) respectively. By considering the proportion of 'hits' and 'false alarms' at different criterion levels, we could construct the ROC curve. The area under the ROC curve is equivalent to the proportion correct that could be achieved in two-way categorization given the distribution of fMRI responses for the two classes of stimuli (Macmillan and Creelman, 2005).

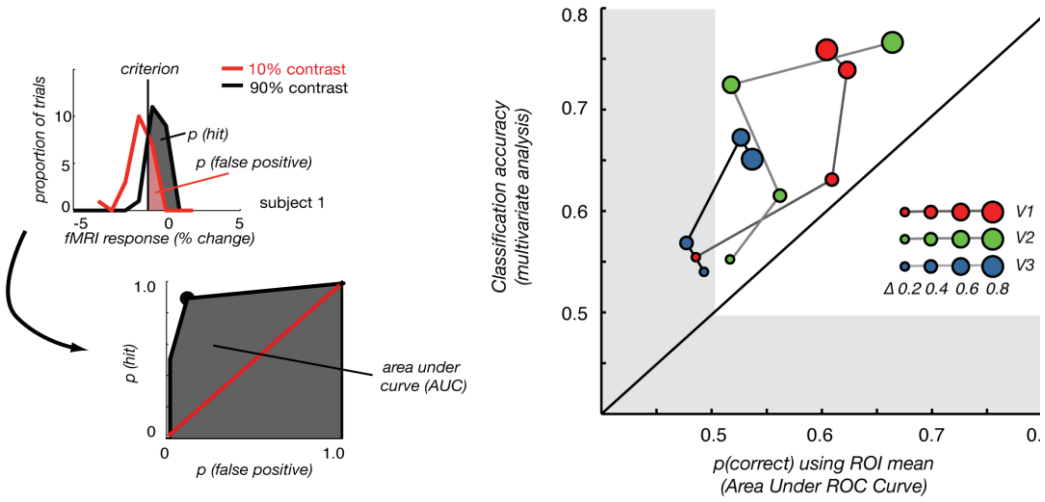

Figure 6.10: Left panel: Illustration of Receiver Operating Characteristic (ROC) and measured Area Under Curve (AUC) for pairwise classification. Left upper: Distributions for fMRI response to 10% (red curve) and 90% (black curve) contrast. Vertical line corresponds to the criterion used for classification of trials of two contrast levels. Trials on the right of this line were labelled as 90% contrast, within which trials as high contrast was referred as hits (grey

area). Since the curves overlap, some trials corresponding to 10% contrast were also greater than the criterion and labelled incorrectly as 90% contrast, thus contributing to the proportion of false positive (red area). Left bottom: ROC curve is plotted with the false positive rates on the x-axis and the hit rates on the y-axis with different criteria. Black dot corresponds to the criterion shown in the upper graph. Red line, chance performance of classification for 10% and 90% contrast. Grey area, area under ROC curve. Right panel: Comparison between proportion correct for pairwise discrimination using only the mean response (area under ROC curve obtained using signal detection theory with the method illustrated in the left panel) and classification accuracy from multivariate analysis in different ROIs. Size of symbols, all pairwise comparisons of trials with a given difference in contrast. Colour of symbols indicates the region of interest used in the analysis. Diagonal line illustrates equivalence of multivariate classification and classification on the mean response in the ROI. Shaded area, cut-off for chance level (50%) performance.

Interestingly, while the classification performance improved as the contrast difference between the two gratings increased, those obtained by only considering the mean response were consistently worse than those obtained by multivariate classification. This indicates that there is significant categorical information present in the pattern of responses that is not captured in the ROI mean, which can be exploited by using multivariate methods.

The scatter plot in Figure 6.10 summarizes the data for the four different levels of contrast difference and four different regions of interest. For all pairwise comparisons of trials with a given difference in contrast (size of symbols), in all the ROIs we considered (colour of symbols), multivariate classification outperformed classification based solely on the mean response in the ROI.

6.3.4 The spatial pattern of responses underlying *contrast decoding*

To characterize the spatial pattern of responses that underlie contrast decoding in our experiment, we subdivided the visual areas into two sets of ROIs: one set based on the eccentricity measurements from retinotopic mapping into a *central* (0.5º- 2.5º eccentricity) and an *eccentric* ROI (2.5º-5º). As a control, we also defined a second set of ROIs corresponding to *upper* and *lower* visual field, which subdivided V1 orthogonally to the central/eccentric split. Figure 6.11 shows the boundaries within V1 in left and right hemispheres on one subject. We compared the responses in these ROIs in two ways. First, we

plotted the contrast-response functions for the two sets of ROIs (three representative curves shown in Figure 6.12) and second, we used the mean time course from the two respective ROIs to create two *supervoxels* (Freeman et al, 2011) which could then be used in the classification analyses. The contrast-response curves are clearly different for the two splits (average contrast-response functions across all subjects illustrated in Figure 6.13), showing a consistent response difference for central/eccentric but not upper/lower visual fields.

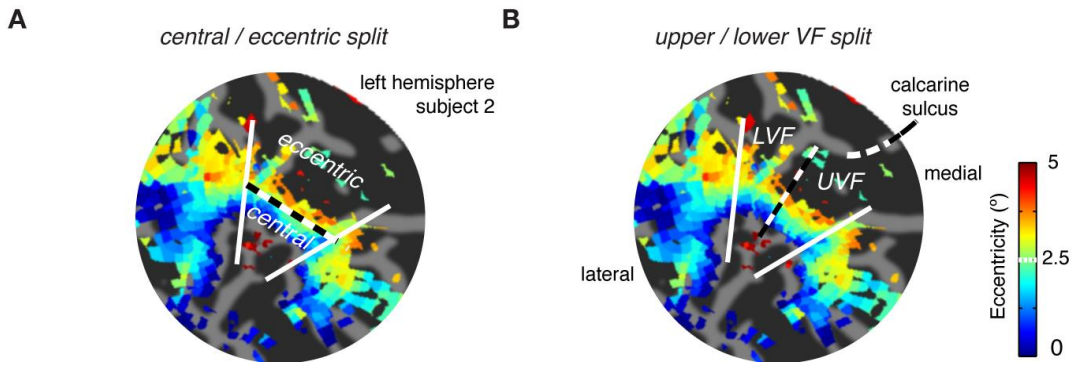

Figure 6.11: Spatial pattern of fMRI responses that drive classification. (A,B) Flat map of visual cortex from one subject showing definition of *central/eccentric* and *lower/upper* visual field ROIs for V1. White dashed lines, borders between V1 and V2v / V2d.

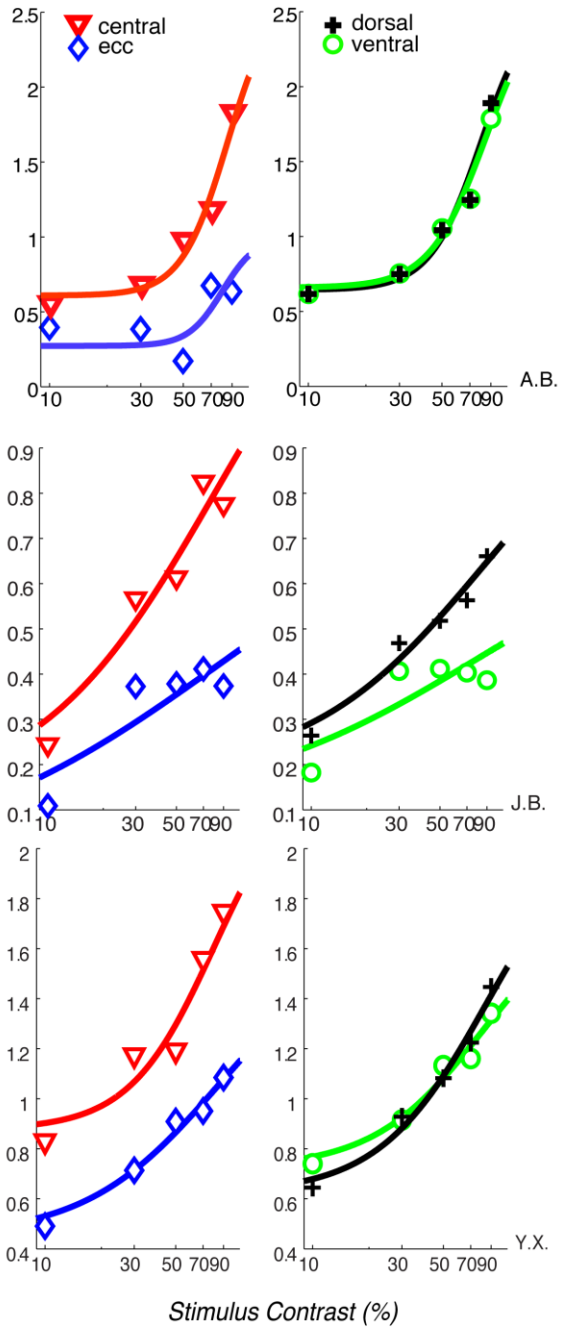

Figure 6.12: FMRI response as a function of stimulus contrast in three representative subjects (r^2 >0.2). The fMRI contrast response curves are different between central and eccentric split ROIs, whereas the response curves are similar for the dorsal and ventral partitions. Contrast response curves from Figure 6.11 left column the central/eccentric split ROIs and Figure 6.11 right column the upper/lower visual field split ROIs.

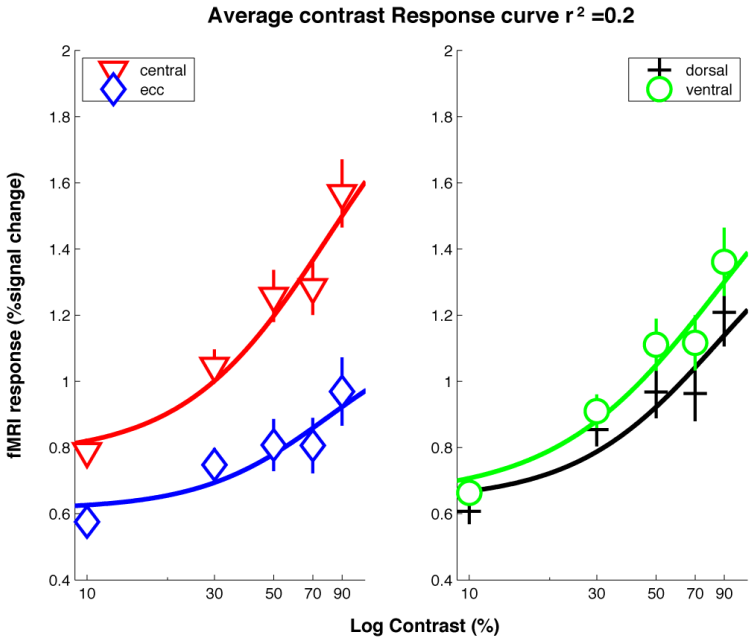

Figure 6.13: FMRI response as a function of stimulus contrast according to eccentricity (left) and angular field (right). Differential response curves are consistent with the patterns illustrated in Figure 6.12. Symbols mean across six subjects. Error bars, SEM across subjects.

Next, we used the responses in the two sets of supervoxels to show that the differences at this large scale can drive classification of perceived contrast, even when only two features are considered: if the supervoxels are constructed from a central/eccentric split, classification is possible. If however, data are reduced to two supervoxels corresponding to the upper and lower visual fields, classification accuracies drop to chance (Figure 6.14).

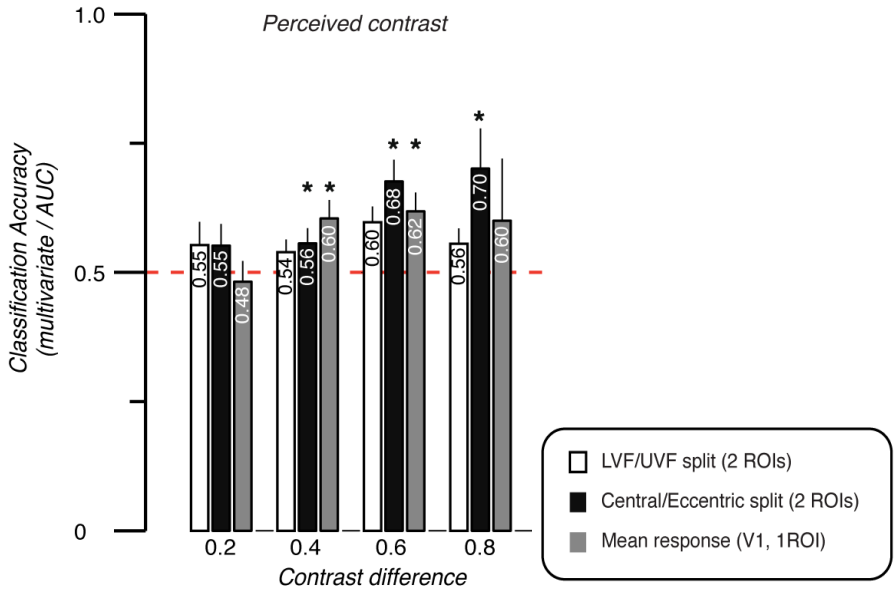

Figure 6.14: Classification accuracies, by contrast difference in stimuli, for the perceived contrast experiment using lower/upper visual field (LVF/UVF) split ROIs (white), central/eccentric split ROIs (black) and the mean response across all voxels included in the V1 ROI (grey). Classification accuracies or AUC using central and eccentric splits increase as the difference of contrast pair increases, which are higher than using the mean response, indicating that even using two supervoxels in multivariate pattern classification is more sensitive than the mean response. These results are in contrast to the nonsignificant classification outcome using the two partitions based on visual angle. Mean across subjects. Error bars, SEM across subjects.

In addition, we examined whether increasing the number of supervoxels would affect our result. We found no appreciable effect on the pattern of results when we divided V1 into four parts according to eccentricity and angle, respectively (Figure 6.15). Averaging data into two or four supervoxels within restricted eccentricity bands (dark grey lines in Figure 6.15) clearly preserves classification accuracies, while averaging within visual field (angle) segments or randomly across voxels in V1 does not.

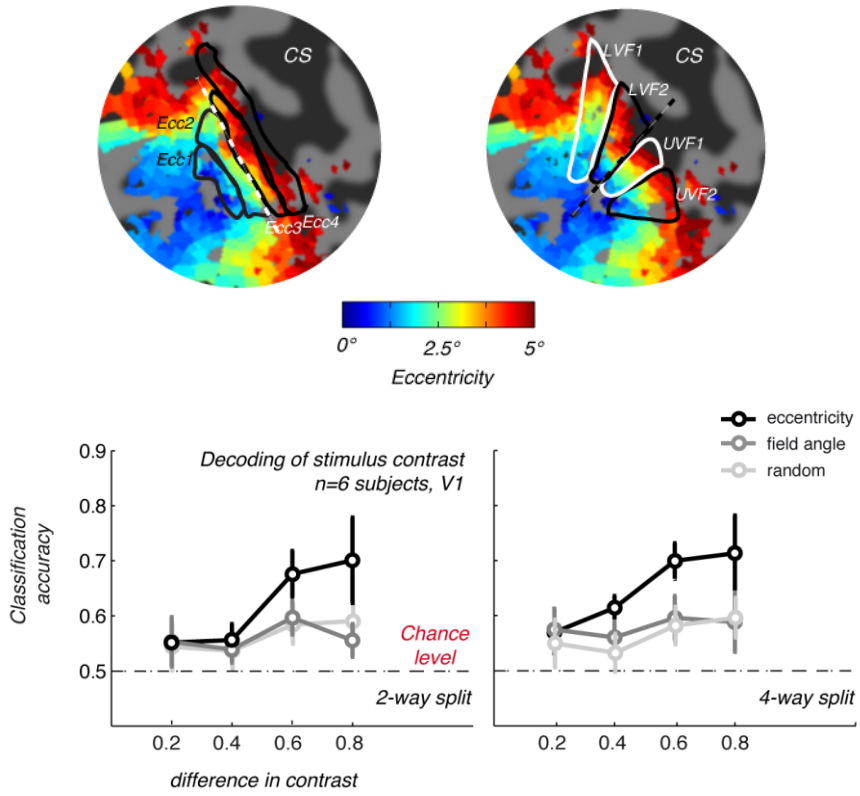

Figure 6.15: Robustness of spatial patterns that drive classification (controls). Upper panel: Flat map of visual cortex from one subject showing definition of 4 bands according to eccentricity and angle in visual field in V1, respectively. Lower panel: Classification accuracies, by contrast difference in stimuli, for the perceived contrast experiment. FMRI responses were averaged in two (Left lower panel also see in Figure 6.11 for the ROI definition) or four (Right lower panel) partitions of voxels, split according to either their eccentricity (black lines, symbols), visual field segment (dark grey) or by random sampling from all voxels in the V1 ROI (light grey). The results from 2-way split are consistent with those from 4-way split.

6.4 Discussion and conclusion

Here we show that the fMRI responses in early visual cortex can be used to decode orientation, but more importantly, our result suggests that the stimulus contrasts presented to the subjects can also be decoded from the signals in these areas. The ability to classify trials with different contrast levels is in itself not surprising because there is a well-known shift in the mean level of response with increasing contrast. This has previously been measured and well-characterized in early visual cortex (Ohzawa et al., 1985; Boynton, et al., 1999; Reich, et

al., 2001; Albrecht & Hamilton, 1982; Gardner et al., 2005). Most neurons in early visual cortex exhibit a monotonic increase in their responses as a function of contrast, though some cells show very different patterns of response saturation (and even supersaturation) with contrast (see Ledgeway et al., 2005; Peirce, 2007; Hu, et al., 2011). However, unlike for stimulus *orientation* there is no known columnar organisation for neurons with similar contrast-response functions. Nonetheless despite the lack of orderly clustering in structure, there may still be spatially local inhomogeneous changes in the fMRI responses to contrast in early visual cortex. Using a multivariate classification analysis that does not take into account shifts in the mean response in the ROI can therefore not untangle whether the ability to classify is simply due to a global shift in the response of the majority of neurons, or some re-distribution of a differential signal.

In a more fine-grained analysis, we therefore evaluated (a) multivariate classification between stimuli at pairwise contrast levels, and (b) the predicted performance using a univariate (signal detection type) analysis using only the (global) average response in each ROI. We found that multivariate classification became increasingly more accurate with larger contrast differences in the stimuli (see Figure 6.9 and also Smith et al., 2011). In our hands, even trials that are close in contrast could be discriminated using SVM, whereas considering only the mean response in the ROI failed to classify trials correctly. This adds further support to MVPA's increased sensitivity compared to univariate methods (Kriegeskorte et al., 2006).

We found that it was possible to decode stimulus contrast by the mean increase in response across the ROI, but it was consistently outperformed by multivariate classification (see Figure 6.10). Especially in the cases of distinguishing trials with small contrast differences, multivariate classification clearly dominated the simple ROI mean based analysis. Classification accuracy grew as the difference in stimulus contrast increased.

These results suggest that there is a spatially specific response to different contrasts that can drive the improved classification performance. To characterize the spatial pattern (and scale)

of responses underlying this multivariate contrast decoding seen here, we subdivided the visual areas into two sets of ROIs: one set based on the eccentricity measurements from retinotopic mapping corresponding to a *central* and an *eccentric* portion of our stimuli, as contrast sensitivity is known to change as a function of eccentricity (Legge et al., 1987). As a control, we also defined a second set of ROIs corresponding to the *upper* and the *lower* visual fields, where such asymmetries might be less pronounced. We found that even when we reduced the multivariate fMRI responses to only two features, responses in a central and eccentric ROI, classification was possible. This suggests that a large-scale bias with eccentricity can drive classification for perceived contrast. Our results here do not directly address the question of whether information is present only at the level of a coarser scale (eccentricity) map or also at fine columnar architecture, an issue that is currently the subject of much debate (Gardner, et al., 2008; Op de Beeck et al., 2008; Swisher, et al., 2010; Freeman et al., 2011; Beckett et al., 2012).

In general, we found that multivariate analyses can be used to decode the visually presented features of a stimulus (orientation and contrast) in this chapter. However, it is unclear whether its cortical representation is similar when subjects *perceive* and *remember* such stimuli. Therefore, we performed another experiment in the next chapter using delayed discrimination of contrast in combination with multivariate classification to address this issue.

Chapter 7: Decoding working memory of stimulus contrast in early visual cortex

Abstract

One recent study has demonstrated that the memorized orientation of a visual stimulus can be decoded from the pattern of fMRI responses in early visual areas (Harrison & Tong, 2009). On the other hand, our result from last chapter has illustrated that perceived contrast can be decoded within the same regions. Thus, it raised a question of whether information about *remembered* contrast can also be decoded in these early cortical stations of visual stream. Our data shows that pattern classification enables the decoding of contrasts when they are stored in memory as well. Together with our observation of two distinguishable activation patterns of remembered orientations (during periods when no stimulus is displayed) in early visual areas, we conclude that V1-V3 are involved in memory of visual stimulus features, such as orientation and contrast. Furthermore, we show that classifiers generalise from remembered contrast to the fMRI data from last chapter for perceived contrast, and vice versa. Finally, we found that classification accuracies were significantly higher for behaviourally correct than incorrect trials, indicating that signals from early visual cortex contribute significantly to VSTM of stimulus contrast. Our results also suggest that responses from incorrect trials add substantial noise to the contrast VSTM signals used in decoding.

7.1 Introduction

Several lines of research suggest that the human brain has a specific cognitive system for holding information to be manipulated and executed - so called working memory. Visual short-term memory (VSTM) is a specific sub-type that allows the robust maintenance of stimulus attributes such as contrast, orientation, spatial frequency, speed, etc. with high fidelity (for review see Pasternak and Greenlee, 2005; Luck & Vogel, 1997).

Functional brain imaging has enabled the exploration of the anatomical and functional correlates underlying VSTM first discovered by neurophysiological techniques (see Fuster, 1995 and eg Braver, et al., 1997; Curtis and D'Esposito, 2003; Pessoa et al., 2002). Although studies largely agree on the involvement of higher-level cortical areas in this cognitive process (Haxby et al., 2000; Postle and D'Esposito, 1999), there is still some controversy about the role of early visual cortex in working memory. Recent fMRI evidence suggests that early sensory areas may be involved in retaining visual stimulus representations, e.g. of orientation (Pessoa et al., 2002; Serences, et al., 2009), and spatial frequency (Baumann, Endestad et al., 2008; Sneve, et al., 2011; Greenlee, et al., 2000). However, the sustained responses detected in early visual cortex may be related to visual attention rather than VSTM (Offen et al., 2009, 2010; see also Pooresmaeili et al., 2010). Harrison & Tong (2009) used multivariate pattern analysis, MVPA, to search for potential signatures of working memory for orientation in the pattern of fMRI responses in early visual areas. They found that *remembered* orientation could be decoded and that same neural circuitry that mediates early visual processing (and perception) of orientation is also recruited during the working memory period.

In this chapter, our aim was to examine whether representation of a different stimulus property – the contrast of a stimulus – could be decoded when subjects remembered stimuli. In order to control for slight methodological differences between our study and that of Harrison & Tong, we also conducted an orientation memory experiment in a separate session to see whether their result is replicable.

7.2 Materials and Methods

7.2.1 Subjects

The six observers who participated in the perceived contrast experiments also took part in this contrast memory experiment. The same subject who participated in the experiment described in the last chapter also took part in the remembered *orientation* experiment.

7.2.2 Functional MRI acquisition

Each subject participated in the same scanning sessions as they did in the last chapter. This included one session of retinotopic functional scans and high-resolution anatomical T1-weighted MPRAGE images of the whole brain. Another session included two localizer scans and functional MRI scans for the memory conditions. For these scans, we used a standard T2* (gradient-echo) echo planar imaging pulse sequence with same values of the parameters as in the measure shown in Chapter 6.

7.2.3 Visual Stimuli

Identical toolboxes were used to generate the corresponding stimuli for localizer scans, orientation memory and contrast memory experiments as was used for the visual contrast stimuli presented in the last chapter.

7.2.4 Localizer scans

For both orientation and contrast memory experiments, we included a localizer scan at the beginning and the end of each scanning session. The purpose of these localizer scans is to identify voxels within V1-V3 that correspond to the retinotopic stimulus locations (See details for the corresponding stimulus attributes in the section of Localizer scans in last chapter).

7.2.5 Contrast working memory scans - Experiment 1

In line with the experimental paradigm used by Harrison and Tong (2009), we used an event-related design in which each trial comprised (i) visual stimuli presentation, (ii) a retention period, and (iii) a test interval (see Figure 1). During the stimulus presentation at the beginning of each trial two gratings with different contrasts (30% and 70%) were presented

sequentially. Each grating presentation (in a circular aperture, radius 5º, centered at fixation) was accompanied by a small text label (‘1’ or ‘2’), rendered in red and displayed with a small offset from the fixation cross; the assignment of the label to the higher or lower contrast grating was randomized on each trial. The orientation of both gratings in each trial was chosen to be either 45º or 135º, but remained constant throughout the trial. Following the presentation of the two sample stimuli, the numeric cue indicated which of the two contrast stimuli the subjects should remember and retain in memory for the delay period (fixed, 8.4 s). Finally at the end of each trial, a matching grating (contrast ± 20% of the to be remembered grating) was displayed, and the subjects were asked to indicate with a press of a button whether the remembered (sample) or matching grating had the higher contrast.

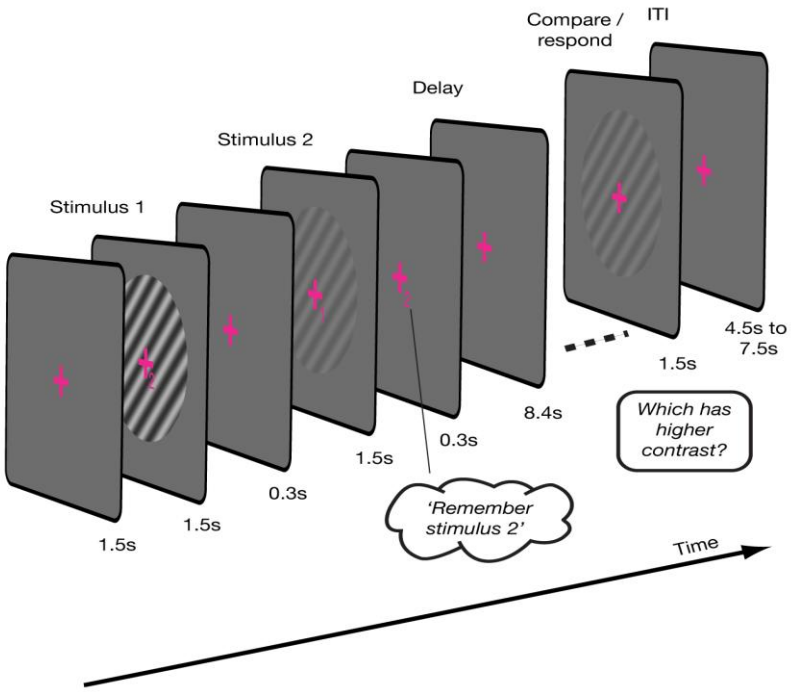

Figure 7.1 Visual working memory task of contrast performed by subjects in the scanner. On each trial, two grating stimuli of different contrasts were presented for 1.5 s each, separated by 300 ms. Each stimulus was labelled by a number (‘1’ or ‘2’, rendered in red close to the fixation cross, order randomized). There followed a 300 ms period during which subjects were cued to remember the grating / contrast corresponding to the given text label. The delay period during which subjects had to retain information in working memory was 8.4 s and was followed by a comparison stimulus, which differed in terms of contrast from the grating to be remembered by up to 20%. In a two-interval forced choice setting, subjects had to respond by pressing a button whether the remembered stimulus or the comparison stimulus had higher contrast. The next trial started after an inter-trial interval of 4.5 s – 7.5 s.

7.2.6 Orientation working memory scans - Experiment 2

To control the slight alteration of methods used in our study as compared with that of Harrison & Tong's study, we performed *orientation* memory experiment with our parameters and paradigm. During each trial, the subject was instructed to remember one of the two orientations (45º or 135º, slightly jittered) of moving gratings (100% contrast) shown at the beginning of each trial. At the end of the trials, another moving grating with a different orientation is presented to test whether the information of the cued grating is retained robustly in the memory. These matching stimuli had an orientation of ±5º (close to threshold) to maximize the requirement to keep an accurate representation of the orientation of gratings. The subject's task was to choose between this matching stimulus and the one cued to remember- which of the gratings was more clock-wise. Feedback was given after subjects pressed a corresponding button.

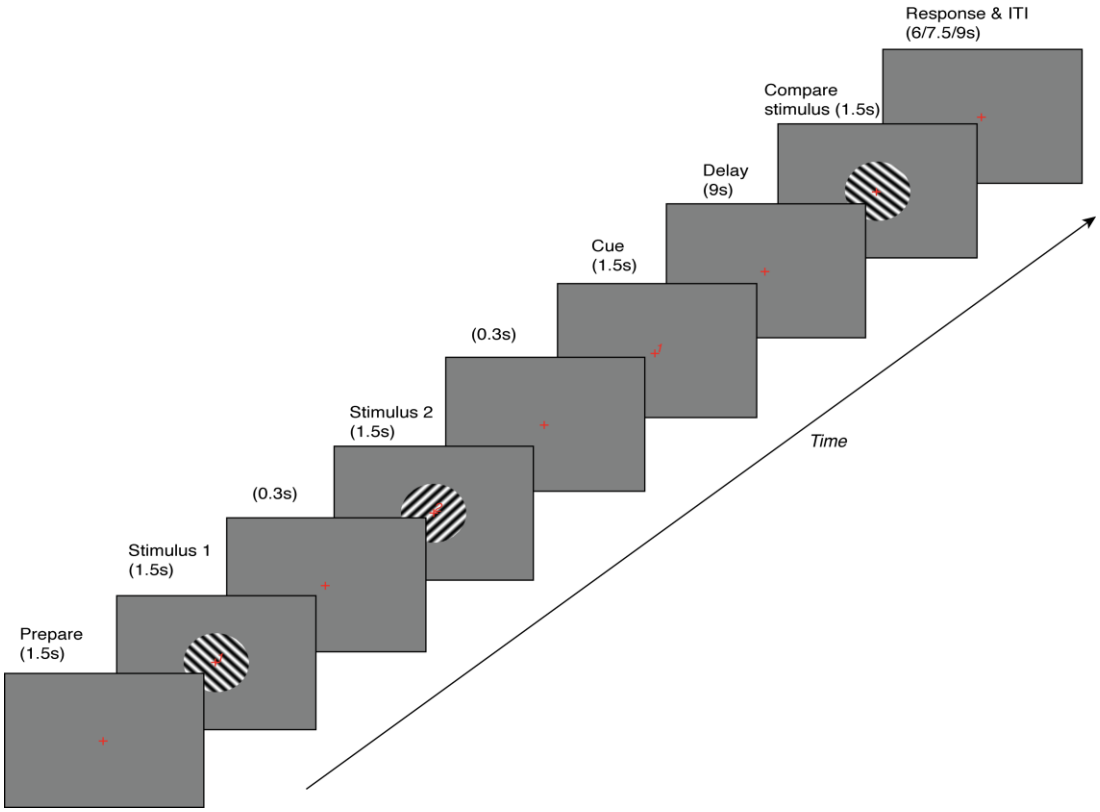

Figure 7.2 Visual working memory task of orientation performed by subjects in the scanner. On each trial, two grating stimuli of different oirentations were presented for 1.5 s each, separated by 300 ms. Each stimulus was labelled by a number ('1' or '2', rendered in red close to the fixation cross, order randomized). There followed a 300 ms period during which subjects were cued to remember the grating / orientation corresponding to the given text label.

The delay period during which subjects had to retain information in working memory was 9 s and was followed by a comparison stimulus, which differed ±5° in terms of orientation from the grating to be remembered. In a two-interval forced choice setting, subjects had to respond by pressing a button whether the remembered stimulus or the comparison stimulus was more clock-wise oriented. The next trial started after an inter-trial interval of 6 s – 9 s.

For both experiments, we ascertained that there were no systematic response amplitude differences in the average event-related fMRI response between the two trial types as this could be a potential confounding factor for the multivariate classification analysis (see Figure 7.3 and Figure7.4).

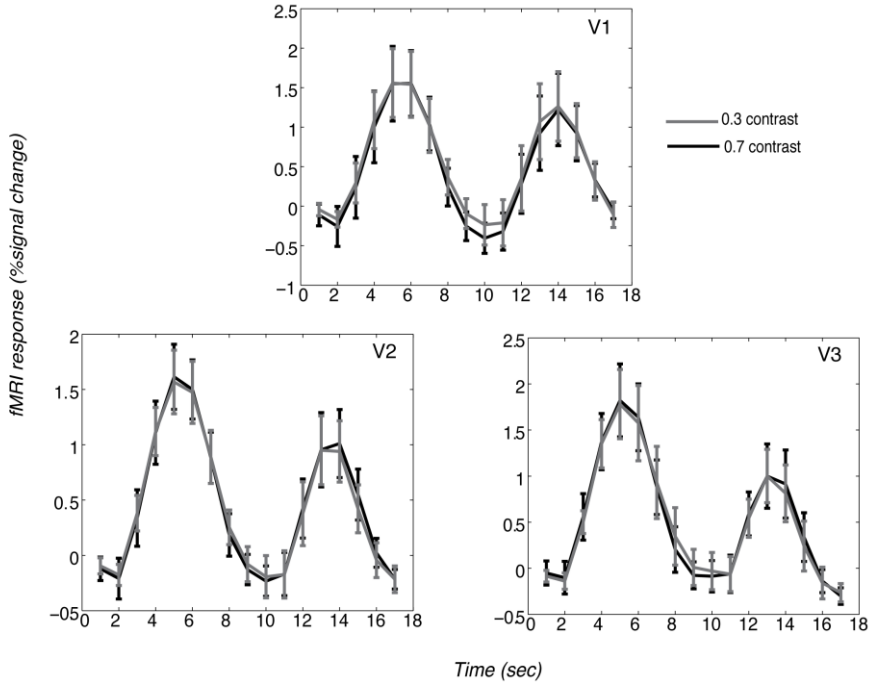

Figure7.3: Event-related responses from the contrast working memory experiment. Plot shows average responses in V1, V2 and V3 during trials in which the remembered contrasts were 0.3 and 0.7 respectively (mean + SEM across subjects). The curves show a typical pattern of response with a large transient following the presentation of the two stimuli and cue at fixation at the beginning of each trial, followed by a reduced response during the delay period and another transient increase in response after the presentation of the comparison stimulus.

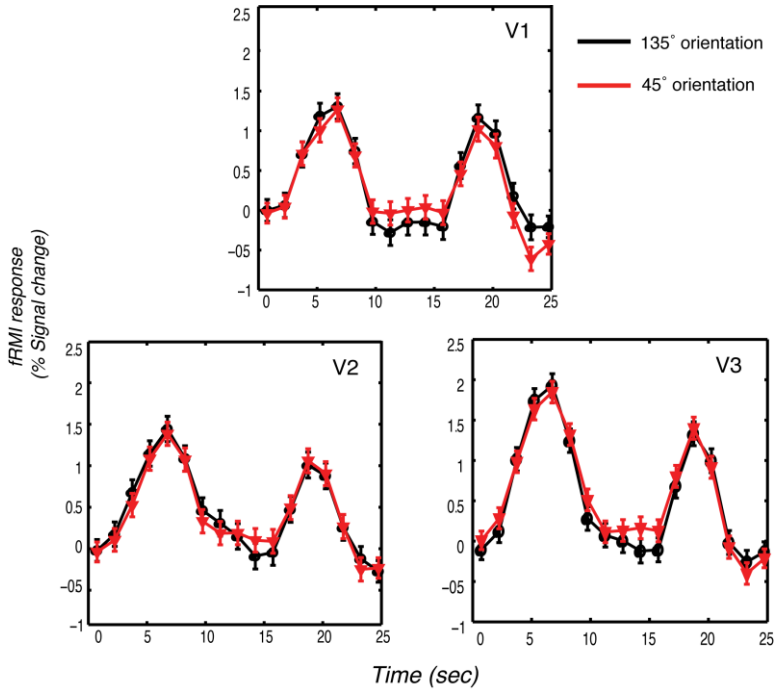

Figure 7.4: Event-related responses from the orientation working memory experiment. Plot shows average responses in V1, V2 and V3 during trials in which the remembered orientations were 45° and 135° respectively (mean + SEM across subjects). The curves show a typical pattern of response with a large transient following the presentation of the two stimuli and cue at fixation at the beginning of each trial, followed by a reduced response during the delay period and another transient increase in response after the presentation of the comparison stimulus.

7.2.7 fMRI response time courses

Imaging data were analyzed using a combination of custom-written software (mrTools, NYU, Heeger lab, NYU; VISTA, Stanford) running in Matlab 7.4 (Mathworks, Natick, MA). We used the standard event-related analysis methods (Burock et al., 1998; Dale, 1999; Burock and Dale, 2000) to reconstruct the time course of fMRI response for each trial type at each voxel in the ROIs with no predefined assumption of the hemodynamic response function.

7.2.8 Multivariate classification

We used multivariate pattern classification (MVPA) to analyze data from both of these memory experiments. Linear support vector machine (SVM classification) was implemented in custom-written Matlab (MathWorks, Natick, MA) functions to perform the classification.

The data for the classification analysis was the average across the time points corresponding to retention period after the stimulus presentation selected for each subject (TRs 5-7, i.e. 7.5s-10.5s after stimulus onset). The reason for including these response data is to maximise the coverage of the memory period while avoiding the contamination of the next event given the hemodynamic delay for each subject (see also Harrison & Tong, 2009).

A linear SVM provides optimal parameter values (weights and bias) for a hyperplane to categorize two classes of data, collected under two different stimulus conditions within such N-dimensional space. To access how generalizable the classification was, we tested our analysis with a 10-fold (or 5-fold) cross-validation scheme with the two classes approximately matched in each fold: 90% (80%) of data were used to train a classifier and the remaining, hold-out, 10% (20%) of data to test. We report the mean classification accuracy across these 10 (5) folds. The statistical analysis utilised the same procedure as described in the last chapter.

7.3 Results

7.3.1 Multivariate classification of remembered contrast

In this study, we addressed whether BOLD responses in early visual cortex could be used to classify the *remembered* stimulus contrast of a pattern. We recorded the BOLD responses when two levels of contrasts ('low', 30% or 'high', 70%) were remembered. Average time courses in V1 for the two types of trials across 6 subjects showed no apparent differences between the responses during trials when subjects had to remember the low or high contrast pattern (refer back to Figure 7.3). All subjects' responses across V2 and V3 in this task showed a similar profile.

The first transient increase in the event-related responses follows the presentation of the sample gratings and cue at the beginning of each trial. The second transient response corresponds to the presentation of the test grating. The period in between corresponds to the

interval during which subjects had to remember the contrast of the grating to allow them to perform the task. We averaged the four time points in this time window (see Materials and Methods) and used these data as input for our classification analysis.

To ensure that the pattern of results in the classification accuracies obtained did not depend critically on our choice of voxel number, we performed the following analysis. We randomly selected a range of 2-210 voxels (increments of 15) from the 210 candidate voxels in each V1, V2, and V3 and performed the classification analysis with this subset of features. We then repeated this analysis in 100 bootstrapped replications for each subject and plotted classification accuracy as a function of the number of voxels included. Figure 7.15 shows the mean (± 1 SEM) for data in V1 across 6 subjects, indicating that there are small differences in classification accuracy that depend on voxel number, but importantly the overall pattern of results remained. (The dashed line indicates the classification accuracy for n=180 voxels, the lowest common number of voxels available across ROIs and subjects, rounded down to a multiple of 10). Results in the working memory decoding are significant in 5 of 6 subjects as determined by a bootstrapping method. We include here the graphs in which we show the dependence of classification accuracy on the number of voxels included in the analysis (Figure 7.6).

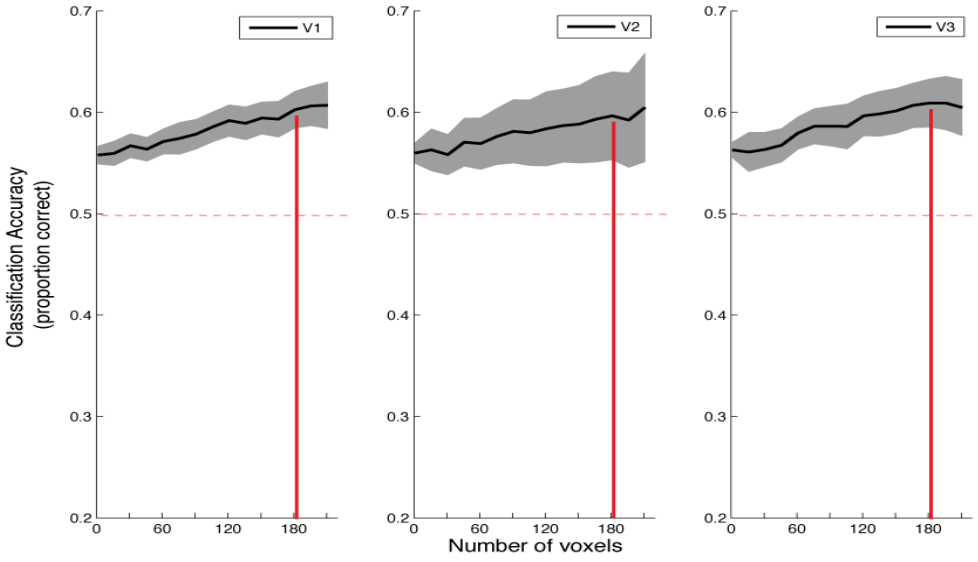

Figure 7.5 Relationship between classification accuracy and the number of voxels included in the MVPA analysis. The red line indicates the classification accuracy for n = 180 voxels, the

lowest common number of voxels available across ROIs and subjects rounded down to a multiple of 10. Shaded areas: standard error of the mean across 6 subjects.

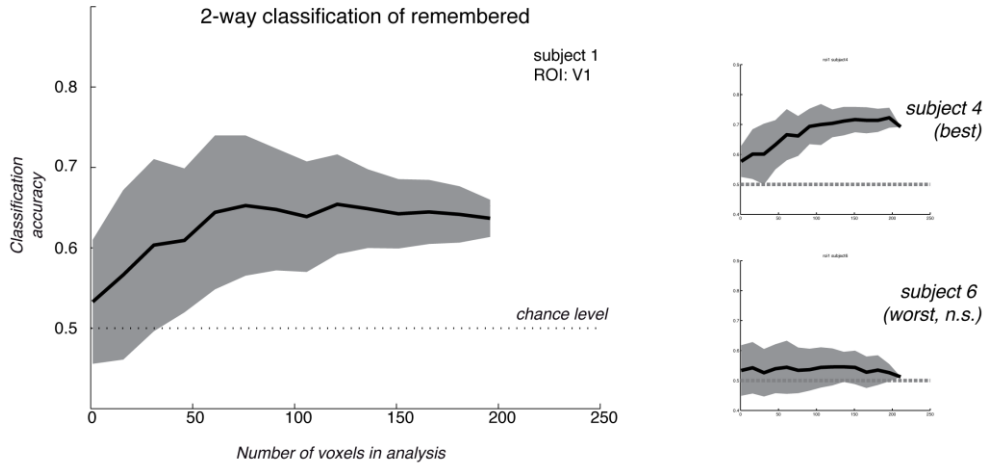

Figure 7.6: Dependence of classification accuracy on the number of voxels included in the MVPA analysis for individual subjects. These plots include data from subject 1 as well as plots for the "best" and "worst" subjects in each case. Shaded areas: standard deviation of the 100 bootstrapped replications.

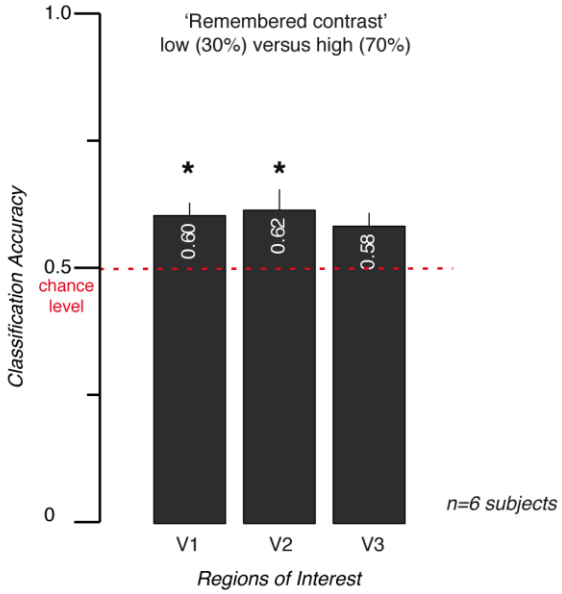

Figure 7.7: Proportion correct classification (30% contrast versus 70% contrast) from delayed periods in the working memory task. Error bars, SEM across subjects. Asterisks demonstrate the ROIs that reach the classification accuracy above 50% chance level ($p < 0.05$, two-tailed t test).

Using multivariate classification on the 180 voxels, we could successfully categorize the remembered contrast trials with accuracies significantly above chance level (Figure 7.7). This result was consistent across data from early visual areas V1 and V2. Results for V3 showed a similar trend, but failed to reach significance.

7.3.2 Analysis of correct / incorrect trials

We also split the fMRI data according to behavioural performance on each trial and considered classification accuracies for correct and incorrect trials respectively. This analysis revealed that decoding remembered contrast levels from early visual cortex was significantly better when subjects had correctly remembered the stimuli (Figure 7.8, n=4 subjects, for which there was a sufficient number of incorrect trials to perform the analysis). This suggests that the pattern of fMRI responses was more consistent and reproducible across 'correct' trials than 'incorrect' trials indicating an increased consistency of response patterns that leads to higher classification accuracies. The behavioural performance of our subjects in the working memory task for contrast indicated that the participants performed the task reliably. There was no significant difference in performance for maintaining in memory a pattern with contrast of 30% and 70% (74.1% correct versus 73.8% correct; $t(6) = 0.471$), implying that task difficulty was nearly matched across the two conditions. This may indicate that errors are more related to memory lapses or the inability to respond in time rather than difficulties with encoding the contrast level during the presentation of the sample pattern.

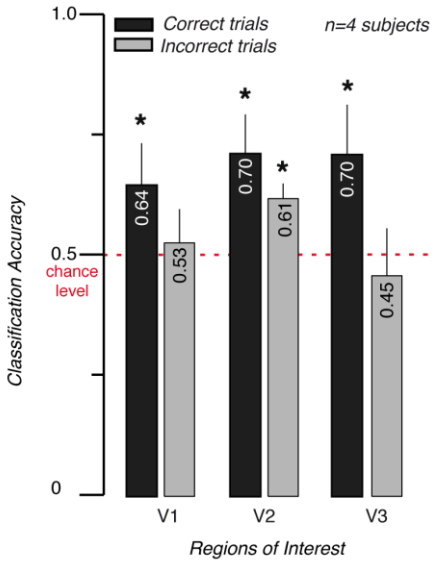

Figure 7.8: Predictions of remembered contrast levels using correct versus incorrect trials. Data were combined across (n = 4) subjects. Error bars, SEM across subjects. Colours, dark bars, using only correct trials; lighter bars, with only incorrect trials. Asterisks demonstrate the ROIs and conditions that reach the classification accuracy above 50% chance level ($p < 0.05$, two-tailed *t* test).

7.3.3 Generalization analysis

To further examine the role of early visual areas in maintaining a working memory representation for contrast, we tried to predict the remembered contrast during the memory task (30% and 70% contrast) using the SVM classifier trained with the data collected during last chapter when stimulus contrast was viewed. If the response patterns of *perceived* stimuli could be generalized to those of *remembered* stimuli successfully, this would provide additional evidence to implicate the function of early visual cortex in short-term memory for contrast.

To match the amount of data used in training and test of classification, the following 10-fold cross-validation procedure was used: 90% of data samples from perceiving experiment were used to train an SVM classifier, whose ability to classify was tested with 10% of data from contrast working memory experiment. Classification accuracies in this analysis were above chance for V1 and V2, with a similar trend for V3 (see Figure 7.9).

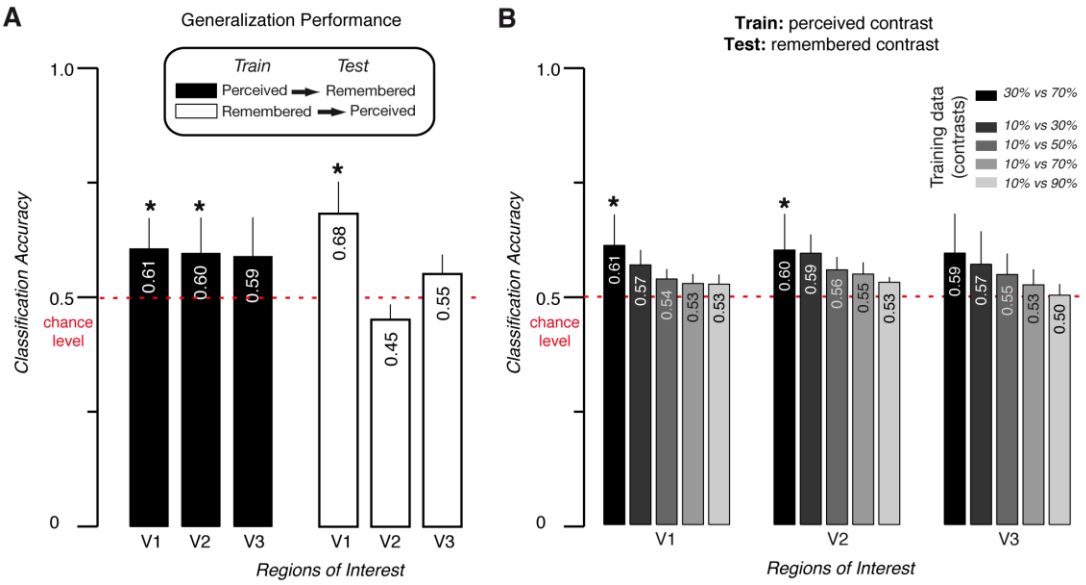

Figure 7.9: A. Generalization performance. Dark grey bars show performance when the classifier from experiment 1 (perceived contrast) was used to decode which contrast was remembered in experiment 2 (remembered contrast). Light grey bars show performance generalization by a classifier from experiment 2 (remembered contrast) to experiment 1 (perceived contrast). Error bars, SEM across subjects. B. Generalization from perceived to remembered stimulus is most consistent when contrast for training and test data are matched (black bars). Error bars indicate SEM subjects. *p <0.05, two-tailed t test.

In the converse analysis, training on memory trials and then testing on data from *perceived* stimuli - performance also exceeded chance level for V1. We also found that generalization from perceived to remembered stimuli was most consistent when the contrast for training and test data are matched (Figure 7.9B, black bars) and are reduced to chance for increasingly dissimilar training stimuli. These results provide compelling evidence that the patterns of response in early visual cortex associated with subjects performing the visual short-term memory task and perceiving stimuli are highly similar, although this does not imply a causal role of these responses in visual working memory.

7.3.4 The spatial pattern of representation underlying *contrast decoding*

To investigate the spatial pattern underlying the visual working memory of contrast, we conducted a corresponding analysis for data of the memory experiment. Similarly, V1 was

divided into two ROIs according to eccentricity. And another two ROIs corresponding to upper and lower visual fields served as control. Our result shows that an eccentricity bias also drives the classification in the working memory experiment above chance-level performance (Figure 7.10 C). This suggests that inhomogeneity in the spatial pattern of visual cortex responses – potentially driven by a feedback signal or attention – underlies the memory "decoding".

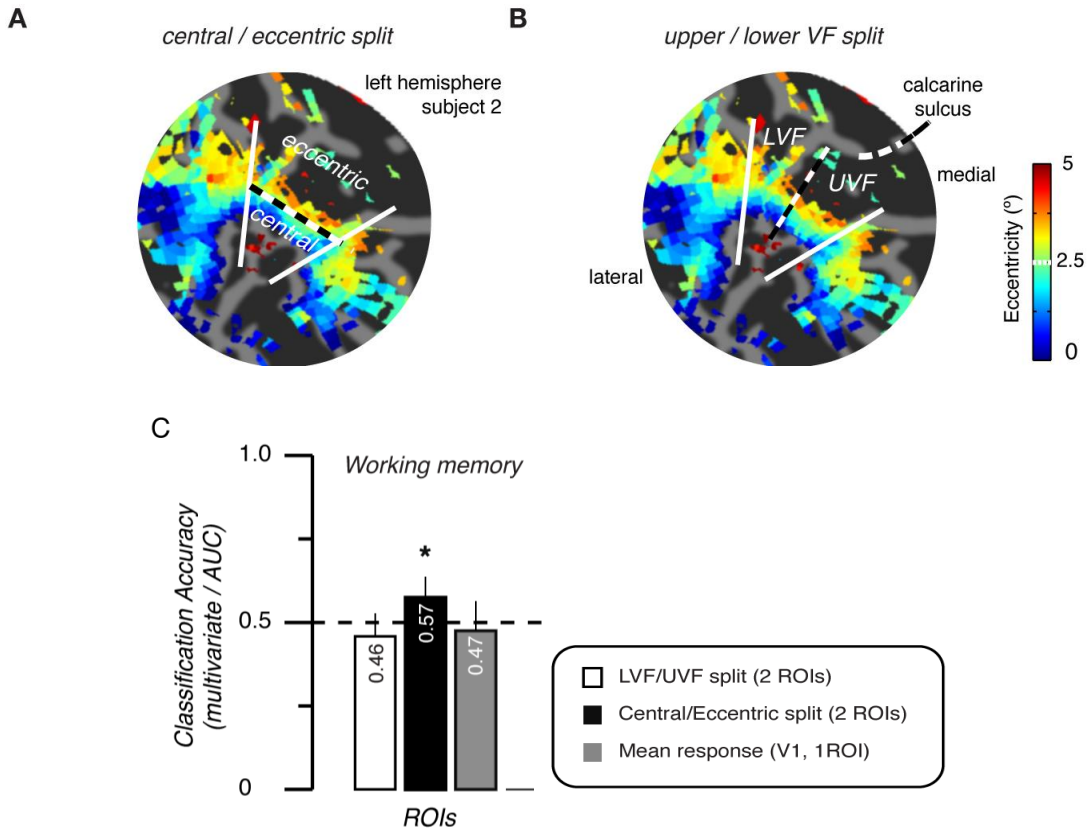

Figure 7.10 Spatial patterns of fMRI responses that drive classification. (A, B) Flat map of visual cortex from one subject showing definition of *central/eccentric* and *lower/upper* visual field ROIs for V1. White dashed lines, borders between V1 and V2v / V2d. C. Classification accuracies for decoding of remembered contrast. For multivariate classification, accuracies represent cross-validated values obtained with linear SVM, which are higher than the classification results using the mean time course across ROI. *p <0.05, two-tailed t test.

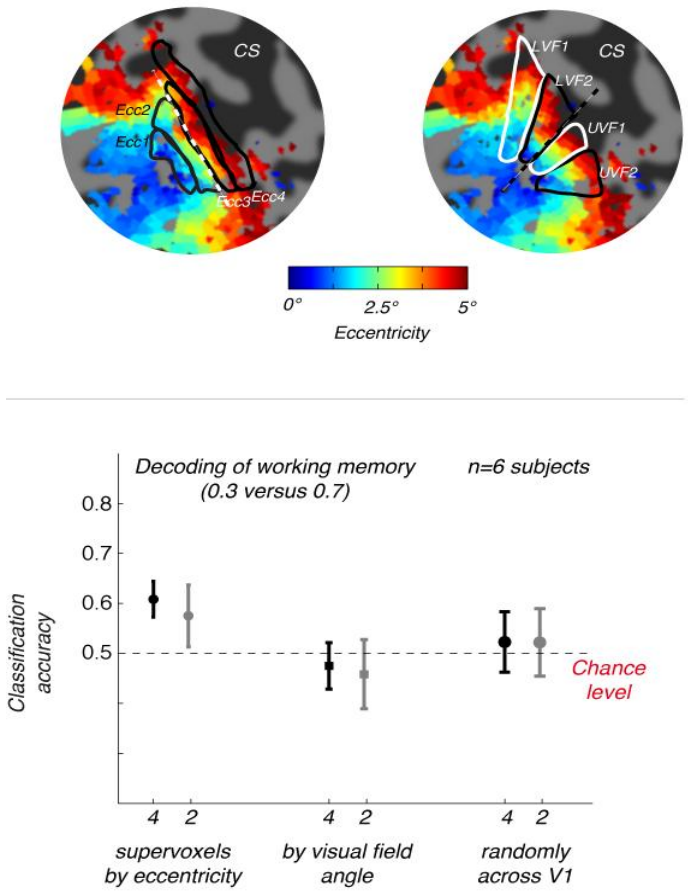

Figure 7.11: Robustness of spatial patterns that drive classification (controls). Upper panel: Flat map of visual cortex from one subject showing definition of 4 regions according to *eccentricity* (left) and 4 areas based on the *angle* visual field ROIs (right) for V1. Lower panel: Classification accuracies for the working memory trials obtained with fMRI response averaged in two (ROIs showed in Figure 7.10 A and B) or four (ROIs showed in upper panel) partitions of voxels split according to their eccentricity, visual field segment or by random sampling from all voxels in V1. Classification accuracies using either 4 or 2 supervoxels by eccentricity are consistently higher than those by visual field angle and random selection Symbols, mean across n=6 subjects. Error bars, ± 1 SEM.

7.3.5 Multivariate classification of remembered orientation

To control the slight difference in methods compared to Harrison & Tong (2009), we also used the fMRI decoding approach to determine whether activity in early visual areas might reflect which orientation was held in memory. Our study successfully reproduced the result from Harrison and Tong's report (2009) that orientation information from cortical activity sample at 3 mm^3 voxel resolution could predict the contents of working memory. The behavioural accuracy reaches 74%, which shows that the orientation information was

efficiently remembered. V1, V2 and V3 showed similar levels of orientation decoding performance with 180 voxels: Our classification shows significant performance (above 50% chance level) in all these areas (Average accuracystandard deviation across two sessions: V1, 0.6465±0.0065; V2, 0.5061±0.1061; V3, 0.6063±0.0263), except one session in V2. Once again, our data suggests that early visual cortex is involved in the maintaining of orientation of gratings.

7.4 Discussion

Following the demonstrations reported by Kamitani and Tong (2005b), and Haynes and Rees (2005), a wealth of studies have confirmed that multivariate classification can be used to *decode* basic features of stimuli that participants were viewing or even to predict attended stimulus features, in particular the orientation of gratings (Kamitani & Tong, 2006; Mannion, et al., 2009; Sapountzis, et al., 2010; Swisher, et al., 2010). However, there is substantial debate concerning the source of the underlying signal that allows this decoding to be performed both for stimulus orientation in particular (Freeman et al., 2011) and other stimulus parameters in general (Kriegeskorte et al., 2009).

To test whether MVPA could also be used to probe the mechanisms underlying working memory of stimulus contrast, we analyzed the fMRI responses obtained during a delay period in a visual working memory task. Given previous findings (Ester, Serences and Awh, 2009; Harrison and Tong, 2009) and our result from Experiment 2 in this chapter indicating that there is a significant working memory trace for specific orientations in early visual cortex, we wanted to investigate whether a similar result would hold for contrast.

Crucially, we found that there is indeed information in the fMRI responses during working memory trials that could be used to decode whether a low contrast or high contrast visual

pattern was retained in memory[1]. Intriguingly, when we reduced the multivariate responses into those of two *supvervoxels* corresponding to a *central* and an *eccentric* portion of our stimuli, classification of remembered contrasts was still possible. This suggests that a large-scale bias with eccentricity can drive classification for remembered contrast.

Another interesting finding is that there was no significant difference in the mean level of response in early visual cortex when subjects had to remember a low contrast stimulus compared to a high contrast stimulus, suggesting that the overall response level across the population of neurons is *not* the representation used for remembering stimulus contrast. The *pattern* of fMRI responses in early visual cortex, however, contained sufficient information to allow decoding of trials into the two categories. This result is consistent with those of Offen et al., (2009), who pointed out a possible explanation for the absence of (mean) delay period activity in early visual areas during visual working memory tasks: there may be opposing excitatory and inhibitory responses coming from different sub-populations of neurons in these regions, which may have been offset against each other in the average BOLD signal. Any delay period activity in early visual cortex may therefore be obscured in individual voxels or the mean responses across regions of interest.

To address the key issue of whether or not the pattern of fMRI responses obtained when subjects *perceived* a given stimulus contrast is similar to when they *remembered* it, we assessed the ability of our classifiers to generalize across the different tasks (Kamitani and Tong, 2005b, 2006; Dinstein et al., 2008; Kay et al., 2008; Brouwer and Heeger, 2009; Harrison and Tong, 2009). In Harrison and Tong's (2009) study on working memory for *orientation*, they predicted which of two orientations were retained in memory with a classifier trained on data from visual activity patterns induced by unattended gratings. In the

[1] It should be noted that the experimental design used here (in line with Harrison and Tong's paradigm) is not ideally suited to estimate sustained delay period activity, as the delay duration is fixed (see Schluppeck et al., 2006 for discussion) and by necessity always directly follows a cue. Exact estimation of delay period activity in such a paradigm is therefore ill-posed. However, to the extent that sustained delay period activity can be estimated, there was variability across our four subjects in the amount of sustained response, which is in agreement with previous reports (Harrison & Tong, 2009).

present study, generalization was tested by comparing classification with *perceived* (Experiment 2 in last chapter) versus *remembered* stimulus contrasts (Experiment 1 in this chapter). In our analyses, we found that classification generalized both, from perceived to remembered and vice-versa, strongly suggesting that the representation of information in early visual cortex (specifically V1) is similar for both perceived and remembered contrast.

Moreover, we observed a strong dependence of classification performance on the behavioural performance of our subjects in agreement with previous reports (Scolari and Serences, 2010; Williams et al., 2007). In one key analysis, we split trials according to correct and incorrect behavioural performance and found that *classification* accuracies for correct trials were significantly higher than for incorrect trials. This suggests that the pattern of responses in early visual cortex is more *consistent and repeatable* across correct trials than incorrect trials. This could be attributed to a number of factors: if the multivariate classification analysis relies on signals that are directly related to neural activity supporting working memory function, then this increased consistency in fMRI responses may correspond to decreased noise and a more reliable neural signal. Activity in early visual cortex during incorrect trials may also be less consistent, because there are several different reasons for making errors, hence causing more variability across those trials. Errors may be due to lapses or drifts in attention, short eye blinks and failure to encode or retain the matching stimulus and finger (response) errors.

Some studies suggest that both task-relevant and task-irrelevant features may be encoded together in VSTM (O'Craven et al., 1999; Wheeler and Treisman, 2002), while others have argued for a task-selective activity pattern in primary visual cortex (Woodman and Vogel, 2008; Serences et al., 2009). One previous fMRI experiment used color or orientation as selected features to evaluate prediction accuracy of MVPA in a working memory task (Serences et al., 2009). They found a significant change of performance when subjects' attention was switched between the alternate features in different runs. Here, we did not directly test whether the information of two orientations that were task-irrelevant were retained in memory (subjects only performed the task on the stimulus contrast), but like others

(eg Serences et al., 2009), we used two primary stimulus attributes (orientation and stimulus contrast), to reduce adaptation effects across trials.

7.5 Conclusion

Combined with the result from Chapter 6, our studies show that fMRI responses in early visual cortex could be used to decode stimulus contrast of a *perceived* stimulus and that responses in these areas also supported the classification of contrast when the stimulus only had to be *remembered*. Importantly, classifiers trained on data from each experiment generalized to the other: data from perceived experiment could be used to decode data from memory experiment and vice versa, suggesting that signals in early visual cortex contribute significantly to working memory for stimulus contrast on the timescale of seconds and that the same signals are present during *perception* and visual short term *memory* for this stimulus property. Importantly, we found that a large scale bias in the responses with eccentricity can drive classification for remembered as well as perceived stimuli, raising the possibility that a consistent attentional or feedback signal rather than activity related to working memory *per se* may underlie the significant (but modest) classification accuracies found in this and related studies.

Finally, we found substantially improved pattern classification when we compared data from correct to incorrect trials. When we considered only data from correct trials for classification, accuracies approximately matched subjects' behavioural performance on the task. This highlights the fact that fMRI responses from incorrect trials add substantial noise to the contrast VSTM signals that are used in decoding, an important consideration for future studies.

Chapter 8: Spatial properties of working memory and attentional signals in visual cortex

Abstract

Functional MRI evidence has shown that attention can modulate the neuronal activity in human visual areas when subjects attend to one particular spatial location. However, it is not clear the effect of visual attention on primary visual area when subjects maintain visual information online at the same time. To disentangle the contributions of VSTM and visual attention, we added uncertainty of the spatial location of the second stimulus in a simple two spatial interval forced choice procedure of a delayed orientation discrimination task. However, it is not known whether the spatial uncertainty enhances the activity at each possible spatial locations or the modulational effect may be weakened as the attention is redistributed across these different places. Our result demonstrated that attention modulates the average activity of the primary visual cortex during the delay interval but not working memory. This may suggest that average fMRI response may not be sufficiently sensitive as an indicator of the undergoing process of VSTM. Moreover, the responses increase less at each possible location of the second stimulus during the task when spatial uncertainty is involved, compared to the condition when subjects knew precisely the stimulus location. This result supports our second presumption that when attention was allocated among all the possible regions in space, which lessened the effect of modulation. Finally, our data confirmed that attention modulation of cortical activity follows the retinotopic organization.

8.1 Introduction

As defined for the purposes of this thesis, visual working memory refers to the ability of maintaining and manipulating information online without the presence of a visual stimulus. Previous working memory (WM) studies using neuroimaging methods have mostly considered the involvement of given cortical areas in the process of WM by examining if they

display sustained delay period activity. Based on this criterion, several previous studies found that the early visual cortex is also involved in WM. However, a recent study showed that the BOLD response increased as perceptual demands of a memory probe increased, suggesting that the overall activity changes in these areas could be attributed to the spatial attention at preparatory state rather than WM (Offen, Schluppeck and Heeger, 2009).

It is well known that spatial attention modulates the sensitivity to stimuli at specific spatial locations (Posner & Petersen, 1990; Colby, 1999; Posner & Dehaene, 1994; Maunsell, 1995; Mangun, 1995), which is different from feature or object-based attention. Improved sensitivity with spatial attention can be generated by a cue without moving the eyes (covert attention) if a subject's attention is directed and maintained prior to the presentation of a target at certain locations in the visual field (LaBerge, 1995). Using this typical paradigm of directing attention, a considerable number of studies have revealed characteristics about spatial attention in experiments using both psychophysical and neuroimaging methods. It has been found that the fMRI response increases at the representations of the attended target during the delay period. This parallels similar changes during WM tasks in visual areas (Serences & Awh, 2009), making it difficult to untangle the cause for the amplified response in those regions when a cognitive task requires both working memory and spatial attention. Furthermore, behaviourally it was found that working memory is highly dependent on attention. Given this distributed anatomical network and overlapped functional consequences, it is crucially important to clarify the role of attention. This thesis has described one pilot experiment on distinguishing attention and working memory in early visual cortex using a motion coherence stimulus. Here we take advantage of different task structures to keep the demand of working memory constant in order to measure the intensity of attentional modulation on cortical activity using BOLD fMRI and – in the first instance – univariate analysis.

The present study consisted of three experiments and used the orientation of sinusoidal gratings as the visual feature. Three delay intervals were used in the first and the second

experiments (see table 8.1 for the experimental structure). In these two tasks, we modulated spatial certainty but attempted to keep temporal certainty constant. Subjects were cued in both experiments 0.5s before the onset of delay intervals. In the first experiment, attention was actively directed by a symbolic cue to *one* spatial location; whereas in Experiment 2 *four* possible target locations were cued and spatial uncertainty was therefore introduced. The spatial uncertainty could bring two consequences. Subjects may direct more spatial attention at preparatory state to the four cued locations to offset the spatial uncertainty. If this were the case, the activity during the delay interval at the target location should be higher than the one evoked in Experiment 1. Alternatively, if the spatial attention is disturbed among the potential target locations (Experiment 2), then the intensity should be weaker during the delay period compared to the first experiment. In addition, the responses of target and non-target locations should be similar because all were attended. In Eexperiment 3, two stimuli were simultaneously presented to the subjects at two cued locations in the two visual fields. Therefore, no working memory and spatial uncertainty is involved. However, since the stimuli were displayed at the same time at two hemifields, it is possible that the visual attention is engaged, which can be demonstrated by the behaviroal change and/or activity amplitude at both target locations.

In the present chapter, the first experiment also addressed the question of whether the BOLD response in early visual areas could reflect task difficulty of working memory (see the fourth column in Table 8.1). A few fMRI studies have asked this question but mainly focus on the higher cortical regions. Duncan and Owen (2000) reviewed the cortical locations involved in a variety of tasks with different cognitive demands such as task novelty, WM loads, response conflict and so on. Regardless of the task and stimulus types, a common network of regions has been identified, including frontoparietal regions, prefrontal cortex and subregions in cingulate cortices. It has been pointed out that the enhanced activations in these cortical areas are correlated with increased levels of task difficulty. We increased the WM demand by manipulating the perceptual difference between first and second stimuli in Experiment 1.

Since the attentional modulation by the spatial cueing was maintained at the same level within this experiment, we were able to investigate the effect of WM task difficulty on the change of fMRI response in human primary visual cortex.

Table 8.1: Experimental design and structure in Chapter 8 (Y: Yes; N: No).

Domain	**Temporal (WM)**	**Spatial uncertainty**	**Task difficulty**
Task (Experiment #)	2IFC Orientation discrimination (which grating is more clockwised?)		
1	Y	N	Easy/Hard
2	Y	Y	Hard
3	N	N (but may require spatial attention)	Hard

Another currently open debate in the field of WM is how visual information is actually stored in the brain. While some recent reports proposed the "sensory recruitment theory", other evidence suggested that information is not only modulated by top-down activation from higher visual regions but also represented in these regions, including intraparietal sulcus (IPS) (Sereno et al., 2001; Bisley & Goldberg, 2003; Silver et al., 2005; Serences & Yantis, 2007; Saygin & Sereno, 2008) and prefrontal cortex (PFC) (Sereno et al, 2001; Serences & Yantis, 2007; Saygin & Sereno, 2008). To investigate how different cortical areas perform and cooperate during WM and their relation to attention, we also looked at the fMRI acitivity at higher regions beyond the visual system.

8.2 Materials and methods

8.2.1 Subjects

Three experienced subjects with normal or corrected-to-normal vision took part in this study with written consent. The procedures were approved by the Medical School Research Ethics Committee at the University of Nottingham. Each subject participated in two scanning sessions, including one session for retinotopic mapping and one session for the functional scans for the main experiment.

8.2.3 Visual stimuli

In all experiments, the stimuli were generated on an Apple MacBook Pro running Matlab and the MGL toolbox (http://justingardner.net/doku.php/mgl). In the fMRI experiments stimuli (on a median grey background) were projected from a LCD projector onto a display screen at the feet of our subjects. The display resolution was 1024×768 pixels, covering 20.4º (width) × 15.4º (height) of visual angle. Subjects were in the supine position in the scanner bore and viewed the display through an angled mirror. A white cross was presented and remained on the centre of the display throughout each run. Subjects were asked to maintain fixation at this location to stabilize eye position in all scans for collecting response within precisely defined visual field locations (see below). All the stimuli in the main experiments were sinusoidal gratings (radius, 4°; spatial frequency, 0.75 cycles/°; contrast, 40%) presented within six identical circular apertures at six different peripheral locations, which were centered at the same eccentricity (5° of visual angle) around the fixation. The right visual field and left visual field each contained three locations. In detail, two locations were set on the right and left side of the fixation cross, respectively, along the horizontal meridian of the display. Others were distributed in the four quadrants, 54° diagonal from the central fixation. The shortest distance from the edge of apertures to the vertical meridian of the screen was 1° of visual angle. Figure 8.1 illustrates the stimulus locations as described. This setup of visual stimulus locations was used in order to confine ROIs within one hemisphere. Meanwhile, in order to prevent overlap of stimuli, the angle between the tangents of any adjacent apertures within each hemi-field

was 10.4°. Subjects conducted three different tasks ("Experiments 1, 2, and 3") with this scheme of stimulus independently according to the following procedures.

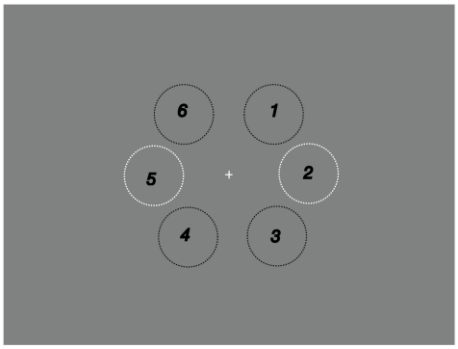

Figure 8.1. Stimulus spatial locations in the localizer scan and main experiments. For the sake of clarification, the six locations of possible stimuli were numbered as on a clock-face. The numbering of stimulus location was in a clock-wise sequence by starting from up-right quadrant. In the actual experiments, there was no number displayed on the screen. White dashed circles, possible locations for sample stimulus; Black dashed circles, possible locations for target stimulus.

8.2.4 Experimental procedures

All experiments utilized an event-related design procedure. Experiment 1 and 2 applied the delayed sample-target paradigm typically used in working memory studies. At the onset of a trial, a white dashed circle indicated the location of the sample stimulus randomly chosen between the two horizontal locations. Then, a grating (contrast, 70%; spatial frequency, 0.75 cycles/deg; phases (0 and 180); orientation, 45° or 135°) was displayed at the cued position for 500 ms. Subjects were then cued by a second brief spatial cue (a black circle presented for 300 ms) to the (possible) location(s) of the target stimulus. Following a variety of delays (3 s, 5 s, or 7 s), the target stimulus was displayed at a target location randomly selected from the four locations in quadrants. The position of the target was varied from trial to trial. The duration of the delay period was also randomized to discourage subjects' anticipation of the impending stimulus. Subjects were asked to maintain the orientation of this sample stimulus in memory and to compare it with the orientation of the target stimulus presented at the end of the trial. When the colour of the fixation changed into yellow, they reported a judgement of

which stimulus was more clockwise-oriented. Finally, feedback was given to indicate whether subjects answered correctly (fixation cross turned green) or not (red). Inter-trial intervals were chosen randomly from three values (1 s, 2 s, and 4 s). Though different stimulus locations were involved in this study, subjects were instructed to remember the orientation of the sample stimulus not the spatial location. Therefore, no spatial working memory was required. The following sections describe the characteristics of task structures in Experiment 1, 2 and 3. The paradigm of each experiment, including timing and spatial locations of the stimuli, is illustrated in Figure 8.2 (A, B, C).

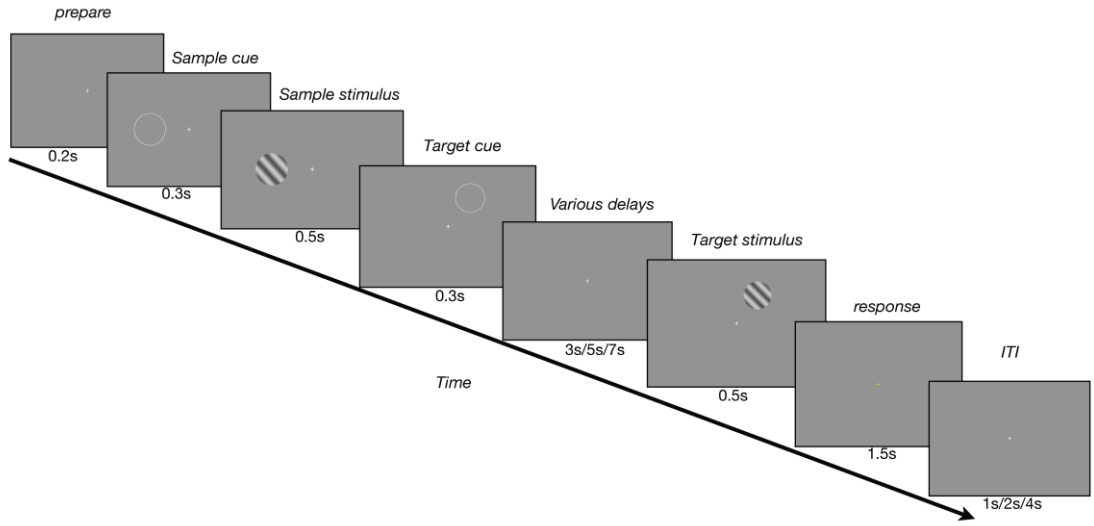

Figure 8.2. Stimulus and behavioral tasks from the three main experiments. **A**, task scheme of Experiment 1: Subjects were instructed to fixate centrally throughout each of the scans. A dotted white circle was displayed at the exact location of the sample stimulus location. A peripheral grating with an orientation was to be remembered for a variable delay interval (3s, 5s and 7s). Then a dotted black circle cued the target stimulus of a grating with a different orientation. A colour change of fixation signaled the subjects to make a decision of which orientation was more clock-wised. The next trial began after a variable intertribal interval (ITI) (1 s, 2 s or 4 s).

8.2.4.1 Experiment 1: Delayed orientation comparison task

After the sample stimulus and just before the onset of the delay period, a black dashed circle briefly marked the exact location of the target stimulus. Therefore, no spatial uncertainty is involved in Experiment 1. Even though the delay duration was jittered among three different

delay intervals, the temporal structure of this task did not require intensive attention to detect the onset of the target stimulus because it was a salient supra-threshold stimulus (50% contrast). To manipulate the working memory difficulty, two levels of orientation differences were used. Subjects were instructed to discriminate two stimulus orientations with either one JND (Difficult) or three JND (Easy) in the scanner. The just noticeable difference (JND) is the baseline orientation discrimination threshold for each particular subject. It was acquired in a practice run prior to scanning.

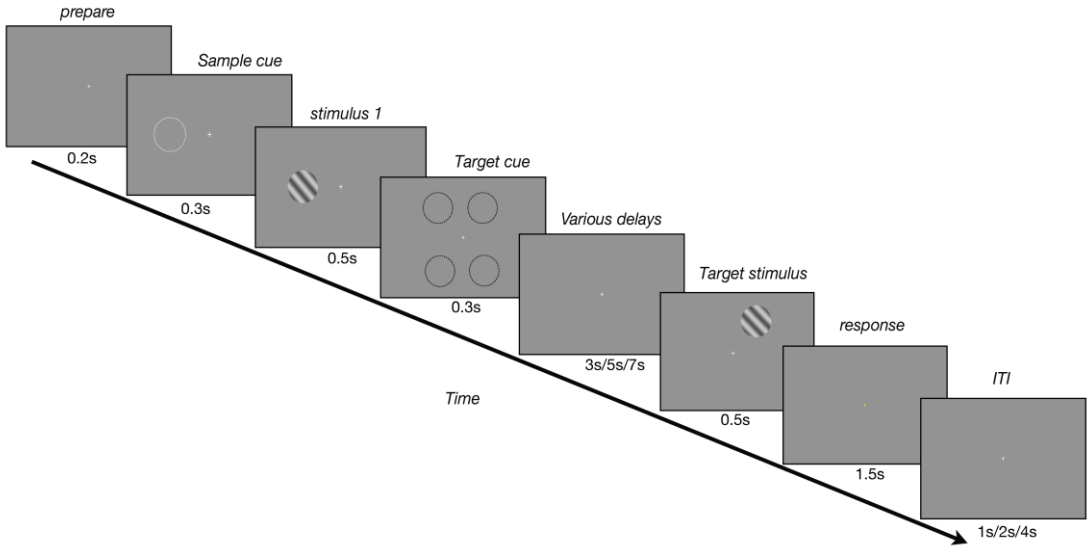

Figure 8.2 **B**, task scheme of Experiment 2: Similar to the delayed discrimination task in Experiment 1, Experiment 2 cued all possible positions in quadrants (four black dashed circles), signaling that the target stimulus could be presented in any of the four locations.

8.2.4.2 Experiment 2: Delayed orientation comparison task with spatial uncertainty

Similar to Experiment 1, this task also requires the memory of the initial stimulus and participants did not have to be attentive in the temporal domain. However, the location of the impending target stimulus was not certain. Before the delay period, four dashed circles were displayed as cues to indicate the possible locations of the target stimulus. To allow independent measurements in the ROIs for sample and target processing, we specifically separated the location of the four possible *targets* and two patches for the *sample* stimulus

along the horizontal meridian of the screen. By cueing all possible target locations, we incorporated spatial uncertainty to this experiment while keeping the WM demands the same as Experiment 1. Only one JND difference of orientation was used for maintaining subjects' performance at 70% correct in the scanner.

8.2.4.3 Experiment 3: Concurrent orientation comparison task

In contrast to the first two experiments that involved retaining orientation information online to compare with the upcoming stimulus, Experiment 3 was a spatial 2AFC orienation discrimination task. Two gratings at same contrast with orientations differing by one JND were presented to subjects simultaneously for 500 ms. One of the stimuli was presented in one of the horizontal locations and the other was always displayed within one of the two remaining quadrants in the opposite visual field. No spatial uncertainty was involved since these two locations were cued precisely before the presence of stimuli. JNDs for each subject was measured for this task prior to scanning. Subjects were asked to press a one of two buttons to indicate on which visual field (left or right) the grating appeared more clockwise.

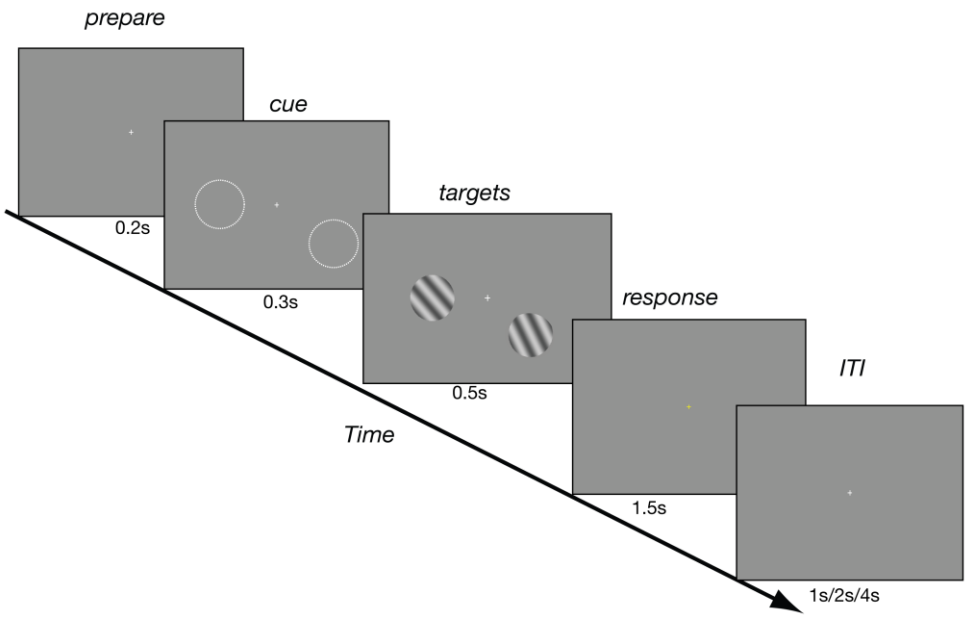

Figure 8.2 **C**: task scheme of Experiment 3: Subjects fixed at the central cross while two contralateral targets were briefly and simultaneously (~500 ms) presented at two locations, including one of the sample locations (# 2 or # 5 in Figure 8.1) and one of the four target locations (# 1 / 3 / 4 / 6). Subjects gave a response at the end of each trial which orientation was more clock-wise oriented (left or right), followed by a feedback.

8.2.5 Threshold estimation

Subjects performed a similar orientation discrimination task before they were scanned. Individual performance was estimated for each of the three tasks using a modified 1-up-3-down staircase adaptive procedure. The orientation difference was varied from trial to trial to allow a convergence at 70% correct (Levitt, 1971). The mean of the last six reversals in each staircase was used to estimate threshold. For the delayed discrimination tasks (Experiment 1 and 2), the delay interval was kept constant at 5 seconds during this session outside the scanner. Each subject performed 2 runs of staircase for each experiment.

8.2.6 Functional MRI acquisition

MR imaging was performed at 3 T (Philips Achieva, Philips Healthcare, Best, the Netherlands) using a 32-channel Philips SENSE head coil. Foam padding was used to minimize head movements. In session one we obtained a set of 10-12 functional scans to measure the retinotopic organisation in the early visual cortex allowing us to functionally define V1, V2 and V3 with standard methods. For subjects who had no previous anatomical scans, we also acquired high-resolution anatomical T1-weighted MPRAGE images of the whole brain for segmentation and cortical flattening in the same session. In the second session, we obtained fMRI data while subjects were performing tasks which manipulated the requirements of working memory and attention. During each session, we acquired several functional scans, including a scan for localizing the regions in early visual cortex representing the stimulus and six to eight scans for the three main experiments according to the pre-defined order. Two participants had three scans for the first two experiments, and two scans for Experiment 3 in order to collect similar number of trials for each type of task. All the functional imaging was performed with same scanning parameters: 33/32 oriented slices were acquired using a blood-oxgenation level dependent (BOLD) T2*-weighted (gradient-echo) with echo-planar imaging sequence (repetition time (TR): 2000 ms; echo time (TE), 35 ms; flip angle (FA), 78°; voxel size, 3×3×3 mm^3; field of view (FOV), 192×192 mm^2; interleaved acquisition). We used parallel imaging (acceleration SENSE factor 2). The slices covered the

whole brain volume. At the beginning of each fMRI scan, 4 dummy volumes were acquired to avoid T1-saturation effects. Structural T1-weighted images with the same scanning orientation and coverage were collected as well. These anatomical images were used to co-register the high-resolution 2D-MRAGE images and functional images for each individual.

8.2.7 Retinotopic mapping

For each participarnt, we used a combination of tools (FreeSurfer, MGH, Harvard; FSL distribution, FMRIB Software Library (Smith et al., 2004) for segmentation and cortial flattening of the retinotopic mapping session (Schluppeck et al., 2006; Sanchez-Panchuelo et al., 2010). Early visual areas (V1, V2 and V3) for each subject were then identified based on the standard travelling-wave method using rotating wedges and expanding rings (Engel, et al., 1997; DeYoe, et al., 1996; for a review see Wandell et al, 2007). The responses to the rings and wedges are used to estimate the eccentricity and polar angle of the visual field representation, respectively. Following standard methods we defined areas V1, V2, and V3 in our subjects after locating the upper, lower and horizontal meridian representations using the phase reversals in the polar angle maps (see more details in Chapter 2).

8.2.8 Localizer scans

To identify the corresponding visual regions of each stimulus location, we used a phased-locked localizer to measure the response from the stimulated areas at the beginning and the end of each scan session. During the scans, subjects viewed 4-Hz flickering gratings presented at each of the stimulus locations in a clockwise sequence starting from the top right quadrant to the top left quadrant with a period of 24s and a 50% duty cycle. The orientation of the grating was randomly assigned to be either 45° or 135°. Other parameters for generating the stimuli were identical to those used in the main experiments. In order to keep their gaze maintained on the central fixation marker, they were asked to perform a contrast discrimination task at fixation with a staircase procedure (as same as the one used in retinotopic mapping session).

8.2.9 fMRI Data Analysis

8.2.9.1 Pre-processing and motion correction

fMRI data anlysis was performed in MATLAB using the software package mrTools and additional custom-built functions. The preprocessing of the BOLD signal included the following steps: First, linear trend in the time series was removed, and a high-pass filter was applied to compensate for the low-frequency drifts at each voxel with a cutoff frequency at 0.01 Hz (Biswal, et al., 1997; Offen, Schluppeck & Heeger, 2009). Next, the time series of each voxel was normalised with its mean intensity to convert the data to percent signal change.

8.2.9.2 Localizer in early visual areas

Data from the localizer scans for each subject were analyzed using a standard correlation analysis between the signal in each voxel and a sinusoid of 4s period. Given the previously described (and well known) topography in early visual areas, the localizer time series reflects the locations of six stimuli displayed in clockwise direction (from the right-up quadrants to the left-up quadrants) as time progresses. The correlation between the time series and the sinusoid was calculated and a coherence value was assigned to each voxel in the defined V1, V2 and V3. Then we selected the voxels with coherence exceeding the threshold criterion (coherence > 0.5). Boundaries of the six regions of interstest (ROIs) – three in each hemipshere V1 – were delineated on the flattened cortical map. These ROIs from the localizer scan are thus completely indepdent of the result from main experiments.

8.2.9.3 Voxel selection

Instead of arbitrarily choosing a r^2 threshold for data analyzed in the framework of the GLM, we adopted a permutation procedure to perform voxel selection (Gardner et al., 2005; Costagli et al., 2012). The r^2 values were re-calculated for all voxels in the ROIs within V1 for 10 randomizations of the stimulus onset times. Then we combined all the r^2 values from this randomization procedure into a single (null) distribution to compare with the real r^2 distribution. By taking the right-tailed 5% r^2 values of the randomization-derived distribution, we could assign a cutoff value to select voxels with $P<0.05$ (Figure 8.3). The following fMRI

data analyses for different experimental manipulations were all based on this voxel selection procedure.

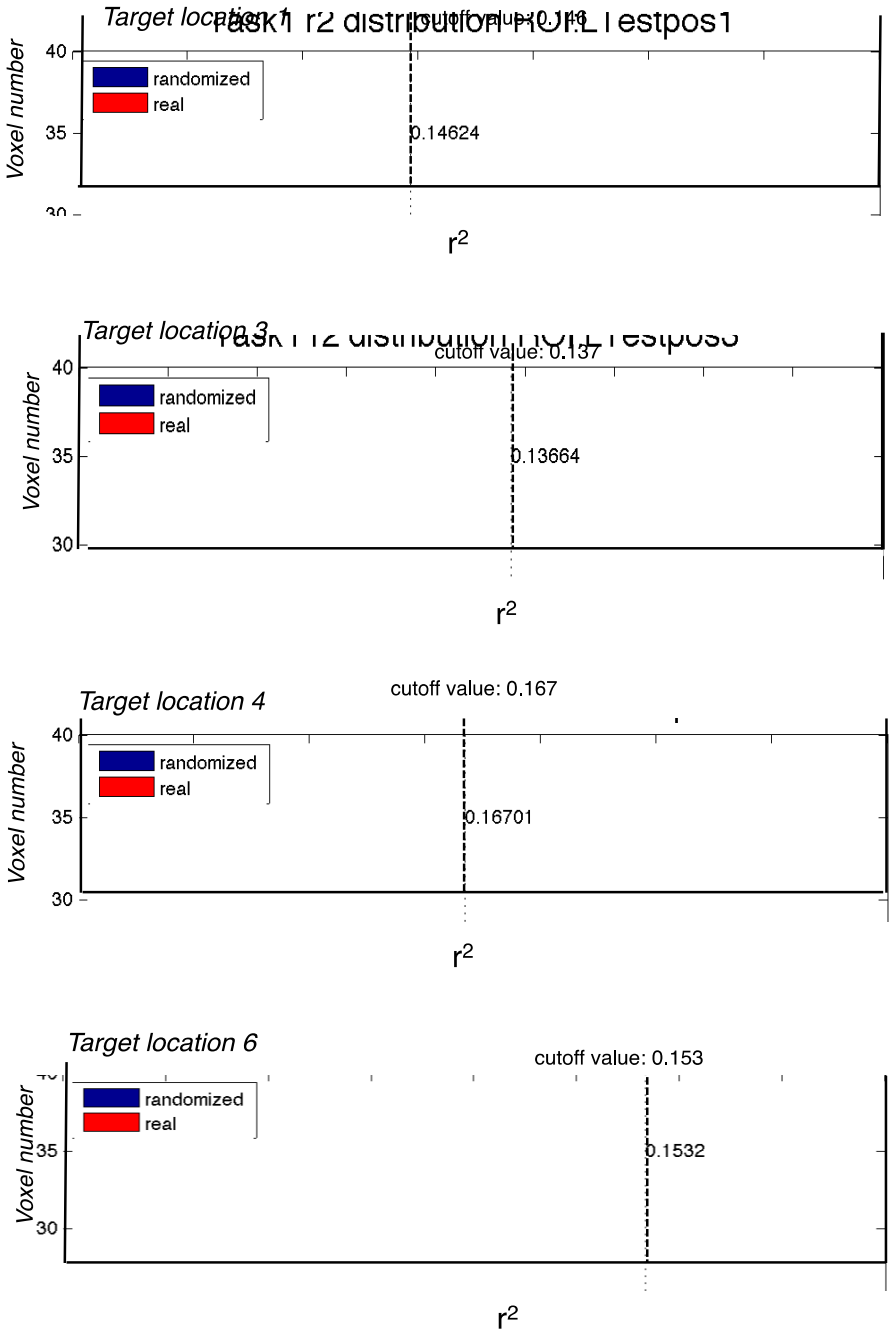

Figure 8.3: Examples of distribution of r^2 values obtained for the real data (red) and when the stimulus times were randomly shuffled (blue) at different target locations. Dashed vertical line marks the r^2 cutoff value chosen on the basis of the randomized distribution for Experiment 1.

8.2.9.4 fMRI responses

We used the typical univariate analysis to investigate the activity for each ROI (Curtis &

D'Esposito, 2003). A standard event-related method with a set of deconvolution models was applied to estimate the actual hemodynaic responses for different experimental conditions (Glover, 1999; also see more details in section of GLM analysis, Chapter 2). With this computed fMRI response of all types of trials for each voxel, we then calculated the ROI activity by averaging the time series across the set of voxels that represent the stimulus delivered in the main experiments. For the purposes of measurement power and visualisation, the time courses displayed in most of the following analysis are combined across all the target locations or sample locations for different delay intervals. We also computed the proportion of variance accounted for in the measured fMRI responses (r^2) to quantify the model fitting.

8.2.9.5 fMRI response amplitudes

To quantify the BOLD activity for experimental conditions, we also estimated the response amplitude in ROIs. As illustrated in the section on the hemodynamic response function and linear systems (Chapter 2), the amplitudes of fMRI responses to each of the three events (sample, delay and target intervals) can be estimated by multiple linear regression. Each trial was modelled with three components as follows: (1) a transient at the start of each trial, which represented sample visual stimulus at the sample location (marked as S), (2) a component that lasted throughout different delay periods (delay duration, marked as d), and (3) another transient component at the end of each trial that reflected the target stimulus at the test locations (marked as T). Each of the components (S, d, and T) in the neuronal response model was then convolved with a two-gamma canonical model of the hemodynamic response function (Jezzard, Matthews, & Smith, 2003; Friston et al., 1995) to yield three regressors of the fMRI measurements. This model is demonstrated in Figure 8.4. Linear regression was used to estimate the three responses amplitudes (which scale the three regressors) separately for each scan over time. However, because the sample and target locations were separated spatially, we grouped the three events according to the stimulus locations in the following way: (1) the sample, delay and test activities at the sample location and (2) the delay and test activities at the target locations.

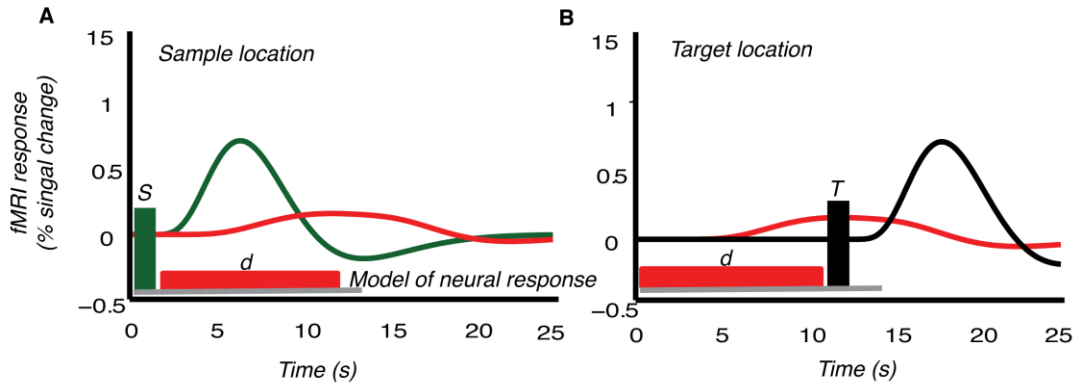

Figure 8.4: Model simulation. Data were modeled with three components: a transient for the sample (S), a constant for the duration of the delay (d), and target visual stimulus (T). Their response amplitudes were represented in green, red and black, respectively. The predicted fMRI responses were calculated by convolving the neuronal response model with a canonical hemodynamic response function (HRF) (See Material and Methods). Green, red and black curves show the predicted fMRI response time courses contributed from each component (S, d, and T), respectively. Summation of these curves achieves the total predicted fMRI response. **A**, possible fMRI responses at the sample location. **B**, possible fMRI responses at the target location.

8.3 Results

8.3.1 Behavioural data

The discrimination thresholds (mean±std) of the main experiments outside the scanner were summarized in Table 8.1. We only used the mean value in the actual experiments.

Table 8.1: The Just Noticeable Difference of experiments for the three subjects

	Experiment 1 (°)	**Experiment 2 (°)**	**Experiment 3 (°)**
Subject 1 (A.B.)	6.3 ± 0.45	5 .2± 0.53	7 .4± 0.52
Subject 2 (M.S.)	5 .2± 0.53	5 .3± 0.32	10.5 ± 1.1
Subject 3 (D.H.)	5 .1± 0.56	5 .5± 0.26	7 .3± 0.63

(i) The behavioral performance for two difficulty levels in Experiment 1

The average behavorial accuracies (percent correct) on delayed orientation discrimination task in Experiment 1 (3JND difference: 62.5%; 1JND difference: 52.8%). As expected, trials with 3JND difference were higher than 1JND trials. This measurement confirms that our threshold

manipulation successfully increased task difficulty for WM.

(ii) Behavioral performance of main experiments

The average behavorial accuracy of experiment 1 (without certainty) was equivalent to the performance of task 2 (with uncertainty). No performance difference on the discrimination tasks was observed for the two possible sample locations (stimulus was present left or right hemifield) nor for the two orientations (~45° or ~135°). In addtion, the results of statistical analysis showed that behavioral performance was independent of delay duration for all set of delays. The average accuracy of experiment 3 was around 70% across three subjects.

8.3.2 Localizing the stimulus representation in V1

To better visualize V1, we unfolded the grey matter and flattened the visual cortex into a map for each participant. V1 was further limited to the representation of sub-regions according to the localizing stimuli. For these experiments, it is crucially important to separate the regions corresponding to sample and target stimuli. Besides the relatively large area of V1 compared to V2 and V3, we found the boundaries of subregions in V2 and V3 began to overlap as the size of receptive fields (RF) increases when moving along the visual pathway. In addition, for two simultaneous stimuli in visual areas with larger RF, neurons may mutually inhibit each other in V2 and V3 (Bles et al., 2006). To avoid this confouding factor for Experiment 3 and also for other listed reasons, here we only focus on the representation of stimuli within V1, colour coded in RGB in Figure 8.5.

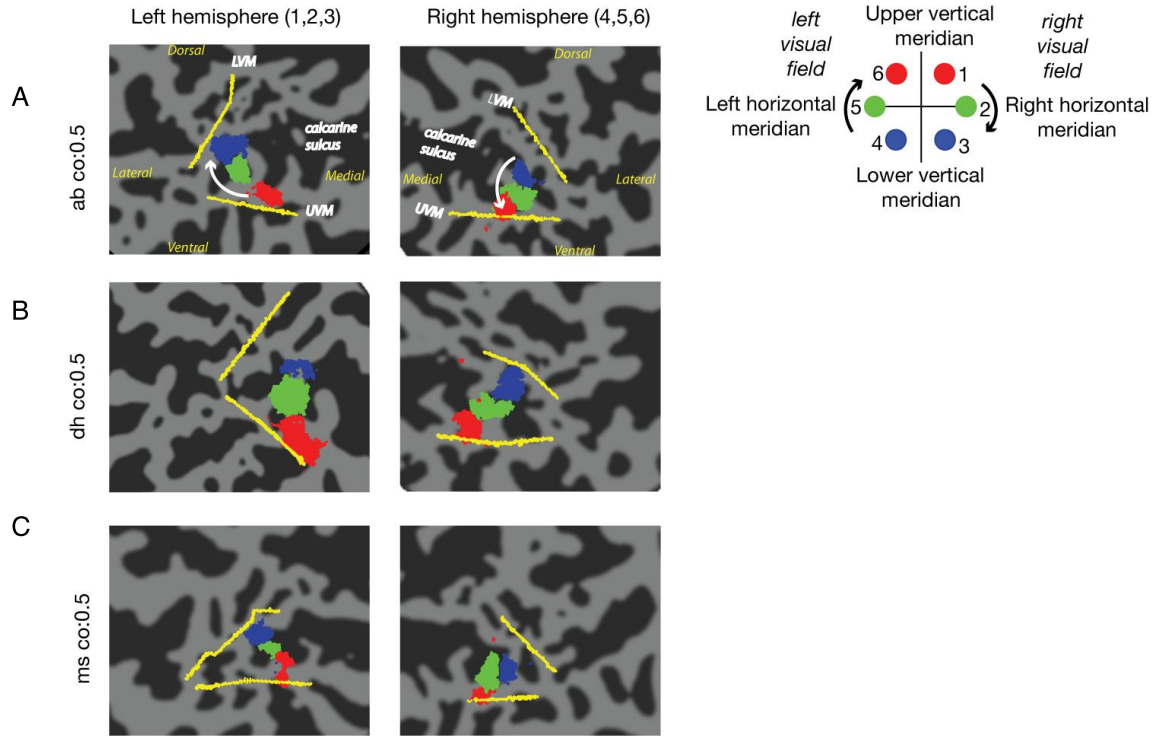

Figure 8.5: Representation of localizing stimuli in primary visual cortex, visualized on a flattened patch of the left and right occipital cortex. Activation evoked by the stimuli used in the localizer scan is marked in V1 for different subregions in each hemisphere. A, B, and C show the spatial location of ROIs in each of the subjects, respectively. Meridians are marked in yellow lines. The inset indicates each location on an imagery clock-face with different colours.

8.3.3 Activity at sample location in Experiment 1 & 2

The fMRI responses at sample locations were similar for the first experiment (Figure 8.6). A clear, transient response to the first presentation (of the *sample* stimulus) was found at the sample locations. The amplitude of the sample period activity that best fit the measured time courses were computed individually for experiment 1 and 2 (Figure 8.7), and they did not show significant difference when tested with two-tailed t-test ($p < 0.1$) ($t = 0.1547$, $p = 0.8913$). In addition, no significant activity (vesus zero baseline) in the sample locations was observed during the delay and test periods. In contrast to the increase in activity in the attended sample location in all subjects, the unattended sample locations showed either small negative responses or no difference compared to baseline activity.

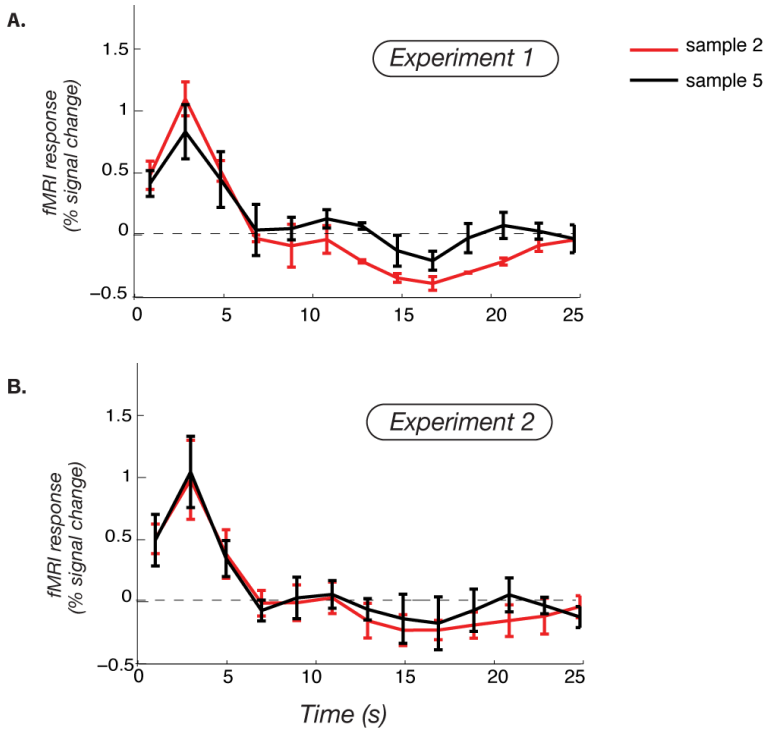

Figure 8.6: The hemodynamic response evoked by the sample stimulus (# 2 and #5 in Figure 8.1) in Experiment 1 (***A***) and Experiment 2 (***B***). The fMRI responses at the sample locations are similar in both experiments and theses transcient responses correspond to stimulus presented during the stimulus intervals. No response is shown when stimulus was presented elsewhere during the delay and the target interval. Error bars: SEM across subjects.

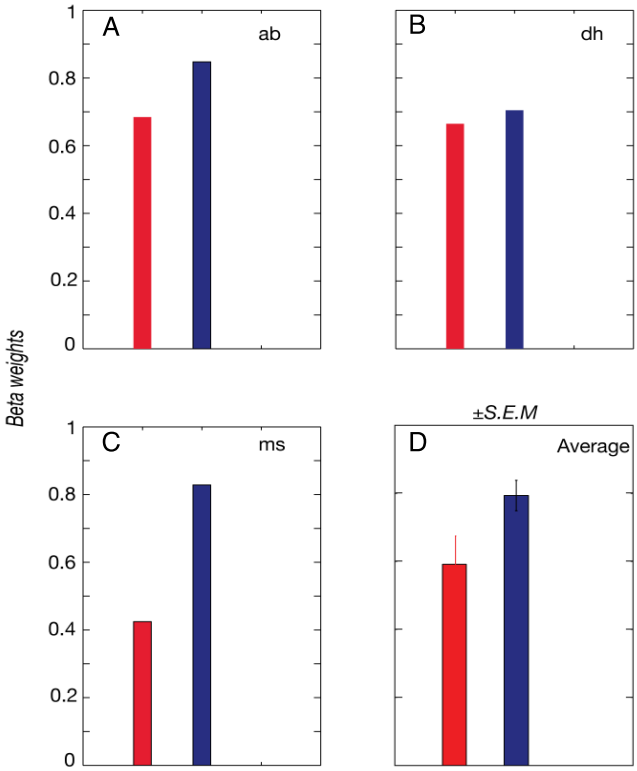

Figure 8.7: Amplitude of the *sample* period activity that best fits the measured time courses in experiment 1 (Red bar) and 2 (Blue bar) at the sample locations (# 2 and #5 in Figure 8.1). ***A***-

C, Sample activity for the three participants. **D**, The average amplitude of sample activity across subjects plotted and noted as in A-C. Error bars denote SEM.

8.3.4 Sustained activity of attentional modulation

There were three delay periods between the attentional cue and target stimulus. Figure 8.8A and Figure 8.8B show time courses split according to the three different delays for Experiment 1 and 2, respectively. To summarize data, the responses were collapsed across the four possible cued target locations. Then we averaged the response across subjects. It appears that the responses measured at the target locations show a combination of transient responses (due to the target stimulus) and sustained activity (during the delay duration), suggesting that V1 is involved in the maintenance of attention in these trials.

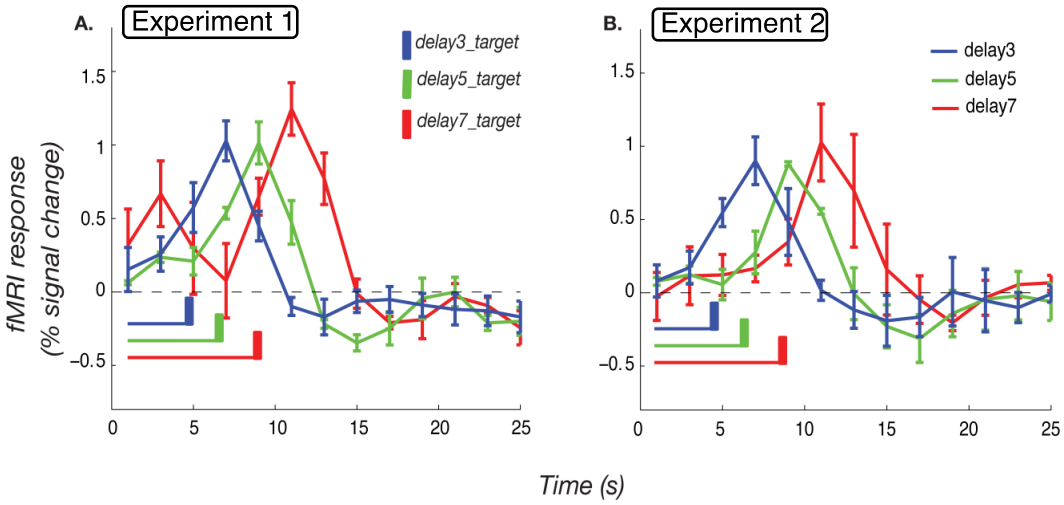

Figure 8.8: **A**, Average response time course at the cued target locations for different delay durations across three subjects in Experiment 1. **B**, Average response time course at the cued target locations for different delay durations across three subjects in Experiment 2. Error bars denote SEM across subjects. Thin blue, green, and red horizontal lines illustrate the delay durations of 3s, 5s and 7s, respectively. Blue, green, and red vertical bars mark the onset of the second stimulus at the target location. The transcient rises of the fMRI response after the vertical bars are evoked by the presence of second stimulus at the target locations. Compared to the delay activity shown in the Experiment 2, the responses during the delay intervals (indicated by the horizontal lines) in Experiment 1 are stronger.

If it was not the case, the amplitude during the delay interval should drop immediately after the attentional cue, and this should be especially visible for the longer delays. However, our

result from Experiment 1 (Figure 8.8A) demonstrated a sustained delay activity throughout the entire delay interval and the duration of the sustained fMRI response was positively correlated with the delay durations. This maintained activity was not caused by the visual stimuli and it is time-locked (taking into account the sluggishness of the hemodynamic response, ~4s) to the duration when participants were attentive to the target location.

The observed responses are unlikely to be the sensory consequence of the presentation of the cue. First, one or four dashed circles was/were presented briefly (300ms) to cue the possible target location(s) in the first two experiments. If the cue evoked a transient activity, it should diminish after a fixed hemodynamic delay. Instead, the delay activity was still reliably present even in the longer delay conditions (i.e. 5s and 7s). Moreover, the cue-evoked amplitude should appear during the delay duration in Experiment 2 as well because identical cues were presented at all the possible targets, but we did not observe a transient or similar amplitude of sustained response in that experiment (see Figure 8.8B). In the light of this, we can exclude the possibility that delay-activation was induced by a cue signal.

However, one may argue that the sustained response could have been induced by WM load, because participants were asked to remember the orientation of the sample stimulus. Experiment 2 was designed to have different demands on attention while maintaining a fixed WM load (similar to Experiment 1). Therefore, the intensity of WM should have been the same across the two experiments. However, the result of Experiment 2 was different from Experiment 1, showing even smaller maintained activity when all four possible target locations were cued. Figure 8.8B shows the averaged timeseries for the three delays across subjects in this experiment.

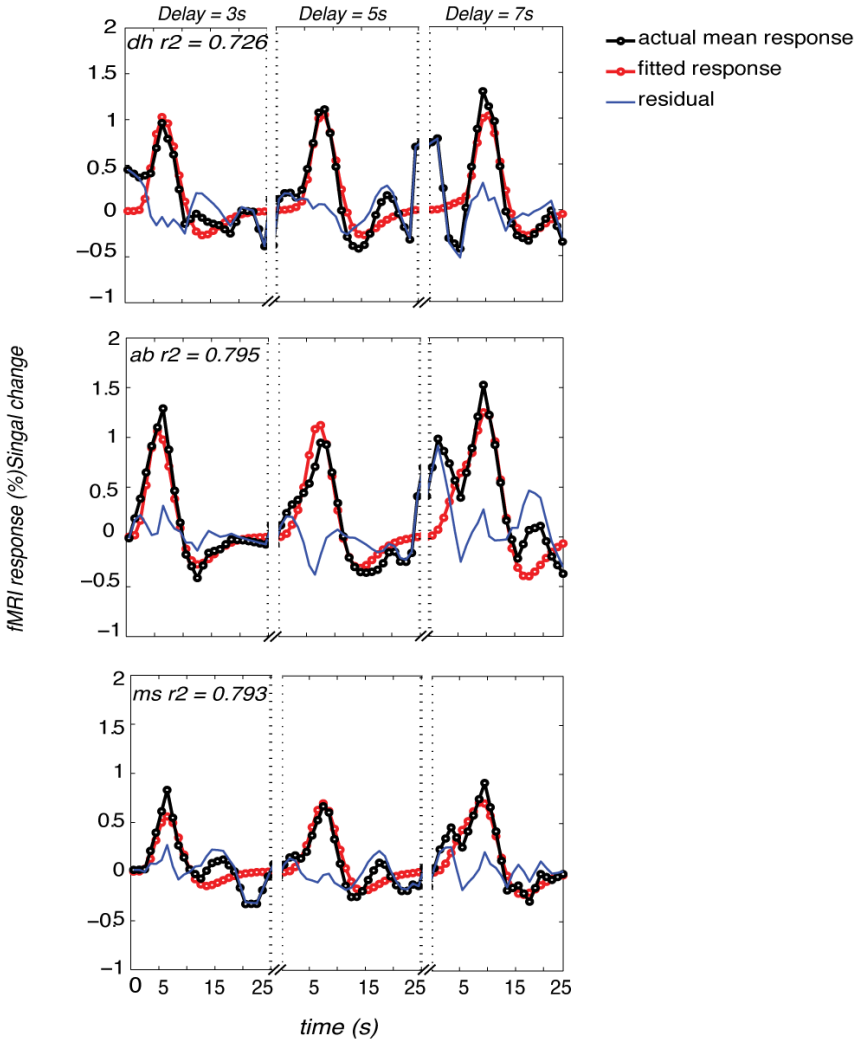

Figure 8.9: The individual best fitting of measured fMRI response for delay and target periods in Experiment 1. Data were modeled with two components (see Methods section): d, sustained delay period activity; T, transient response to the target stimulus interval. Rows, data from three different subjects. Columns, data from three different dleay periods (3, 5, 7s). Goodness of fit comparing the measured average fMRI response collapsed across all the target location (black curves) and the model (red curves) was quantified by computing the r^2 at the left corner of each row.

Figure 8.9 and Figure 8.10 illustrate the individual best fit of measured fMRI response for both experiments. The amplitude activity during the delay and test periods were computed as well (Figure 8.11). The result of one-tailed t-test (H_0: mean = 0) at $p<0.1$ illustrated that the though the amplitudes of sustained activity during the delay interval in Experiment 1 is small, they are significantly higher than the zero baseline (t-statistic = 2.4461, p=0.0671), whereas the beta weights measured from Experiment 2 were not significantly different from baseline (t

= 1.1833, p = 0.1791). By incorporating spatial uncertainty, we investigated whether the response during the delay would be different between these two experiments because any response difference during this interval should be attributed to attentional modulation rather than WM. As can be seen in Figure 8.11, the sustained activation in Experiment 2 is lower than those in Experiment 1, while the stimulus-evoked activities at the target locations did not show a statistical difference with two-tailed t-test at $p < 0.1$ (t-statistic = -0.6669, p =0.5735).

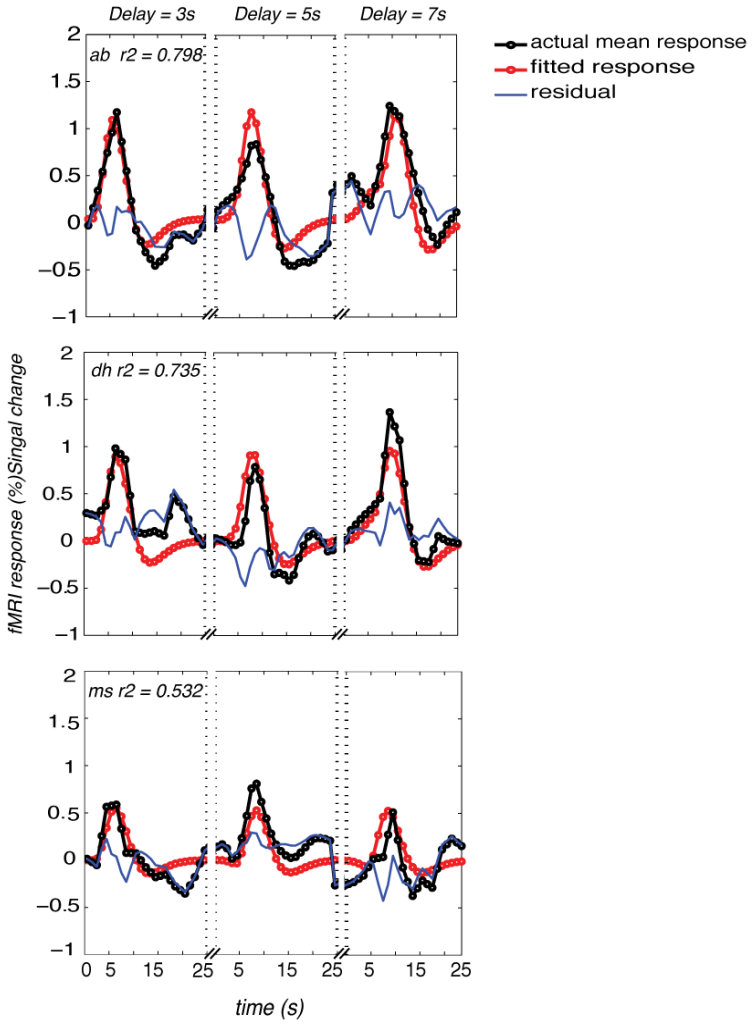

Figure 8.10: The individual best fitting of measured fMRI response for delay and target periods in Experiment 2. Data were modeled with two components (see Methods section): d, sustained delay period activity; T, transient response to the target stimulus interval. Rows, data from three different subjects. Columns, data from three different dleay periods (3, 5, 7s). Goodness of fit comparing the measured average fMRI response collapsed across all the target location and the model was quantified by computing the r^2 at the left corner of each row.

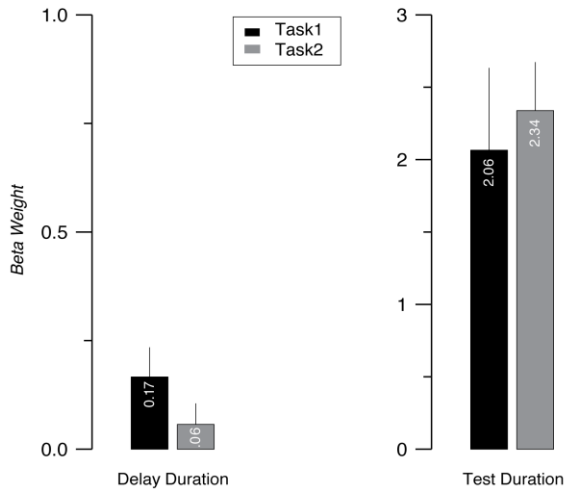

Figure 8.11: The average amplitude of activity during the delay and target periods across subjects. Left panel: the average amplitude of delay period in Experiment 1 (darker bar) is higher than that in Experiment 2 (lighter bar). Right panel: the average amplitude of target period in Experiment 1 (darker bar) is similar to that of the Experiment 2 (lighter bar). Error bars: SEM across subjects.

Though there is sustained activity during the delay period, the amplitude of the response was small. It could be caused by the small baseline activity. Therefore, we computed an attentional modulation index for each target subregion by comparing the baseline when the location was not cued in Experiment 1 (cued - uncued)/ (cued + uncued). Figure 8.12 shows that attention indeed affects the activity markedly. Taking all the evidence together, we claim that the activity in early visual cortex is sustained during the process of attention.

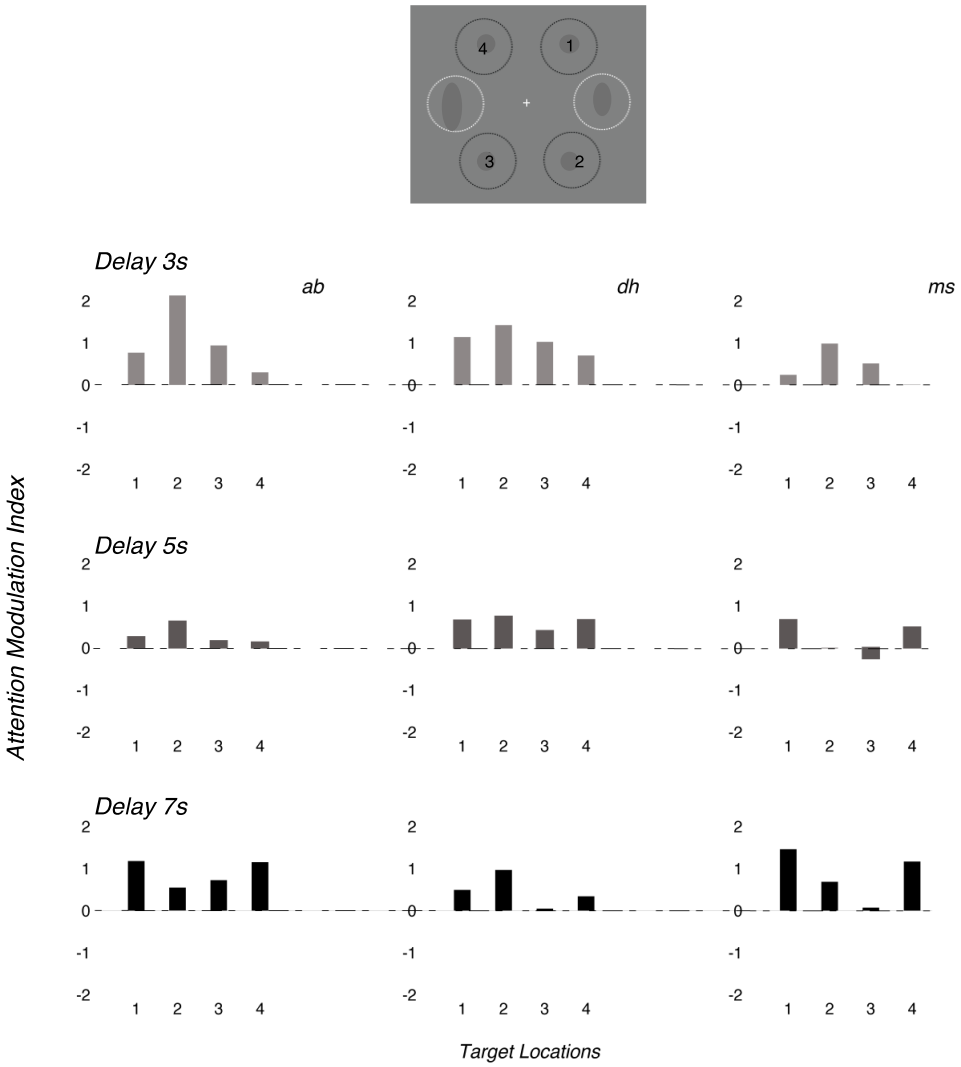

Figure 8.12: Attention modulation index for each subject is calculated by using the trials when the stimulus appears at the cued location compared to the response obtained with trials when location is not cued: (cued - uncued)/ (cued + uncued). Top graph indicates the indices of target locations that were measured for attention modualation index. Most of the modulation index is above the zero baseline, suggesting that the activities at the target locations are affected by the attention rather than the fluctuation of baseline activity. Each column corresponds to one subject and each row corresponds to one delay condition in Experiment 1.

8.3.5 The retionotopy of visual spatial attention

A considerable number of reports have shown that attention modulation is consistent with retinal location in extrastriate visual areas (Jeffreys & Axfor, 1972; Butler et al, 1987). The result of comparison between Experiment 1 and 2 in our present study confirmed this retinotopic characteristic of attention. During the first sample interval in both experiments, the

unattended (and unstimulated) parts of the visual field did not show any siginificant activity. And the sample location did not respond to the stimulus show at the four possible target locations during the delay and test durations. In addition, we found decreased levels of fMRI response in the same target locations when attention was directed at retinotopically different locations. This result also supports the previous findings that subjects were depending on the cue to perform the task for orientation discrimination (Figure 8.13). Moreover, Figure 8.14 shows the average fMRI response for one cued location is much stronger than three uncued locations in the same trial in Experiment 1.

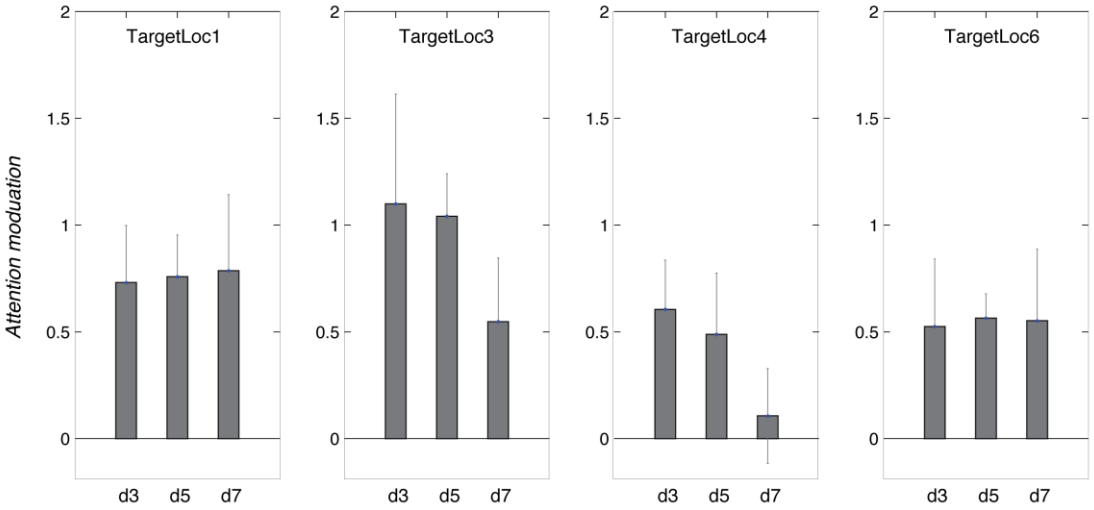

Figure 8.13: The attention modulation index in cued or un-cued trials across subjects for three delay conditions in each target location (Experiment 1). The data is the averaged result from Figure 8.12. The horizontal line indicates the baseline for visualization purposes. Error bars: SEM across subjects.

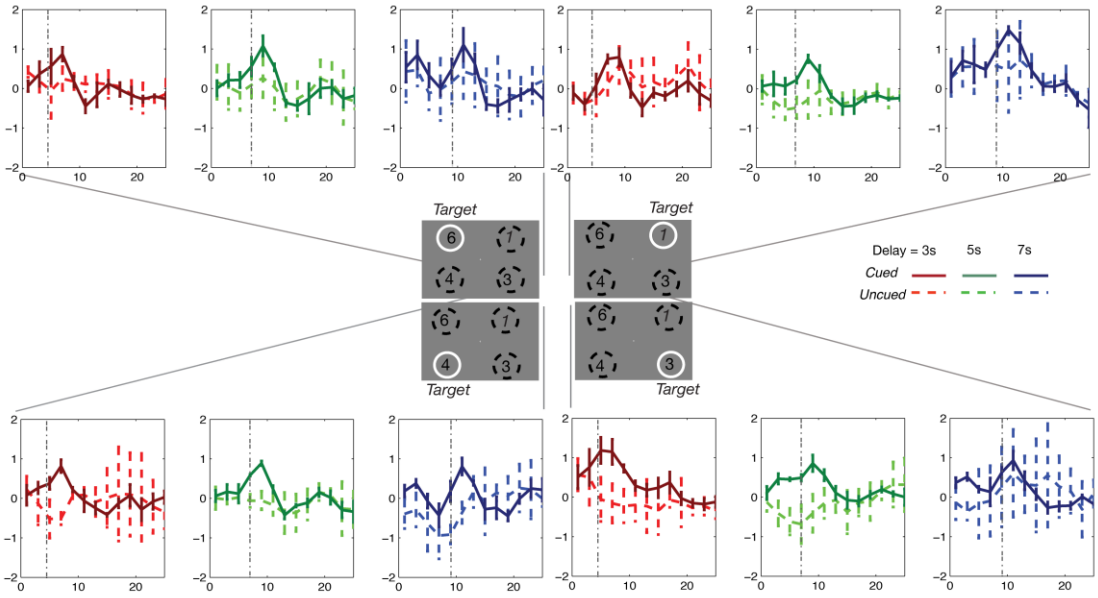

Figure 8.14: Time courses for the cued (white solid circles) and the collapsed non-cued locations (white dashed circles) in Experiment 1 averaged across the three subjects for three delays. The average fMRI response for one cued location is much stronger than three uncued locations in the same trial in Experiment 1, indicating that the modulating effect of attention follows the retinitopic manner. Error bars: SEM across subjects.

8.3.6 Effect of spatial uncertainty on attention

We found evidence of sustained activity during the delay period in the target locations when its position was signalled in advance (Experiment 1). However, the delay period activity was reduced when participants were uncertain about the stimulus location of the target (Experiment 2). This difference in the sustained delay response in Experiment 1 and 2 indicates the role of attention when spatial uncertainty was involved. As we proposed, if the attention was allocated among all the possible target locations in the second experiment, one would expect sustained activity in Experiment 2 that is significantly lower than Experiment 1. On the other hand, if the brain assembles more neuronal activations to resolve spatial uncertainty, the fMRI response should be higher in the four possible locations than the cued one in the first experiment. We therefore examined the activities at the target and non-target locations during the delay interval individually. The reponses at the target location in Experiment 1 are higher while the responses at the nontarget locations fall below baseline (Figure 8.15 Left panel), indicating spatial attention enhanced the neuronal response while

possibly suppressing the other un-cued locations. We used two-tailed t-test at $p < 0.1$ and found a significant difference of the response amplitudes (beta weights) between the cued location and other three un-cued locations during the delay interval (t-statistic = -6.0251, p = 0.0265). In contrast, in Experiment 2, we found that the positive responses between the target and nontargets show no significant difference when all the possible test locations were cued (attended) (Figure 8.15 Right panel), suggesting that the spatial uncertainty caused attention to be redistributed (t-statistic = -2.0435, p = 0.1777). But alternatively, higher amplitude responses might also be present as a result of a stronger prepartory attention at the single (exactly) cued target location in Experiment 1, leading to the disparity between those two experiments (more details will be explored in the Discussion).

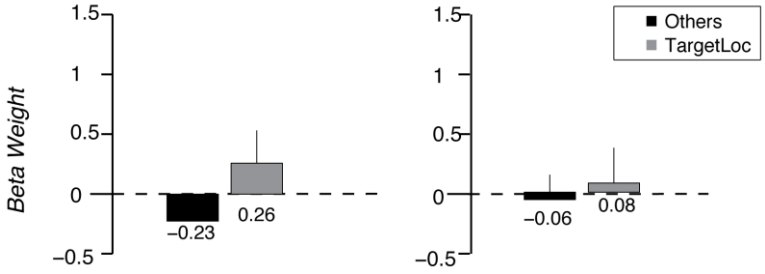

Figure 8.15: Estimated amplitude for the cued and the collapsed non-cued locations in Experiment 1 & 2 averaged across the three subjects and three delays. The amplitude is estimated from the model of fMRI response during the delay intervals showed in Figure 8.14, again demonstrating that the attention increased the activity at the cued (target) location during the delay interval in Experiment 1 compared to other non-cued locations. Additionally, the sustained amplitude in the only one cued location (Experiment 1) is higher than the activity measured in the four possible cued locations in Experiment 2. Error bars denote SEM.

8.3.7 Effect of task difficulty in Experiment 1

In experiment 1, the orientation differences of the two stimuli displayed during sample and test phases were either 1JND (difficult) or 3JND (easy), which allowed us to examine the effect of task difficulty of WM in V1. We found that there were no main effects of task difficulty in any of the target regions, but the fMRI response for the difficult condition is

stronger than that in the easier condition for two of our subjects (Figure 8.16).

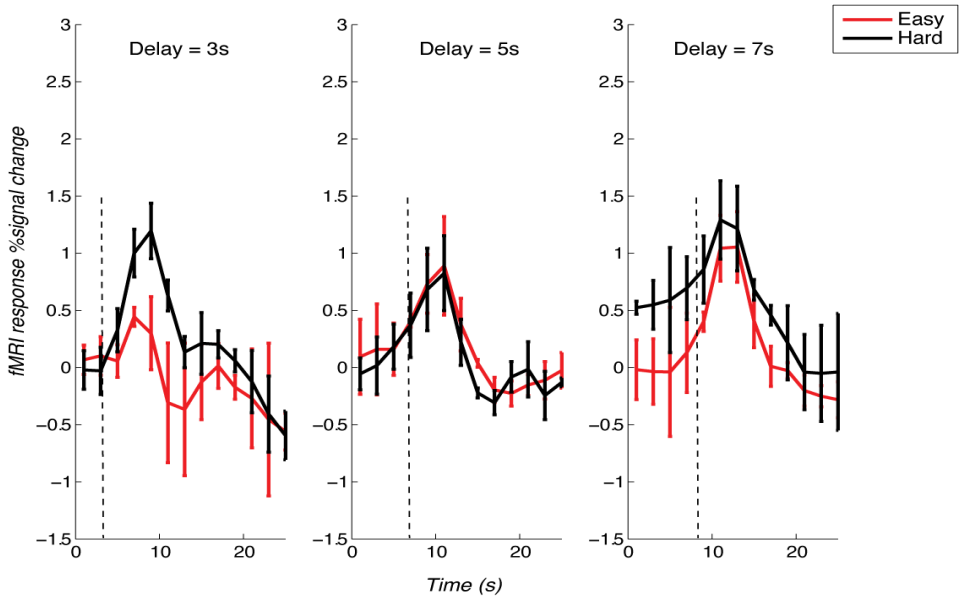

Figure 8.16: Effect of task difficulty in Experiment 1. Average fMRI responses with different task difficulty (discrimination difference) at the target locations during the three delay durations (3s, 5s and 7s). Red curves, easy task with 3JND; Black curves, hard task with 1JND. Dashed vertical line: the offset of the delay duration. Error bars: SEM across subjects.

Besides the primary visual cortex, we also searched for other higher-level regions that may be sensitive to task difficulty. ROIs were defined individually for each subject by the regions active (P<0.05, FDR corrected) during the difficult (1JND) versus easy (3JND) trials. Figure 8.17 illustrates the regions that may be related to task difficulty effect in both hemispheres of a subject in our experiment.

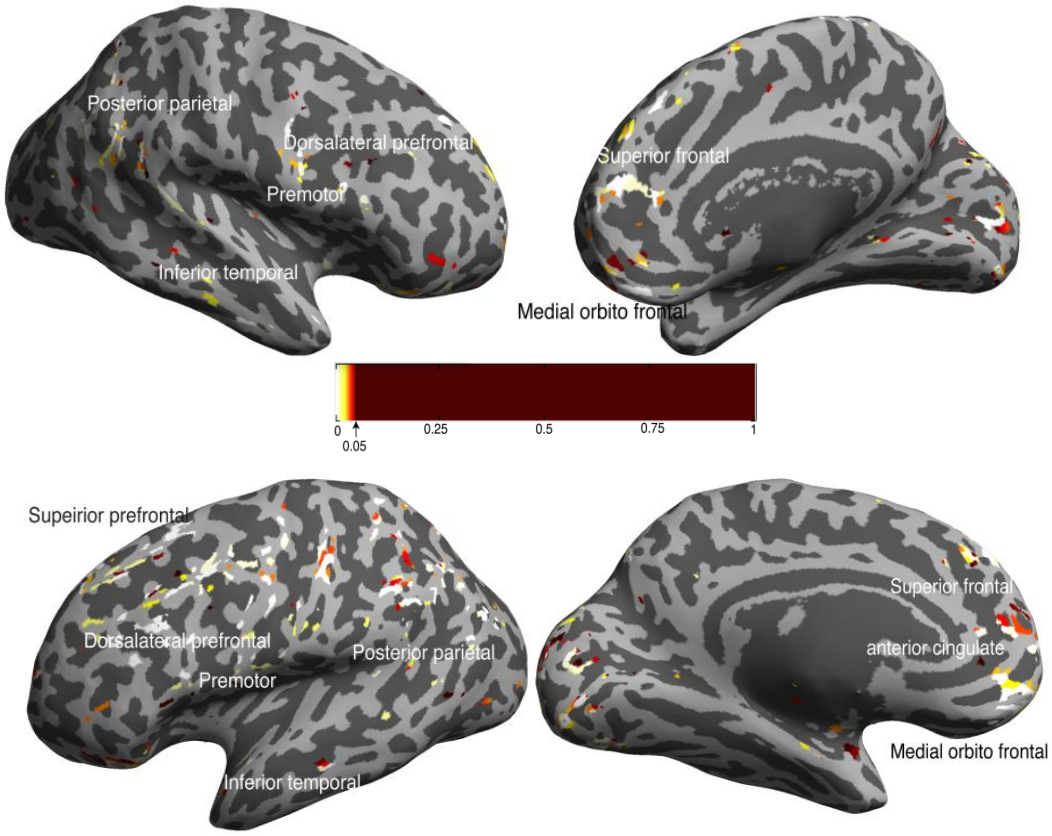

Figure 8.17. Regions that may be related to the task difficulty effect in the whole brain. Coloured areas on the inflated cortical surface of the brain represent the voxels that respond significantly different in the difficult condition (1 JND) from the easy task (3 JND) (P<0.05, FDR corrected). Note that data were not smoothed for this GLM analysis.

8.3.8 Response to concurrent stimuli in Experiment 3

As a control experiment, we used a version of the experiment in which subjects were instructed to discriminate two orientations in space rather than in time. In order to examine the BOLD activity when spatial attention is divided by visual stimuli, we displayed two gratings simultaneously to different visual hemifields. In early visual cortex, the representations of these are therefore in different cortical hemispheres. Again, we found that the concurrent stimuli evoked transient response at the two target locations according to the retinotopical arrangement. By comparing with the stimulus-evoked response at sample locations during the sample interval in the preceding two experiments, reduction of response magnitude was observed (Figure 8.18).

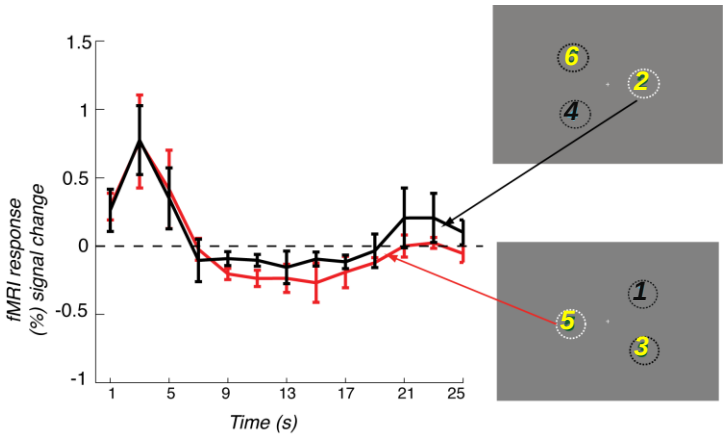

Figure 8.18: Hemodynamic response evoked by the simultaneous stimuli in Experiment 3. Black curve: fMRI response when sample 2 is one of the targets simultaneously stimulated with one of the contralateral target locations (4 or 6). Red curve: fMRI response when sample 5 is one of the targets simultaneously stimulated with one of the contralateral target locations (1 or 3). The responses from the two sample locations in this Experiment 3 are similar and are not significantly different from the responses from those in the Experiment 1 and 2. Error bars denote SEM.

8.4 Discussion

Offen et al. (2009) investigated the processe of WM and attention in two separate tasks. In one of their tasks – an "attention task" – the perceptual experience of the first stimulus did not contribute to the completion of the task. Subjects only needed to attend to the upcoming stimlus which was of low contrast. In their "working memory task", subjects were asked to remember the orientation of the first sample stimulus. Sustained activity during the delay period was only clearly present when attention was required, but not in the memory task. In real life, however, the two cognitive processes are likely to occur concurrently. A few studies have explored the role of higher visual areas in visual attention and the maintenance of the representation of stimulus features. However, how the mechanisms of WM and attention interact in early visual areas, especially in V1, remains unclear. Our present study shows that even by considering a relatively simple fMRI measure, the mean responses of neuronal populations in a region of interest, in different task structures can provide insight about the mechanisms underlying the process of spatial attention when WM is also involved. Instead of using detection judgements, we employed a two-alternative forced-choice (2AFC)

discrimination task, which draws on sustained attention more than the former procedure (Bashinski & Bacharach, 1980; Bonnel & Miller, 1994; Downing, 1988; Shaw, 1984; Muller & Findlay, 1987). For such experimental procedure, it is important to maintain subjects' fixation. We used a small fixation cross of high contrast in the center of the screen to minimize effects of eye movements. Moreoever, the design of the third experiment restricted the subjects to move eyes because the two stimuli were presented to two visual fields simontaneously within a very brief period (500ms). In addition, if subjects had moved their eyes toward the target stimulus in the frist two experiments, then we would expect better performance than the third experiment. However, it is not the case. Last but not least, our retinotopical organization of attentional modulation and the precise correspondence with localizing result both demonstrated that it is unlikey subjects moved their eyes during the stimulus intervals.

8.4.1 Attentional modulation in primary visual cortex

The modulation of attention produced in V1 is completely endogenous since it is generated in the absence of any stimulus. An increase in BOLD responses in V1 at the retinotopic locations of the targets has been reported in several attention studies (Li et a., 2008; Buracas & Boynton, 2007; Kanwisher & Wojciulik, 2000; Watanabe et al., 1998). We observed the same retinotopic stimulus-specific modulation due to attention regardless of the duration between cueing and target stimulus. This increased sustained activity is neither the result of WM nor a remainder of activation from the sample visual stimulus from neighbouring locations (as detailed in the Result section of this chapter). These results are consistent with recent results, suggesting that spatial attention enhances visual responses in human V1 (Tootell et al., 1998b; Gandhi et al., 1999) despite a relatively lower intensity than in extrastriate areas in the visual hierarchy (Desimone & Duncan, 1995; Maunsell, 1995). As shown in these attentional modulation studies (Luck et a., 1997a; Seidemann & Newsome, 1999), the size of the effect is not particularly large. To exclude the possibility that this revealed enhancement for those ROIs simply represents trivial changes in the baseline activity, we also evaluated the impact

of attention by computing an attentional modulation index with the uncued condition. The robust change above the baseline indicates the reliable impact of attention on V1. Previous studies (Luck et al., 1997a) stated that the small size of attentional modification in V1 may be due to the modest demands of tasks since we defined the discrimination thresholds at ~70% accuracy. Moreover, a similarly small magnitude has been reported by other comparable electrophysiological studies (Motter, 1993; Conner et al., 1997).

An alternative hypothesis is that the modulation we observed in V1 may reflect general arousal and /or attentional alerting (Posner & Petersen, 1990). However, the responses from the uncued condition were around the zero-baseline. In addition, no clear relationship between the task difficulty and the magnitude of modulation was revealed. Therefore, these enhancements were likely not the result of global factors, which should modulate all neurons and therefore the overall fMRI response in a given ROI. What is more, they are not caused by anticipation or expectation because any possible target locations have equal chance to be the target location.

8.4.2 The retinotopy of spatial attention

Many studies of attention have used an apparent signal (i.e. a arrow) to cue the observers about the relevant properties of the subsequent visual stimulus. In experiment 1, we used transiently presented circles to instruct subjects to covertly direct their attention to the location of the forthcoming stimulus, therefore no uncertainty was involved. We then measured the activity in these cued regions and compared them with those of uncued locations in each trial. We also compared the responses in cued versus non-cued trials for one location. Our findings show that spatial attention affects the activity of local populations, rather than modulating responses across the whole visual area in a global manner. Specifically, three results support the presence of a retinotopic attention signal in V1: (1) in Experiment 1, sustained attention was directed to a specific (cued) spatial location during the delay-period, whereas other non-

target locations were not well driven or engaged in a task. Data from all delay intervals showed a similar pattern of response: Neurons respond significantly more to one location when it is the locus of the attention. (2) Signals were reduced at the same location when attention was directed to elsewhere. (3) The response of the population is biased towards its attended location for the *sample* stimulus as well. This includes the one presentation of stimulus in the first two experiments and the cortical distribution of BOLD activity with the attended locations in Experiment 3 when two stimuli were simultaneously presented. These results are in line with previous results showing that attentional instruction amplifies the responses of neurons in the primary visual cortex according to the retinotopic locations in both single-unit studies with behaving macaque and human MRI studies (Kastner et a., 1999; Luck et al, 1997b; Ress et al., 2000; Moran & Desimone, 1985). It was found that attention-related retinotopy almost precisely corresponds to the retinotopic organization from sensory stimulation, suggesting that both processes shared a similar receptive field substrate. Moreover, our results are consistent with the idea that varying the location of attention evokes a reliable and retinotopically-based modulation of endogenous activity in V1. A set of preceding studies manipulated the covert attention between two individual stimuli at different hemifields. Their results showed that attention produced preferential activation in the hemisphere contralateral to the attended target (Mangun et al., 1993; 1997; Heinze et al., 1994; Mangun, 1995; Clark & Hillyard, 1996; Woldorff et al, 1997; Gandhi, Heeger & Boynton, 1999), supporting our claim that the increased responses in V1 is spatial selective as a result of covert spatial attention.

8.4.3 Possible mechanism of attentional modulation

To investigate the possible mechanism of spatial attention, we measured the amount of attention in two experiments with match-to-sample procedure. Experiment 1 in our study used a cue to indicate the incoming target stimulus whereas spatial uncertainty was imposed in Experiment 2. The sustained intensity of attention in Experiment 1 was significantly higher

than baseline. In contrast, when attention was directed to all possible locations, the amplitude of modulation decreased. There could be two possibilities explaining the differential intensity of response during the delay period in these experiments. It is likely that this stronger amplitude in Experiment 1 is due to the signal enhancement at the cued (attended) location and reduced (or even suppressed) activity at unattended location outside its locus. Alternatively, it is also possible that the attention was distributed among the possible locations, meaning less attention was allocated to each of the four candidates in Experiment 2. Currently, our results cannot distinguish between these two possible interpretations. However, it seems that our data supported both possibilities, which may suggest that spaital attention is task-dependent (see Figure 8.11).

Explanations of the differential modulation of attention range from the proposals that focused attention increases the signal, to those stating that attention enhances sensitivity by reducing external noise (Buracas & Boynton, 2007; Li et al., 2008; Liu et al., 2005, Murray, 2008), and to other hypothesis that when spatial uncertainty is not involved, observers are optimal at making decisions/selections. Our data from Experiment 1 suggests that these three mechanisms are not mutually exclusive, but rather complementary (Eckstein et al., 2000; Lu & Dosher, 1999, 2000; Palmer et al., 2000; Pestilli & Carrasco, 2005). First, the pre-cue in this experiment allowed observers to monitor only the location of the second incoming stimulus with spatial certainty. Second, it increased the neuronal activation at the target location, while reducing or inhibiting activity of all three un-cued locations in each trial, suggesting that the attention reduced the interference of noise from non-target location as well (Baldassi & Burr, 2000; Cameron et al., 2004; Kinchla, 1992; Shiu & Pashler, 1994). Previous fMRI findings with multiple stimuli also support the idea that the visual spatial attention involves a ‘push-pull’ mechanism. It is suggested that activity amplification at an attended location comes hand-in-hand with a decrease in activity at non-attended locations. According to the biased-competition (efficiency) hypothesis, when participants attend to a stimulus at one location, the competition is biased to the local neurons at the cost of the

resources at the unattended location in visual cortex. It shifts the baseline of response across the neuronal population relevant to the target locations, and hence, weighs more for the subsequent input (for a review, see Desimone & Duncan, 1995). It is noticeable that our data shows a difference in the BOLD response among the attended location when we averaged the activity according to the attention location of different trials. These shifts in amplitude of activity may indicate the top-down biases from higher-level regions, consistent with the result from neuronal population recordings for spontaneous firing rate (Luck et al., 1996).

8.4.3.1 The effect of spatial uncertainty

Contrary to the first experiment, spatial uncertainty was introduced in the second experiment. All four possible locations of the target stimulus were precued, causing the processing resources spread evenly among them. The result from this experiment may support the resource allocation model (limited resource model) in terms of BOLD activity. When the duration between the offset of cue and the test stimulus is sufficient for attention to be allocated among multiple possible locations, the corresponding fMRI signal elicited by attention become proportionally lower than in the case when there was no uncertainty involved. According to the limited resource model, the amount of resources available for perceiving and processing stimuli is limited, (Broadbent, 1958; Kahneman, 1973; Moray, 1967; Wickens, 1984), and thus allocating resources to process important or relevant stimulus will withdraw the resources from irrelevant stimulus. Similar to our behavioural finding, previous psychophysical experiments using analogous spatial cueing paradigms have reported that performance can be optimized by allocating a relatively high proportion of processing capacity to stimuli at the cued location in contrast of a deteriorated performance if the target is presented at an uncued location (Luck & Hillyard, 1990; Treisman & Gelade, 1980).

Although limited neuronal capacity can explain the effect of spatial uncertainty for the contrasting result shown in our first two experiments, one may still consider the result as a consequence of hemodynamic effect, which we will discuss in the last section.

8.4.3.2 Attention allocation- simultaneous visual stimuli

Experiment 3 assessed the activity in target locations (one sample + one target location in Experiment 1 & 2) with the complete absence of spatial uncertainty, temporal uncertainty and working memory. But in this case, two stimuli were displayed to different hemifields simultaneously. In this experiment, we found that the sensory activity at both target locations is slightly lower than the transient response at the sample or test locations in Experiment 1 & 2. This result is in line with other previous studies, which may be explained by the small RF size in V1. For example, single cell experiments have used multiple stimuli displayed simultaneously to a neuron's receptive field in V1, V2 or V4. Compared with the neuronal response when a single visual stimulus is presented to a RF, simultaneous stimuli mutually suppress each other in a range of areas in the rhesus monkey brain in V4 but not V1 (Luck et al., 1997a; Miller, Gochin & Gross, 1993). Using the same paradigm but at multiple distinct spatial locations, other fMRI studies also reported that paired stimuli evoke a weaker response, but the magnitude difference of response is much lower in striate areas than ventral and dorsal extrastriate regions (Beck & Kastner, 2005, 2007; Kastner et al., 1998; Kastner, 2001; Luck et al., 1997a; Miller, et al., 1963; Moran & Desimore, 1985; Pinsk, Doniger & Kastner, 2004; Recanzone, et al., 1997; Reynolds et al., 1999; Snowden et al., 1991).

8.4.4 Relationship between behavioural performance and attention

We set the threshold at 70% accuracy for all main experiments. Thus, performances were matched across subjects in these tasks, but the actual thresholds increased in the order of Experiment 1, 2 and 3. These results can be explained by considering the demands on the decision-making process. Attention improves performance by improving the signal to noise ratio via reducing the impact of noise or enhancing the signal in early visual cortex, including V1. Similar to our data in Experiment 1, it was demonstrated that the speed and sensitivity of detection were enhanced when attention was instructed to the target stimulus location (Posner, 1980; Carrasco & McElree, 2001; Pestilli & Carrasco, 2005; Lu & Dosher, 1999). Some

previous studies (Foley & Schwarz, 1998) instructed attention to different locations when multiple stimuli were concurrently displayed. Investigators found that participants could make their decision only based on the relevant responses irrespective to the noisy irrelevant activation at non-target locations if no spatial uncertainty was engaged.

When spatial uncertainty was introduced, earlier psychophysical experiments and our experiment 2 demonstrate a behavioural cost, leading to an increase of threshold as a result. Analoguously, in other experiments, performance degraded as the number of distractors increased (Davis, Kraner & Graham, 1983). One interpretation of these reports is that as noise from the non-targets get added, more confusion with the target signal is introduced (Foley & Schwarz, 1998; Cohn, 1981; Pelli, 1985; Nachmias & Koher, 1970).

Finally, we found that thresholds in experiment 3 were higher than the single-stimulus working memory experiment even though maintenance of the first stimulus over time is not needed. This result is compatible with the hypothesis of a limited-attention resource as two stimuli need to be processed simultaneously (see the discussion above, Duncan, Ward & Shapiro, 1994; Luck et al., 1996).

8.4.5 Effect of task difficulty

Our result demonstrates that the fMRI response in the primary visual cortex (V1) is largely invariant with task difficulty of working memory even though the fMRI responses for the difficult condition are stronger than that in the easy trials for two of our subjects. Some previous studies have reported similar results using other stimulus features (Buracas, Fine and Boynton, 2005). However, there are other neuroimaging studies showing that difficulty changes the response due to attention (Ress & Heeger, 2003; Backus, Fleet & Heeger, 2001; Huk & Heeger, 2000). Besides, one prior electrophysiological study found that task difficulty modulates neuronal firing rate of specific neuronal populations in a colour detection task (Chen et al., 2008). By dividing the attention-modulated V1 neurons into two groups:

inhibitory and excitatory neurons, the authors revealed that spatial attention influences the activity of these two populations of neurons in target locations. It seems that there was no consistent effect of task difficulty on the magnitude of attentional modulation. However, this discrepancy might be due to differences in the specific aspects of the tasks used. Other experiments have manipulated the perceptual difficulty in a detection task to require more "perceptual" attention. Here instead, we decreased the discrimination difference to increase the difficulty of working memory. Along similar lines, it has been demonstrated that the magnitude of delay activity in visual cortex during WM does not necessarily depend on WM demand, but reflects the expected perceptual demands related with the memory probe (Lepsien, Thornton & Nobre, 2011). This may imply that increasing the difficulty (discrimination difference) of working memory is independent to the attention requirement level.

8.4.6 Cortical distribution of spatial attention

8.4.6.1 Functional regions associated with attention and working memory

It is well known that the majority of the attention-related modulation in V1 comes from the projection from higher visual areas. Moreover, there are a growing number of studies in humans using TMS and functional imaging methods supporting that covert attention is allocated voluntarily through these top-down inputs (Corbetta et al., 2008). An overlapping network for attention and WM has also been proposed, including parietal, frontal areas and the superior colliculus. For example, previous studies assessed the effect of memory load on BOLD signal change and reported a monotonic relationship between them in prefrontal and parietal cortices (Braver et al., 1997; Carlson et al., 1998; Cohen et al., 1997; Kammer et al., 1997), though some showed subject-dependent variation (Callicott et al., 1999). In experiments looking at distraction of attention, prefrontal cortex is found to be involved in suppressing distractors during memory periods (Miller, 2000; Miller & Cohen, 2001). Further, activation in supracallosal anterior cingulate cortex has been reported in WM tasks when

different demands of attention were applied (Paus et al., 1998). However, it was proposed that the activity in this area may be associated with non-mnemonic factors such as initiation and willed control of behaviour (Paus, 2001; Posner et al., 1988; George et al., 1993). Consistent with the majority of earlier studies, we found that both cognitive processes preferentially activate parietal and prefrontal cortical regions like other neuroimaging studies showed (Haxby et al., 1994; Corbetta, 1993; Culnam et al., 1998), suggesting that these regions are functionally interconnected and are responsible for sending feedback information to early visual areas to direct attention in the WM task (Bisley & Goldberg, 2012).

8.4.6.2 Functional regions associated with task difficulty

In our study, we examined the association between task difficulty (discrimination difference) and the activation in V1, but we did not to find significantly differential activity in the retinotopically-defined subregions that represent the stimuli in this earliest visual area in cortex, though two of our subjects exhibited higher activation in the difficult condition. In contrast to reports using changes in memory load or distractors, we manipulated the orientation difference of the stimuli (discrimination threshold) to change the difficulty level. Our result showed that frontal, parietal and inferior temporal regions are sensitive to the level of difficulty. This result also pointed out the functional involvement of middle and inferior frontal gyri and dorsolateral prefrontal cortex (DLPFC) when task difficulty increased, which is in agreement with other task difficulty investigations (Carlson et al., 1998; Jonides et al., 1997; Klingberg et al., 1997; Rypma et al., 1999; Cohen, Braver and O'Reilly, 1996; Braver, Cohen and Servan-Schreiber, 1995).

8.4.7 Possible physiological foundation for attentional modulation

Besides modulating firing rates, electrophysiological studies also found that attention influences sustained neuronal activity in other ways. It was discovered that the synchronization of local field potential in V4 (Fries et al., 2001; Fries et al., 2008) increases as attention was directed to one particular location. Attentional modulation has also been

previously associated with the reduction of interneuronal correlation (Cohen & Maunsell, 2009). That particular result also showed that the spike count correlations between pairs of neurons in opposite hemispheres became weak. From the view of hemodynamics, attention has been attributed to the mechanism of oxygen metabolism: there may be increases of blood flow to the cortical representation of the attended location and decreases at cortical representations that are distant to the attention focus. Indeed, our findings reveal a few negative BOLD responses at the uncued sample or test locations, suggesting a decrease in blood flow as a result of an increase of a vascular resources elsewhere (Bressler et al., 2007), which is possibly related to the increasing neuronal activity in the cued location. In terms of neuronal activity, several neuroimaging studies have demonstrated same result as we do that an increase of neuronal activity at the attended region, and a reduction in neuronal and BOLD response at the unattended locations even when there is no stimulus present (Muller & Kleinschmidt, 2004; Tootell et al., 1998b; Kastner et al., 1999; Brefczynski & De Yoe, 1999; Desimone & Duncan, 1995; Luck et al., 1997a; Maunsell & Cook, 2002; Moran & Desimone, 1985; Somers et al., 1999). Again, it allows a boost of relevant signals while inhibiting or decreasing the level of noise, which may account for the better performance at the attended locations.

Chapter 9: General discussion

9.1 Summary of findings

Visual working memory reflects the ability to store, for a short period, visual information that is no longer in view, so that it can to be used in the subsequent actions (McKeefry et al., 2007; Pasternak & Greenlee, 2005). The majority of previous working memory studies have focused on the functional contribution of higher-level brain regions to the performance of WM. Furthermore, the early stages of cortical visual analysis (V1, V2 and V3) have been regarded as the regions that are mostly involved in processing visual information relevant to perception (e.g. spatial frequency, orientation, contrast or direction of motion). More recently, however, evidence from electrophysiological, psychophysical and neuroimaging studies has come to suggest that these early visual areas may also play a role in retaining stimulus representations in memory (Bisley & Pasternak, 2000; Gibson & Maunsell, 1997; Magnussen & Greenlee, 1999; Magnussen, 2000; Pasterna & Greenlee, 2005; Serences et al., 2009, Harrison & Tong, 2009; Ester, Serences, & Awh, 2009; Miller et al, 1996; Super et al., 2001). Most of these studies predominately worked with elemental visual features such as orientation, spatial frequency, motion direction and speed. Since early visual areas have shown different response characteristics to different visual attributes, we raised the question of whether this involvement of early visual cortex in WM also extends to other visual features. This thesis addressed the issue mainly with two properties: stimulus contrast and motion coherence. Two experimental techniques have been used: psychophysics and neuroimaging methods (fMRI). The work presented thus adds significant evidence to the investigation of the roles played by early visual areas in human WM. Furthermore, it also serves as a foundation for future studies.

Chapter 4 (the first experimental chapter) looked at behavioural evidence of the role of early visual areas in WM for motion coherence with psychophysical methods. In this study, the discrimination thresholds were nearly invariant across ISI, suggesting that motion coherence

is preserved with relatively high accuracy during the delay period. Building on this initial result, we applied a 'memory-masking' procedure where an irrelevant stimulus was introduced in the temporal delay between the sample and test stimuli. Our results showed that the coherence discrimination thresholds significantly increased when a transient memory mask (250ms) was delivered 125ms after the offset of the sample stimulus. This finding indicates that the fidelity of stored representation was degraded by viewing an irrelevant masker, suggesting that those early visual areas that process sensory motion coherence may be also involved in maintaining this information.

Moreover, we also found that the memory mask effect varied with the coherence of the mask. During the delay period, a motion mask that contained either random motion or a coherent motion signal (at the mean coherence level used in the study) was presented briefly (500ms) either at the beginning, in the middle or at the end of the delay interval. The result showed that a mask containing motion coherence had more disruptive effects than a mask with 0% coherence (random motion). This suggests selective interference with the representation of the memorized feature rather than a non-specific form of deterioration caused by, say, distraction. This result is consistent with previous studies, which illustrated the selectivity of working memory for many stimulus attributes, such as orientation, spatial frequency, texture, motion direction and speed (Bisley & Pasternak, 2000; Bisley et al., 2004; Bisley et al., 2000; Magnussen & Greenlee, 1992, 1999; Magnussen et al., 1991; Pasternak & Zaksas, 2003; for a review, see: Pasternak & Greenlee, 2005). For example, no threshold elevation was observed when the test and mask were identical and became more apparent when they differed along the stimulus dimension (Pasternak & Zaksas, 2003; Magnussen et al., 1991). This has been explained with the multichannel memory array (DeValois & De Valois, 1988; Olzak & Thomas, 1986) and the lateral inhibition model (for detail see Discussion in Chapter 4). Evidence opposing the results from the motion direction memory experiments has been reported in a recent study (Pasternak & Zaksas, 2003), demonstrating that the masking effect of motion direction and speed memory was maximal when the corresponding features

matched that of the remembered sample. The authors of that study ascribed this discrepancy to their distinct task structure: rather than judging local motion in a single spatial location, their task required temporal integration of motion signals at multiple locations to construct a global motion percept (Pavan et al., 2013).

To gain more insight into the temporal properties of WM, we also manipulated the timing of the mask presented during the delay interval. Our results show that the precise timing and the duration of mask (at least for the 250 ms and 500 ms stimuli we used) did not exert different disruptive effect to visual WM of motion coherence. The very early (125ms after the offset of the sample stimulus), early, middle, and late mask exhibited equivalent effects. However, this seemingly comparable effect might be actually induced through different mechanisms. It is possible that the two masks presented at the earliest timing points during the delay interval disrupted the memory when the coherence information was still stored in an iconic buffer (Sperling, 1960, 1963) and had not yet entered the stabilizing phase of WM. This agrees with previous studies that investigated the temporal characteristics of WM for motion direction (Pasternak & Zaksas, 2003; Pavan et al., 2013). However, slightly different from those two experiments, our result showed that a mask that appeared at later points during the retention interval also affected the mnemonic representation of motion coherence. This outcome is consistent with our assumption that if neurons in early visual areas stored information throughout the memory period, then the perceived masking stimulus should interfere at any time points within the delay interval. One may argue that the performance should be improved as feedback input or the recurrent network begins to operate at the later stage of retention period (the middle and late time points of delay interval), which is not the case in our report. However, it is possible that their effect was counterbalanced by increased noise or decreased signal as time passed. Thus, our result is not incompatible with the feedback hypothesis.

Chapter 5 investigated both the temporal and spatial properties of WM when participants were instructed to remember the contrast of visual stimuli. In the first part of that study, I measured the temporal characteristics of working memory for image contrast with three psychophysical

experiments. In agreement with previous contrast working memory studies with gratings (Greenlee et al., 1991; Magnussen et al., 1996), we found that the contrast information degraded as a function of ISI for both simple gratings and random visual noise patterns. The interference of memory was also not caused by the complexity of the spatially two-dimensional pattern since the task using pixel noise image did not show more disruption compared to that of a simple grating stimulus. Therefore, it is possible that the deterioration of memory precision is related to the endogenously increasing noise, as time progresses, during the memory process as has been proposed previously (Magnussen et al., 1996).

The results from Chapter 4 and Chapter 5 clearly demonstrated a differential ability of maintaining different visual stimulus features in short-term memory: a degrading memory for contrast (Chapter 5) versus a robust retention of motion coherence (Chapter 4). This discrepancy has been shown in other previous reports as well. For instance, memory experiments that have studied spatial frequency and contrast of simple gratings have shown that participants were able to retain spatial frequency information for up to 30s almost perfectly (Magnussen et al., 1990), whereas contrast information decayed over time. They tentatively attributed this differential precision of retention to the neuronal representation for extensive and intensive visual features (Magnussen & Greenlee, 1992). Specifically, for extensive attributes such as velocity and spatial frequency, only a population of neurons that prefer certain specific stimulus features are recruited for encoding and retention. However, in terms of contrast encoding it is widely assumed that different contrast levels are represented by the overall activity changes in ensembles of neurons. They proposed that the different memory performance for these types of visual attributes might be related to such differences in the distribution of activity. However, our results from experiments with motion coherence, which like contrast is also thought to be represented uniformly over the cortical surface in motion-responsive regions (Rees et al., 2000), showed faithful maintenance. Moreover, the short-term memory for orientation has also been reported to decay during the delay interval (Magnussen & Greenlee, 1985; Vogels & Orban, 1986), which did not follow the model

proposed by Magnussen and Greenlee (1992). Our discrepant results for motion coherence and contrast supports a mechanism that WM, similar to perceptual encoding, may also process different visual features via independent and parallel channels, suggesting that different neuronal representations may underlie the maintenance of different types of visual attributes (Tulving, 1991; Tulving & Schacter, 1990).

Another important contribution of Chapter 5 is that we explored the potential mechanism of the memory for stimulus contrast. It is possible that a relatively straightforward pictorial representation of contrast is encoded and kept in memory to facilitate the maintenance of contrast information rather than an abstracted contrast signal. This possibility was supported by an experiment using a 'memory mask' procedure. We showed that regardless of the contrast of the masker, all masking stimuli with the same spatial pattern as the to-be-remembered stimulus did not disrupt performance on a delayed contrast discrimination task as strongly as those with a completely different pattern. Again, this indicates that the pattern information has been exploited to some degree for remembering contrast. Furthermore, this result from the memory mask experiment supports our inference in Chapter 4 that sensory processing and visual short-term memory may share a common anatomical basis.

Chapter 5 in this thesis also examined how the stimulus contrast of a pixel noise pattern could be maintained along the spatial domain. Participants were required to remember and judge the contrast of a noise pattern presented either on the same side of the visual field or a different side in separate blocks. In the contralateral condition, subjects showed more impairment in terms of discrimination thresholds, and longer ISI led to more severe deterioration. This result is consistent with results from our contrast discrimination task along the temporal domain, which showed that contrast information decays over time. In addition, based on our previous result, we may infer that when subjects performed this task in space, their brain transferred the "pictorial information with contrast" within/across hemispheres rather than contrast alone.

The behavioural measurements from our psychophysical experiments provided indirect evidence that the early visual areas are likely to be involved in the process of short-term information storage, in particular for the contrast and motion coherence of simple visual stimuli. This was consolidated by our neuroimaging experiments in which we sought to probe the neuronal correlates of visual working memory (Chapter 6 and Chapter 7) and other higher-level cognitive process (i.e. attention in Chapter 8).

Recent work suggests that the sustained activity during the delay interval is caused by attention rather than WM (Offen et al., 2009). The investigators used two different experiments: one utilized an orientation detection task with a high demand on attention but no involvement of working memory, and another used a typical sample-to-match discrimination task where no intensive attention, but some degree of working memory, was needed. In this thesis, we conducted one pilot MRI experiment (described in the second part of Chapter 5) on motion coherence with a similar experimental paradigm. The key findings are that the primary visual cortex exhibited a sustained response in both discrimination and detection tasks, whereas MT/V5 only showed delayed activity in the detection task. This surprising result may be related to the experimental design in that there were random moving dots presented on the display even during the delay interval. As discussed in the corresponding part in Chapter 5, it could be explained by the findings from one previous study: V1 is more responsive to incoherent motion, whereas the activity amplitude in MT/V5 is positively correlated with motion coherence. Therefore, it is possible that the fMRI response in MT/V5 reflects the differential effect of WM (discrimination task) and attention (detection task), whereas the sustained activity shown in the discrimination task in V1 is only a side effect of an unselective neuronal response to motion. However, it is not straightforward to make any strong conclusion based on this result. Moreover, even if there was no incoherent movement during the delay interval, the univariate analysis methods we used to analyze the data are more vulnerable to possibly missing task-related patterns in BOLD activity when averaging across different voxels (Offen et al., 2009; Harrison & Tong, 2009). This may also explain why

previous univariate analyses failed to find consistent, sustained activity in V1 during the memory period (Harrison & Tong, 2009; Super et al., 2001).

Based on the results of this pilot MRI experiment, we modified the experimental design to make the *contrast* of gratings the feature of interest of the visual stimulus, to avoid these potential ambiguities brought about by motion coherence (see Discussion in Chapter 6 for more details). Moreover, we introduced another more sophisticated MRI analysis (MVPA) that exploits multivariate information across individual voxels to investigate the role of early visual areas in visual working memory. Previous memory studies with MVPA found that fMRI responses obtained during the delay period between two presentations of an oriented visual stimulus can be used to decode the *remembered* stimulus orientation, direction and speed of motion (Harrison & Tong, 2009; Christophel et al., 2012). In Chapter 6 and Chapter 7, we obtained neuroimaging evidence to test whether or not this phenomenon generalises to working memory traces of other visual features, such as contrast. Strikingly, we found that fMRI responses not only enable the decoding of the perceived contrast of a stimulus, but also support performance when the contrast of a stimulus had to be *remembered*. Our results suggest these signals contribute significantly to working memory for contrast on the timescale of seconds. Furthermore, classification generalized from *perceived* to *remembered* stimuli and vice-versa, implying that the corresponding pattern of responses in early visual cortex were highly consistent in both cases. Interestingly, classification accuracies obtained from data collected on correct trials were significantly higher than for incorrect trials, indicating that fMRI responses during incorrect trials add substantial noise to the VSTM signals exploited in the decoding.

In the work described in Chapters 6 and 7, we also addressed the spatial pattern of responses underlying contrast decoding. We found that a large-scale bias with eccentricity can drive classification for remembered as well as perceived contrast of grating patterns. However, this does not preclude the possibility that information is present also at a finer level than that of this coarse scale map. Over the past decade, many studies reported above-chance performance

using pattern classification, but the answer to what drives these results are discrepant and it is still a subject of debate (Clifford et al., 2011). Earlier studies using MVPA attributed this success to fine-spatial information. For example, in the case of decoding of orientation, it was proposed that each voxel in an fMRI image contains a large population of orientation columns, each of which has a unique orientation preference. As a result, every voxel yields a small bias of oriented response, and when considering all these correlated voxels together, the region of interest shows distinct patterns in response to different visual orientations (Haynes & Rees, 2005; Kamitani & Tong, 2005b). However, challenges to this rationale have emerged recently. One antagonistic camp argues that classification for orientation depends on coarser scale map rather than fine columnar architecture, at least for V1 (Freeman et al., 2011; Op de Beeck et al., 2008; Swisher, et al., 2010). Freeman et al. estimated the accuracy of decoding using an angular-position-based map in V1 with six orientated stimuli, evenly spread within the range spanning from 0° to 180°, and found that instead of sampling a subtle spatial bias from each voxel, signals from large-scale maps are sufficient for discrimination. They also calculated the decoding accuracy after removing the angular position components and found that the performance dropped to chance-level. Therefore, they suggested that such topographic map is also a necessary structure for classifying the underlying response patterns in their data. Moreover, their model was supported by other spatial filter methods which suggested that smoothing in the spatial domain does not deteriorate the accuracy of classification for orientation in V1 (Op de Beeck 2008, Gardner et al., 2005), and under some circumstances may even enhance performance (Thompson, et al., 2011).

Other investigators reasoned that the vasculature might play a crucial role in successful classification. They proposed that the information used for pattern classification maybe sampled from vascular signals itself, rather than a representation within a subvoxel scale. One possibility is that cortical vascular organization may be constructed on the basis of functional need in the cortex, extracting oxygen or draining deoxygenated hemoglobin through a shared vascular architecture (Gardner, 2010). Other than this systemic explanation, another

hypothesis holds that vasculature is a complex spatio-temporal filter, which may modify the original information conveyed from cortical columns (Kriegeskorte et al., 2009). Thompson et al. (2011) investigated the source of the classification information in MVPA from a methodological perspective. They compared gradient echo (GRE) sequences that have been used by the majority of fMRI experiments, to data acquired with spin echo (SE) methods. Their results showed that the most discriminative information employed by MVPA was from voxels associated with larger draining veins, to which the former sequence is more sensitive. On the contrary, the classification results from SE, which should be more spatially selective, were not significantly different from chance. This finding supports the proposal that vasculature contributes considerably to pattern analysis (although it should be noted that a potential weakness of this study is that the intrinsic SNR of SE acquisitions is much lower than that of GRE). They also suggested that higher magnetic field strengths might help unveil more precise information of how vasculature is involved in MVPA. One recent study using fMRI at 7T successfully replicated the result reported previously for orientation classification with MVPA and confirmed that a relatively large scale spatial map is also sufficient for decoding directions of motion (Beckett et al., 2012)

Taking together the results of Chapters 6 and 7, we have shown that a highly similar response pattern was evoked during the perceiving and remembering of contrast; however, it does not necessarily indicate that activity in early visual cortex was the result of memory *per se*. Instead, it may suggest that a consistent attentional or feedback signal modulates the activity during both tasks. Though using multivariate pattern analysis could reveal more information about the properties of neuronal populations, it is still difficult to discern the effects of working memory and attention individually. Therefore, we manipulated the task structure to disentangle these two cognitive processes with another fMRI experiment described in Chapter 8. Participants were asked to perform three (delayed) orientation discrimination tasks that were designed to probe different aspects of working memory and attention. The result of this MRI experiment was similar to those of previous studies, showing that the sustained mean

activity in the early visual cortex during the delay interval might not be a good proxy for the operation of working memory (Harrison & Tong, 2009; Offen et al., 2009). In addition, our result consistently indicates that attention modulates the neuronal activity on a retinotopic basis. By using three different delay intervals, we also verified that this spatial specificity is not an after-effect of a sensory stimulus being presented locally to the visual fields because even for the longest delay (7 seconds), there was significant delayed activity in the corresponding subregions in V1.

In this study, we introduced spatial uncertainty to assess its effect on the extent of attentional modulation by comparing the response when the exact location of the upcoming test stimulus was known by the subject (Experiment 1) versus not (Experiment 2) while keeping the demand of memory constant. It was found that the BOLD response in the cued location was stronger than the average response of four cued possible test locations, indicating that spatial uncertainty made the modulation power at each location weaker. Therefore, this suggests that like working memory, spatial attention may also be capacity limited. This hypothesis is supported by the behavioural measurement of Experiment 3 described in Chapter 8. Larger discrimination thresholds were found in this task when subjects had to discriminate between two oriented gratings visually displayed simultaneously. Since no working memory is involved, we were able to measure the response in each location where a stimulus was presented with the influence of spatial attention only. For sensory-evoked responses, no significant difference was found between the conditions when attention was required to perceive one (experiment 1 and 2) and two stimuli (experiment 3). However, this might be a result of using the larger discrimination difference to reach the same accuracy performance as the working memory tasks did. Therefore, we could not exclude the possibility that the response decreases when attention is allocated. Moreover, it is also likely that the amplitude of reduction is linked to the number of attended stimuli. In our current study, we used one stimulus pair to allow a simultaneous discrimination task, as well as enabling subjects to perform the task at a relatively high level within a brief period of time. Finally, the work

presented in Chapter 8 also demonstrated that task difficulty might be a potential modulator of neural activity.

9.2 Future directions

9.2.1 Extending investigation of memory of motion with RDKs

First, analogous to other previous studies on accessing the selectivity of stimulus representation in WM, one future direction would be to broaden the range of mask coherences to explore the dependence on this parameter. With a larger spectrum of coherence levels, we would be able to explore in more detail the characteristics of the stimulus-specific mechanism of visual WM. Second, to further determine how the multichannel model in WM system could account for the data, we could extend our investigation by manipulating another visual stimulus feature. For instance, a variety of channels each tuned to a particular motion direction have been postulated (Pavan et al., 2013). Building on our current memory-masking paradigm, we could present a masker with either the same or a different direction to the remembered stimulus while keeping the mask coherence the same to see whether features outside the memorized stimulus dimension would exert a disruptive effect. Third, our current pilot work only had one subject in the fMRI motion coherence memory experiment, so it would be worthwhile recruiting more participants and also applying MVPA analysis in MT/ V5 and other early visual areas to investigate whether information can be used to decode the motion coherence retained in these regions as we illustrated with psychophysical methods.

9.2.2 Extending investigation of contrast WM with random pixel noise pattern

This thesis demonstrates that the memory for contrast may be closely related to the pattern that represents luminance differences. However, further study needs to be conducted to investigate whether the local or (global) pictorial information is made use of when the contrast of a visual stimulus is to be remembered. If the local spatial pattern information is sufficient

for discriminating contrast over time, are there any particularly important locations in the visual field? Does the spatial (and gray-level value) distribution of the dark/bright elements distributed in the image play any important role in the memory for the pixel patterns? Different sizes of mask at spatially varied retinotopic locations and different spatial patterns may be helpful for gaining more insight into this question.

9.2.3 Mechanism underlying the differential mnemonic ability for different visual features

The work in this thesis has shown differences concerning the memory precision for contrast and motion coherence of a stimulus, but the precise mechanism underlying each of these phenomena is still unclear. It is possible that it is related to the neuronal coding and representation of these different visual features in early visual cortex. However, it is also likely that it is linked to feedback from other cortical areas along the visual stream. Application of TMS pulse at different visual regions may provide useful information to address this feedback issue.

9.2.4 Finer details of spatial pattern of representation for perceived and memorized visual stimulus

Chapter 6 and 7 discussed that a large-scale bias with eccentricity can drive classification for both perceived and remembered contrast levels. Moreover, it seems that this reflects a spatially local inhomogeneity of response to contrast. However, we found no readily apparent consistent spatial patterns of contrast representation across our subjects, even though similar populations of neurons participated in both the memory and perception of contrast within each individual. A carefully designed follow-on study and detailed analysis of the spatial patterns (e.g. cross-correlation of spatial pattern of BOLD signal obtained in these two experiments) may be able to reveal whether a consistent contrast signal is present and can be visualized on an individual basis.

9.3 Concluding remarks

The work presented in this thesis provides new evidence to support the idea that the early visual areas that encode visual information are also recruited for storage during visual working memory. In addition, the work considerably enhances our understanding of the modulating effect of visual spatial attention on neuronal activity in primary visual cortex during WM. Moreover, I believe the work provides a valuable and substantial foundation to direct future study in this area.

Reference

Abbott LF, Chance FS (2002) Rethinking the taxonomy of visual neurons. Nature Neuroscience 5:391-392.

Aboitiz F, Ide A, Olivares R (2003) Corpus Callosum Morphology In Relation To Cerebral Asymmetries In The Postmortem Human. In: The Parallel Brain: The Cognitive Neuroscience Of The Corpus Callosum (Zaidel E, Iacoboni M, Eds), Pp 33-46. Cambridge, Mass: MIT Press.

Adams DL, Sincich LC, Horton JC (2007) Complete pattern of ocular dominance columns in human primary visual cortex. Journal of Neuroscience 27:10391-10403.

Adelson EH, Bergen JR (1985) Spatiotemporal energy models for the perception of motion. J Opt Soc Am A 2:284-299.

Albrecht DG (1978) Analysis of Visual Form. In. University of California, Berkeley.

Albrecht DG (1995) Visual-cortex neurons in monkey and cat - effect of contrast on the spatial and temporal phase-transfer functions. Visual Neuroscience 12:1191-1210.

Albrecht DG, Hamilton DB (1982) Striate cortex of monkey and cat: contrast response function. J Neurophysiol 48:217-237.

Albright TD (1984) Direction and orientation selectivity of neurons in visual area MT of the macaque. Journal of Neurophysiology 52:1106-1130.

Allison JD, Casagrande VA, Debruyn EJ, Bonds AB (1993) Contrast adaptation in striate cortical-neurons of the nocturnal primate bush-baby (galago-crassicaudatus). Visual Neuroscience 10:1129-1139.

Allman J, Miezin F, McGuinness E (1985) Stimulus specific responses from beyond the classical receptive-field - neurophysiological mechanisms for local global comparisons in visual neurons. Annual Review of Neuroscience 8:407-430.

Allman JM, Kaas JH (1971) Representation Of Visual Field In Striate And Adjoining Cortex Of Owl Monkey (Aotus-Trivirgatus). Brain Research 35:89.

Alonso JM, Martinez LM (1998) Functional connectivity between simple cells and complex cells in cat striate cortex. Nature Neuroscience 1:395-403.

Amano K, Wandell BA, Dumoulin SO (2009) Visual field maps, population receptive field sizes, and visual field coverage in the human MT+ complex. J Neurophysiol 102:2704-2718.

Amaro E, Brammer MJ, Williams SCR, Andrew C, Curtis V, Ahmad F (1999) Event-related fMRI without scanner acoustic noise. NeuroImage 5:S331.

Andersen RA (1997) Neural mechanisms of visual motion perception in primates. Neuron 18:865-872.

Andrews TJ, Halpern SD, Purves D (1997) Correlated size variations in human visual cortex, lateral geniculate nucleus, and optic tract. J Neurosci 17:2859-2868.

Andrews TJ, Schluppeck D, Homfray D, Matthews P, Blakemore C (2002) Activity In The Fusiform Gyrus Predicts Conscious Perception Of Rubin's Vase-Face Illusion. Neuroimage 17:890-901.

Anzai A, Bearse MA, Freeman RD, Cai D (1995) Contrast coding by cells in the cat's striate cortex: monocular vs. binocular detection. Vis Neurosci 12:77-93.

Arezzo J, Legatt AD, Vaughan HG (1979) Topography and intracranial sources of somatosensory evoked-potentials in the monkey 1 Early components. Electroencephalography and Clinical Neurophysiology 46:155-172.

Austin G, Laffin D, Hayward W (1974) Physiologic factors in selection of patients for superficial temporal artery to middle cerebral-artery anastomosis. Surgery 75:861-868.

Avidan G, Behrmann M (2002) Correlations between the fMRI BOLD signal and visual perception. Neuron 34:495-497.

Awh E, Jonides J (2001) Overlapping mechanisms of attention and spatial working memory. Trends in Cognitive Sciences 5:119-126.

Awh E, Anllo-Vento L, Hillyard SA (1999) The time course of visual modulations during

spatial rehearsal in working memory. Journal of Cognitive Neuroscience:25-25.
Backus BT, Fleet DJ, Parker AJ, Heeger DJ (2001) Human cortical activity correlates with stereoscopic depth perception. Journal of Neurophysiology 86:2054-2068.
Baddeley A (2000) The episodic buffer: a new component of working memory? Trends Cogn Sci 4:417-423.
Baddeley A (2003) Working memory: Looking back and looking forward. Nature Reviews Neuroscience 4:829-839.
Baddeley AD, Hitch G (1974) Working memory. In: The psychology of learning and motivation: Advances in research and theory (Bower GH, ed), pp 47–89. New York: Academic Press.
Baddeley A, Wilson B (1988) Frontal amnesia and the dysexecutive syndrome. Brain Cogn 7:212-230.
Baldassi S, Burr DC (2000) Feature-based integration of orientation signals in visual search. Vision Research 40:1293-1300.
Banich MT, Belger A (1990) Interhemispheric interaction - how do the hemispheres divide-and-conquer a task. Cortex 26:77-94.
Banich MT, Nicholas C (1998) Integration of reading processing between the hemispheres. In: Right Hemisphere language comprehension: Perspectives from cognitive neuroscience (Beeman M CC, ed), pp 51–77. Hillsdale, N.J.: Lawrence Erlbaum Associates.
Barlow HB, Kaushal TP, Hawken M, Parker AJ (1987) Human contrast discrimination and the threshold of cortical-neurons. Journal of the Optical Society of America a-Optics Image Science and Vision 4:2366-2371.
Bartels A, Logothetis NK, Moutoussis K (2008) fMRI and its interpretations: an illustration on directional selectivity in area V5/MT. Trends Neurosci 31:444-453.
Bashinski HS, Bacharach VR (1980) Enhancement of perceptual sensitivity as the result of selectively attending to spatial locations. Perception & Psychophysics 28:241-248.
Baumann O, Endestad T, Magnussen S, Greenlee MW (2008) Delayed discrimination of spatial frequency for gratings of different orientation: behavioral and fMRI evidence for low-level perceptual memory stores in early visual cortex. Exp Brain Res 188:363-369.
Beauchamp MS, Cox RW, DeYoe EA (1997) Graded effects of spatial and featural attention on human area MT and associated motion processing areas. Journal of Neurophysiology 78:516-520.
Beck DM, Kastner S (2005) Stimulus context modulates competition in human extrastriate cortex. Nature Neuroscience 8:1110-1116.
Beck DM, Kastner S (2007) Stimulus similarity modulates competitive interactions in human visual cortex. Journal of Vision 7.
Beck J (1983) Textural segmentation, 2nd-order statistics, and textural elements. Biological Cybernetics 48:125-130.
Beckers G, Zeki S (1995) The consequences of inactivating areas V1 and V5 on visual motion perception. Brain 118 (Pt 1):49-60.
Beckett A, Peirce J, Sanchez-Panchuelo R, Francis S, Schluppeck D (2012) Contribution of large scale biases in decoding of direction-of-motion from high-resolution fMRI data in human early visual cortex. Neuroimage 63:1623-1632.
Benedek G, Janaky M, Benedek K, Keri S (2006) [Parallel processing of visual information]. Ideggyogy Sz 59:241-248.
Benton CP, Johnston A, McOwan PW (1997) Perception of motion direction in luminance- and contrast-defined reversed-phi motion sequences. Vision Res 37:2381-2399.
Bergen JR, Adelson EH (1988) Visual texture segmentation based on energy measures J Opt Soc Am A 3:98-101.
Bergen JR, Landy MS (1991) Texture segregation and orientation gradient. Vision Research 31:679-691.
Berkley MA, Watkins DW (1973) Grating resolution and refraction in cat estimated from evoked cerebral potentials. Vision Research 13:403-415.

Bird CM, Henning GB, Wichmann FA (2002) Contrast discrimination with sinusoidal gratings of different spatial frequency. Journal of the Optical Society of America a-Optics Image Science and Vision 19:1267-1273.

Birn RM, Saad ZS, Bandettini PA (2001) Spatial heterogeneity of the nonlinear dynamics in the FMRI BOLD response. Neuroimage 14:817-826.

Bisley JW, Pasternak T (2000) The Multiple Roles Of Visual Cortical Areas MT/MST In Remembering The Direction Of Visual Motion. Cerebral Cortex 10:1053-1065.

Bisley JW, Goldberg ME (2003) Neuronal activity in the lateral intraparietal area and spatial attention. Science 299:81-86.

Bisley JW, Zaksas D, Droll JA, Pasternak T (2004) Activity of Neurons in Cortical Area MT During a Memory for Motion Task. Journal of Neurophysiology 91:286-300.

Bisti S, Maffei L (1974) Behavioral contrast sensitivity of cat in various visual meridians. Journal of Physiology-London 241:201-210.

Biswal B, Hudetz AG, Yetkin FZ, Haughton VM, Hyde JS (1997) Hypercapnia reversibly suppresses low-frequency fluctuations in the human motor cortex during rest using echo-planar MRI. Journal of Cerebral Blood Flow and Metabolism 17:301-308.

Blake R, Cepeda NJ, Hiris E (1997) Memory for visual motion. Journal of Experimental Psychology-Human Perception and Performance 23:353-369.

Blamire AM, Ogawa S, Ugurbil K, Rothman D, McCarthy G, Ellermann JM, Hyder F, Rattner Z, Shulman RG (1992) Dynamic mapping of the human visual-cortex by high-speed magnetic-resonance-imaging. Proceedings of the National Academy of Sciences of the United States of America 89:11069-11073.

Blasdel GG, Salama G (1986a) Visualization of striate cortical activity in macaque monkeys using voltage sensitive dyes. Journal of Neuroscience Methods 17:175-176.

Blasdel GG, Salama G (1986b) Voltage-sensitive dyes reveal a modular organization in monkey striate cortex. Nature 321:579-585.

Bles M, Schwarzbach J, De Weerd P, Goebel R, Jansma BM (2006) Receptive field size-dependent attention effects in simultaneously presented stimulus displays. Neuroimage 30:506-511.

Bloch F, Hansen WW, Packard M (1946) Nuclear induction. Physical Review 69:127-127.

Bonds AB (1991) Temporal dynamics of contrast gain in single cells of the cat striate cortex. Vis Neurosci 6:239-255.

Bonhoeffer T, Grinvald A (1991) Iso-orientation domains in cat visual cortex are arranged in pinwheel-like patterns. Nature 353:429-431.

Bonnel AM, Miller J (1994) Attentional effects on concurrent psychophysical discriminations - investigations of a sample-size model. Perception & Psychophysics 55:162-179.

Born RT, Tootell RBH (1992) Segregation of global and local motion processing in primate middle temporal visual area. Nature 357:497-499.

Born RT, Bradley DC (2005) Structure and function of visual area MT. Annual Review of Neuroscience 28:157-189.

Boynton GM, Finney EM (2003) Orientation-specific adaptation in human visual cortex. J Neurosci 23:8781-8787.

Boynton GM, Engel SA, Glover GH, Heeger DJ (1996) Linear systems analysis of functional magnetic resonance imaging in human V1. Journal of Neuroscience 16:4207-4221.

Boynton GM, Demb JB, Glover GH, Heeger DJ (1999) Neuronal basis of contrast discrimination. Vision Res 39:257-269.

Braddick OJ, O'Brien JM, Wattam-Bell J, Atkinson J, Hartley T, Turner R (2001) Brain Areas Sensitive To Coherent Visual Motion. Perception 30:61-72.

Bradley DC, Qian N, Andersen RA (1995) Integration of motion and stereopsis in middle temporal cortical area of macaques. Nature 373:609-611.

Bradley R, Skottun BC (1984) The effects of large orientation and spatial frequency differences on spatial discriminations. Vision Research 24:1889.

Brainin M, Seiser A, Matz K (2008) The mirror world of motor inhibition: the alien hand syndrome in chronic stroke. Journal of Neurology Neurosurgery and Psychiatry

79:246-252.
Braver TS, Cohen JD, Servanschreiber D (1995) Neural-network simulations of schizophrenic performance in a variant of the CPT-AX. Biological Psychiatry 37:634-634.
Braver TS, Cohen JD, Nystrom LE, Jonides J, Smith EE, Noll DC (1997) A parametric study of prefrontal cortex involvement in human working memory. Neuroimage 5:49-62.
Brefczynski JA, DeYoe EA (1999) A physiological correlate of the 'spotlight' of visual attention. Nature Neuroscience 2:370-374.
Breitmeyer BG (1984) Visual masking: An integrative approach. New York: Oxford University Press.
Brelsfor.Jw, Shiffrin RM, Atkinson RC (1968) Multiple Reinforcement Effects In Short-Term Memory. British Journal of Mathematical & Statistical Psychology 21:1.
Bressler D, Spotswood N, Whitney D (2007) Negative BOLD fMRI Response in the Visual Cortex Carries Precise Stimulus-Specific Information. Plos One 2: e410.
Brindley GS, Gautiers.Pc, Lewin W (1969) Cortical Blindness And Functions Of Non-Geniculate Fibres Of Optic Tracts. Journal of Neurology Neurosurgery and Psychiatry 32:259.
Britten KH, Newsome WT (1998) Tuning bandwidths for near-threshold stimuli in area MT. Journal of Neurophysiology 80:762-770.
Britten KH, Shadlen MN, Newsome WT, Movshon JA (1992) The analysis of visual-motion - a comparison of neuronal and psychophysical performance. Journal of Neuroscience 12:4745-4765.
Broadbent ED (1958) Perception and communication. New York: Pergamum Press.
Brockway JP (2000) Two functional magnetic resonance imaging f(MRI) tasks that may replace the gold standard, Wada testing, for language lateralization while giving additional localization information. Brain Cogn 43:57-59.
Brouwer GJ, Heeger DJ (2009) Decoding and reconstructing color from responses in human visual cortex. J Neurosci 29:13992-14003.
Bruce V, Green PR, Georgeson MA (1996) Visual Perception: Physiology, Psychology and Ecology, 3rd Edition: Hove & London: Psychology Press.
Buckner RL, Bandettini PA, Ocraven KM, Savoy RL, Petersen SE, Raichle ME, Rosen BR (1996) Detection of cortical activation during averaged single trials of a cognitive task using functional magnetic resonance imaging. Proceedings of the National Academy of Sciences of the United States of America 93:14878-14883.
Buklina SB (2005) The corpus callosum, interhemisphere interactions, and the function of the right hemisphere of the brain. Neuroscience and behavioral physiology 35:473-480.
Buracas GT, Fine I, Boynton GM (2005) The relationship between task performance and functional magnetic resonance imaging response. J Neurosci 25:3023-3031.
Buracas GT, Boynton GM (2007) The effect of spatial attention on contrast response functions in human visual cortex. Journal of Neuroscience 27:93-97.
Burock MA, Dale AM (2000) Estimation and detection of event-related fMRI signals with temporally correlated noise: a statistically efficient and unbiased approach. Hum Brain Mapp 11:249-260.
Burock MA, Buckner RL, Woldorff MG, Rosen BR, Dale AM (1998) Randomized event-related experimental designs allow for extremely rapid presentation rates using functional MRI. Neuroreport 9:3735-3739.
Burton MW, Small SL (1999) An introduction to functional magnetic resonance imaging. Neurologist 5:145-158.
Butler SR, Georgiou GA, Glass A, Hancox RJ, Hopper JM, Smith KRH (1987) Cortical Generators Of The Ci Component Of The Pattern-Onset Visual Evoked-Potential. Electroencephalography and Clinical Neurophysiology 68:256-267.
Buxton RB, Wong EC, Frank LR (1998) Dynamics of blood flow and oxygenation changes during brain activation: the balloon model. Magn Reson Med 39:855-864.
Caldemeyer KS, Buckwalter KA (1999) The basic principles of computed tomography and

magnetic resonance imaging. Journal of the American Academy of Dermatology 41:768-771.

Callaway EM (2005) Structure and function of parallel pathways in the primate early visual system. In: J Physiol, pp 13-19. England.

Callaway EM, Katz LC (1993) Photostimulation Using Caged Glutamate Reveals Functional Circuitry In Living Brain-Slices. Proceedings of the National Academy of Sciences of the United States of America 90:7661-7665.

Callicott JH, Mattay VS, Bertolino A, Finn K, Coppola R, Frank JA, Goldberg TE, Weinberger DR (1999) Physiological characteristics of capacity constraints in working memory as revealed by functional MRI. Cereb Cortex 9:20-26.

Cameron EL, Tai JC, Eckstein MP, Carrasco M (2004) Signal detection theory applied to three visual search tasks - identification, yes/no detection and localization. Spatial Vision 17:295-325.

Campbell FW, Gubisch RW (1966) Optical quality of human eye. Journal of Physiology-London 186:558.

Campbell FW, Maffei L, Piccolin.M (1973) Contrast sensitivity of cat. Journal of Physiology-London 229:719.

Campbell FW, Cooper GF, Robson JG, Sachs MB (1969) Spatial selectivity of visual cells of cat and squirrel monkey. Journal of Physiology-London 204:P120.

Cannestra AF, Pouratian N, Bookheimer SY, Martin NA, Becker DP, Toga AW (2001) Temporal spatial differences observed by functional MRI and human intraoperative optical imaging. Cerebral Cortex 11:773-782.

Cao A (2001) Neural responses to relative motion in V1 and V2 of macaque monkeys. In: Massachusetts Institute of Technology. Dept. of Brain and Cognitive Sciences.: Massachusetts Institute of Technology.

Carandini M, Heeger DJ, Movshon JA (1997) Linearity and normalization in simple cells of the macaque primary visual cortex. Journal of Neuroscience 17:8621-8644.

Carlson S, Martinkauppi S, Rama P, Salli E, Korvenoja A, Aronen HJ (1998) Distribution of cortical activation during visuospatial n-back tasks as revealed by functional magnetic resonance imaging. Cerebral Cortex 8:743-752.

Carlson TA, Schrater P, He S (2003) Patterns of activity in the categorical representation of objects. J Cogn Neurosci 15:704-717.

Carrasco M, McElree B (2001) Covert attention accelerates the rate of visual information processing. Proceedings of the National Academy of Sciences of the United States of America 98:5363-5367.

Casey BJ, Davidson M, Rosen B (2002) Functional magnetic resonance imaging: basic principles of and application to developmental science. Developmental Science 5:301-309.

Cavanaugh JR, Bair W, Movshon JA (2002) Nature and interaction of signals from the receptive field center and surround in macaque V1 neurons. Journal of Neurophysiology 88:2530-2546.

Cavina-Pratesi C, Bricolo E, Pellegrini B, Marzi CA (2004) At what stage of manual visual reaction time does interhemispheric transmission occur: controlled or ballistic? Experimental Brain Research 155:220-230.

Celsis P, Boulanouar K, Doyon B, Ranjeva JP, Berry I, Nespoulous JL, Chollet F (1999) Differential fMRI responses in the left posterior superior temporal gyrus and left supramarginal gyrus to habituation and change detection in syllables and tones. Neuroimage 9:135-144.

Jacobsen CF (1936) Studies of cerebral function in primates. I. The functions of the frontal association areas in monkeys. Comp Psychol Monogr 13:1–60.

Chance FS, Nelson SB, Abbott LF (1999) Complex cells as cortically amplified simple cells. Nature Neuroscience 2:277-282.

Chao LL, Knight RT (1995) Human Prefrontal Lesions Increase Distractibility To Irrelevant Sensory Inputs. Neuroreport 6:1605-1610.

Chen Y, Martinez-Conde S, Macknik SL, Bereshpolova Y, Swadlow HA, Alonso JM (2008)

Task difficulty modulates the activity of specific neuronal populations in primary visual cortex. Nat Neurosci 11:974-982.

Cheng K, Waggoner RA, Tanaka K (2001) Human ocular dominance columns as revealed by high-field functional magnetic resonance imaging. Neuron 32:359-374.

Chiang T-C, Walsh V, Lavidor M (2004) The cortical representation of foveal stimuli: evidence from quadrantanopia and TMS-induced suppression. Brain research Cognitive brain research 21:309-316.

Chiarello C, Nuding S (1987) Visual-Field Effects For Processing Content And Function Words. Neuropsychologia 25:539-548.

Christophel TB, Hebart MN, Haynes J-D (2012) Decoding The Contents Of Visual Short-Term Memory From Human Visual And Parietal Cortex. Journal Of Neuroscience 32:12983-12989.

Chubb C, Nam JH (2000) Variance of high contrast textures is sensed using negative half-wave rectification. Vision Research 40:1677-1694.

Chubb C, Econopouly J, Landy MS (1994) Histogram contrast analysis and the visual segregation of iid textures. Journal of the Optical Society of America a-Optics Image Science and Vision 11:2350-2374.

Chubb C, Landy MS, Econopouly J (2004) A visual mechanism tuned to black. Vision Research 44:3223-3232.

Chun MM, Potter MC (1995) A 2-stage model for multiple-target detection in rapid serial visual presentation. Journal of Experimental Psychology-Human Perception and Performance 21:109-127.

Chung S, Ferster D (1998) Strength and orientation tuning of the thalamic input to simple cells revealed by electrically evoked cortical suppression. Neuron 20:1177-1189.

Clark VP, Hillyard SA (1996) Spatial selective attention affects early extrastriate but not striate components of the visual evoked potential. Journal of Cognitive Neuroscience 8:387-402.

Clarke S (2003) Complexity of human interhemispheric connections. In: The parallel brain: the cognitive neuroscience of the corpus callosum (Zaidel E, Iacoboni M, eds), pp 47-49. Cambridge, Mass: MIT Press.

Clifford CW (2011) Are Coarse-Scale Orientation Maps Really Necessary For Orientation Decoding. Available online at: http://www.jneurosci.org/content/31/13/4792/reply.

Clithero JA, Smith DV, Carter RM, Huettel SA (2011) Within- and cross-participant classifiers reveal different neural coding of information. Neuroimage 56:699-708.

Cohen JD, Braver TS, O'Reilly RC (1996) A computational approach to prefrontal cortex, cognitive control and schizophrenia: Recent developments and current challenges. Philosophical Transactions of the Royal Society B-Biological Sciences 351:1515-1527.

Cohen JD, Perlstein WM, Braver TS, Nystrom LE, Noll DC, Jonides J, Smith EE (1997) Temporal dynamics of brain activation during a working memory task. Nature 386:604-608.

Cohen MR, Maunsell JHR (2009) Attention improves performance primarily by reducing interneuronal correlations. Nature Neuroscience 12:1594-U1148.

Cohn TE (1981) Absolute Threshold - Analysis In Terms Of Uncertainty. Journal of the Optical Society of America 71:783-785.

Colby CL, Goldberg ME (1999) Space and attention in parietal cortex. Annual Review of Neuroscience 22:319-349.

Colvin MK, Funnell MG, Gazzaniga MS (2005) Numerical processing in the two hemispheres: Studies of a split-brain patient. Brain and Cognition 57:43-52.

Conner CE, Preddie DC, Gallant JL, Vanessen DC (1997) Spatial Attention Effects In Macaque Area V4. Journal Of Neuroscience 17:3201-3214.

Constantinidis C, Franowicz MN, Goldman-Rakic PS (2001) The sensory nature of mnemonic representation in the primate prefrontal cortex. Nature Neuroscience 4:311-316.

Cook EP, Maunsell JHR (2002) Dynamics of neuronal responses in macaque MT and VIP during motion detection. Nature Neuroscience 5:985-994.

Corballis MC (2002) Hemispheric interactions in simple reaction time. Neuropsychologia 40:423-434.

Corbetta M (1993) Positron Emission Tomography As A Tool To Study Human Vision And Attention. Proceedings of the National Academy of Sciences of the United States of America 90:10901-10903.

Corbetta M, Patel G, Shulman GL (2008) The reorienting system of the human brain: from environment to theory of mind. Neuron 58:306-324.

Corbetta M, Miezin FM, Dobmeyer S, Shulman GL, Petersen SE (1990) Attentional Modulation Of Neural Processing Of Shape, Color, And Velocity In Humans. Science 248:1556-1559.

Corbetta M, Miezin FM, Dobmeyer S, Shulman GL, Petersen SE (1991) Selective And Divided Attention During Visual Discriminations Of Shape, Color, And Speed - Functional-Anatomy By Positron Emission Tomography. Journal of Neuroscience 11:2383-2402.

Coren S, Ward LM, Enns JT (1994) Sensation and Perception, 4th Edition. Toronto: Harcourt Brace.

Cornette L, Dupont P, Salmon E, Orban GA (2001) The Neural Substrate Of Orientation Working Memory. J Cogn Neurosci 13:813-828.

Costagli M, Ueno K, Sun P, Gardner JL, Wan X, Ricciardi E, Pietrini P, Tanaka K, Cheng K (2012) Functional Signalers of Changes in Visual Stimuli: Cortical Responses to Increments and Decrements in Motion Coherence. Cereb Cortex.

Courtney SM, Ungerleider BG, Keil K, Haxby JV (1997) Transient and sustained activity in a distributed neural system for human working memory. Nature 386:608-611.

Cox DD, Savoy RL (2003) Functional magnetic resonance imaging (fMRI) "brain reading": detecting and classifying distributed patterns of fMRI activity in human visual cortex. Neuroimage 19:261-270.

Culham JC, Brandt SA, Cavanagh P, Kanwisher NG, Dale AM, Tootell RB (1998) Cortical fMRI activation produced by attentive tracking of moving targets. J Neurophysiol 80:2657-2670.

Curtis CE, D'Esposito M (2003) Persistent activity in the prefrontal cortex during working memory. Trends Cogn Sci 7:415-423.

Curtis CE, D'Esposito M (2004) The effects of prefrontal lesions on working memory performance and theory. Cognitive Affective & Behavioral Neuroscience 4:528-539.

D'Esposito M, Zarahn E, Aguirre GK (1999a) Event-related functional MRI: Implications for cognitive psychology. Psychological Bulletin 125:155-164.

D'Esposito M, Postle BR, Rypma B (2000) Prefrontal cortical contributions to working memory: evidence from event-related fMRI studies. Experimental Brain Research 133:3-11.

D'Esposito M, Ballard D, Aguirre GK, Zarahn E (1998) Human prefrontal cortex is not specific for working memory: A functional MRI study. Neuroimage 8:274-282.

D'Esposito M, Postle BR, Jonides J, Smith EE (1999b) The neural substrate and temporal dynamics of interference effects in working memory as revealed by event-related functional MRI. Proc Natl Acad Sci U S A 96:7514-7519.

D'Esposito M, Postle BR, Ballard D, Lease J (1999c) Maintenance versus manipulation of information held in working memory: an event-related fMRI study. Brain Cogn 41:66-86.

De Valois RL, De Valois KK (1988) Spatial Vision.

Dale AM (1999) Optimal experimental design for event-related fMRI. Hum Brain Map 8:109-114.

Dale AM, Buckner RL (1997) Selective averaging of rapidly presented individual trials using fMRI. Human Brain Mapping 5:329-340.

Damasio AR, Chui HC, Corbett J, Kassel N (1980) Posterior callosal section in a non-epileptic patient. Journal of Neurology Neurosurgery and Psychiatry 43:351-356.

Daniel PM, Whitteridge D (1961) Representation Of Visual Field On Cerebral Cortex In Monkeys. Journal of Physiology-London 159:203.
Das A, Gilbert CD (1997) Distortions of visuotopic map match orientation singularities in primary visual cortex. Nature 387:594-598.
Davatzikos C (2005) Classifying spatial patterns of brain activity with machine learning methods: application to lie detection. Neuroimage 28:663-668.
Davis ET, Kramer P, Graham N (1983) Uncertainty about spatial-frequency, spatial position, or contrast of visual-patterns. Perception & Psychophysics 33:20-28.
De Martino F, Valente G, Staeren N, Ashburner J, Goebel R, Formisano E (2008) Combining multivariate voxel selection and support vector machines for mapping and classification of fMRI spatial patterns. Neuroimage 43:44-58.
Dean AF (1981) The relationship between response amplitude and contrast for cat striate cortical neurones. J Physiol 318:413-427.
Delis DC, Robertson LC, Efron R (1986) Hemispheric specialization of memory for visual hierarchical stimuli. Neuropsychologia 24:205-214.
Desimone R, Gross CG (1979) Visual areas in the temporal cortex of the macaque. Brain Res 178:363-380.
Desimone R, Ungerleider LG (1986) Multiple visual areas in the caudal superior temporal sulcus of the macaque. Journal of Comparative Neurology 248:164-189.
Desimone R, Duncan J (1995) Neural mechanisms of selective visual-attention. Annual Review of Neuroscience 18:193-222.
Deutsch JA, Deutsch D (1963) Attention - some theoretical considerations. Psychological Review 70:80-90.DeYoe EA, Bandettini P, Neitz J, Miller D, Winans P (1994) Functional Magnetic- Resonance-Imaging (Fmri) Of The Human Brain. Journal Of Neuroscience Methods 54:171-187.DeYoe EA, Carman GJ, Bandettini P, Glickman S, Wieser J, Cox R, Miller D, Neitz J (1996) Mapping striate and extrastriate visual areas in human cerebral cortex. Proc Natl Acad Sci U S A 93:2382-2386.
Dimond S, Beaumont G (1971) Hemisphere function and vigilance. Quarterly Journal of Experimental Psychology 23:443-448.
Dimond SJ (1971) Hemisphere function and word registration. Journal of Experimental Psychology 87:183-186.
Dinstein I, Hasson U, Rubin N, Heeger DJ (2007) Brain areas selective for both observed and executed movements. J Neurophysiol 98:1415-1427.
Dinstein I, Gardner JL, Jazayeri M, Heeger DJ (2008) Executed and observed movements have different distributed representations in human aIPS. J Neurosci 28:11231-11239.
Dobelle WH, Mladejovsky MG (1974) Directions For Future Research On Sensory Prostheses. Transactions American Society for Artificial Internal Organs B 20:425-429.
Dobelle WH, Turkel J, Henderson DC, Evans JR (1979) Mapping the representation of the visual-field by electrical-stimulation of human visual-cortex. American Journal of Ophthalmology 88:727-735.
Doty RW (1983) Nongeniculate afferents to striate cortex in macaques. Journal of Comparative Neurology 218:159-173.
Doty RW, Negrao N, Yamaga K (1973) Unilateral Engram. Acta Neurobiologiae Experimentalis 33:711-728.
Doty RW, Ringo JL, Lewine JD (1988) Forebrain commissures and visual memory - a new approach. Behavioural Brain Research 29:267-280.
Doty RW, Ringo JL, Lewine JD (1994) Interhemispheric sharing of visual memory in macaques. Behav Brain Res 64:79-84.
Dougherty RF, Koch VM, Brewer AA, Fischer B, Modersitzki J, Wandell BA (2003) Visual field representations and locations of visual areas V1/2/3 in human visual cortex. Journal of Vision 3:586-598.
Downing CJ (1988) Expectancy and visual spatial attention - effects on perceptual quality. Journal of Experimental Psychology-Human Perception and Performance 14:188-

202.
Dragoi V, Sur M (2001) Inhomogeneities in the structure of V1 orientation maps and their consequences for cortical function. Society for Neuroscience Abstracts 27:1625-1625.
Dragoi V, Sharma J, Sur M (2000) Adaptation-induced plasticity of orientation tuning in adult visual cortex. In: Neuron, pp 287-298. United States.
Druzgal TJ, D'Esposito M (2003) Dissecting contributions of prefrontal cortex and fusiform face area to face working memory. Journal of Cognitive Neuroscience 15:771-784.
Duda RO, Hart PE, Stork DG (2000) Pattern Classification, 2nd Edition.
Dumoulin SO, Wandell BA (2008) Population Receptive Field Estimates In Human Visual Cortex. Neuroimage 39:647-660.
Duncan J, Ward R, Shapiro K (1994) Direct Measurement Of Attentional Dwell Time In Human Vision. Nature 369:313-315.
Duyn JH, Kellman P, van Gelderen P, de Zwart JA, Jansma M, Fukunaga M, Chu R (2003) Temporal dynamics of the BOLD signal. Society for Neuroscience Abstract Viewer and Itinerary Planner 2003:Abstract No. 863.818-Abstract No. 863.818.
Eacott MJ, Gaffan D (1989) Interhemispheric-Transfer Of Visual Learning In Monkeys With Intact Optic Chiasm. Experimental Brain Research 74:348-352.
Eckstein MP, Thomas JP, Palmer J, Shimozaki SS (2000) A signal detection model predicts the effects of set size on visual search accuracy for feature, conjunction, triple conjunction, and disjunction displays. Perception & Psychophysics 62:425-451.
Edelstein WA, Glover GH, Hardy CJ, Redington RW (1986) The intrinsic signal-to-noise ratio in NMR imaging. Magnetic Resonance in Medicine 3:604-618.
Edwards DP, Purpura KP, Kaplan E (1995) Contrast sensitivity and spatial-frequency response of primate cortical-neurons in and around the cytochrome-oxidase blobs. Vision Research 35:1501-1523.
Egner T, Hirsch J (2005) Where Memory Meets Attention: Neural Substrates Of Negative Priming. Journal Of Cognitive Neuroscience 17:1774-1784.
Engel SA, Glover GH, Wandell BA (1997) Retinotopic organization in human visual cortex and the spatial precision of functional MRI. Cereb Cortex 7:181-192.
Engel SA, Rumelhart DE, Wandell BA, Lee AT, Glover GH, Chichilnisky EJ, Shadlen MN (1994) fMRI of human visual cortex. Nature 369:525.
Ester EF, Serences JT, Awh E (2009) Spatially global representations in human primary visual cortex during working memory maintenance. J Neurosci 29:15258-15265.
Ethofer T, Mader I, Seeger U, Helms G, Erb M, Grodd W, Ludolph A, Klose U (2003) Comparison of longitudinal metabolite relaxation times in different regions of the human brain at 1.5 and 3 Tesla. Magnetic Resonance in Medicine 50:1296-1301.
Fabri M, Del Pesce M, Paggi A, Polonara G, Bartolini M, Salvolini U, Manzoni T (2005) Contribution of posterior corpus callosum to the interhemispheric transfer of tactile information. Brain research Cognitive brain research 24:73-80.
Fahle M, Harris JP (1992) Visual Memory For Vernier Offsets. Vision Research 32:1033-1042.
Feinberg TE, Schindler RJ, Flanagan NG, Haber LD (1992) 2 Alien hand syndromes. Neurology 42:19-24.
Felleman DJ, Van Essen DC (1991) Distributed Hierarchical Processing in the Primate Cerebral Cortex. Cerebral Cortex 1:1-47.
Ferbert A, Priori A, Rothwell JC, Day BL, Colebatch JG, Marsden CD (1992) Interhemispheric inhibition of the human motor cortex. Journal of Physiology-London 453:525-546.
Ferrera VP, Rudolph KK, Maunsell JHR (1994) Responses Of Neurons In The Parietal And Temporal Visual Pathways During A Motion Task. Journal Of Neuroscience 14:6171-6186.
Fischl B, Dale AM (2000) Measuring the thickness of the human cerebral cortex from magnetic resonance images In: (Raichle ME, ed). St. Louis, MO: Washington University School of Medicine.

Fitzpatrick D, Usrey WM, Schofield BR, Einstein G (1994) The sublaminar organization of corticogeniculate neurons in layer-6 of macaque striate cortex. Visual Neuroscience 11:307-315.

Fogel I, Sagi D (1989) Gabor filters as texture discriminator. Biological Cybernetics 61:103-113.

Foley JM, Yang YD (1991) Forward pattern masking - effects of spatial-frequency and contrast. Journal of the Optical Society of America a-Optics Image Science and Vision 8:2026-2037.

Foley JM, Schwarz W (1998) Spatial attention: effect of position uncertainty and number of distractor patterns on the threshold-versus-contrast function for contrast discrimination. Journal of the Optical Society of America a-Optics Image Science and Vision 15:1036-1047.

Foltz WD, Jaffray DA (2012) Principles of Magnetic Resonance Imaging. Radiation Research 177:331-348.

Fox PT, Raichle ME (1986) Focal Physiological Uncoupling Of Cerebral Blood-Flow And Oxidative-Metabolism During Somatosensory Stimulation In Human-Subjects. Proceedings Of The National Academy Of Sciences Of The United States Of America 83:1140-1144.

Freeman J, Brouwer GJ, Heeger DJ, Merriam EP (2011) Orientation decoding depends on maps, not columns. J Neurosci 31:4792-4804.

Fries P, Reynolds JH, Rorie AE, Desimone R (2001) Modulation of oscillatory neuronal synchronization by selective visual attention. Science 291:1560-1563.

Fries P, Womelsdorf T, Oostenveld R, Desimone R (2008) The effects of visual stimulation and selective visual attention on rhythmic neuronal synchronization in macaque area v4. Journal of Neuroscience 28:4823-4835.

Frisch HL, Julesz B (1966) Figure-ground perception and random geometry. Perception & Psychophysics 1:389-398.

Friston K (2006) Dynamic causal modelling of brain responses. Journal of Psychophysiology 20:322-322.

Friston KJ, Frith CD, Frackowiak RS, Turner R (1995) Characterizing dynamic brain responses with fMRI: a multivariate approach. Neuroimage 2:166-172.

Friston KJ, Mechelli A, Turner R, Price CJ (2000) Nonlinear responses in fMRI: the Balloon model, Volterra kernels, and other hemodynamics. Neuroimage 12:466-477.

Friston KJ, Holmes AP, Price CJ, Buchel C, Worsley KJ (1999) Multisubject fMRI studies and conjunction analyses. In: Neuroimage, pp 385-396. United States: 1999 Academic Press.

Friston KJ, Holmes AP, Worsley KJ, Poline JP, Frith CD, Frackowiak RSJ (1994) Statistical parametric maps in functional imaging: A general linear approach. Human Brain Mapping 2:189-210.

Friston KJ, Fletcher P, Josephs O, Holmes A, Rugg MD, Turner R (1998) Event-related fMRI: Characterizing differential responses. Neuroimage 7:30-40.

Friston KJ, Glaser DE, Henson RN, Kiebel S, Phillips C, Ashburner J (2002) Classical and Bayesian inference in neuroimaging: applications. In: Neuroimage, pp 484-512. United States: 2002 Elsevier Science (USA).

Funahashi S, Bruce CJ, Goldmanrakic PS (1989) Mnemonic Coding Of Visual Space In The Monkeys Dorsolateral Prefrontal Cortex. Journal of Neurophysiology 61:331-349.

Fuster JM (1995) Memory in the cortex of the primate. Biol Res 28:59-72.

Fuster JM (2008) The prefrontal cortex. London: Academic Press.

Fuster JM, Alexander GE (1971) Neuron activity related to short-term memory. Science 173:652-654.

Gandhi SP, Heeger DJ, Boynton GM (1999) Spatial attention affects brain activity in human primary visual cortex. Proceedings of the National Academy of Sciences of the United States of America 96:3314-3319.

Gardner JL (2010) Is Cortical Vasculature Functionally Organized? Neuroimage 49:1953-1956.

Gardner JL, Anzai A, Ohzawa I, Freeman RD (1999) Linear and nonlinear contributions to orientation tuning of simple cells in the cat's striate cortex. Visual Neuroscience 16:1115-1121.

Gardner JL, Merriam EP, Movshon JA, Heeger DJ (2008) Maps of visual space in human occipital cortex are retinotopic, not spatiotopic. J Neurosci 28:3988-3999.

Gardner JL, Sun P, Waggoner RA, Ueno K, Tanaka K, Cheng K (2005) Contrast adaptation and representation in human early visual cortex. Neuron 47:607-620.

Gattass R, Gross CG, Sandell JH (1981) Visual topography of V2 in the macaque. J Comp Neurol 201:519-539.

Gattass R, Sousa APB, Gross CG (1988) Visuotopic organization and extent of v3 and v4 of the macaque. Journal of Neuroscience 8:1831-1845.

Gawne TJ, Kjaer TW, Richmond BJ (1996) Latency: Another potential code for feature binding in striate cortex. Journal of Neurophysiology 76:1356-1360.

Gazzaniga MS (2000) Cerebral specialization and interhemispheric communication - Does the corpus callosum enable the human condition? Brain 123:1293-1326.

Gazzaniga.MS, Young ED (1967) Effects Of Commissurotomy On Processing Of Increasing Visual Information. Experimental Brain Research 3:368.

Geisler WS, Albrecht DG (1997) Visual cortex neurons in monkeys and cats: detection, discrimination, and identification. Vis Neurosci 14:897-919.

Gelman N, Gorell JM, Barker PB, Savage RM, Spickler EM, Windham JP, Knight RA (1999) MR imaging of human brain at 3.0 T: Preliminary report on transverse relaxation rates and relation to estimated iron content. Radiology 210:759-767.

George MS, Ketter TA, Parekh PI, Rosinsky N, Ring H, Casey BJ, Trimble MR, Horwitz B, Herscovitch P, Post RM (1993) Regional Brain Activity When Selecting a Response Despite Interference: An H-2-15O PET Study of the Stroop and an Emotional Stroop. Human Brain Mapping 1:194-209.

Ghez C (1991a) Voluntary movement. In: Principles of neural science, 3rd Edition (E.R. Kandel JHSaTMJ, ed), pp 609-625. Norwalk, Connecticut: Appleton & Lange.

Ghez C (1991b) Posture. In: Principles of neural science, 3rd Edition (E.R. Kandel JHSaTMJ, ed), pp 596-608. Norwalk, Connecticut: Appleton & Lange.

Ghez C (1991c) The control of movement. In: Principles of neural science, 3rd Edition (E.R. Kandel JHSaTMJ, ed), pp 533-547. Norwalk, Connecticut: Appleton & Lange.

Gibby WA (2005) Basic principles of magnetic resonance imaging. Neurosurgery Clinics of North America 16:1.

Gibson JR, Maunsell JH (1997) Sensory Modality Specificity Of Neural Activity Related To Memory In Visual Cortex. J Neurophysiol 78:1263-1275.

Giesbrecht B, Di Lollo V (1998) Beyond the attentional blink: Visual masking by object substitution. Journal of Experimental Psychology-Human Perception and Performance 24:1454-1466.

Gleissner U, Helmstaedter C, Kurthen M, Elger CE (1997) Evidence of very fast memory consolidation: an intracarotid amytal study. Neuroreport 8:2893-2896.

Glickstein M (2009) Paradoxical inter-hemispheric transfer after section of the cerebral commissures. Experimental Brain Research 192:425-429.

Glover GH (1999) Deconvolution of impulse response in event-related BOLD fMRI. In: Neuroimage, pp 416-429. United States: 1999 Academic Press.

Goldman-Rakic PS (1987) Circuitry of primate prefrontal cortex and regulation of behaviour by representational memory In: Handbook of physiology (Plum F, Mouncastle U, eds), pp 373–417. Washington, DC: The American Physiological Society.

Goldman-Rakic PS (1995) Architecture of the prefrontal cortex and the central executive. Structure and Functions of the Human Prefrontal Cortex 769:71-83.

Goodale MA, Milner AD (1992) Separate visual pathways for perception and action. Trends Neurosci 15:20-25.

Goodyear BG, Menon RS (2001) Brief visual stimulation allows mapping of ocular dominance in visual cortex using fMRI. Hum Brain Mapp 14:210-217.

Goris RLT, Wichmann FA, Henning GB (2009) A neurophysiologically plausible population

code model for human contrast discrimination. Journal of Vision 9.
Gott PS (1973) Cognitive abilities following right and left hemispherectomy. Cortex 9:266-274.
Graham N (1991) Complex channels, early local nonlinearities, and normalization in texture segregation. In: Computational Models of Visual Processing (Landy M, Movshon JA, eds), pp 273-290. Cambridge, MA: MIT Press.

Greenlee MW, Georgeson MA, Magnussen S, Harris JP (1991) The Time Course Of Adaptation To Spatial Contrast. Vision Res 31:223-236.
Green DM, Swets JA (1966) Signal detection theory and psychophysics: Wiley New York.
Greenlee MW, Thomas JP (1993) Simultaneous discrimination of the spatial frequency and contrast of periodic stimuli. J Opt Soc Am A 10:395-404.
Greenlee MW, Magnussen S, Reinvang I (2000) Brain regions involved in spatial frequency discrimination: evidence from fMRI. Exp Brain Res 132:399-403.
Greenlee MW, Koessler M, Cornelissen FW, Mergner T (1997) Visual discrimination and short-term memory for random patterns in patients with a focal cortical lesion. Cerebral Cortex 7:253-267.
Griffith H, Davidson M (1966) Long-term changes in intellect and behaviour after hemispherectomy. Journal of Neurology Neurosurgery and Psychiatry 29:571.
Grill-Spector K (2003) The neural basis of object perception. Curr Opin Neurobiol 13:159-166.
Grill-Spector K, Malach R (2001) Fmr-Adaptation: A Tool For Studying The Functional Properties Of Human Cortical Neurons. Acta Psychologica 107:293-321.
Grinvald A, Lieke E, Frostig RD, Gilbert CD, Wiesel TN (1986) Functional Architecture Of Cortex Revealed By Optical Imaging Of Intrinsic Signals. Nature 324:361-364.
Gu H, Stein EA, Yang Y (2005) Nonlinear responses of cerebral blood volume, blood flow and blood oxygenation signals during visual stimulation. Magn Reson Imaging 23:921-928.
Gur M, Kagan I, Snodderly DM (2005) Orientation and direction selectivity of neurons in V1 of alert monkeys: Functional relationships and laminar distributions. Cerebral Cortex 15:1207-1221.
Guyon, Elisseeff (2003) An Introduction To Variable And Feature Selection. J Mach Learn Res 3:1157-1182.
Haenny PE, Maunsell JHR, Schiller PH (1988) State dependent activity in monkey visual-cortex .2. Retinal and extraretinal factors in v4. Experimental Brain Research 69:245-259.
Hansen LK (2007) Multivariate strategies in functional magnetic resonance imaging. Brain and Language 102:186-191.
Hanson SJ, Matsuka T, Haxby JV (2004) Combinatorial codes in ventral temporal lobe for object recognition: Haxby (2001) revisited: is there a "face" area? Neuroimage 23:156-166.
Harrison SA, Tong F (2009) Decoding reveals the contents of visual working memory in early visual areas. Nature 458:632-635.
Harvey BM, Dumoulin SO (2011) The relationship between cortical magnification factor and population receptive field size in human visual cortex: constancies in cortical architecture. J Neurosci 31:13604-13612.
Harvey LO, Klix F, Hagendorf H (1986) Human memory and cognitive capabilities.
Hashemi R, Bradley W, Christopher L (2003) MRI the basics, Second Edition. U.S.A: Lippincott Williams & Wilkins.
Hastie T, Zhu M (2001) Dimension reduction and visualization in discriminant analysis - Discussion. Australian & New Zealand Journal of Statistics 43:179-185.
Hawken MJ, Parker AJ, Lund JS (1988) Laminar organization and contrast sensitivity of direction-selective cells in the striate cortex of the old-world monkey. Journal of Neuroscience 8:3541-3548.
Haxby JV (2012) Multivariate pattern analysis of fMRI: The early beginnings. Neuroimage

62:852-855.
Haxby JV, Petit L, Ungerleider LG, Courtney SM (2000) Distinguishing the functional roles of multiple regions in distributed neural systems for visual working memory. Neuroimage 11:380-391.
Haxby JV, Horwitz B, Ungerleider LG, Maisog JM, Pietrini P, Grady CL (1994) The functional-organization of human extrastriate cortex - a pet-rcbf study of selective attention to faces and locations. Journal of Neuroscience 14:6336-6353.
Haxby JV, Gobbini MI, Furey ML, Ishai A, Schouten JL, Pietrini P (2001) Distributed and overlapping representations of faces and objects in ventral temporal cortex. In: Science, pp 2425-2430. United States.
Haynes J-D, Rees G (2006) Decoding mental states from brain activity in humans. Nature Reviews Neuroscience 7:523-534.
Haynes J-D, Sakai K, Rees G, Gilbert S, Frith C, Passingham RE (2007) Reading hidden intentions in the human brain. Current Biology 17:323-328.
Haynes JD, Rees G (2005) Predicting the orientation of invisible stimuli from activity in human primary visual cortex. Nat Neurosci 8:686-691.
Heeger DJ (1991) Nonlinear model of neural responses in cat visual cortex. Computational models of visual processing:119-133.
Heeger DJ (1992) Normalization of cell responses in cat striate cortex. In: Vis Neurosci, pp 181-197. England.
Heeger DJ, Ress D (2002) What does fMRI tell us about neuronal activity? Nat Rev Neurosci 3:142-151.
Heeger DJ, Huk AC, Geisler WS, Albrecht DG (2000) Spikes versus BOLD: what does neuroimaging tell us about neuronal activity? Nat Neurosci 3:631-633.
Heinze HJ, Mangun GR, Burchert W, Hinrichs H, Scholz M, Munte TF, Gos A, Scherg M, Johannes S, Hundeshagen H, Gazzaniga MS, Hillyard SA (1994) Combined spatial and temporal imaging of brain activity during visual selective attention in humans. Nature 372:543-546.
Hellige JB (1993) Hemispheric Asymmetry: what's right and what's left. Cambridge: Harvard University Press.
Henriksson L, Karvonen J, Salminen-Vaparanta N, Railo H, Vanni S (2012) Retinotopic maps, spatial tuning, and locations of human visual areas in surface coordinates characterized with multifocal and blocked FMRI designs. PloS one 7:e36859-e36859.
Henschen SE (1893) On the visual path and centre. Brain 16:170–180.
Hodos W, Ghim MM, Potocki A, Fields JN, Storm T (2002) Contrast sensitivity in pigeons: A comparison of behavioral and pattern ERG methods. Documenta Ophthalmologica 104:107-118.
Hofer S, Frahm J (2006) Topography of the human corpus callosum revisited - Comprehensive fiber tractography using diffusion tensor magnetic resonance imaging. Neuroimage 32:989-994.
Hoge RD, Atkinson J, Gill B, Crelier GR, Marrett S, Pike GB (1999) Linear coupling between cerebral blood flow and oxygen consumption in activated human cortex. Proc Natl Acad Sci U S A 96:9403-9408.
Holtzman JD, Gazzaniga MS (1985) Enhanced Dual Task-Performance Following Corpus Commissurotomy In Humans. Neuropsychologia 23:315-321.
Hoptman MJ, Davidson RJ (1994) How And Why Do The 2 Cerebral Hemispheres Interact. Psychological Bulletin 116:195-219.
Horner AJ, Andrews TJ (2009) Linearity of the fMRI response in category-selective regions of human visual cortex. Hum Brain Mapp 30:2628-2640.
Horton JC (2006) Ocular Integration In The Human Visual Cortex. Canadian Journal Of Ophthalmology-Journal Canadien D Ophtalmologie 41:584-593.
Horton JC, Hoyt WF (1991) The Representation Of The Visual-Field In Human Striate Cortex - A Revision Of The Classic Holmes Map. Archives Of Ophthalmology 109:816-824.
Hu M, Wang Y (2011) Rapid dynamics of contrast responses in the cat primary visual cortex.

PLoS One 6:e25410.
Huang CM, Buchwald JS (1977) Interpretation Of Vertex Short-Latency Acoustic Response - Study Of Single Neurons In Brain-Stem. Brain Research 137:291-303.
Hubel DH, Wiesel TN (1963) Receptive Fields Of Cells In Striate Cortex Of Very Young, Visually Inexperienced Kittens. Journal of Neurophysiology 26:994.
Hubel DH, Wiesel TN (1965) Binocular Interaction In Striate Cortex Of Kittens Reared With Artificial Squint. Journal of Neurophysiology 28:1041.
Hubel DH, Livingstone MS (1990) Color And Contrast Sensitivity In The Lateral Geniculate-Body And Primary Visual-Cortex Of The Macaque Monkey. Journal of Neuroscience 10:2223-2237.
Huettel S, Song A, McCarthy G (2009) Functional Magnetic Resonance Imaging, Second Edition. Sunderland, Massachusetts U.S.A.: Sinauer Associates, Inc.
Huk AC, Heeger DJ (2000) Task-related modulation of visual cortex. Journal of Neurophysiology 83:3525-3536.
Huk AC, Heeger DJ (2002) Pattern-motion responses in human visual cortex. In: Nat Neurosci, pp 72-75. United States.
Huk AC, Ress D, Heeger DJ (2001) Neuronal basis of the motion aftereffect reconsidered. In: Neuron, pp 161-172. United States.
Intraub H (1981) Dissociation Of Concurrently Presented Visual Information. Bulletin of the Psychonomic Society 18:69-69.
Jarvis JR, Wathes CM (2008) A mechanistic inter-species comparison of spatial contrast sensitivity. Vision Research 48:2284-2292.
Jeffreys DA, Axford JG (1972) Source Locations Of Pattern-Specific Components Of Human Visual Evoked-Potentials .1. Component Of Striate Cortical Origin. Experimental Brain Research 16:1.
Jensen O, Gelfand J, Kounios J, Lisman JE (2002) Oscillations in the alpha band (9-12 Hz) increase with memory load during retention in a short-term memory task. Cerebral Cortex 12:877-882.
Jezzard P MP, Smith SM (2003) Functional magnetic resonance imaging: an introduction to methods. Oxford: Oxford UP.
Jolicoeur P, Dell' Acqua R (1998) The demonstration of short-term consolidation. Cognitive Psychology 36:138-202.
Jones JP, Palmer LA (1987) An evaluation of the two-dimensional Gabor filter model of simple receptive fields in cat striate cortex. J Neurophysiol 58:1233-1258.
Jonides J, Schumacher EH, Smith EE, Lauber EJ, Awh E, Minoshima S, Koeppe RA (1997) Verbal Working Memory Load Affects Regional Brain Activation As Measured By PET. Journal Of Cognitive Neuroscience 9:462-475.
Jonides J, Smith EE, Marshuetz C, Koeppe RA, Reuter-Lorenz PA (1998) Inhibition in verbal working memory revealed by brain activation. Proceedings of the National Academy of Sciences of the United States of America 95:8410-8413.
Josephs O, Henson RNA (1999) Event-related functional magnetic resonance imaging: modelling, inference and optimization. Philosophical Transactions of the Royal Society B-Biological Sciences 354:1215-1228.
Josephs O, Turner R, Friston K (1997) Event-related fMRI. Human Brain Mapping 5:243-248.
Julesz B (1965) Texture And Visual Perception. Scientific American 212:38.
Julesz B (1975) Experiments In Visual-Perception Of Texture. Scientific American 232:34-43.
Julesz B, Oswald HP (1978) Binocular Utilization Of Monocular Cues That Are Undetectable Monocularly. Perception 7:315-322.
Kahneman D (1973) Attention and effort. Englewood Cliffs, NJ: Prentice Hall.
Kamitani Y, Tong F (2005a) Decoding motion direction from activity in human visual cortex. J Vision 5:152a.
Kamitani Y, Tong F (2005b) Decoding the visual and subjective contents of the human brain. Nature Neuroscience 8:679-685.

Kamitani Y, Tong F (2006) Decoding seen and attended motion directions from activity in the human visual cortex. Curr Biol 16:1096-1102.

Kammer T, Bellemann ME, Gückel F, Brix G, Gass A, Schlemmer H, Spitzer M (1997) Functional MR imaging of the prefrontal cortex: specific activation in a working memory task. Magn Reson Imaging 15:879-889.

Kamondi A, Acsady L, Buzsaki G (1998) Dendritic spikes are enhanced by cooperative network activity in the intact hippocampus. Journal of Neuroscience 18:3919-3928.

Kandel E, Schwartz J, Jessell T (2000) Principles Of Neural Science, 4, Revised Edition. Maidenhead/US: Mcgraw-Hill Education - Europe.

Kanwisher N, Wojciulik E (2000) Visual attention: Insights from brain imaging. Nature Reviews Neuroscience 1:91-100.

Kanwisher N, McDermott J, Chun MM (1997) The fusiform face area: a module in human extrastriate cortex specialized for face perception. J Neurosci 17:4302-4311.

Kaplan JT, Meyer K (2012) Multivariate pattern analysis reveals common neural patterns across individuals during touch observation. Neuroimage 60:204-212.

Kastner S, Ungerleider LG (2000) Mechanisms of visual attention in the human cortex. Annual Review of Neuroscience 23:315-341.

Kastner S, De Weerd P, Desimone R, Ungerleider LC (1998) Mechanisms of directed attention in the human extrastriate cortex as revealed by functional MRI. Science 282:108-111.

Kastner S, Pinsk MA, De Weerd P, Desimone R, Ungerleider LG (1999) Increased activity in human visual cortex during directed attention in the absence of visual stimulation. Neuron 22:751-761.

Kastner S, De Weerd P, Pinsk MA, Elizondo MI, Desimone R, Ungerleider LG (2001) Modulation of sensory suppression: Implications for receptive field sizes in the human visual cortex. Journal of Neurophysiology 86:1398-1411.

Kastner S, O'Connor DH, Fukui MM, Fehd HM, Herwig U, Pinsk MA (2004) Functional imaging of the human lateral geniculate nucleus and pulvinar. J Neurophysiol 91:438-448.

Kavcic V, Doty RW (2002) Efficiency of the forebrain commissures: memory for stimuli seen by the other hemisphere. Acta Neurobiol Exp (Wars) 62:235-242.

Kay KN, Naselaris T, Prenger RJ, Gallant JL (2008) Identifying natural images from human brain activity. Nature 452:352-355.

Kay S (1998) Fundamentals of Statistical Signal Processing, Volume 2: Detection Theory: Prentice Hall PTR.

Kelley WM, Miezin FM, McDermott KB, Buckner RL, Raichle ME, Cohen NJ, Ollinger JM, Akbudak E, Conturo TE, Snyder AZ, Petersen SE (1998) Hemispheric Specialization in Human Dorsal Frontal Cortex and Medial Temporal Lobe for Verbal and Nonverbal Memory Encoding. Neuron 20:927-936.

Kileny P, Ryu JH, McCabe BF, Abbas PJ (1980) Neuronal habituation in the vestibular nuclei of the cat. Acta Otolaryngol 90:175-183.

Kim DY, Duran WR, Kobayashi I, Daniels AJ, Duran WN (1994) Microcirculatory Dynamics Of Neuropeptide-Y. Microvascular Research 48:124-134.

Kim SG, Richter W, Ugurbil K (1997) Limitations of temporal resolution in functional MRI. Magnetic Resonance in Medicine 37:631-636.

Kinchla RA (1992) Attention. Annual Review of Psychology 43:711-742.

Kippenhan JS, Barker WW, Pascal S, Nagel J, Duara R (1992) Evaluation Of A Neural-Network Classifier For Pet Scans Of Normal And Alzheimers-Disease Subjects. Journal of Nuclear Medicine 33:1459-1467.

Klimesch W, Vogt F, Doppelmayr M (1999) Interindividual differences in alpha and theta power reflect memory performance. Intelligence 27:347-362.

Klingberg T, Osullivan BT, Roland PE (1997) Bilateral activation of fronto-parietal networks by incrementing demand in a working memory task. Cerebral Cortex 7:465-471.

Knight RT, Staines WR, Swick D, Chao LL (1999) Prefrontal cortex regulates inhibition and excitation in distributed neural networks. Acta Psychologica 101:159-178.

Kriegeskorte N, Bandettini P (2007) Combining the tools: activation- and information-based fMRI analysis. Neuroimage 38:666-668.
Kriegeskorte N, Goebel R, Bandettini P (2006) Information-based functional brain mapping. Proc Natl Acad Sci USA 103:3863-3868.
Kriegeskorte N, Simmons WK, Bellgowan PS, Baker CI (2009) Circular analysis in systems neuroscience: the dangers of double dipping. Nat Neurosci 12:535-540.
Kubota K, Niki H (1971) Prefrontal cortical unit activity and delayed alternation performance in monkeys. J Neurophysiol 34:337-347.
Kulikowski JJ (1976) Effective Contrast Constancy And Linearity Of Contrast Sensation. Vision Research 16:1419-1431.
Kusunoki M, Sigala N, Gaffan D, Duncan J (2009) Detection of Fixed and Variable Targets in the Monkey Prefrontal Cortex. Cerebral Cortex 19:2522-2534.
Laberge D (1995) Computational and anatomical models of selective attention in object identification. The cognitive neurosciences:649-663.
Lai S, Hopkins AL, Haacke EM, Li D, Wasserman BA, Buckley P, Friedman L, Meltzer H, Hedera P, Friedland R (1993) Identification of vascular structures as a major source of signal contrast in high-resolution 2d and 3d functional activation imaging of the motor cortex at 1.5t - preliminary-results. Magnetic Resonance in Medicine 30:387-392.
Laconte S, Strother S, Cherkassky V, Anderson J, Hu X (2005) Support Vector Machines For Temporal Classification Of Block Design Fmri Data. Neuroimage 26:317-329.
Lakrimi M, Thomas AM, Hutton G, Kruip M, Slade R, Davis P, Johnstone AJ, Longfield MJ, Blakes H, Calvert S, Smith M, Marshall CA (2011) The principles and evolution of magnetic resonance imaging. In: Condensed Matter and Materials Physics Conference (Inglesfield JE, ed).
Lalonde J, Chaudhuri A (2002) Task-dependent transfer of perceptual to memory representations during delayed spatial frequency discrimination. Vision Research 42:1759-1769.
Larsson J (2001) Imaging vision: Functional mapping of intermediate visual processes in man. In: Karolinska Institutet.
Larsson J, Heeger DJ (2006) Two retinotopic visual areas in human lateral occipital cortex. J Neurosci 26:13128-13142.
Larsson J, Heeger DJ, Landy MS (2010) Orientation selectivity of motion-boundary responses in human visual cortex. J Neurophysiol 104:2940-2950.
Larsson J, Schluppeck D, Landy MS, Heeger DJ (2003) Orientation - selective adaptation to first - and second - order stimuli in human visual cortex measured with fMRI. Society for Neuroscience Abstract Viewer and Itinerary Planner 2003:Abstract No. 911.917-Abstract No. 911.917.
Lavidor M, Walsh V (2004) Opinion - The nature of foveal representation. Nature Reviews Neuroscience 5:729-735.
Lawton TB (1982) Effect Of A Patterns Frequency Structure On Phase Discrimination. Journal of the Optical Society of America 72:1757-1757.
Lebihan D (1992) Theoretical Principles Of Perfusion Imaging - Application To Magnetic-Resonance-Imaging. Investigative Radiology 27:S6-S11.
Ledgeway T (1994) Adaptation to second-order motion results in a motion aftereffect for directionally-ambiguous test stimuli. Vision Res 34:2879-2889.
Ledgeway T, Smith AT (1994a) The duration of the motion aftereffect following adaptation to first-order and second-order motion. Perception 23:1211-1219.
Ledgeway T, Smith AT (1994b) Evidence for separate motion-detecting mechanisms for first- and second-order motion in human vision. Vision Res 34:2727-2740.
Ledgeway T, Hess RF (2002) Rules for combining the outputs of local motion detectors to define simple contours. Vision Res 42:653-659.
Ledgeway T, Hutchinson CV (2006) Is the direction of second-order, contrast-defined motion patterns visible to standard motion-energy detectors: a model answer? Vision Res 46:556-567.

Ledgeway T, Zhan C, Johnson AP, Song YN, Baker CL (2005) The direction-selective contrast response of area 18 neurons is different for first- and second-order motion. Visual Neuroscience 22:87-99.

Lee AT, Glover GH, Meyer CH (1995) Discrimination Of Large Venous Vessels In Time-Course Spiral Blood-Oxygen-Level-Dependent Magnetic-Resonance Functional Neuroimaging. Magnetic Resonance in Medicine 33:745-754.

Lee B, Harris J (1996) Contrast transfer characteristics of visual short-term memory. Vision Research 36:2159-2166.

Legge G, Kersten D, Burgess A (1987) Contrast Discrimination In Noise. Journal of the Optical Society of America a-Optics Image Science and Vision 4:391-404.

Legge GE (1981) A Power Law For Contrast Discrimination. Vision Research 21:457-467.

Legge GE, Foley JM (1980) Contrast Masking In Human-Vision. Journal of the Optical Society of America 70:1458-1471.

Lepsien J, Griffin IC, Devlin JT, Nobrea AC (2005) Directing spatial attention in mental representations: Interactions between attentional orienting and working-memory load. Neuroimage 26:733-743.

Lepsien J, Thornton I, Nobre AC (2011) Modulation Of Working-Memory Maintenance By Directed Attention. Neuropsychologia 49:1569-1577.

Leuba G, Kraftsik R (1994) Changes In Volume, Surface Estimate, 3-Dimensional Shape And Total Number Of Neurons Of The Human Primary Visual-Cortex From Midgestation Until Old-Age. Anatomy and Embryology 190:351-366.

Levinson E, Sekuler R (1975) Independence Of Channels In Human Vision Selective For Direction Of Movement. Journal of Physiology-London 250:347-366.

Levitt H (1971) Transformed Up-Down Methods in Psychoacoustics. The Journal of the Acoustical Society of America 49:467-477.

Levy I, Schluppeck D, Heeger DJ, Glimcher PW (2007) Specificity of human cortical areas for reaches and saccades. Journal of Neuroscience 27:4687-4696.

Lewine JD, Doty RW, Astur RS, Provencal SL (1994) Role Of The Forebrain Commissures In Bihemispheric Mnemonic Integration In Macaques. Journal of Neuroscience 14:2515-2530.

Li CY, Creutzfeldt O (1984) The representation of contrast and other stimulus parameters by single neurons in area 17 of the cat. Pflugers Arch 401:304-314.

Li X, Lu ZL, Tjan BS, Dosher BA, Chu W (2008) Blood oxygenation level-dependent contrast response functions identify mechanisms of covert attention in early visual areas. Proc Natl Acad Sci U S A 105:6202-6207.

Liederman J (1986) Subtraction In Addition To Addition - Dual Task-Performance Improves When Tasks Are Presented To Separate Hemispheres. Journal of Clinical and Experimental Neuropsychology 8:486-502.

Liederman J (1998) The dynamics of interhemispheric collaboration and hemispheric control. Brain and Cognition 36:193-208.

Liederman J, Merola JL, Hoffman C (1986) Longitudinal data indicate that hemispheric independence increases during early adolescence. Developmental Neuropsychology 2:183-201.

Linden DE, Bittner RA, Muckli L, Waltz JA, Kriegeskorte N, Goebel R, Singer W, Munk MH (2003) Cortical capacity constraints for visual working memory: dissociation of fMRI load effects in a fronto-parietal network. Neuroimage 20:1518-1530.

Liu T, Hospadaruk L, Zhu DC, Gardner JL (2011) Feature-specific attentional priority signals in human cortex. J Neurosci 31:4484-4495.

Liu TS, Pestilli F, Carrasco M (2005) Transient attention enhances perceptual performance and fMRI response in human visual cortex. Neuron 45:469-477.

Liu TT, Frank LR, Wong EC, Buxton RB (2001) Detection power, estimation efficiency, and predictability in event-related fMRI. Neuroimage 13:759-773.

Logothetis NK (2003) MR imaging in the non-human primate: studies of function and of dynamic connectivity. Curr Opin Neurobiol 13:630-642.

Logothetis NK (2008) What we can do and what we cannot do with fMRI. Nature 453:869-

878.
Logothetis NK, Pfeuffer J (2004) On the nature of the BOLD fMRI contrast mechanism. Magn Reson Imaging 22:1517-1531.
Logothetis NK, Pauls J, Augath M, Trinath T, Oeltermann A (2001) Neurophysiological investigation of the basis of the fMRI signal. Nature 412:150-157.
Loubinoux I, Carel C, Alary F, Boulanouar K, Viallard G, Manelfe C, Rascol O, Celsis P, Chollet F (2001) Within-session and between-session reproducibility of cerebral sensorimotor activation: a test--retest effect evidenced with functional magnetic resonance imaging. J Cereb Blood Flow Metab 21:592-607.
Lu HD, Roe AW (2007) Optical Imaging of Contrast Response in Macaque Monkey V1 and V2. Cerebral Cortex 17:2675-2695.
Lu ZL, Dosher BA (1999) Characterizing human perceptual inefficiencies with equivalent internal noise. Journal of the Optical Society of America a-Optics Image Science and Vision 16:764-778.
Lu ZL, Dosher BA (2000) Spatial attention: Different mechanisms for central and peripheral temporal precues? Journal of Experimental Psychology-Human Perception and Performance 26:1534-1548.
Lubin J (1992) Interactions among motion-sensitive mechanisms in human vision. In: University of Pennsylvania.
Lucas PA (1967) Green,DM - Signal Detection Theory And Psychophysics. British Journal of Mathematical & Statistical Psychology 20:112.
Luck SJ, Hillyard SA (1990) Electrophysiological Evidence For Parallel And Serial Processing During Visual-Search. Perception & Psychophysics 48:603-617.
Luck SJ, Vogel EK (1997) The capacity of visual working memory for features and conjunctions. Nature 390:279-281.
Luck SJ, Hillyard SA, Mouloua M, Hawkins HL (1996) Mechanisms of visual-spatial attention: Resource allocation or uncertainty reduction? Journal of Experimental Psychology-Human Perception and Performance 22:725-737.
Luck SJ, Chelazzi L, Hillyard SA, Desimone R (1997a) Neural mechanisms of spatial selective attention in areas V1, V2, and V4 of macaque visual cortex. Journal of Neurophysiology 77:24-42.
Luck SJ, Girelli M, McDermott MT, Ford MA (1997b) Bridging the gap between monkey neurophysiology and human perception: An ambiguity resolution theory of visual selective attention. Cognitive Psychology 33:64-87.
Lueck CJ, Zeki S, Friston KJ, Deiber MP, Cope P, Cunningham VJ, Lammertsma AA, Kennard C, Frackowiak RSJ (1989) The Color Center In The Cerebral-Cortex Of Man. Nature 340:386-389.
Lund JS, Boothe RG (1975) Interlaminar Connections And Pyramidal Neuron Organization In Visual-Cortex, Area 17, Of Macaque Monkey. Journal of Comparative Neurology 159:305-334.
Lüsebrink F, Wollrab A, Speck O (2013) Cortical Thickness Determination Of The Human Brain Using High Resolution 3T And 7T MRI Data. Neuroimage 70:122-131.
Machielsen WC, Rombouts SA, Barkhof F, Scheltens P, Witter MP (2000) FMRI of visual encoding: reproducibility of activation. In: Hum Brain Mapp, pp 156-164. United States.
Macmillan N, Creelman C (2005) Detection theory: a user's guide. NJ: Erlbaum: Mahwah.
Magnussen S (2000) Low-level memory processes in vision. Trends in Neurosciences 23:247-251.
Magnussen S (2009) Implicit visual working memory. Scandinavian Journal of Psychology 50:535-542.
Magnussen S, Greenlee MW (1985) Marathon adaptation to spatial contrast: saturation in sight. Vision Res 25:1409-1411.
Magnussen S, Greenlee MW (1992) Retention and disruption of motion information in visual short-term memory. J Exp Psychol Learn Mem Cogn 18:151-156.
Magnussen S, Greenlee MW (1997) Competition and sharing of processing resources in

visual discrimination. J Exp Psychol Hum Percept Perform 23:1603-1616.
Magnussen S, Greenlee MW (1999) The psychophysics of perceptual memory. Psychological Research-Psychologische Forschung 62:81-92.
Magnussen S, Greenlee MW, Thomas JP (1996) Parallel processing in visual short-term memory. J Exp Psychol Hum Percept Perform 22:202-212.
Magnussen S, Idas E, Myhre SH (1998) Representation of orientation and spatial frequency in perception and memory: A choice reaction-time analysis. Journal of Experimental Psychology-Human Perception and Performance 24:707-718.
Magnussen S, Greenlee MW, Asplund R, Dyrnes S (1990) Perfect visual short-term memory for periodic patterns. European Journal of Cognitive Psychology 2:345-362.
Magnussen S, Greenlee MW, Asplund R, Dyrnes S (1991) Stimulus-specific mechanisms of visual short-term memory. Vision Res 31:1213-1219.
Malach R, Reppas JB, Benson RR, Kwong KK, Jiang H, Kennedy WA, Ledden PJ, Brady TJ, Rosen BR, Tootell RB (1995) Object-related activity revealed by functional magnetic resonance imaging in human occipital cortex. Proc Natl Acad Sci U S A 92 :8135-8139.
Maldonado PE, Godecke I, Gray CM, Bonhoeffer T (1997) Orientation selectivity in pinwheel centers in cat striate cortex. Science 276:1551-1555.
Malmo RB (1942) Interference factors in delayed response in monkeys after removal of frontal lobes. Journal of Neurophysiology 5:295-308.
Mangun GR (1995) Neural Mechanisms Of Visual Selective Attention. Psychophysiology 32:4-18.
Mangun GR, Hillyard SA, Luck SJ (1993) Electrocortical Substrates Of Visual Selective Attention. In: Attention and Performance Xiv: Synergies in Experimental Psychology, Artificial Intelligence and Cognitive Neuroscience (Meyer DE, Kornblum S, eds), pp 219-243.
Mangun GR, Hopfinger JB, Kussmaul CL, Fletcher EM, Heinze HJ (1997) Covariations in ERP and PET measures of spatial selective attention in human extrastriate visual cortex. Human Brain Mapping 5:273-279.
Mannion DJ, McDonald JS, Clifford CW (2009) Discrimination of the local orientation structure of spiral Glass patterns early in human visual cortex. Neuroimage 46:511-515.
Mansfield P (1977) Multi-Planar Image-Formation Using NMR Spin Echoes. Journal of Physics C-Solid State Physics 10:L55-L58.
Marsolek CJ, Nicholas CD, Andresen DR (2002) Interhemispheric communication of abstract and specific visual-form information. Neuropsychologia 40:1983-1999.
Marzi CA (1986) Transfer Of Visual Information After Unilateral Input To The Brain. Brain and Cognition 5:163-173.
Marzi CA, Perani D, Tassinari G, Colleluori A, Maravita A, Miniussi C, Paulesu E, Fazio F (1998) Brain imaging studies of callosal transmission. International Journal of Psychophysiology 30:75-75.
Mather G, Moulden B (1983) Thresholds For Movement Direction - 2 Directions Are Less Detectable Than One. Quarterly Journal of Experimental Psychology Section a-Human Experimental Psychology 35:513-518.
Mathiesen C, Caesar K, Akgoren N, Lauritzen M (1998) Modification of activity-dependent increases of cerebral blood flow by excitatory synaptic activity and spikes in rat cerebellar cortex. Journal of Physiology-London 512:555-566.
Maunsell JHR (1995) The Brains Visual World - Representation Of Visual Targets In Cerebral-Cortex. Science 270:764-769.
Maunsell JHR, Vanessen DC (1983) Functional-Properties Of Neurons In Middle Temporal Visual Area Of The Macaque Monkey .1. Selectivity For Stimulus Direction, Speed, And Orientation. Journal of Neurophysiology 49:1127-1147.
Maunsell JHR, Vanessen DC (1987) Topographic Organization Of The Middle Temporal Visual Area In The Macaque Monkey - Representational Biases And The Relationship To Callosal Connections And Myeloarchitectonic Boundaries. Journal

of Comparative Neurology 266:535-555.
Maunsell JHR, Cook EP (2002) The role of attention in visual processing. Philosophical Transactions of the Royal Society of London Series B-Biological Sciences 357:1063-1072.
McGowan JC (2008) Basic Principles of Magnetic Resonance Imaging. Neuroimaging Clinics of North America 18:623-636.
McKeefry DJ, Burton MP, Vakrou C (2007) Speed selectivity in visual short term memory for motion. Vision Research 47:2418-2425.
McKeefry DJ, Watson JD, Frackowiak RS, Fong K, Zeki S (1997) The activity in human areas V1/V2, V3, and V5 during the perception of coherent and incoherent motion. In: Neuroimage, pp 1-12. United States.
McLeod P, Heywood C, Driver J, Zihl J (1989) Selective deficit of visual search in moving displays after extrastriate damage. Nature 339:466-467.
Mechler F, Ringach DL (2002) On The Classification Of Simple And Complex Cells. Vision Research 42:1017-1033.
Meng J, Liu R, Wang K, Hua T, Lu Z-L, Xi M (2013) Neural correlates of stimulus spatial frequency-dependent contrast detection. Experimental brain research Experimentelle Hirnforschung Experimentation cerebrale 225:377-385.
Menon RS, Goodyear BG (1999) Submillimeter functional localization in human striate cortex using BOLD contrast at 4 Tesla: implications for the vascular point-spread function. Magn Reson Med 41:230-235.
Menon RS, Kim SG (1999) Spatial and temporal limits in cognitive neuroimaging with fMRI. Trends Cogn Sci 3:207-216.
Menon RS, Luknowsky DC, Gati JS (1998) Mental chronometry using latency-resolved functional MRI. Proceedings of the National Academy of Sciences of the United States of America 95:10902-10907.
Menon RS, Ogawa S, Tank DW, Ugurbil K (1993) Tesla gradient recalled echo characteristics of photic stimulation-induced signal changes in the human primary visual cortex. Magn Reson Med 30:380-386.
Miezin FM, Maccotta L, Ollinger JM, Petersen SE, Buckner RL (2000) Characterizing the hemodynamic response: Effects of presentation rate, sampling procedure, and the possibility of ordering brain activity based on relative timing. Neuroimage 11:735-759.
Miller EK (2000) The Prefrontal Cortex And Cognitive Control. Nature Reviews Neuroscience 1:59-65.
Miller EK, Cohen JD (2001) An integrative theory of prefrontal cortex function. Annual Review of Neuroscience 24:167-202.
Miller EK, Erickson CA, Desimone R (1996) Neural mechanisms of visual working memory in prefrontal cortex of the macaque. J Neurosci 16:5154-5167.
Miller EK, Gochin PM, Gross CG (1993) Suppression Of Visual Responses Of Neurons In Inferior Temporal Cortex Of The Awake Macaque By Addition Of A 2nd Stimulus. Brain Research 616:25-29.
Milner B (1963) Effects Of Different Brain Lesions On Card Sorting - Role Of Frontal Lobes. Archives of Neurology 9:90.
Misaki M, Kim Y, Bandettini PA, Kriegeskorte N (2010) Comparison of multivariate classifiers and response normalizations for pattern-information fMRI. Neuroimage 53:103-118.
Mitchell TM, Hutchinson R, Niculescu RS, Pereira F, Wang X (2004) Learning to decode cognitive states from brain images. Machine Learning 57:145-175.
Montaser-Kouhsari L, Landy MS, Heeger DJ, Larsson J (2007) Orientation-selective adaptation to illusory contours in human visual cortex. J Neurosci 27:2186-2195.
Moran J, Desimone R (1985) Selective Attention Gates Visual Processing In The Extrastriate Cortex. Science 229:782-784.
Moray N (1967) Where Is Capacity Limited. A Survey And A Model. Acta Psychologica 27:84.

Morin RL, Gray JE (1990) Basic Principles And Terminology Of Magnetic Resonance Imaging.

Norman KA, Polyn SM, Detre GJ, Haxby JV (2006) Beyond mind-reading: multi-voxel pattern analysis of fMRI data. Trends Cogn Sci 10:424-430.

Motter BC (1993) Focal Attention Produces Spatially Selective Processing In Visual Cortical Areas V1, V2, And V4 In The Presence Of Competing Stimuli. Journal Of Neurophysiology 70:909-919.

Movshon J, Adelson E, Gizzi M, Newsome W (1986) The analysis of moving visual patterns. In: Experimental brain research supplementum 2: Pattern recognition mechanisms (Chagas C, Gattass R, Gross C, eds), pp 117-151. New York: Springer-Verlag.

Movshon JA, Newsome WT (1996) Visual response properties of striate cortical neurons projecting to area MT in macaque monkeys. Journal of Neuroscience 16:7733-7741.

Mukamel R, Harel M, Hendler T, Malach R (2004) Enhanced temporal non-linearities in human object-related occipito-temporal cortex. Cereb Cortex 14:575-585.

Muller HJ, Findlay JM (1987) Sensitivity And Criterion Effects In The Spatial Cueing Of Visual-Attention. Perception & Psychophysics 42:383-399.

Muller JR, Metha AB, Krauskopf J, Lennie P (1999) Rapid adaptation in visual cortex to the structure of images. In: Science, pp 1405-1408. United States.

Muller NG, Kleinschmidt A (2004) The attentional 'spotlight's' penumbra: center-surround modulation in striate cortex. Neuroreport 15:977-980.

Munk MHJ, Linden DEJ, Muckli L, Lanfermann H, Zanella FE, Singer W, Goebel R (2002) Distributed cortical systems in visual short-term memory revealed by event-related functional magnetic resonance imaging. Cerebral Cortex 12:866-876.

Mur M, Bandettini PA, Kriegeskorte N (2009) Revealing representational content with pattern-information fMRI an introductory guide. Social Cognitive and Affective Neuroscience 4:101-109.

Murray SO (2008) The effects of spatial attention in early human visual cortex are stimulus independent. Journal of Vision 8.

Nachmias J, Kocher EC (1970) Visual Detection And Discrimination Of Luminance Increments. Journal of the Optical Society of America 60:382.

Nachmias J, Sansbury RV (1974) Grating Contrast - Discrimination May Be Better Than Detection. Vision Research 14:1039-1042.

Nemes VA, Whitaker D, Heron J, McKeefry DJ (2011) Multiple spatial frequency channels in human visual perceptual memory. Vision Res 51:2331-2339.

Nestares O, Heeger DJ (2000) Robust multiresolution alignment of MRI brain volumes. Magn Reson Med 43:705-715.

Newsome WT, Pare EB (1988) A Selective Impairment Of Motion Perception Following Lesions Of The Middle Temporal Visual Area (MT). Journal of Neuroscience 8:2201-2211.

Newsome WT, Wurtz RH, Komatsu H (1988) Relation Of Cortical Areas Mt And Mst To Pursuit Eye-Movements .2. Differentiation Of Retinal From Extraretinal Inputs. Journal of Neurophysiology 60:604-620.

Nichols DF, Betts LR, Wilson HR (2010) Decoding of faces and face components in face-sensitive human visual cortex. Front Psychol 1:28.

Norman KA, Polyn SM, Detre GJ, Haxby JV (2006) Beyond mind-reading: multi-voxel pattern analysis of fMRI data. Trends in Cognitive Sciences 10:424-430.

Oberauer K, Kliegl R (2001) Beyond Resources: Formal Models Of Complexity Effects And Age Differences In Working Memory. European Journal Of Cognitive Psychology 13:187-215.

O'Craven KM, Downing PE, Kanwisher N (1999) fMRI evidence for objects as the units of attentional selection. Nature 401:584-587.

O'Craven KM, Rosen BR, Kwong KK, Treisman A, Savoy RL (1997) Voluntary Attention Modulates Fmri Activity In Human MT-MST. Neuron 18:591-598.

O'Keefe LP, Levitt JB, Kiper DC, Shapley RM, Movshon JA (1998) Functional organization

of owl monkey lateral geniculate nucleus and visual cortex. Journal of Neurophysiology 80:594-609.
O'Toole AJ, Jiang F, Abdi H, Haxby JV (2005) Partially distributed representations of objects and faces in ventral temporal cortex. Journal of Cognitive Neuroscience 17:580-590.
O'Toole AJ, Jiang F, Abdi H, Penard N, Dunlop JP, Parent MA (2007) Theoretical, statistical, and practical perspectives on pattern-based classification amoroaches to the analysis of functional neuroimaging data. Journal of Cognitive Neuroscience 19:1735-1752.
Oberauer K, Kliegl R (2001) Beyond resources: Formal models of complexity effects and age differences in working memory. European Journal of Cognitive Psychology 13:187-215.
Offen S, Schuppeck D, Heeger DJ (2009) The role of early visual cortex in visual short-term memory and visual attention. Vision Research 49:1352-1362.
Offen S, Gardner JL, Schluppeck D, Heeger DJ (2010) Differential roles for frontal eye fields (FEFs) and intraparietal sulcus (IPS) in visual working memory and visual attention. Journal of Vision 10.
Ogawa S, Lee TM, Kay AR, Tank DW (1990) Brain Magnetic-Resonance-Imaging With Contrast Dependent On Blood Oxygenation. Proceedings of the National Academy of Sciences of the United States of America 87:9868-9872.
Ogden JA (1989) Visuospatial And Other Right-Hemispheric Functions After Long Recovery Periods In Left-Hemispherectomized Subjects. Neuropsychologia 27:765-776.
Ohki K, Chung S, Kara P, Huebener M, Bonhoeffer T, Reid RC (2006) Highly ordered arrangement of single neurons in orientation pinwheels. Nature 442:925-928.
Ohzawa I, Sclar G, Freeman RD (1982) Contrast Gain-Control In The Cat Visual-Cortex. Nature 298:266-268.
Ohzawa I, Sclar G, Freeman RD (1985) Contrast gain control in the cat's visual system. J Neurophysiol 54:651-667.
Olzak LA, Thomas P, Boff K, Kaufman L, Thomas JP (1986) Handbook Of Perception And Performance. Vol. 1: Sensory Processes And Perception.
Op de Beeck HP, Dicarlo JJ, Goense JB, Grill-Spector K, Papanastassiou A, Tanifuji M, Tsao DY (2008) Fine-scale spatial organization of face and object selectivity in the temporal lobe: do functional magnetic resonance imaging, optical imaging, and electrophysiology agree? J Neurosci 28:11796-11801.
Oppenheim A (1978) Applications of Digital Signal Processing: Prentice-Hall.
Palmer J, Verghese P, Pavel M (2000) The psychophysics of visual search. Vision Research 40:1227-1268.
Pantle A (1974) Visual Information Processing Of Complex Imagery. In: Aerospace Medical Research Laboratory Report.
Pantle AJ (1983) Temporal determinants of spatial sine-wave masking. In: Vision Res, pp 749-757. England.
Parrish TB, Gitelman DR, LaBar KS, Mesulam MM (2000) Impact of signal-to-noise on functional MRI. Magnetic Resonance in Medicine 44:925-932.
Pasternak T, Zaksas D (2003) Stimulus specificity and temporal dynamics of working memory for visual motion. Journal of Neurophysiology 90:2757-2762.
Pasternak T, Greenlee MW (2005) Working memory in primate sensory systems. Nat Rev Neurosci 6:97-107.
Patterson JT, Head PA, McNeill DL, Chung K, Coggeshall RE (1989a) Ascending Unmyelinated Primary Afferent-Fibers In The Dorsal Funiculus. Journal of Comparative Neurology 290:384-390.
Patterson K, Varghakhadem F, Polkey CE (1989b) Reading With One Hemisphere. Brain 112:39-63.
Paus T, Castro-Alamancos MA, Petrides M (2001) Cortico-cortical connectivity of the human mid-dorsolateral frontal cortex and its modulation by repetitive transcranial

magnetic stimulation. European Journal of Neuroscience 14:1405-1411.
Paus T, Koski L, Caramanos Z, Westbury C (1998) Regional differences in the effects of task difficulty and motor output on blood flow response in the human anterior cingulate cortex: a review of 107 PET activation studies. Neuroreport 9:R37-R47.
Pavan A, Langgartner D, Greenlee MW (2013) Visual short-term memory for global motion revealed by directional and speed-tuned masking. Neuropsychologia 51:809-817
Peirce JW (2007) The potential importance of saturating and supersaturating contrast response functions in visual cortex. J Vis 7:13.
Pelli DG (1985) Uncertainty Explains Many Aspects Of Visual Contrast Detection And Discrimination. Journal of the Optical Society of America a-Optics Image Science and Vision 2:1508-1532.
Pereira F, Mitchell T, Botvinick M (2009) Machine learning classifiers and fMRI: A tutorial overview. Neuroimage 45:S199-S209.
Pessoa L, Gutierrez E, Bandettini P, Ungerleider L (2002) Neural correlates of visual working memory: fMRI amplitude predicts task performance. Neuron 35:975-987.
Pestilli F, Carrasco M (2005) Attention enhances contrast sensitivity at cued and impairs it at uncued locations. Vision Research 45:1867-1875.
Peterson WW, Birdsall TG, Fox W (1954) The theory of signal detectability. Information Theory, Transactions of the IRE Professional Group on 4:171-212.
Phillips WA (1974) Distinction Between Sensory Storage And Short-Term Visual Memory. Perception & Psychophysics 16:283-290.
Phillips WA, Christie DFM (1977a) Components Of Visual Memory. Quarterly Journal of Experimental Psychology 29:117-133.
Phillips WA, Christie DFM (1977b) Interference With Visualization. Quarterly Journal of Experimental Psychology 29:637-650.
Pinsk MA, Doniger GM, Kastner S (2004) Push-pull mechanism of selective attention in human extrastriate cortex. Journal of Neurophysiology 92:622-629.
Poffenberger AT (1912) Reaction time to retinal stimulation with special reference to the time lost in conduction through nerve centers. In, pp 1-73. New York: Columbia university.
Poldrack RA (2006) Can cognitive processes be inferred from neuroimaging data? Trends Cogn Sci 10:59-63.
Poldrack RA (2007) Region of interest analysis for fMRI. Social Cognitive and Affective Neuroscience 2:67-70.
Poline JB, Worsley KJ, Holmes AP, Frackowiak RSJ, Friston KJ (1995) Estimating Smoothness In Statistical Parametric Maps - Variability Of P-Values. Journal of Computer Assisted Tomography 19:788-796.
Pollen DA, Ronner SF (1981) Phase-Relationships Between Adjacent Simple Cells In The Visual-Cortex. Science 212:1409-1411.
Pollmann S, Maertens M, von Cramon DY, Lepsien J, Hugdahl K (2002) Dichotic listening in patients with splenial and nonsplenial callosal lesions. Neuropsychology 16:56-64.
Pooresmaeili A, Poort J, Thiele A, Roelfsema PR (2010) Separable Codes for Attention and Luminance Contrast in the Primary Visual Cortex. Journal of Neuroscience 30:12701-12711.
Posner MI (1980) Orienting Of Attention. Quarterly Journal of Experimental Psychology 32:3-25.
Posner MI, Petersen SE (1990) The Attention System Of The Human Brain. Annual Review of Neuroscience 13:25-42.
Posner MI, Dehaene S (1994) Attentional Networks. Trends in Neurosciences 17:75-79.
Posner MI, Petersen SE, Fox PT, Raichle ME (1988) Localization Of Cognitive Operations In The Human-Brain. Science 240:1627-1631.
Postle BR, D'Esposito M (1999) "What" - Then - "where" in visual working memory: An event-related, fMRI study. Journal of Cognitive Neuroscience 11:585-597.
Postle BR, Berger JS, D'Esposito M (1999) Functional neuroanatomical double dissociation of mnemonic and executive control processes contributing to working memory

performance. Proc Natl Acad Sci U S A 96:12959-12964.
Puce A, Constable RT, Luby ML, McCarthy G, Nobre AC, Spencer DD, Gore JC, Allison T (1995) Functional Magnetic-Resonance-Imaging Of Sensory And Motor Cortex - Comparison With Electrophysiological Localization. Journal of Neurosurgery 83:262-270.
Purcell EM, Torrey HC, Pound RV (1946) Resonance Absorption By Nuclear Magnetic Moments In A Solid. Physical Review 69:37-38.
Qian N, Andersen RA (1994) Transparent Motion Perception As Detection Of Unbalanced Motion Signals .2. PHYSIOLOGY. Journal of Neuroscience 14:7367-7380.
Qian N, Andersen RA, Adelson EH (1994) Transparent Motion Perception As Detection Of Unbalanced Motion Signals .1. Psychophysics. Journal of Neuroscience 14:7357-7366.
Raj D, Anderson AW, Gore JC (2001) Respiratory effects in human functional magnetic resonance imaging due to bulk susceptibility changes. Physics in Medicine and Biology 46:3331-3340.
Ranganath C (2006) Working memory for visual objects: Complementary roles of inferior temporal, medial temporal, and prefrontal cortex. Neuroscience 139:277-289.
Ranganath C, D'Esposito M (2005) Directing the mind's eye: prefrontal, inferior and medial temporal mechanisms for visual working memory. Current Opinion in Neurobiology 15:175-182.
Ranganath C, DeGutis J, D'Esposito M (2004) Category-specific modulation of inferior temporal activity during working memory encoding and maintenance. Brain research Cognitive brain research 20:37-45.
Raybaud C (2010) The corpus callosum, the other great forebrain commissures, and the septum pellucidum: anatomy, development, and malformation. Neuroradiology 52:447-477.
Recanzone GH, Wurtz RH, Schwarz U (1997) Responses of MT and MST neurons to one and two moving objects in the receptive field. Journal of Neurophysiology 78:2904-2915.
Rees G, Friston K, Koch C (2000) A direct quantitative relationship between the functional properties of human and macaque V5. Nature Neuroscience 3:716-723.
Rees G, Howseman A, Josephs O, Frith CD, Friston KJ, Frackowiak RS, Turner R (1997) Characterizing the relationship between BOLD contrast and regional cerebral blood flow measurements by varying the stimulus presentation rate. Neuroimage 6:270-278.
Regan D, Beverley KI (1985) Postadaptation Orientation Discrimination. Journal of the Optical Society of America a-Optics Image Science and Vision 2:147-155.
Reich DS, Mechler F, Victor JD (2001) Temporal coding of contrast in primary visual cortex: when, what, and why. J Neurophysiol 85:1039-1050.
Reinhard J, Trauzettel-Klosinski S (2003) Nasotemporal overlap humans: A functional of retinal ganglion cells in study. Investigative Ophthalmology & Visual Science 44:1568-1572.
Reppas JB, Niyogi S, Dale AM, Sereno MI, Tootell RBH (1997) Representation of motion boundaries in retinotopic human visual cortical areas. Nature (London) 388:175-179.
Ress D, Heeger DJ (2003) Neuronal correlates of perception in early visual cortex. Nat Neurosci 6:414-420.
Ress D, Backus BT, Heeger DJ (2000) Activity in primary visual cortex predicts performance in a visual detection task. Nature Neuroscience 3:940-945.
Reynolds JH, Chelazzi L, Desimone R (1999) Competitive mechanisms subserve attention in macaque areas V2 and V4. Journal of Neuroscience 19:1736-1753.
Richter W, Ugurbil K, Georgopoulos A, Kim SG (1997) Time-resolved fMRI of mental rotation. Neuroreport 8:3697-3702.
Ringach DL, Shapley RM, Hawken MJ (2002) Orientation selectivity in macaque V1: Diversity and Laminar dependence. Journal of Neuroscience 22:5639-5651.
Ringo JL (1993) The Medial Temporal-Lobe In Encoding, Retention, Retrieval And

Interhemispheric-Transfer Of Visual Memory In Primates. Experimental Brain Research 96:387-403.

Risse GL, Gates J, Lund G, Maxwell R, Rubens A (1989) Interhemispheric-Transfer In Patients With Incomplete Section Of The Corpus-Callosum - Anatomic Verification With Magnetic-Resonance Imaging. Archives of Neurology 46:437-443.

Rodieck RW (1973) Inhibition In Cat Lateral Geniculate Nucleus Role Of Y System. Proceedings of the Australian Physiological and Pharmacological Society 4:167-167.

Rodman HR, Albright TD (1989) Single-unit analysis of pattern-motion selective properties in the middle temporal visual area (MT). Exp Brain Res 75:53-64.

Rodriguez AO (2004) Principles of magnetic resonance imaging. Revista Mexicana De Fisica 50:272-286.

Rogers LJ (2000) Evolution of Hemispheric Specialization: Advantages and Disadvantages. Brain and Language 73:236-253.

Rombouts SA, Barkhof F, Hoogenraad FG, Sprenger M, Scheltens P (1998) Within-subject reproducibility of visual activation patterns with functional magnetic resonance imaging using multislice echo planar imaging. In: Magn Reson Imaging, pp 105-113. United States.

Rombouts SA, Barkhof F, Hoogenraad FG, Sprenger M, Valk J, Scheltens P (1997) Test-retest analysis with functional MR of the activated area in the human visual cortex. AJNR Am J Neuroradiol 18:1317-1322.

Rosen BR, Buckner RL, Dale AM (1998) Event-related functional MRI: Past, present, and future. Proceedings of the National Academy of Sciences of the United States of America 95:773-780.

Rowe JB, Toni I, Josephs O, Frackowiak RSJ, Passingham RE (2000) The prefrontal cortex: Response selection or maintenance within working memory? Science 288:1656-1660.

Ruge MI, Victor J, Souweidane MM, Bilsky M, Gutin PH, Hirsch J (1999) Identification of pre- and post central sulcus by functional magnetic resonance imaging and electrophysiology: Comparison in 11 cases. Journal of Cognitive Neuroscience:30-30.

Rypma B, Prabhakaran V, Desmond JE, Glover GH, Gabrieli JDE (1999) Load-dependent roles of frontal brain regions in the maintenance of working memory. Neuroimage 9:216-226.

Salzman CD, Murasugi CM, Britten KH, Newsome WT (1992) Microstimulation in visual area MT: effects on direction discrimination performance. J Neurosci 12:2331-2355.

Sanchez Panchuelo RM (2009) High Resolution Anatomical And Functional Imaging. In: School Of Physics And Astronomy. UK: University Of Nottingham.

Sanchez-Panchuelo RM, Francis S, Bowtell R, Schluppeck D (2010) Mapping human somatosensory cortex in individual subjects with 7T functional MRI. J Neurophysiol 103:2544-2556.

Sanchez-Panchuelo RM, Francis ST, Schluppeck D, Bowtell RW (2012a) Correspondence of human visual areas identified using functional and anatomical MRI in vivo at 7 T. Journal of Magnetic Resonance Imaging 35:287-299.

Sanchez-Panchuelo RM, Besle J, Beckett A, Bowtell R, Schluppeck D, Francis S (2012b) Within-Digit Functional Parcellation of Brodmann Areas of the Human Primary Somatosensory Cortex Using Functional Magnetic Resonance Imaging at 7 Tesla. Journal of Neuroscience 32:15815-15822.

Sapountzis P, Schluppeck D, Bowtell RW, Peirce JW (2008) Comparing Orientation-Specific Adaptation And Pattern Classification Analyses In Human V1 Using High-Field fMRI. Perception 37:164-164.

Sapountzis P, Schluppeck D, Bowtell R, Peirce JW (2010) A comparison of fMRI adaptation and multivariate pattern classification analysis in visual cortex. Neuroimage 49:1632-1640.

Sasaki Y, Rajimehr R, Kim BW, Ekstrom LB, Vanduffel W, Tootell RBH (2006) The radial

bias: A different slant on visual orientation sensitivity in human and nonhuman primates. Neuron 51:661-670.
Savoy R, O'Craven K, Weisskoff R, Davis T, Baker J, Rosen B (1994) Exploring the temporal boundaries of fMRI: Measuring responses to very brief visual stimuli. . Miami.
Savoy R, Bandettini P, Weisskoff R, Kwong K, Davis T, Baker J (1995) Pushing the temporal resolution of fMRI: Studies of very brief visual stimuli, onset variability and asynchrony, and stimulus-correlated changes in noise In: Proceedings of the SMR3rd Annual Meeting,, p 450. Nice, France.
Saxe R, Moran JM, Scholz J, Gabrieli J (2006) Overlapping and non-overlapping brain regions for theory of mind and self reflection in individual subjects. Social Cognitive and Affective Neuroscience 1:229-234.
Saygin AP, Sereno MI (2008) Retinotopy and attention in human occipital, temporal, parietal, and frontal cortex. Cerebral Cortex 18:2158-2168.
Schade OH (1956) Optical And Photoelectric Analog Of The Eye. Journal of the Optical Society of America 46:721-739.
Schepelmann F, Prull G, Fellmann A, Becker W, Rossing H (1976) Clinical Picture, Motor-Activity, Electro-Encephalographic, Neurophysiologic And Linguistic Findings In A Case Of Left-Sided Hemispherectomy. Fortschritte Der Neurologie Psychiatrie 44:381-432.
Schira MM, Tyler CW, Breakspear M, Spehar B (2009) The Foveal Confluence in Human Visual Cortex. Journal of Neuroscience 29:9050-9058.
Schluppeck D, Glimcher P, Heeger DJ (2005) Topographic organization for delayed saccades in human posterior parietal cortex. Journal of Neurophysiology 94:1372-1384.
Schluppeck D, Curtis CE, Glimcher PW, Heeger DJ (2006) Sustained activity in topographic areas of human posterior parietal cortex during memory-guided saccades. Journal of Neuroscience 26:5098-5108.
Schonhoff TA, Giordano AA (2006) Detection and Estimation Theory and Its Applications. New Jersey: Pearson Education.
Schulder M, Maldjian JA, Liu WC, Holodny AI, Kalnin AT, Mun IK, Carmel PW (1998) Functional image-guided surgery of intracranial tumors located in or near the sensorimotor cortex. Journal of Neurosurgery 89:412-418.
Schumacher JF, Thompson SK, Olman CA (2011) Contrast Response Functions For Single Gabor Patches: ROI-Based Analysis Over-Represents Low-Contrast Patches For GE BOLD. Frontiers In Systems Neuroscience 5:19-19.
Schwartz O, Simoncelli EP (2001) Natural signal statistics and sensory gain control. Nature Neuroscience 4:819-825.
Schwarzkopf DS, Rees G (2011) Pattern Classification Using Functional Magnetic Resonance Imaging. Wiley Interdisciplinary Reviews-Cognitive Science 2:568-579.
Sclar G (1987) Expression Of Retinal Contrast Gain-Control By Neurons Of The Cats Lateral Geniculate-Nucleus. Experimental Brain Research 66:589-596.
Sclar G, Freeman RD (1982) Orientation Selectivity In The Cats Striate Cortex Is Invariant With Stimulus Contrast. Experimental Brain Research 46:457-461.
Sclar G, Ohzawa I, Freeman RD (1985) Contrast Gain-Control In The Kittens Visual-System. Journal of Neurophysiology 54:668-675.
Sclar G, Lennie P, Depriest DD (1989) Contrast Adaptation In Striate Cortex Of Macaque. Vision Research 29:747-755.
Scolari M, Serences JT (2010) Basing perceptual decisions on the most informative sensory neurons. J Neurophysiol 104:2266-2273.
Seidemann E, Newsome WT (1999) Effect of spatial attention on the responses of area MT neurons. Journal of Neurophysiology 81:1783-1794.
Serences JT, Boynton GM (2007) Feature-based attentional modulations in the absence of direct visual stimulation. Neuron 55:301-312.
Serences JT, Yantis S (2007) Spatially selective representations of voluntary and stimulus-

driven attentional priority in human occipital, parietal, and frontal cortex. Cerebral Cortex 17:284-293.
Serences JT, Ester EF, Vogel EK, Awh E (2009) Stimulus-specific delay activity in human primary visual cortex. Psychol Sci 20:207-214.
Sereno MI (1995) Borders of multiple visual areas in humans revealed by functional magnetic resonance imaging. Science 268:889-893.
Sereno MI, Pitzalis S, Martinez A (2001) Mapping of contralateral space in retinotopic coordinates by a parietal cortical area in humans. Science 294:1350-1354.
Shadlen MN, Newsome WT (1994) Noise, neural codes and cortical organization. Curr Opin Neurobiol 4:569-579.
Shannon M, Roemer RC (1990) Physical And Imaging Principles Of Magnetic Resonance.
Shapley RM, Victor JD (1978) The effect of contrast on the transfer properties of cat retinal ganglion cells. J Physiol 285:275-298.
Shaw ML (1984) Division Of Attention Among Spatial Locations - A Fundamental Difference Between Detection Of Letters And Detection Of Luminance Increments. Attention and Performance 10:109-121.
Shiu LP, Pashler H (1994) Negligible Effect Of Spatial Precuing On Identification Of Single Digits. Journal of Experimental Psychology-Human Perception and Performance 20:1037-1054.
Siegmund DO, Worsley KJ (1995) Testing For A Signal With Unknown Location And Scale In A Stationary Gaussian Random-Field. Annals Of Statistics 23:608-639.
Silver MA, Ress D, Heeger DJ (2005) Topographic maps of visual spatial attention in human parietal cortex. J Neurophysiol 94:1358-1371.
Silver MA, Ress D, Heeger DJ (2007) Neural correlates of sustained spatial attention in human early visual cortex. Journal of Neurophysiology 97:229-237.
Silver MA, Landau AN, Lauritzen TZ, Prinzmetal W, Robertson LC (2010) Isolating human brain functional connectivity associated with a specific cognitive process. In: Human Vision and Electronic Imaging XV. San Jose, CA.
Skottun BC, Bradley A, Sclar G, Ohzawa I, Freeman RD (1987) The Effects Of Contrast On Visual Orientation And Spatial-Frequency Discrimination - A Comparison Of Single Cells And Behavior. Journal of Neurophysiology 57:773-786.
Sligte I, van Moorselaar D, Vandenbroucke A (2013) Decoding the Contents of Visual Working Memory: Evidence for Process-Based and Content-Based Working Memory Areas? Journal of Neuroscience 33:1293-1294.
Smith A, Kosillo P, Williams A (2011) The confounding effect of response amplitude on MVPA performance measures. Neuroimage 56:525-530.
Smith SM, Jenkinson M, Woolrich MW, Beckmann CF, Behrens TE, Johansen-Berg H, Bannister PR, De Luca M, Drobnjak I, Flitney DE, Niazy RK, Saunders J, Vickers J, Zhang Y, De Stefano N, Brady JM, Matthews PM (2004) Advances in functional and structural MR image analysis and implementation as FSL. Neuroimage 23 Suppl 1:S208-219.
Sneve MH, Alnæs D, Endestad T, Greenlee MW, Magnussen S (2011) Modulation of activity in human visual area V1 during memory masking. PLoS One 6:e18651.
Snowden RJ, Treue S, Andersen RA (1992) The response of neurons in areas V1 and MT of the alert rhesus monkey to moving random dot patterns. Exp Brain Res 88:389-400.
Snowden RJ, Treue S, Erickson RG, Andersen RA (1991) The Response Of Area Mt And V1 Neurons To Transparent Motion. Journal of Neuroscience 11:2768-2785.
Sokoloff L (1977) Relation Between Physiological Function And Energy-Metabolism In Central Nervous-System. Journal of Neurochemistry 29:13-26.
Sokoloff L, Reivich M, Kennedy C, Desrosiers MH, Patlak CS, Pettigrew KD, Sakurada O, Shinohara M (1977) Deoxyglucose-C-14 Method For Measurement Of Local Cerebral Glucose-Utilization - Theory, Procedure, And Normal Values In Conscious And Anesthetized Albino-Rat. Journal of Neurochemistry 28:897-916.
Soltysik DA, Peck KK, White KD, Crosson B, Briggs RW (2004) Comparison of hemodynamic response nonlinearity across primary cortical areas. Neuroimage

22:1117-1127.
Soma S, Shimegi S, Suematsu N, Sato H (2013) Cholinergic modulation of response gain in the rat primary visual cortex. Sci Rep 3:1138.
Somers DC, Dale AM, Seiffert AE, Tootell RBH (1999) Functional MRI reveals spatially specific attentional modulation in human primary visual cortex. Proceedings of the National Academy of Sciences of the United States of America 96:1663-1668.
Sowden PT, Rose D, Davies IRL (2002) Perceptual learning of luminance contrast detection: specific for spatial frequency and retinal location but not orientation. Vision Research 42:1249-1258.
Sperling G (1960) Visual Information-Storage. Acta Psychologica 16:558-559.
Sperling G (1963) A Model For Visual Memory Tasks. Human Factors 5:19-31.
Sperry RW, Zaidel E, Zaidel D (1979) Self Recognition And Social Awareness In The Deconnected Minor Hemisphere. Neuropsychologia 17:153-166.
Spiridon M, Kanwisher N (2002) How distributed is visual category information in human occipito-temporal cortex? An fMRI study. Neuron 35:1157-1165.
Stanisz GJ, Odrobina EE, Pun J, Escaravage M, Graham SJ, Bronskill MJ, Henkelman RM (2005) T-1, T-2 relaxation and magnetization transfer in tissue at 3T. Magnetic Resonance in Medicine 54:507-512.
Stoner GR, Albright TD (1992) Neural correlates of perceptual motion coherence. Nature 358:412-414.
Stromeyer CF, Kronauer RE, Madsen JC, Klein SA (1984) Opponent-Movement Mechanisms In Human-Vision. Journal of the Optical Society of America a-Optics Image Science and Vision 1:876-884.
Stromeyer CF, 3rd, Klein S (1974) Spatial frequency channels in human vision as asymmetric (edge) mechanisms. In: Vision Res, pp 1409-1420. England.
Sugishita M, Otomo K, Yamazaki K, Shimizu H, Yoshioka M, Shinohara A (1995) Dichotic-Listening In Patients With Partial Section Of The Corpus-Callosum. Brain 118:417-427.
Super H, Spekreijse H, Lamme VAF (2001) A neural correlate of working memory in the monkey primary visual cortex. Science 293:120-124.
Suwanwela NC, Leelacheavasit N (2002) Isolated corpus callosal infarction secondary to pericallosal artery disease presenting as alien hand syndrome. Journal of Neurology Neurosurgery and Psychiatry 72:533-536.
Swift DJ, Smith RA (1983) Spatial-Frequency Masking And Weber Law. Vision Research 23:495-505.
Swisher JD, Gatenby JC, Gore JC, Wolfe BA, Moon CH, Kim SG, Tong F (2010) Multiscale pattern analysis of orientation-selective activity in the primary visual cortex. J Neurosci 30:325-330.
Talbot SA (1942) A lateral localization in the cat's visual cortex. In: Fed. Proc, pp 1255-1263.
Talbot SA, Marshall WH (1940) Multiple responses in the optic tract and optic cortex of cat. Am J Physiol 129:478.
Tanaka K (2000) Basic principles of magnetic resonance imaging. Rinsho byori The Japanese journal of clinical pathology 48:614-620.
Tanaka M, Weber H, Creutzfeldt OD (1986) Visual Properties And Spatial-Distribution Of Neurons In The Visual Association Area On The Prelunate Gyrus Of The Awake Monkey. Experimental Brain Research 65:11-37.
Tanner WP, Swets JA (1954) A Decision-Making Theory Of Visual Detection. Psychological Review 61:401-409.
Teo PC, Heeger DJ (1994) Perceptual Image Distortion.
Teo PC, Heeger DJ (1995) A General Mechanistic Model Of Spatial Pattern Detection. Investigative Ophthalmology & Visual Science 36:S439-S439.
Thompson R, Correia M, Cusack R (2011) Vascular contributions to pattern analysis: comparing gradient and spin echo fMRI at 3T. Neuroimage 56:643-650.
Thompson JM, Woolsey CN, Talbot SA (1950) Visual areas I and 2 of cerebral cortex of

rabbit. J Neurophysiol 13:277-288.
Thulborn KR, Waterton JC, Matthews PM, Radda GK (1982) Oxygenation dependence of the transverse relaxation time of water protons in whole blood at high field. Biochimica et Biophysica Acta (BBA) - General Subjects 714:265-270.
Tolhurst DJ, Thompson ID (1982) Organization Of Neurons Preferring Similar Spatial-Frequencies In Cat Striate Cortex. Experimental Brain Research 48:217-227.
Tolias AS, Smirnakis SM, Augath MA, Trinath T, Logothetis NK (2001) Motion processing in the macaque: Revisited with functional magnetic resonance imaging. Journal of Neuroscience 21:8594-8601.
Tootell RB, Hamilton SL, Switkes E (1988) Functional anatomy of macaque striate cortex. 4. Contrast and magno-parvo streams. J Neurosci 8:1594-1609.
Tootell RBH, Taylor JB (1995) Anatomical Evidence For Mt And Additional Cortical Visual Areas In Humans. Cerebral Cortex 5:39-55.
Tootell RBH, Tsao D, Vanduffel W (2003) Neuroimaging weighs in: Humans meet macaques in "primate" visual cortex. Journal of Neuroscience 23:3981-3989.
Tootell RBH, Mendola JD, Hadjikhani NK, Liu AK, Dale AM (1998a) The representation of the ipsilateral visual field in human cerebral cortex. Proceedings of the National Academy of Sciences of the United States of America 95:818-824.
Tootell RBH, Hadjikhani NK, Vanduffel W, Liu AK, Mendola JD, Sereno MI, Dale AM (1998b) Functional analysis of primary visual cortex (V1) in humans. Proceedings of the National Academy of Sciences of the United States of America 95:811-817.
Tootell RBH, Reppas JB, Kwong KK, Malach R, Born RT, Brady TJ, Rosen BR, Belliveau JW (1995) Functional-Analysis Of Human MT And Related Visual Cortical Areas Using Magnetic-Resonance-Imaging. Journal of Neuroscience 15:3215-3230.
Treisman AM, Gelade G (1980) Feature-Integration Theory Of Attention. Cognitive Psychology 12:97-136.
Treue S, Maunsell JHR (1996) Attentional modulation of visual motion processing in cortical areas MT and MST. Nature 382:539-541.
Treue S, Trujillo JCM (1999) Feature-based attention influences motion processing gain in macaque visual cortex. Nature 399:575-579.
Trevarthen C (1972) Specialized Lesions The Split Brain Technique. Myers, RD (Ed) Methods in Psychobiology, Vol 2 Specialized Laboratory Techniques in Neuropsychology and Neurobiology Xii+398p Illus Academic Press: London, England; New York, NY, USA:251-284.
Triantafyllou C, Hoge RD, Wald LL (2006) Effect of spatial smoothing on physiological noise in high-resolution fMRI. Neuroimage 32:551-557.
Tsao DY, Freiwald WA, Knutsen TA, Mandeville JB, Tootell RB (2003) Faces and objects in macaque cerebral cortex. Nat Neurosci 6:989-995.
Tulving E (1991) Concepts Of Human Memory. In: Memory Organization And Locus Of Change (Squire L, Lynch GN, Eds), Pp 387-396. N.J.: Erlbaum: Hillsdale.
Tulving E, Schacter DL (1990) Priming And Human-Memory Systems. Science 247:301-306.
Uhlrich DJ, Essock EA, Lehmkuhle S (1981) Cross-Species Correspondence Of Spatial Contrast Sensitivity Functions. Behavioural Brain Research 2:291-299.
Urban FM (1910) The method of constant stimuli and its generalizations. Psychological Review 17:229-259.
van de Ven V, Jacobs C, Sack AT (2012) Topographic contribution of early visual cortex to short-term memory consolidation: a transcranial magnetic stimulation study. J Neurosci 32:4-11.
Van der Knaap LJ, Van der Ham IJM (2011) How does the corpus callosum mediate interhemispheric transfer? A review. Behavioural Brain Research 223:211-221.
Van Essen DC, Maunsell JHR, Bixby JL (1981) The Middle Temporal Visual Area In The Macaque Macaca-Fascicularis Myelo Architecture Connections Functional Properties And Topographic Organization. Journal of Comparative Neurology 199:293-326.
Van Geuns RJM, Wielopolski PA, de Bruin HG, Rensing BJ, van Ooijen PMA, Hulshoff M,

Oudkerk M, de Feyter PJ (1999) Basic principles of magnetic resonance imaging. Progress in Cardiovascular Diseases 42:149-156.
Van Santen JP, Sperling G (1984) Temporal covariance model of human motion perception. J Opt Soc Am A 1:451-473.
Vazquez AL, Noll DC (1998) Nonlinear aspects of the BOLD response in functional MRI. Neuroimage 7:108-118.
Virsu V, Rovamo J (1979) Visual Resolution, Contrast Sensitivity, and the Cortical Magnification Factor. Experimental Brain Research 37:475-494.
Vogel EK, Woodman GF, Luck SJ (2006) The time course of consolidation in visual working memory. Journal of Experimental Psychology-Human Perception and Performance 32:1436-1451.
Vogels R, Orban GA (1986) Decision processes in visual discrimination of line orientation. J Exp Psychol Hum Percept Perform 12:115-132.
Wandell BA (1999) Computational Neuroimaging Of Human Visual Cortex. Annual Review Of Neuroscience 22:145.
Wandell BA, Dumoulin SO, Brewer AA (2007) Visual field maps in human cortex. Neuron 56:366-383.
Ward R, Duncan J, Shapiro K (1996) The slow time-course of visual attention. Cognitive Psychology 30:79-109.
Warden MR, Miller EK (2007) The representation of multiple objects in prefrontal neuronal delay activity. In: Cereb Cortex, pp i41-50. United States.
Wassle H, Grunert U, Rohrenbeck J, Boycott BB (1990) Retinal Ganglion-Cell Density And Cortical Magnification Factor In The Primate. Vision Research 30:1897-1911.
Watanabe T, Sasaki Y, Miyauchi S, Putz B, Fujimaki N, Nielsen M, Takino R, Miyakawa S (1998) Attention-regulated activity in human primary visual cortex. Journal of Neurophysiology 79:2218-2221.
Watson AB, Robson JG (1981) Summation of grating patches indicates many types of detector at one retinal location. Vision Research 21:1115.
Watson JDG, Myers R, Frackowiak RSJ, Hajnal JV, Woods RP, Mazziotta JC, Shipp S, Zeki S (1993) Area-V5 Of The Human Brain - Evidence From A Combined Study Using Positron Emission Tomography And Magnetic-Resonance-Imaging. Cerebral Cortex 3:79-94.
Wehrli FW, Atlas SW (1991) Fast Imaging Principles Techniques And Clinical Applications. Atlas, S W (Ed) Magnetic Resonance Imaging of the Brain and Spine Xiii+1137p Raven Press: New York, New York, USA Illus:1013-1078.
Westheimer G (2001) The Fourier theory of vision. Perception 30:531-541.
Wheeler ME, Treisman AM (2002) Binding in short-term visual memory. J Exp Psychol Gen 131:48-64.
Whittle P (1986) Increments And Decrements - Luminance Discrimination. Vision Research 26:1677-1691.
Wickens CD (1984) Processing resources in attention. In: Varieties of attention (Parasuraman R, Daview DRD, eds), pp 63-102. London: Academic Press.
Wickens TD (2002) Elementary Signal Detection Theory. New York: Oxford University Press.
Wiener E, Schad LR, Baudendistel KT, Essig M, Muller E, Lorenz WJ (1996) Functional MR imaging of visual and motor cortex stimulation at high temporal resolution using a flash technique on a standard 1.5 Tesla scanner. Magnetic Resonance Imaging 14:477-483.
Williams MA, Dang S, Kanwisher NG (2007) Only some spatial patterns of fMRI response are read out in task performance. Nat Neurosci 10:685-686.
Wilson HR, Gelb DJ (1984) Modified Line-Element Theory For Spatial-Frequency And Width Discrimination. Journal of the Optical Society of America a-Optics Image Science and Vision 1:124-131.
Wiser AK, Callaway EM (1996) Contributions of individual layer 6 pyramidal neurons to local circuitry in macaque primary visual cortex. Journal of Neuroscience 16:2724-

2739.
Witelson SF (1974) Hemispheric Specialization for Linguistic and Nonlinguistic Tactual Perception Using a Dichotomous Stimulation Technique. Cortex 10:3-17.
Witzel T, Halgren E, Fischl BR, Liu AK, Ahlfors SP, Dale AM (2001) Spatiotemporal imaging of brain activation using FreeSurfer. Neuroimage 13:S286-S286.
Woldorff MG, Fox PT, Matzke M, Lancaster JL, Veeraswamy S, Zamarripa F, Seabolt M, Glass T, Gao JH, Martin CC, Jerabek P (1997) Retinotopic organization of early visual spatial attention effects as revealed by PET and ERPs. Human Brain Mapping 5:280-286.
Wong-Riley M (1979) Changes in the visual system of monocularly sutured or enucleated cats demonstrable with cytochrome oxidase histochemistry. Brain Res 171:11-28.
Woodman GF, Vogel EK (2008) Selective storage and maintenance of an object's features in visual working memory. Psychon Bull Rev 15:223-229.
Worden MS, Foxe JJ, Wang N, Simpson GV (2000) Anticipatory biasing of visuospatial attention indexed by retinotopically specific alpha-band electroencephalography increases over occipital cortex. Journal of Neuroscience 20:art. no.-RC63.
Worsley KJ, Friston KJ (1995) Analysis Of fmri Time-Series Revisited - Again. Neuroimage 2:173-181.
Xu X, Bosking W, Sary G, Boyd J, Jones M, Khaytin I, Stefansic J, Shima D, Fitzpatrick D, Casagrande V (2002) Orientation Preference Domains And Their Relation To Cytochrome Oxidase (Co) Modules In Owl Monkey Visual Cortex. Society for Neuroscience Abstract Viewer and Itinerary Planner 2002:Abstract No. 325.313-Abstract No. 325.313.
Yabuta NH, Callaway EM (1998) Functional streams and local connections of layer 4C neurons in primary visual cortex of the macaque monkey. Journal of Neuroscience 18:9489-9499.
Yamamoto H, Fukunaga M, Takahashi S, Mano H, Tanaka C, Umeda M, Ejima Y (2012) Inconsistency and uncertainty of the human visual area loci following surface-based registration: Probability and Entropy Maps. Human Brain Mapping 33:121-129.
Yoshioka T, Levitt JB, Lund JS (1994) Independence And Merger Of Thalamocortical Channels Within Macaque Monkey Primary Visual-Cortex - Anatomy Of Interlaminar Projections. Visual Neuroscience 11:467-489.
Yousry T, Schmid UD, Schmidt D, Heiss D, Jassoy A, Eisner W, Reulen HJ, Reiser M (1995) Cortical Motor Hand Area - Validation Of Functional Magnetic-Resonance-Imaging By Intraoperative Cortical Stimulation Mapping. Radiology 35:252-255.
Zaidel E, Peters AM (1981) Phonological Encoding And Ideographic Reading By The Disconnected Right-Hemisphere - 2 Case Studies. Brain and Language 14:205-234.
Zaksas D, Pasternak T (2006) Directional signals in the prefrontal cortex and in area MT during a working memory for visual motion task. In: J Neurosci, pp 11726-11742. United States.
Zarahn E, Aguirre G, Desposito M (1997) A trial-based experimental design for fMRI. Neuroimage 6:122-138.
Zarahn E, Aguirre GK, D'Esposito M (1999) Temporal isolation of the neural correlates of spatial mnemonic processing with fMRI. Cognitive Brain Research 7:255-268.
Zeki S, Watson JDG, Lueck CJ, Friston KJ, Kennard C, Frackowiak RSJ (1991) A Direct Demonstration Of Functional Specialization In Human Visual-Cortex. Journal of Neuroscience 11:641-649.
Zeki SM (1969) Representation Of Central Visual Fields In Pre-striate Cortex Of Monkey. Brain Research 14:271.
Zeki SM (1974) Functional Organization Of A Visual Area In Posterior Bank Of Superior Temporal Sulcus Of Rhesus-Monkey. Journal of Physiology-London 236:549.
Zemany L, Stromeyer CF, Chaparro A, Kronauer RE (1998) Motion detection on flashed, stationary pedestal gratings: Evidence for an opponent-motion mechanism. Vision Research 38:795-812.
Zenger-Landolt B, Heeger DJ (2003) Response suppression in v1 agrees with psychophysics

of surround masking. J Neurosci 23:6884-6893.
Zhou YD, Fuster JM (1996) Mnemonic neuronal activity in somatosensory cortex. Proceedings of the National Academy of Sciences of the United States of America 93:10533-10537.
Zhou YD, Fuster JM (1997) Neuronal activity of somatosensory cortex in a cross-modal (visuo-haptic) memory task. Experimental Brain Research 116:551-555.